

Synthetic Studies on New Teropyrenophanes and Pyrenophanes

by

© Parisa Ghods Ghasemabadi

A thesis submitted to the
School of Graduate Studies
in partial fulfilment of the requirements
for the degree of Doctor of Philosophy

Department of Chemistry

Memorial University

May 2019

St. John's

Newfoundland

Dedicated to:

My Lovely Family

Without them, none of this would have been possible.

Abstract

Cyclophane chemistry came into existence in the middle of 20th century with Brown and Farthing's synthesis of [2.2]paracyclophane. During the six subsequent decades, interest in cyclophanes has grown significantly due to their interesting structural, spectroscopic, conformational, physical and chemical properties, especially with regards to highly-strained cyclophanes. 1,1,*n,n*-tetramethyl[*n*](2,11)teropyrenophanes are a remarkable class of cyclophanes, which have been successfully synthesized using two related strategies.

The first chapter of this dissertation involves the seminal work on the cyclophane chemistry of teropyrene series including benzene, pyrene and teropyrene. Different general strategies and the chemical, spectral and photophysical properties of each series of cyclophanes have been discussed.

The second chapter focuses on the application of these synthetic strategies and also the development of other approaches for the synthesis of 1,1,6,6-tetramethyl[6](2,11)teropyrenophane, which would become the smallest and most strained member of teropyrenophane series. Although all attempts to arrive at this highly challenging target were unsuccessful, several notable advances were made, and these may open new avenues of investigation.

The third chapter studies a modified protocol for the key teropyrene-forming reaction (a valence isomerization/dehydrogenation (VID) reaction), which has enabled the construction of the teropyrenophanes on a gram-scale. This provided the opportunity to explore new aspects of their chemistry, *i.e.* through *K*-region oxidation and reaction with

o-phenylenediamine, which resulted in the synthesis of larger bent PAHs; quinoxalinoteropyrenophanes.

In the last chapter, some of the aliphatic bridge carbon atoms in teropyrenophane system were replaced with a small aromatic system (pyridine). Titration of this novel cyclophane (pyridinophane) with TFA was performed and a weak charge transfer band was observed in UV-Vis acid titration spectra due to the intramolecular transition between the teropyrene and pyridinium units, which did not exist in neutral pyridinophane. In addition, remarkable progress was made towards the synthesis of pyridine-containing pyrenophane, but more investigation is required in this area. These new types of compounds offer opportunities to investigate their host-guest chemistry and have the potential for application in the design of optoelectronic devices.

Acknowledgements

I would like to express my gratitude to my supervisor, Professor Graham Bodwell, for the support and advice he has provided throughout my Ph.D. research studies. It was a real pleasure for me to study under your guidance.

As members of supervisory committee, I would like to thank Professors Robert Davis and Sunil Pansare for their invaluable suggestions during committee meetings and critical reading and review of this dissertation.

A special thanks to Professor Robert Lucas, who has always believed in me, listened to me and encouraged me, you are such a wonderful teacher.

The services of C-CART and CREAT are greatly appreciated here as well. Specially the assistance of Dr. Celine Schneider (NMR analysis) and Ms. Linda Winsor (mass spectral analysis). I am also grateful to the entire Bodwell group for their support with special mention to Dr. Kiran Unikela.

I would like to thank my amazing parents and brothers for their unconditional love and constant support throughout both undergraduate and graduate programs. Without the inspiration you gave me, I would not be where I am now. Words are not enough to tell you how much you mean to me.

Finally, I extend my sincerest appreciation to my love, Ehsan. Thank you for listening to me, understanding me, standing by my side, supporting me and my dreams, and for always being there during the thick and thin. You are the best thing that has ever happened to me. I love you.

Contents

Dedication.....	ii
Abstract	iii
Acknowledgements.....	v
Contents.....	vi
List of Figures	xii
List of Schemes.....	xvi
List of Tables.....	xx
List of Abbreviations.....	xxii
CHAPTER 1: Introduction.....	1
1.1 Cyclophane Chemistry.....	1
1.1.1 Unlimited Scope of Cyclophane Chemistry.....	1
1.1.2 General Synthetic Considerations.....	2
1.2 [n]Cyclophanes Derived from Polynuclear Aromatic Hydrocarbon (PAH)s.....	4
1.2.1 The [n]Paracyclophanes.....	7
1.2.1.1 Synthesis of [n]Paracyclophane Derivatives.....	8
1.2.1.1.1 Synthesis of [n]Paracyclophanes using the Type I Strategies.....	9
1.2.1.1.2 Synthesis of [n]Paracyclophanes using the Type III Strategy.....	14
1.2.1.2 Consequences of Bending Benzene rings in [n]Paracyclophanes...	19

1.2.2	[<i>n</i>](2,7)Pyrenophanes.....	22
1.2.2.1	Synthesis of [<i>n</i>](2,7)Pyrenophanes.....	24
1.2.2.2	Consequences of Bending the Pyrene Units in the [<i>n</i>](2,7)Pyrenophanes.....	26
1.2.3	[<i>n</i>](2,9)Teropyrenophanes.....	31
1.2.4	[<i>n</i>](2,11)Teropyrenophanes.....	31
1.2.4.1	Synthesis of [<i>n</i>](2,11)Teropyrenophanes.....	31
1.2.4.2	Consequences of Bending the Teropyrene System in [<i>n</i>](2,11)Teropyrenophanes.....	32
1.3	Summary.....	35
1.4	References and Notes.....	36

CHAPTER 2: Attempted Synthesis of 1,1,6,6-Tetramethyl[6](2,11)teropyrenophane.....41

2.1	Introduction.....	41
2.2	Previously Reported Synthesis of a Homologous Series of 1,1, <i>n,n</i> - Tetramethyl[<i>n</i>](2,11)teropyrenophanes.....	43
2.2.1	Synthesis of 1,1, <i>n,n</i> -Tetramethyl[<i>n</i>](2,11)teropyrenophanes 2.6b,c <i>via</i> a Double-McMurry Route.....	44
2.2.2	Synthesis of 1,1, <i>n,n</i> -Tetramethyl[<i>n</i>](2,11)teropyrenophanes 2.6b-e <i>via</i> a Wurtz coupling/McMurry Route.....	47

2.3	Toward the Synthesis of 1,1,6,6-Tetramethyl[6](2,11)teropyrenophane.....	50
2.3.1	1,1,6,6-Tetramethyl[6](2,11)teropyrenophane: A Lower Limit to These Highly Distorted π -Systems or Current Synthetic Route?....	50
2.4	Results and Discussion.....	51
2.4.1	Attempted Synthesis of 1,1,6,6-Tetramethyl[6](2,11)teropyrenophane (2.6a) <i>via</i> a Wurtz/McMurry Route.....	51
2.4.2	Attempted Synthesis of 1,1,6,6-Tetramethyl[6](2,11)teropyrenophane through the Thiacyclophane-based Pathway A.....	55
2.4.3	VT-NMR Spectra and Conformational Behaviours of [n.2](7,1)Pyrenophanes 2.20a and 2.20b	57
2.4.4	Attempted Synthesis of 1,1,6,6-Tetramethyl[6](2,11)teropyrenophane through the Thiacyclophane-based Pathway B.....	63
2.4.5	Attempted Synthesis of 1,1,6,6-Tetramethyl[6](2,11)teropyrenophane through an Oxacyclophane-based Pathway A.....	65
2.4.6	Attempted Synthesis of 1,1,6,6-Tetramethyl[6](2,11)teropyrenophane through a Fourfold Functionalization-based Approach.....	70

2.5	Summary.....	78
	General Experimental Details.....	81
2.6	Experimental Procedures and Characterization Data.....	82
2.7	References and Notes.....	100
	APPENDIX 1.....	104

CHAPTER 3: Optimization of the Valence Isomerization/Dehydrogenation (VID) Reaction in the Synthesis of 1,1,*n,n*-Tetramethyl[*n*](2,11)teropyrenophanes and Further Exploration of the Chemistry of These Aromatic Half-Belts.....118

3.1	Introduction.....	118
3.1.1	Application of the Valence Isomerization/Dehydrogenation (VID) reaction in the Synthesis of (2,7)Pyrenophanes.....	118
3.1.2	Application of the Valence Isomerization/Dehydrogenation (VID) Reaction in the Synthesis of 1,1, <i>n,n</i> -Tetramethyl[<i>n</i>](2,11)teropyrenophanes.....	122
3.1.3	Issues Associated with the VID Reaction in the Original Synthesis of 1,1, <i>n,n</i> -Tetramethyl[<i>n</i>](2,11)teropyrenophanes.....	123
3.1.4	Previous Modified Conditions for the VID Reaction in the Synthesis of 1,1, <i>n,n</i> -Tetramethyl[<i>n</i>](2,11)teropyrenophanes.....	124
3.2	Results and Discussions.....	128

3.2.1	New Conditions for the VID Reaction in the Synthesis of 1,1, <i>n,n</i> -Tetramethyl[<i>n</i>](2,11)teropyrenophanes.....	128
3.2.1.1	Application of Microwave Conditions for the VID Reaction of [7](2,11)teropyrenophane (3.20b).....	128
3.2.1.2	Application of the Thermal Conditions for the VID Reaction of [7](2,11)Teropyrenophane (3.20b).....	131
3.2.1.3	Application of Thermal Conditions for the VID Reaction of [8](2,11)Teropyrenophane (3.20c).....	132
3.2.2	Chemistry of the 1,1, <i>n,n</i> -Tetramethyl[<i>n</i>](2,11)teropyrenophanes.....	133
3.2.2.1	Oxidation of [7]- to [9](2,11)Teropyrenophanes to the Corresponding Diones.....	134
3.2.2.2	Teropyrenophanediones as Precursors to Larger π -Systems.....	139
3.3	Summary.....	143
3.4	Experimental Procedures and Characterization Data.....	144
3.5	References and Notes.....	160
	APPENDIX 2.....	163

CHAPTER 4: Synthesis of Pyridine-Containing Cyclophanes.....176

4.1	Introduction.....	176
4.2	Prevoiusly Synthesized Unsymmetric [<i>n.n</i>]Cyclophanes from the Bodwell Group.....	178

4.3	Results and Discussion.....	184
4.3.1	Attempted Synthesis of Pyridine-Containing Teropyrenophane 4.43 <i>via</i> both McMurry and Wurtz/McMurry Strategies.....	184
4.3.2	Synthesis of Pyridine-Containing Teropyrenophane 4.43 <i>via</i> a Double-Wurtz Coupling Route.....	188
4.3.3.1	Absorption and Emission Spectroscopy of Pyridinophane 4.43 ...	190
4.3.3.2	DFT/TD-DFT Calculations Results of Pyridinophane 4.43	195
4.3.4	Towards the Synthesis of Pyridine-Containing Pyrenophanes....	198
4.4	Summary.....	201
4.5	Experimental Procedures and Characterization Data.....	203
4.6	References and Notes.....	221
	APPENDIX 3.....	223

List of Figures

Figure 1.1	[2.2]Paracyclophane.....	1
Figure 1.2	Basic bridging motifs for aromatic compounds.....	2
Figure 1.3	The ropyrene series of PAHs.....	5
Figure 1.4	The rylene series of PAHs.....	6
Figure 1.5	Some cyclophanes driven from the ropyrene series of PAHs.....	6
Figure 1.6	Definition of α and β angles in $[n]$ paracyclophanes.....	7
Figure 1.7	[4]- to [6]Paracyclophanes.....	8
Figure 1.8	Calculated conformational structures for $[n]$ paracyclophanes ($n=6-7$).....	22
Figure 1.9	Structures of [2.2](2,7)pyrenophanes 1.78-1.79 and $[n](2,7)$ pyrenophane 1.80b	23
Figure 1.10	Some $[n](2,7)$ pyrenophanes reported by Bodwell.....	23
Figure 1.12	(1,3)Peropyrenophane 1.104 – the only reported peropyrenophane.....	31
Figure 2.1	$[n](2,11)$ Teropyrenophanes (2.1), graphene nanoribbons (2.2), (8,8) armchair SWCNTs (2.3) and Vögtle belts (2.4).	41
Figure 2.2	Teropyrene (2.5).....	42
Figure 2.3	$[n](2,11)$ Teropyrenophanes 2.6b-e and synthesized tetrabromides 2.7b-e	42
Figure 2.4	Aromatic region of the ^1H NMR spectra of dialdehydes 2.10a-d	53
Figure 2.5	Conformational ring flip of pyrenophane 2.10a	54
Figure 2.6	The ^1H NMR spectra of $[n.2](7,1)$ pyrenophanes 2.20a and 2.20b	57
Figure 2.7	500 MHz VT-NMR spectrum of [7.2](7,1)pyrenophane 2.20b	58

Figure 2.8	500 MHz VT-NMR spectrum of 2.20a	59
Figure 2.9	Conformational preference in [<i>n.n</i>]metacyclophanes.....	60
Figure 2.10	Conformational ring flip of [6.2](7,1)pyrenophane 2.20a	62
Figure 2.11	The ¹ H NMR spectrum of thiacyclophane 2.26	64
Figure 2.12	The ¹ H NMR spectrum of oxacyclophane 2.29	67
Figure 2.13	The ¹ H NMR spectrum of dioxacyclophane 2.41	73
Figure 2.14	Conformational bridge flips in [3.3]metacyclophanes 2.44 (X=CH ₂ , S, O, NR).....	74
Figure 2.15	Conformational bridge flips in dioxacyclophane 2.41	74
Figure 2.16	Relative energies of 2.41A-2.41D , calculated at B3LYP/6-31G(d) level of theory.....	75
Figure 3.1	Examples of [<i>n</i>](2,7)pyrenophanes synthesized by the Bodwell group....	120
Figure 3.2	Aromatic region of the ¹ H NMR spectra of the crude VID reactions of 3.19b	130
Figure 3.3	Normalized absorption spectra of diones 3.28b-d (first spectrum) and 3.29b-d (second spectrum) measured in CHCl ₃ at room temperature.....	137
Figure 3.4	Deconvoluted UV-Vis absorption spectra of 3.29b-d (first row, left to right) and 3.28b-d (second row, left to right).	138
Figure 3.5	Normalized absorption spectra of quinoxalinoteropyrenophanes 3.33b-d (first spectrum) and 3.34b-d (second spectrum) measured in CHCl ₃ at room temperature.....	141
Figure 3.6	Normalized emission spectra of symmetrical quinoxalinoteropyrenophanes 3.33b-d measured in CHCl ₃ at room temperature.....	142

Figure 3.7	Normalized emission spectra of unsymmetrical quinoxalinoteropyrenophanes 3.34b-d measured in CHCl ₃ at room temperature.....	143
Figure 4.1	A few examples of symmetric [<i>n.n</i>]cyclophanes 4.1-4.2 and mixed [<i>n.n</i>]cyclophanes (4.3-4.5).....	176
Figure 4.2	Symmetric [<i>m.n</i>]cyclophane 4.6 and mixed [<i>m.n</i>]cyclophane 4.7	177
Figure 4.3	Symmetric [<i>n.n</i>]cyclophanes 4.8-4.9 and cyclic oligoarylenes 4.10	177
Figure 4.4	Previously reported [<i>n</i>]pyrenophanes 4.12-4.13 and mixed [2.2]cyclophanes 4.14-4.16	179
Figure 4.5	Pyrenophanes 4.30-4.32	181
Figure 4.6	Incorporation of pyridine in the tether of 4.11 and 4.40	183
Figure 4.7	Target [<i>m.n</i>]cyclophanes 4.43 , 4.44 and 4.45	184
Figure 4.8	The ¹ H NMR spectrum of cyclophane 4.54	187
Figure 4.9	Calculated X-ray value of 4.43 at B3LYP/PM6 level of theory.....	190
Figure 4.10	Normalized absorption and emission spectra of pyridinophane 4.43 measured in CH ₂ Cl ₂ at room temperature.....	191
Figure 4.11	Changes in the emission spectra of pyridinophane 4.43 upon titration with TFA in CH ₂ Cl ₂ at room temperature.....	192
Figure 4.12	Changes in the absorption spectra of pyridinophane 4.43 upon titration with TFA in CH ₂ Cl ₂ at room temperature.....	193
Figure 4.13	Absorption and emission spectra of pyridinophane 4.43 upon titration with copper(II) triflate in CH ₂ Cl ₂ at room temperature.....	194

Figure 4.14	Contour plots (isovalue = 0.02) and eigenvalues of highest occupied molecular orbital (HOMO) and lowest unoccupied molecular orbital (LUMO) of neutral pyridinophane 4.43	196
Figure 4.15	Contour plots (isovalue = 0.02) and eigenvalues of HOMO, LUMO, and LUMO+2 of protonated pyridinophane 4.43	197

List of Schemes

Scheme 1.1	General strategies for the synthesis of cyclophanes.....	3
Scheme 1.2	General strategies for the synthesis of $[n]$ paracyclophanes.....	9
Scheme 1.3	Allinger's synthesis of [8]paracyclophane 1.25	10
Scheme 1.4	Allinger's synthesis of [7]paracyclophane 1.31	11
Scheme 1.5	Misumi's synthesis of [8]paracyclophane (1.34).....	11
Scheme 1.6	Cram's synthesis of [10]paracyclophane (1.40).....	12
Scheme 1.7	Failure of the Wurtz coupling reaction of dibromide 1.41 to deliver 1.34 ...	13
Scheme 1.8	Kanomata's synthesis of [10]paracyclophane (1.40).....	13
Scheme 1.9	Tobe's synthesis of 8-carboxy[6]paracyclophane (1.51).....	15
Scheme 1.10	Tobe's synthesis of 7-methoxycarbonyl[5]paracyclophane (1.54).....	15
Scheme 1.11	Bickelhaupt's synthesis of [5]paracyclophane (1.18).....	16
Scheme 1.12	Tsuji's synthesis of [4]paracyclophane derivative 1.62	17
Scheme 1.13	Tsuji's synthesis of the functionalized [4]paracyclophanes 1.65 and 1.6 ...	18
Scheme 1.14	Tsuji's synthesis of the functionalized [4]paracyclophanes 1.71	18
Scheme 1.15	Selected reactions of strained $[n]$ paracyclophanes.....	20
Scheme 1.16	General strategy for the synthesis of $[n](2,7)$ pyrenophanes (1.13).....	24
Scheme 1.17	Synthesis of [7](2,7)pyrenophane (1.81a) – an example of Bodwell's strategy for the synthesis of $[n](2,7)$ pyrenophanes.....	26
Scheme 1.18	Reduction of $[n](2,7)$ pyrenophanes 1.81a-d	29
Scheme 1.19	Diels-Alder reactions of 1, n -dioxan[n](2,7)pyrenophanes (1.80a-c) with PTAD.....	30

Scheme 1.20	Synthesis of 1,1, <i>n,n</i> -tetramethyl[<i>n</i>](2,11)teropyrenophanes 1.106b-e (<i>n</i> =7-10).....	32
Scheme 1.21	Bromination of 1,1,9,9-tetramethyl[9](2,11)teropyrenophane (1.106d)....	34
Scheme 2.1	Retrosynthetic analysis of teropyrenophane targets 2.6b-e	43
Scheme 2.2	Synthesis of 1,1, <i>n,n</i> -tetramethyl[<i>n</i>](2,11)teropyrenophanes (2.6b-c) using a double-McMurry strategy.....	45
Scheme 2.3	Failure of McMurry reaction in the synthesis of cyclophanediene 2.9a	46
Scheme 2.4	Synthesis of [<i>n</i>](2,11)teropyrenophanes 2.6b-e using a Wurtz/McMurry route.....	49
Scheme 2.5	Attempted synthesis of 1,1,6,6-tetramethyl[6](2,11)teropyrenophanes (2.6a) using a Wurtz coupling/McMurry route.....	52
Scheme 2.6	Attempted synthesis of 1,1,6,6-tetramethyl[6](2,11)teropyrenophane (2.6a) through a thiacyclopentane-based pathway A.....	56
Scheme 2.7	Attempted synthesis of 1,1,6,6-tetramethyl[6](2,11)teropyrenophane (2.6a) through the thiacyclopentane-based pathway B.....	63
Scheme 2.8	Reductive deoxygenation of diaryl ethers reported by Cao and Shi.....	66
Scheme 2.9	Attempted synthesis of 1,1,6,6-tetramethyl[6](2,11)teropyrenophane (2.6a) through an oxacyclopentane-based pathway A.....	66
Scheme 2.10	Solvolysis rate of benzyl bromide and 4-methoxybenzyl bromide.....	68
Scheme 2.11	Inoue's synthesis of dialdehyde 2.33 and Bodwell's synthesis of dialdehyde 2.36	69

Scheme 2.12	Attempted synthesis of 1,1,6,6-tetramethyl[6](2,11)teropyrenophane (2.6a) through an oxacyclophane-based pathway B.....	70
Scheme 2.13	Merner's synthesis of 2.39c via Friedel-Crafts acylation.....	71
Scheme 2.14	Failure of McMurry reaction to afford 2.6a	72
Scheme 2.15	Attempted synthesis of 1,1,6,6-tetramethyl[6](2,11)teropyrenophane through the fourfold functionalization-based approach.....	72
Scheme 2.16	β -H Elimination in the presence of methyl groups at the α -position of ether.....	76
Scheme 2.17	Attempted synthesis of 2.53 through the fourfold functionalization-based approach.....	78
Scheme 3.1	A valence isomerization/dehydrogenation (VID) reaction.....	118
Scheme 3.2	Syn and <i>anti</i> conformers of 3.1 and their valence isomerisation reaction.....	119
Scheme 3.3	VID strategy for constructing nonplanar pyrenes.....	120
Scheme 3.4	General approach for the synthesis of different types of [n](2,7)pyrenophanes.....	121
Scheme 3.5	Application of the VID reaction in the synthesis of [n](2,11)teropyrenophanes 3.20b-e ($x=1-4$).....	123
Scheme 3.6	Reaction of methylated aromatic solvents with DDQ.....	124
Scheme 3.7	Rathore's synthesis of tetramethoxytriphenylene 3.26 using DDQ/CH ₃ SO ₃ H.....	124
Scheme 3.8	Harris' and Bodwell's oxidation of pyrene using RuCl ₃ /NaIO ₄	135
Scheme 3.9	Oxidation of [7]- to [9](2,11)teropyrenophanes using RuCl ₃ /NaIO ₄	135

Scheme 3.10	Karami's synthesis of quinoxaline derivatives 3.32	139
Scheme 3.11	Synthesis of 1,4-aryldiazine derivatives of teropyrenophanes 3.33b-d and 3.34b-d	140
Scheme 4.1	VID strategy for constructing nonplanar pyrenes.....	178
Scheme 4.2	Synthesis of pyrenophane 4.16	180
Scheme 4.3	Müllen's synthesis of hexabenzocorene derivatives 4.29	181
Scheme 4.4	Synthesis of pyrenophane 4.30	182
Scheme 4.5	Attempted synthesis of pyridinophane 4.43 using a double-McMurry route.....	185
Scheme 4.6	Attempted synthesis of pyridinophane 4.43 using a Wurtz/McMurry route.....	186
Scheme 4.7	Synthesis of pyridinophane 4.43 using a double-Wurtz coupling route....	189
Scheme 4.8	Attempted synthesis of pyridine-containing pyrenophane 4.44	199
Scheme 4.9	Attempted synthesis of pyridine-containing pyrenophane 4.45	200

List of Tables

Table 1.1	Strain energies in $[n]$ paracyclophanes and the definition of the bend angles (α and β).....	19
Table 1.2	The ^1H NMR chemical shifts of to the most shielded protons corresponding to the bridging unit (the central methylene units) and the bent benzene ring.....	21
Table 1.3	Bend angles (θ) of some of the $[n](2,7)$ pyrenophanes synthesized in the Bodwell group and the definition of the bend angle θ	27
Table 1.4	The ^1H NMR data for some $[n](2,7)$ pyrenophanes and 1, n -dioxan[n](2,7)pyrenophanes.....	28
Table 1.5	Definition of the total bend angle (θ_{tol}), other bend angles θ_1 , θ_2 , θ_3 and distance between the two terminal carbons (d_1).....	33
Table 3.1	Previous optimization of the VID reaction of $[n.2.2]$ pyrenophanemonoene 3.19d using DDQ/ $\text{CH}_3\text{SO}_3\text{H}$	126
Table 3.2	Previous optimization of the VID reaction of $[n.2.2]$ pyrenophanemonoenes 3.19c	127
Table 3.3	Optimized microwave conditions for the VID reaction of $[n.2.2]$ pyrenophanemonoene 3.19b	129
Table 3.4	Optimized reflux conditions of the VID reaction of $[n.2.2]$ pyrenophanemonoene 3.19b	132
Table 3.5	Optimized thermal conditions of the VID reaction of $[n.2.2]$ pyrenophanemonoene 3.19c	133

Table 4.1	Summary of TD-DFT calculated UV-Vis absorption bands and assignment of related MO contributions (neutral pyridinophane 4.43).....	195
Table 4.2	Summary of TD-DFT calculated UV-Vis absorption bands and assignment of related MO contributions (protonated pyridinophane 4.43).....	196

List of Symbols, Abbreviations and Acronyms

Ac	acetyl
AcOH	acetic acid
AcOEt	ethyl acetate
ASE	aromatic stabilization energy
AM1	Austin model one
Anhyd.	anhydrous
APPI	atmospheric pressure photo ionization
B3LYP	Becke 3-Parameter (Exchange), Lee Yang and Parr
B ₂ Pin ₂	bis(pinacolato)diboran
CT	charge transfer
conc.	concentrated
°C	degree centigrade
CI	chemical ionization
CAM	Coulomb-attenuating method
cm	centimeter(s)
calcd	calculated
CPP	cycloparaphenylene
<i>ca.</i>	circa
Cy	cyclohexyl
ClPPh ₂	chlorodiphenylphosphine
BzCl	benzyl chloride
d	doublet

DBU	1,8-diazabicyclo[5.4.0]undec-7-ene
DCE	1,2-dichloroethane
DDQ	2,3-dichloro-5,6-dicyano-1,4-benzoquinone
DFT	density functional theory
DMF	<i>N,N</i> -dimethylformamide
DPPB	1,4-bis(diphenylphosphino)butane
DMSO	dimethyl sulfoxide
Et	ethyl
EWG	electron withdrawing group
FGI	functional group interconversion
equiv.	equivalent(s)
g	gram(s)
G^\ddagger	free energy of activation
GNR	graphene nanoribbons
h	hour(s)
HOMA	harmonic oscillator model of aromaticity
HOMO	highest occupied molecular orbital
^1H NMR	proton nuclear magnetic resonance
Hz	Hertz
HMPA	hexamethylphosphoramide
HRMS	high resolution mass spectroscopy
Imid.	imidazole
J	coupling constant (Hz) (in NMR)

K	Kelvin
kcal	kilocalorie
L	liter(s)
LDA	lithium diisopropylamine
LCMS	liquid chromatography mass spectroscopy
LUMO	lowest unoccupied (or unfilled) molecular orbital
m	multiplet
<i>m</i> -	meta
<i>m</i> -CPBA	<i>meta</i> -chloroperbenzoic acid
mg	milligram(s)
mL	milliliter(s)
mmHg	millimetres of mercury
min	minute(s)
m.p.	melting point
Me	methyl
MeCN	acetonitrile
MO	molecular orbital
mol	mole(s)
MHz	megahertz
MW	microwave
<i>m/z</i>	mass to charge ratio
<i>n</i>	normal
nm	nanometer(s)

NMR	nuclear magnetic resonance
NICS	nucleus-independent chemical shift
NBS	<i>N</i> -bromosuccinimide
NFP	<i>N</i> -formylpiperidine
NMI	<i>N</i> -methylimidazole
<i>p</i> -	para
PAH	polycyclic aromatic hydrocarbon
Pd/C	palladium/charcoal
Ph	phenyl
pK _a	acid dissociation constant at logarithmic scale
PMHS	polymethylhydrosiloxane
ppm	parts per million
Pyr	pyridine
PTAD	4-phenyl-1,2,4-triazoline-3,5-dione
rt	room temperature
q	quartet
<i>R</i> _f	retention factor
RCM	ring-closing metathesis
s	singlet
<i>SE</i>	strain energy
S _N 2	bimolecular substitution nucleophilic
SWCNT	single-walled carbon nanotube
STO-3G	Slater type orbital-3 Gaussian

T_c	coalescence temperature
$t_{1/2}$	half-life
TLC	thin layer chromatography
Tf	trifluoromethanesulfonyl
Ts	4-toluenesulfonyl or tosyl
TIPSCl	triisopropylsilyl chloride
TMSCl	trimethylsilyl chloride
TMSA	trimethylsilylacetylene
TD-DFT	time-dependent density functional theory
THF	tetrahydrofuran
THF- d_8	deuterated THF
TFA	trifluoroacetic acid
TPP	5,10,15,20-tetraphenyl-21 <i>H</i> , 23 <i>H</i> -porphine
UV-Vis	ultraviolet-visible
VID	valence isomerization/dehydrogenation
VT-NMR	variable temperature nuclear magnetic resonance
W	Watt
δ	chemical shift
$\Delta\delta$	difference in chemical shift
$\Delta\nu_o$	difference in frequency at T_c
θ_{tot}	total bend
Λ	diamagnetic susceptibility exaltation
ϕ	fluorescence quantum yield

CHAPTER 1: Introduction

1.1 Cyclophane Chemistry

Cyclophane chemistry effectively originated in 1949 with Brown and Farthing's discovery of [2.2]paracyclophane (**1.1**)¹ in the pyrolysate of *p*-xylene and Cram's subsequent rational synthesis (Figure 1.1).^{2,3} Cyclophane chemistry then developed quickly into an interesting field of study due to a variety of reasons, such as unusual structural features (*e.g.* nonplanar aromatic systems), interesting conformational behaviour, π - π interactions between non-bonded aromatic units and the chemical and physical properties arising from molecular strain. Hence, a large body of literature on cyclophanes has been reported.⁴

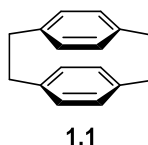


Figure 1.1 [2.2]Paracyclophane.

1.1.1 Unlimited Scope of Cyclophane Chemistry

A cyclophane consists of one or more aromatic systems (*e.g.* benzene) that are connected by one or more chains of atoms (called bridges) at non-adjacent positions. In the case of benzene, the most common aromatic system to have been incorporated into cyclophanes,⁵ there are two possible bridging motifs, namely *para*- (1,4) and *meta*- (1,3) (Figure 1.2). The *ortho*- (1,2) bridging motif is equivalent to ring fusion, thus “orthocyclophanes” are omitted from most discussions of cyclophane chemistry. The open-

ended nature of cyclophanes comes into focus considering that the number and type of the aromatic system(s) can be varied, as can the bridging motif of each aromatic unit. Moreover, the number of bridges, which can be variable in length and constitution, can be as many as permitted by the aromatic system(s).

In naphthalene (the next larger benzenoid aromatic system), on top of the basic bridging motifs present in benzene (intra-ring bridging), new motifs that connect positions in different rings (inter-ring bridging), *e.g.* (2,6) become available (Figure 1.2). As the aromatic system becomes gradually larger, the number of bridging motifs continues to increase. At the same time, the number of known cyclophanes decreases drastically. A plethora of benzene-containing cyclophanes have been reported, but only a few cyclophanes containing an aromatic system with more than four rings have been synthesized.^{4a}

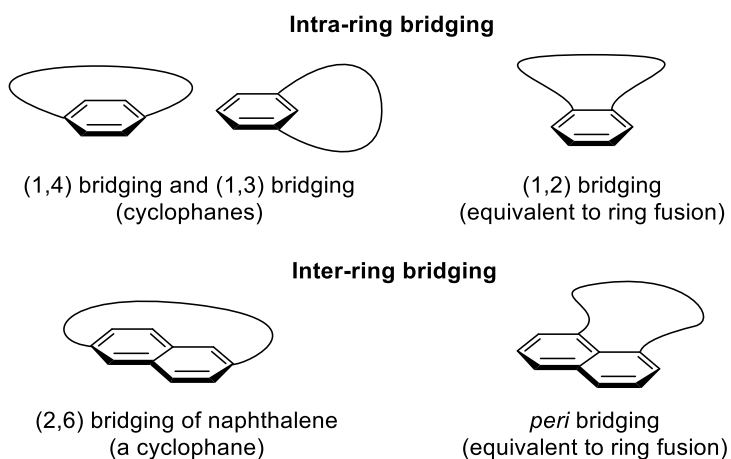
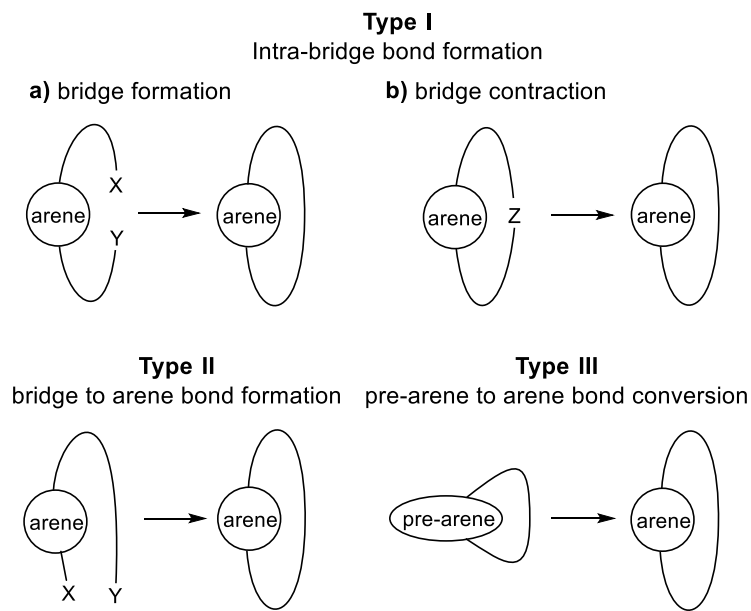


Figure 1.2. Basic bridging motifs for aromatic compounds.

1.1.2 General Synthetic Considerations

The scope of the synthetic methodology that has been exploited to deliver these

bridged aromatic systems pales in comparison to the structural diversity. From a strategic perspective, most cyclophane syntheses can be classified according to the way in which cyclophane formation is accomplished (Scheme 1.1).



Scheme 1.1 General strategies for the synthesis of cyclophanes.

The first strategy (Type I) involves the formation of a bond between two atoms in a bridge, either during bridge formation (Type I-a) or during the contraction of an existing bridge (Type I-b). These strategies are able to deliver moderately strained cyclophanes,⁶ because if bond formation results in the distortion of the aromatic system out of planarity, there will be an energetic cost associated with it. This directly affects the favourability (ΔG and ΔG^\ddagger) of the bond-forming reaction. If the bond-forming reaction is not highly exergonic to start with, then even a relatively small amount of strain energy in the product can render the desired intramolecular reaction unfavourable and intermolecular reactions will become dominant. The intramolecular reactions also must proceed through much more highly-

ordered transition states than their intermolecular counterparts, which makes them entropically challenging. For these reasons, this strategy is ineffective for the synthesis of highly-strained cyclophanes.⁷

The second strategy (Type II) involves the formation of a bond between an atom of the aromatic unit and an atom of the tether. This strategy is similar to Type I strategies (but less common) and generally applied to form relatively unstrained cyclophanes⁸ as the bond-formation reaction in this category is also intramolecular and suffers from same drawbacks as Type I strategies.

The third strategy (Type III) relies upon the generation of the bridged aromatic system from a bridged arene precursor (pre-arene) in the cyclophane-forming step. This strategy is advantageous in that it excludes competing intermolecular reactions. Additionally, the conversion of the pre-arene to the corresponding arene brings with it a significant amount of aromatic stabilization energy (ASE), which can offset the developing strain. This strategy has been the only one that can deliver more highly-strained systems.⁹ Each of these general strategies, has been used to great effect through the application of a variety of synthetic methods, a selection of which is illustrated in the later sections.

1.2 [n]Cyclophanes Derived from Polynuclear Aromatic Hydrocarbons (PAH)s

The simplest class of cyclophanes are the [n]cyclophanes, which are composed of one aromatic system and one bridge. These cyclophanes are especially interesting because variation of the length and nature of the bridge directly affects the conformation of the aromatic system. More specially, systematic changes in the bridge lead to systematic changes in the structure of the aromatic unit and this provides the unique opportunity to

study how this affects the chemical and physical properties of the arene. With the exception of the cyclopropenium system, any aromatic system can potentially be distorted from its lowest energy conformation, whether planar or nonplanar, by incorporating it into an $[n]$ cyclophane. However, this has only been done systematically over a broad range of distortion for benzene, pyrene and more recently, teropyrene.

Benzene, pyrene, and teropyrene are members of a series of polynuclear aromatic hydrocarbons (PAHs) that propagates through the successive linear annulation of phenalene units. This series, which has been called both “pyrenacenes”¹⁰ and “ropyrenes” (Figure 1.3), can be viewed as armchair-edged graphene nanoribbons (GNR). They are closely related to another series of armchair-edged GNRS, the “rylenes”,¹¹ which also propagate by way of phenalene annulation (Figure 1.4). The ropyrenes are more interesting from the cyclophane perspective since bridging them at the two maximally separated positions gives rise to a series of $[n]$ cyclophanes that starts with the $[n]$ paracyclophanes (**1.12**) and propagates to the $[n](2,7)$ pyrenophanes (**1.13**), the $[n](2,9)$ peropyrenophanes (**1.14**) and the $[n](2,11)$ teropyrenophanes (**1.15**) (Figure 1.5, it is worth mentioning that n

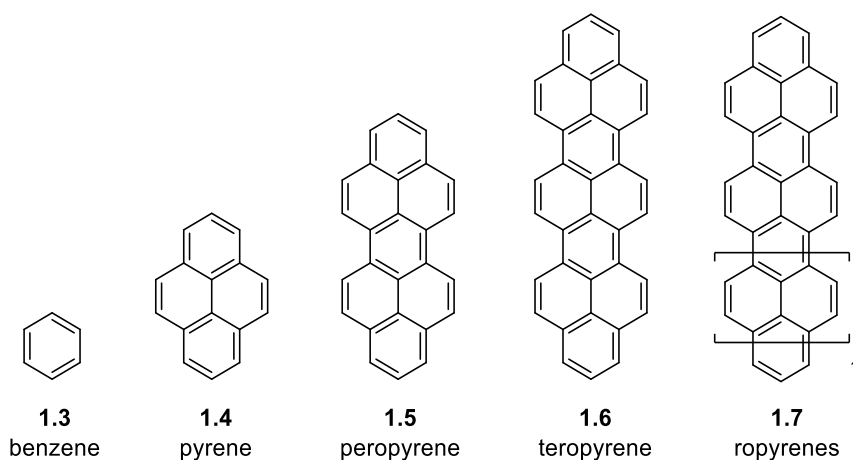


Figure 1.3 The ropyrene series of PAHs.

stands for the number of atoms in the bridge, and the numbers in parentheses indicate one of the available bridging motifs of each system for cyclophane formation).

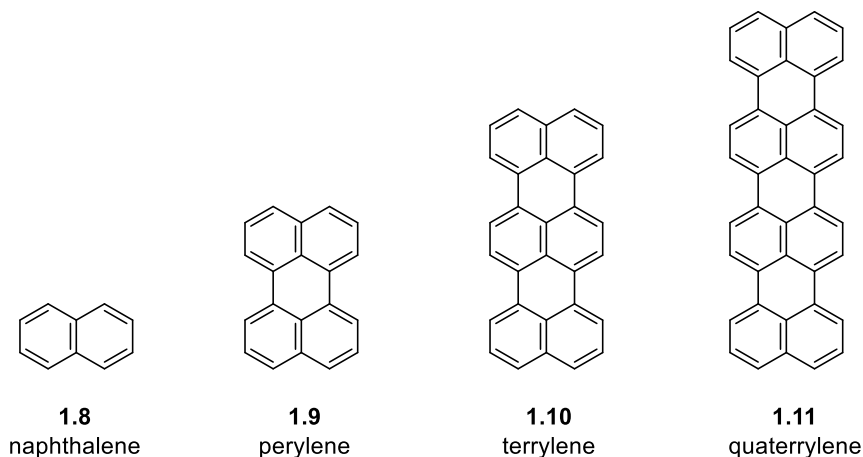


Figure 1.4 The rylene series of PAHs.

A very interesting feature of the ropyrene-derived cyclophanes is that the growing PAH describes an increasingly large part of an aromatic belt. Eventually, wrapping the PAHs onto itself affords aromatic belts **1.16** of the type first described by Vögtle (Figure 1.5).¹² A discussion of the synthesis of this class of cyclophanes and the consequences of bending the benzene unit and other PAHs is presented in the following sections.

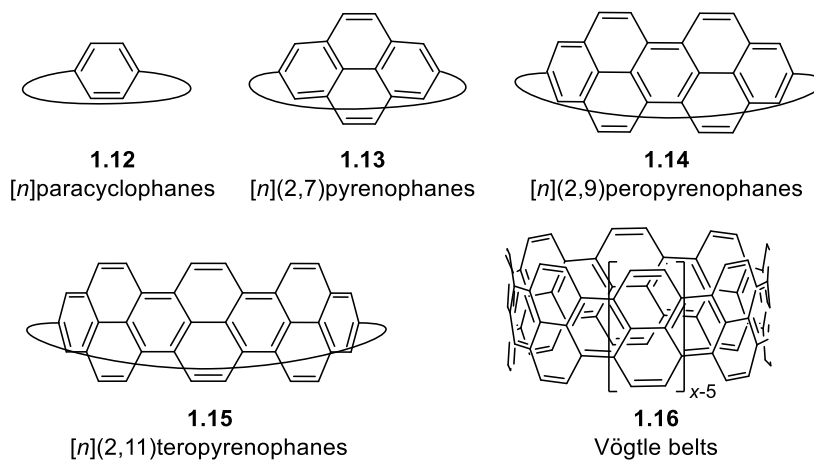


Figure 1.5 Some cyclophanes driven from the ropyrene series of PAHs.

1.2.1 The $[n]$ Paracyclophanes

Benzene (**1.3**) is by far the most common aromatic system to have been incorporated into cyclophanes. The greatest deformation of benzene from planarity can be achieved through bridging the two most remote positions, 1 and 4. The resulting $[n]$ paracyclophanes (**1.12**) have been the subjects of interest for more than six decades,^{4b,5b} starting with the work of Cram and Allinger in 1954.^{13a}

The major objective of this work was to successfully synthesize smaller homologues to establish how far the benzene ring could be distorted from planarity and what the chemical and physical consequences of such distortion would be. The benzene ring in the $[n]$ paracyclophanes with a sufficiently long bridge length ($n > 10$) is nearly planar and it becomes increasingly bent (as measured by the bend angle α) as the bridge becomes shorter (see Section 1.2.1.2 for details) (Figure 1.6).

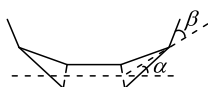


Figure 1.6 Definition of α and β angles in $[n]$ paracyclophanes.

The smallest isolable member of the series is [6]paracyclophane (**1.17**).¹⁴ The next smaller homologue, [5]paracyclophane (**1.18**) exists in equilibrium with its Dewar benzene isomer (Figure 1.7).¹⁵ [4]Paracyclophane (**1.21**) is believed to have been generated at -196°C , where it was trapped by protonation at a bridgehead-carbon atom to give a benzenonium ion, in which the presence of CF_3COO^- led to a bridged 1,4-dihydrobenzene **1.22**.¹⁶ An overview of synthetic approaches to the smaller $[n]$ paracyclophanes is presented below.

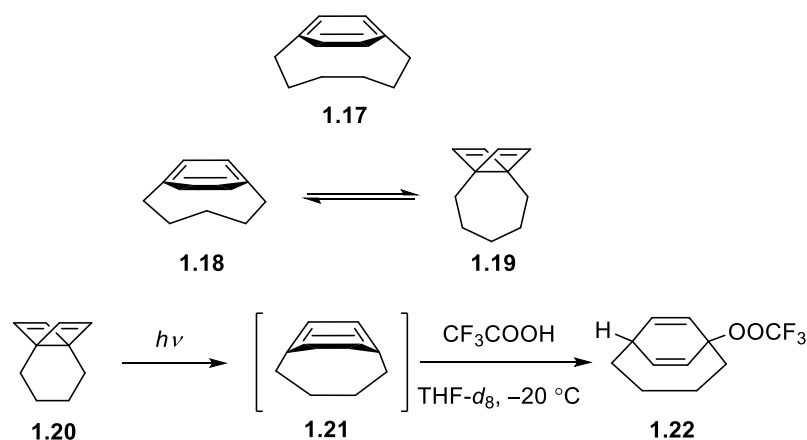


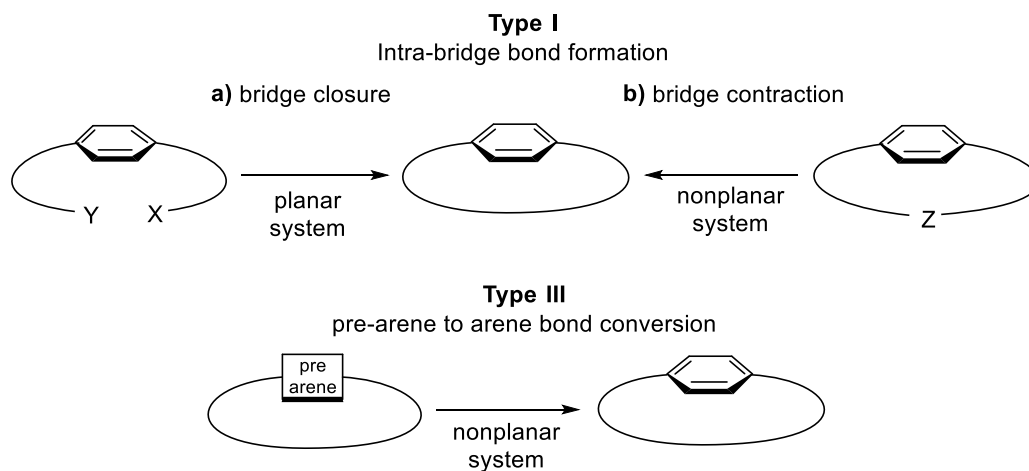
Figure 1.7 [4]- to [6]Paracyclophanes.

1.2.1.1 Synthesis of [*n*]Paracyclophane Derivatives

Sequential shortening of the number of the methylene units that generate the tether of a [*n*]paracyclophane increases the molecular strain.¹⁷ A main part of this strain is established in the distortion of the benzene system. This is the key reason why Type II (and somewhat Type I) strategies are typically ineffective to afford [*n*]paracyclophanes that contain highly distorted π -systems (see Section 1.1.2). A few examples that employ Type I and III strategies will be discussed in the following sections (Scheme 1.2).

The Type Ia strategy, which is a macrocyclic ring closure, involves bond formation in the bridge to generate the cyclophane. This method has never been effectively applied to any [*n*]paracyclophane with $n < 10$ as it is both enthalpically and entropically challenging. In the case of less strained [*n*]paracyclophanes ($n > 10$), it is still an entropically challenging route.

The Type Ib strategy includes application of a ring-contracting reaction to an existing [*n*]paracyclophane and has been successfully applied to small [*n*]paracyclophanes ($n = 7$). Clearly, this strategy is more capable of delivering significantly bent arenes.



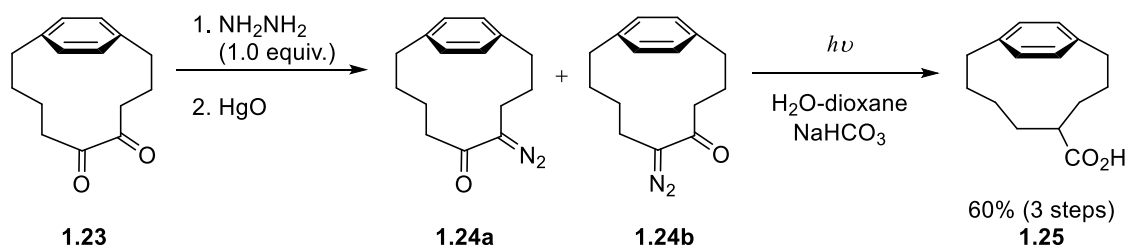
Scheme 1.2 General strategies for the synthesis of $[n]$ paracyclophanes.

The Type III strategy, which includes the conversion of a bridged “pre-arene” system into a bridged benzene ring is easily the most powerful approach because the formation of a benzene ring is accompanied by *ca.* 30 kcal/mol of aromatic stabilization energy (ASE).¹⁸ This large energetic benefit counterbalances developing strain during cyclophane formation. This approach has been utilized for the smallest and most strained $[n]$ paracyclophanes. A few examples of $[n]$ paracyclophanes that have been formed using each of these general approaches are described in the following sections.

1.2.1.1.1 Synthesis of $[n]$ Paracyclophanes using the Type I Strategies

Allinger’s syntheses of [7]paracyclophane **1.31** and [8]paracyclophane **1.25** were accomplished using Strategy Type Ib (Scheme 1.3).¹⁹ They commenced with the reaction of [9]paracyclophane-4,5-dione (**1.23**, prepared from γ -phenylbutyric acid over 5 steps)²⁰ with hydrazine to deliver a mixture of regioisomeric monohydrazones, which were oxidized using mercuric oxide to yield the isomeric α -diazoketones **1.24a** and **1.24b**.

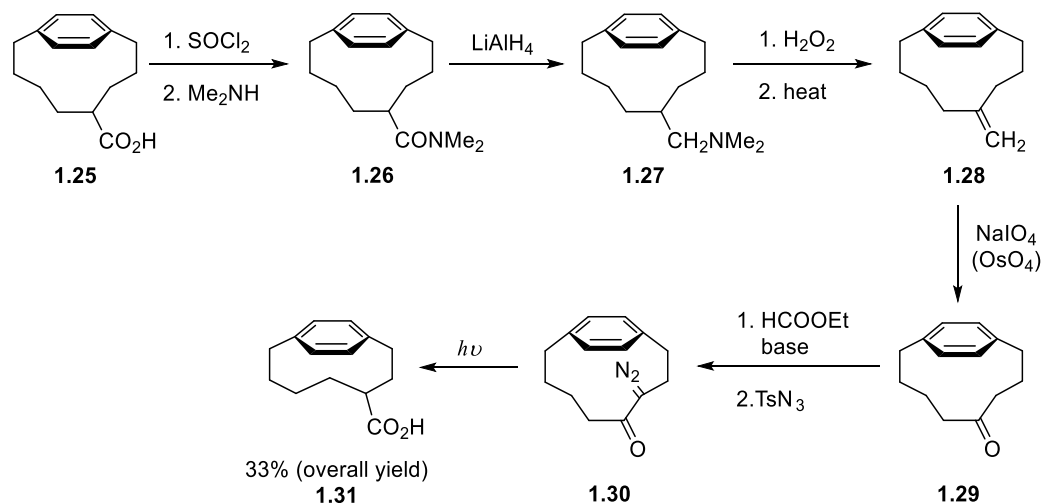
Subjection of the isomer mixture to a Wolff rearrangement upon irradiation with a 250 W sunlamp (100 °C) delivered 4-carboxy[8]paracyclophane (**1.25**) in 60% overall yield for the 3 steps.



Scheme 1.3 Allinger's synthesis of [8]paracyclophane **1.25**.

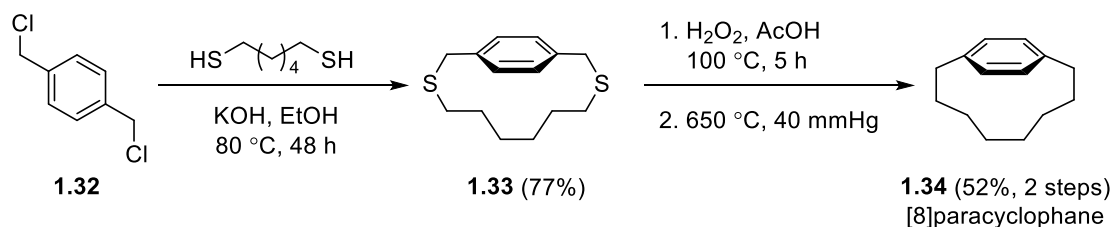
The next lower homologue, 3-carboxy[7]paracyclophane (**1.31**) was synthesized starting from 4-carboxy[8]paracyclophane (**1.25**) *via* a 9-step sequence that commenced with the conversion of acid **1.25** into the corresponding acid chloride using thionyl chloride, followed by reaction with dimethylamine to afford the amide **1.26** (Scheme 1.4).²¹ Reduction of the amide **1.26** provided the tertiary amine **1.27**, which was converted into the corresponding amine oxide and then pyrolyzed to deliver the methylene derivative **1.28** *via* Cope elimination. Oxidative cleavage of **1.28** using a catalytic amount of OsO_4 with NaIO_4 as the stoichiometric oxidant accomplished the synthesis of ketone **1.29**. Reaction of the resulting ketone with ethyl formate and an unspecified base furnished the hydroxymethylene derivative (not shown), which was then converted into the α -diazoketone **1.30** upon treatment with tosyl azide. Photolysis of **1.30** produced the 3-carboxy[7]paracyclophane (**1.31**) in 33% overall yield. It is unknown whether the photochemical Wolff rearrangement would be powerful enough to deliver the next lower

homologue of **1.31**. Presumably, the quantity of **1.31** that was produced was not enough to support another iteration of the 9-step sequence.



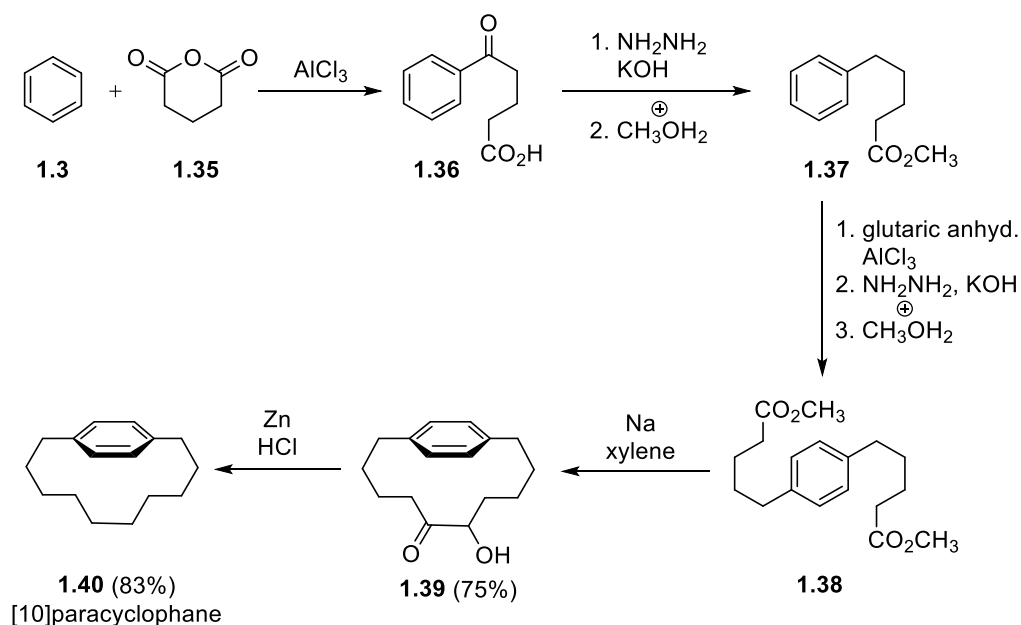
Scheme 1.4 Allinger's synthesis of [7]paracyclopentane **1.31**.

A second example of the Type Ib Strategy is Misumi's²² synthesis of [8]paracyclopentane (**1.34**). *S*-Alkylation of 1,6-hexane dithiol with 1,4-bis(chloromethyl)benzene (**1.32**) in the presence of a base afforded the dithiacyclopentane **1.33** (Scheme 1.5). The resulting dithia[10]paracyclopentane was oxidized to the corresponding disulfone and sulfur dioxide was extruded upon flash vacuum thermolysis at 650 °C and 40 mmHg to furnish [8]paracyclopentane (**1.34**) in 52% yield (2 steps).



Scheme 1.5 Misumi's synthesis of [8]paracyclopentane (**1.34**).

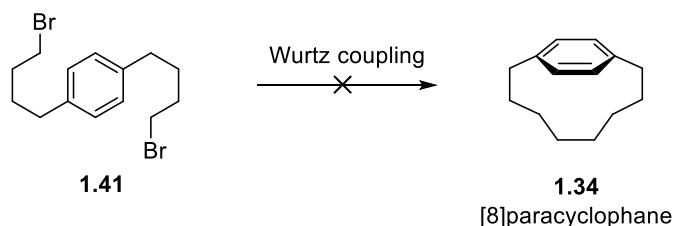
Cram^{13,23} exploited the Type Ia strategy in his syntheses of [10]- and [12]paracyclophane from benzene through an intramolecular acyloin condensation as the cyclophane-forming step (Scheme 1.6). The synthesis commenced with the Friedel-Crafts acylation of benzene (**1.3**) with glutaric anhydride (**1.35**) to afford intermediate **1.36**. Functional group interconversion and another Friedel-Crafts acylation eventually led to diester **1.38**. The [10]paracyclophane derivative **1.39** was then generated by an intramolecular acyloin condensation in 75% yield. The yield for this step is very good, but there is very little strain in the product. Complete reduction of the functional groups of **1.39** produced [10]paracyclophane (**1.40**) in 26% overall yield over 8 steps. The higher homologue [12]paracyclophane was synthesized using the same approach over 16 steps (14% overall yield).^{13b}



Scheme 1.6 Cram's synthesis of [10]paracyclophane (**1.40**).

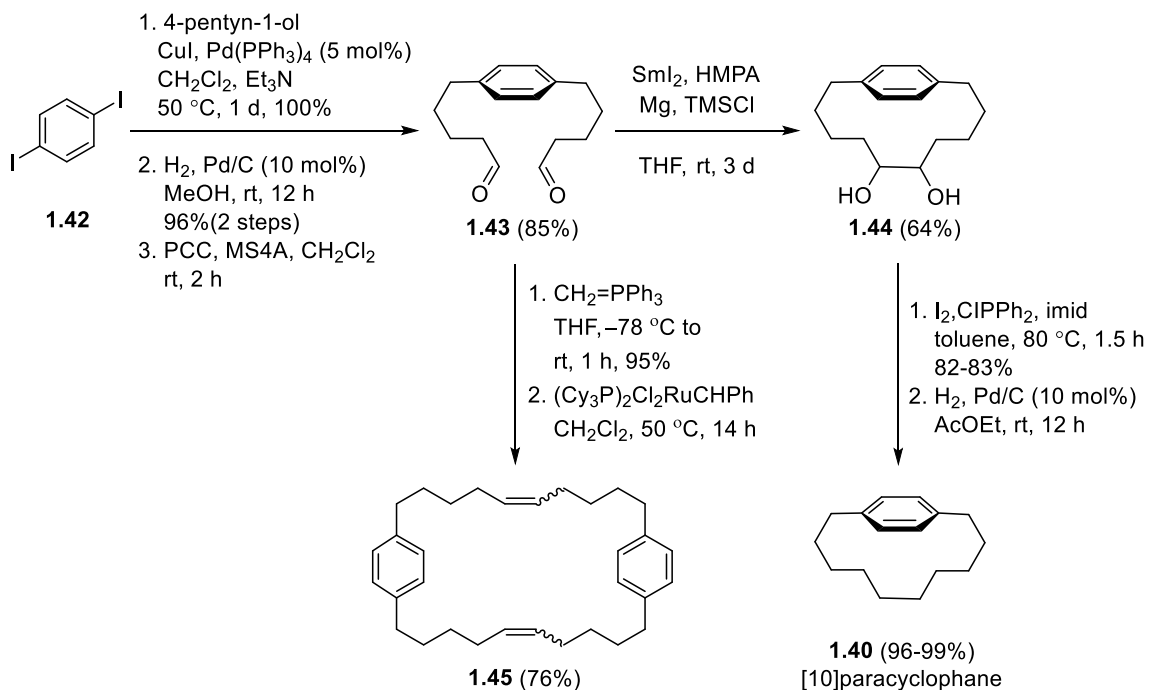
There does not appear to be any report of the use of acyloin condensation to access

smaller [*n*]paracyclophanes. In this regard, it is worth noting that an attempted synthesis of [8]paracyclophane by intramolecular Wurtz coupling of coupling of dibromide **1.41** was not successful (Scheme 1.7).



Scheme 1.7 Failure of the Wurtz coupling reaction of dibromide **1.41** to deliver **1.34**.

Kanomata²⁴ reported the synthesis of [10]paracyclophane (**1.40**) using a samarium-catalyzed pinacol coupling as the key cyclophane-forming step (Scheme 1.8). The synthetic approach, which falls under the Type Ia strategy involved a double Sonogashira reaction of 1,4-diiodobenzene (**1.42**) with 4-pentyn-1-ol, followed by hydrogenation and oxidation to



Scheme 1.8 Kanomata's synthesis of [10]paracyclophane (**1.40**).

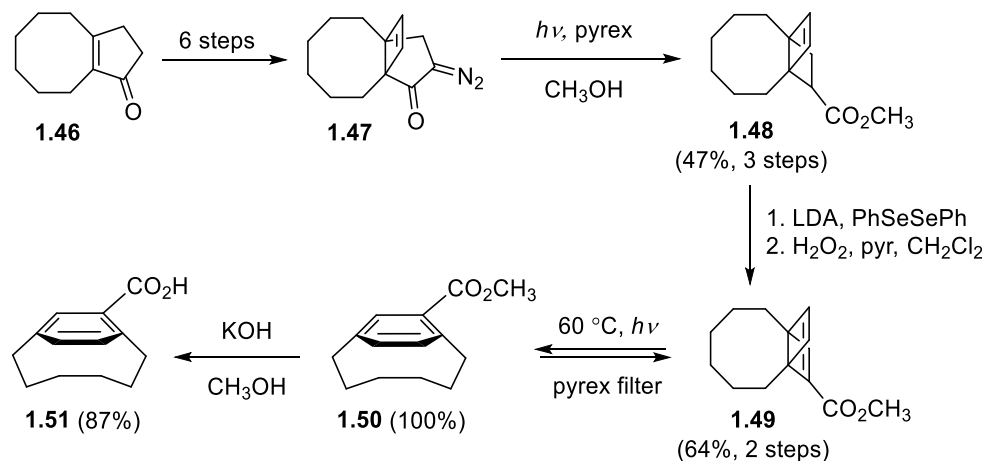
afford dialdehyde **1.43** (82%, over 3 steps). Subjection of dialdehyde **1.43** to a samarium-catalyzed pinacol coupling reaction yielded the corresponding diol **1.44** (64%), which could be converted into [10]paracyclophane (**1.40**) in two steps (79%). It is worth mentioning that the ring-closing metathesis (RCM) of the corresponding diene derived from dialdehyde **1.43** delivered the undesired dimer **1.45** as a less strained product.

1.2.1.1.2 Synthesis of [*n*]Paracyclophanes using the Type III Strategy

As described earlier, the Type III strategy involves the generation of the nonplanar aromatic systems from bridged pre-arenes. Indeed, the final step of this approach is typically an arene-forming reaction and the success or failure of this reaction depends on the encounter between the rising strain and the developing aromatic stabilization energy (ASE) or resonance energy. For the more highly-strained [*n*]paracyclophanes, bridged Dewar benzenes have proved to be very valuable synthetic precursors. Not only does the valence isomerization of a Dewar benzene to a benzene come with *ca.* 30 kcal/mol of aromatic stabilization energy (ASE), but also a significant amount of strain relief as two fused cyclobutenes become a single six-membered ring.

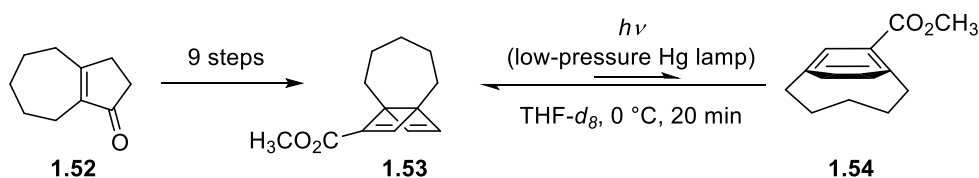
Tobe¹⁴ demonstrated this concept in the synthesis of 8-carboxy[6]paracyclophane (**1.51**). Diazoketone **1.47**, which was synthesized *via* a 6-step sequence from α,β -unsaturated ketone **1.46**, was converted into ester **1.48** through a photochemical Wolff rearrangement in 47% yield over 3 steps (Scheme 1.9). It is worth mentioning that photochemical irradiation, which is employed for the conversion of a Dewar benzene to its Kekulé isomer, can be conducted at very low temperatures. Therefore, this technique

enables the observation of unstable products as it allows them to survive for a reasonable period time under the conditions of their formation.



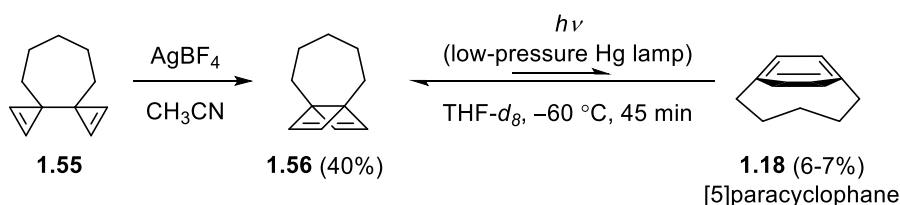
Scheme 1.9 Tobe's synthesis of 8-carboxy[6]paracyclophane (**1.51**).

Selenation of **1.48** followed by oxidation and selenoxide elimination afforded Dewar benzene **1.49** (64%, 2 steps). Irradiation of **1.49** at 60 °C delivered [6]paracyclophane derivative **1.50** in quantitative yield. Saponification then afforded acid **1.51** (87%). The ring opening of a 1,4-bridged Dewar benzene was also successful in the synthesis of the next smaller homologue, 7-methoxycarbonyl[5]paracyclophane (**1.54**).²⁵ The Dewar benzene **1.53** was obtained in a similar way from **1.52** over 9 steps. Irradiation of a THF- d_8 solution of 8-methoxycarbonyl[5.2.2]propelladiene (**1.53**) in a quartz cell with a low-pressure mercury lamp at 0 °C furnished the [5]paracyclophane derivative **1.54**. The formation of **1.54** was confirmed by a 360 MHz ^1H NMR spectrum measured at –60 °C.



Scheme 1.10 Tobe's synthesis of 7-methoxycarbonyl[5]paracyclophane (**1.54**).

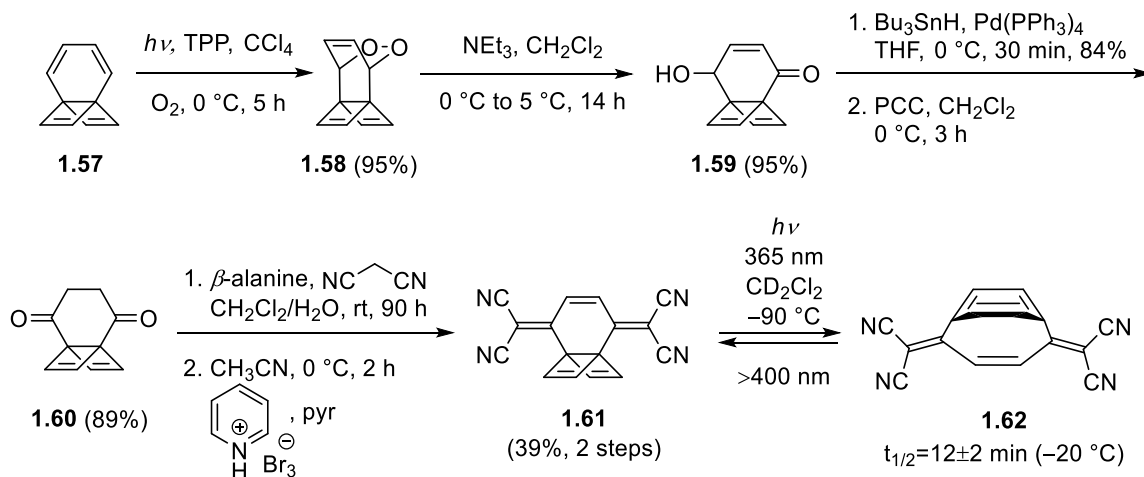
Bickelhaupt²⁶ reported the synthesis of parent [5]paracyclophane (**1.18**) starting with the silver tetrafluoroborate isomerization of 2,2'-bicyclopropenyl substrate **1.55** to Dewar benzene **1.56** (Scheme 1.11). Subsequent irradiation of [5.2.2]propelladiene **1.56** with a low-pressure mercury lamp at $-60\text{ }^{\circ}\text{C}$ for 45 min afforded the highly-strained [5]paracyclophane (**1.18**) in 6-7% yield.



Scheme 1.11 Bickelhaupt's synthesis of [5]paracyclophane (**1.18**).

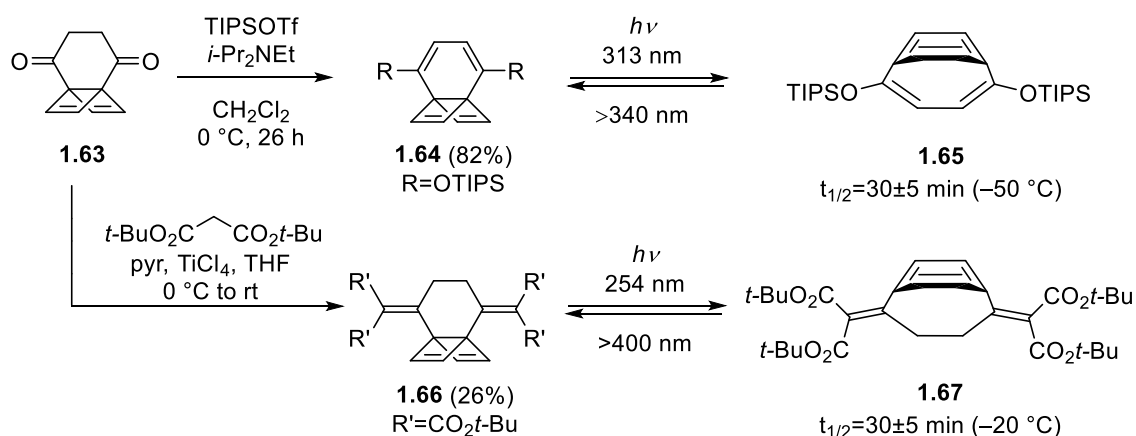
Both Tobe and Bickelhaupt could successfully synthesize [5]paracyclophane derivatives, however, to date there has been no report of the synthesis of an isolable [5]paracyclophane with an appreciable half-life at room temperature. Initial work toward the synthesis of the smallest [*n*]paracyclophanes was disclosed by Tsuji's group in 1997.²⁷ They reported the synthesis of [4]paracyclophane derivative **1.62** from tetraene **1.57** (Scheme 1.12). The [4+2] cycloaddition of the intermediate **1.57**, (which had been already reported by their group)²⁸ with singlet oxygen afforded endoperoxide **1.58** (95%). Treatment of **1.58** with triethylamine in dichloromethane furnished enone **1.59** (95%). The alkene was reduced under radical conditions with Bu_3SnH in the presence of $\text{Pd}(\text{PPh}_3)_4$ and the hydroxyl group was oxidized using pyridinium chlorochromate (PCC) to yield dione **1.60** (75%). The Knoevenagel condensation of **1.60** with malonitrile under the catalysis of β -alanine followed by the bromination/dehydrobromination reaction with pyridinium bromide perbromide furnished the Dewar benzene intermediate **1.61** in 39% yield over 2

steps. Irradiation of **1.61** at 365 nm in deuterated dichloromethane solution at $-90\text{ }^{\circ}\text{C}$ resulted in the formation of the [4]paracyclophane **1.62**, which was stable enough to be characterized. Since this photochemical reaction was completely reversible, **1.61** could be formed upon irradiation of **1.62** at $>400\text{ nm}$.



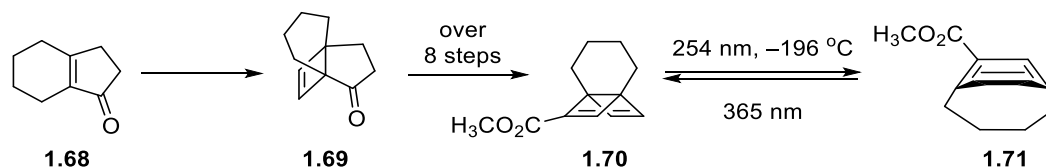
Scheme 1.12 Tsuji's synthesis of [4]paracyclophane derivative **1.62**.

In an attempt to study the extremely bent benzene ring in the [4]paracyclophane system, Tsuji and co-workers^{5d,15} reported the syntheses of other [4]paracyclophane derivatives **1.65** and **1.67** (Scheme 1.13). The synthesis of functionalized [4]paracyclophane **1.65** commenced with the reaction of **1.63** with triisopropylsilyl triflate in *i*-Pr₂NEt to furnish the corresponding bis(silyl enol ether) **1.64** in 82% yield. In parallel, the condensation of dione **1.63** with di-*tert*-butyl malonate under the catalysis of TiCl₄ in pyridine afforded **1.66** (26%). Irradiation of 1,4-bridged Dewar benzenes **1.64** and **1.66** delivered the corresponding functionalized [4]paracyclophanes **1.65** and **1.67** respectively, which underwent efficient cycloreversion upon subsequent electronic excitation at longer wavelength.



Scheme 1.13 Tsuji's synthesis of the functionalized [4]paracyclophanes **1.65** and **1.67**.

Tsuji reported the synthesis of another interesting [4]paracyclophane derivative **1.71** using the approach utilized for the synthesis of **1.51** and **1.54**. Thus, enone **1.68** was converted into 1-carboxy[4]paracyclophane methyl ester **1.71** in 10 steps (Scheme 1.14). The final step was the irradiation of the Dewar benzene **1.70** at 254 nm, which furnished the corresponding [4]paracyclophane **1.71**. This compound also cleanly reverted to **1.70** upon secondary irradiation at 365 nm –196 °C, but it was highly unstable and decomposed in solution at –130 °C. It should be noted that the most kinetically and thermally stable [4]paracyclophane derivative proved to be **1.62** with a half-life 12 ± 2 min at –20 °C.



Scheme 1.14 Tsuji's synthesis of the functionalized [4]paracyclophanes **1.71**.

The benzene rings in these cyclophanes, adopt boat-shaped conformations, which affect their physical and chemical properties such as strain energy, reactivity, aromaticity,

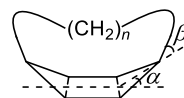
spectroscopic properties, conformational behaviour, *etc.* A summary of the implications of bending the benzene unit is discussed in the following section.

1.2.1.2 Consequences of Bending Benzene Rings in $[n]$ Paracyclophanes

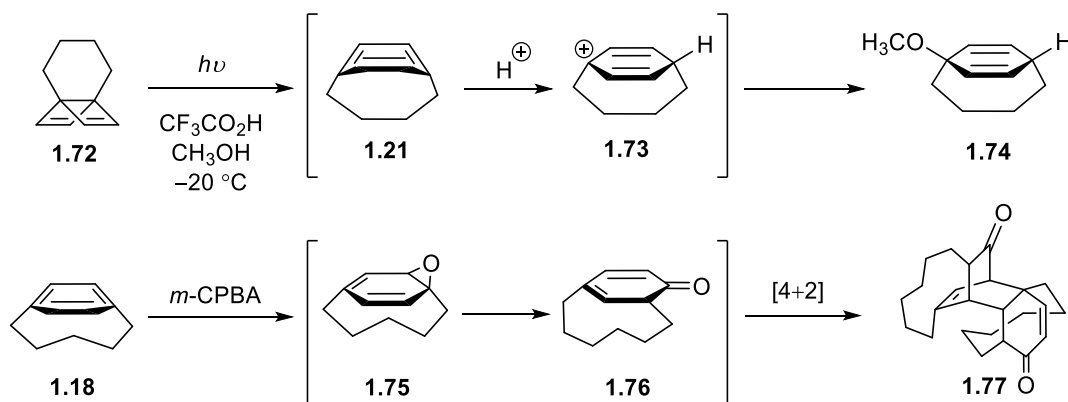
As mentioned earlier, the deformation angle in the benzene system is usually quantified by the parameters α and β . The total bend has been measured by the sum of these two parameters ($\alpha + \beta$). Reducing the number of methylene units in the bridge increases the α angle and the strain energy (SE) that is associated with the distortion of the aromatic unit (Table 1.1).^{13,22,25-28} This energy distributes all over the molecule in a way that minimizes the total strain. Accordingly, the total strain energy (SE_{tot}) in the $[n]$ paracyclophanes can be defined as, $SE_{\text{tot}} = SE_{\text{ring}} + SE_{\text{bridge}}$, where SE_{ring} is the required energy to distort the aromatic ring and SE_{bridge} is the amount of energy required to stretch the bridging chain from its ideal geometry. In the smaller $[n]$ paracyclophanes ($n \leq 6$), the SE_{ring} exceeds the aromatic stabilization energy of benzene (*ca.* 30 kcal/mol), so strain relief becomes a more important consideration than the loss of aromaticity. As such, these cyclophanes are highly

Table 1.1 Strain energies in $[n]$ paracyclophanes and the definition of the bend angles (α and β).

n	α_{exp}	$\alpha_{\text{calculated}}$	SE_{ring} (kcal/mol)	SE_{bridge} (kcal/mol)	SE_{total} (kcal/mol)	per CH_2
3	-	42.5	114.2	12.9	127.1	4.3
4	-	35.5	79.7	7.7	87.4	1.9
5	-	28.4	50.2	8.3	58.5	1.7
6	19.9	22.4	29.1	7.6	36.7	1.3
7	15.1	16.4	15.0	6.7	21.7	1.0
8	9.1	13.3	10.0	6.0	16.0	0.8
9	-	8.4	3.9	5.7	9.6	0.6
10	-	4.9	1.4	7.4	8.8	0.7



reactive compared to higher homologues ($n \geq 7$) and normal aromatic systems. Polymerization, 1,4-addition of dienophiles, alcohols, acids, halogens, *etc.* at the bridgeheads are a few examples of these unusual chemical reactions (Scheme 1.15).^{5c,5d,28,29}



Scheme 1.15 Selected reactions of strained $[n]$ paracyclophanes.

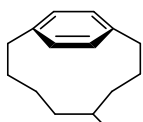
In the case of aromaticity, based on calculations by Dijksha and Lenthe,^{15a} the aromaticity of the ring should be lost as the ring becomes highly distorted and there should be a transition from a preference for the benzene to the Dewar benzene isomer. This is consistent with the suggestions of Schaefer^{15b} that the highly-distorted benzene ring of [4]paracyclophane derivative shows a magnetic susceptibility similar to that of 1,3,5-cyclohexatriene, which reveals a severely diminished ring current. But, based on magnetic criteria (nucleus-independent chemical shift (NICS)) and NMR evidence (diamagnetic susceptibility exaltation (Λ)), the benzene units in [4]paracyclophane derivatives are indeed still aromatic. As proposed by Schleyer^{15c} these parameters can be used as indicators of aromaticity. Large negative values show aromaticity, while the positive ones are indicative of antiaromaticity. The NICS and Λ values for **1.62** were calculated to be -8.0 and -11.5 ppm cgs, respectively, which compare to those of planar benzene -9.7 and -15.1 ppm cgs,

suggest that there is not a major loss of aromaticity in the severely-deformed benzene unit of **1.62**. It should be noted that both UV-Vis and ^1H NMR spectroscopic techniques have been used to characterize the bent aromatic systems in $[n]$ paracyclophanes. The UV-Vis spectra of the strained cyclophanes ($n < 10$) show a gradual bathochromic shift in their longest wavelength band as the bridge becomes shorter.^{9a,30} In contrast, the UV-Vis spectra for the unstrained cyclophanes ($n \geq 10$) are similar to those of non-bridged aromatic compounds.

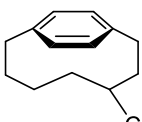
The ^1H NMR spectra of parent $[n]$ paracyclophanes show an increasing upfield shift trend for the aliphatic protons in the central methylene units as the bridge becomes shorter due to the ring current applied by the benzene system (Table 1.2).^{9a,30} In the case of substituted cyclophanes **1.25** and **1.31** the central methylene protons are shifted upfield by

Table 1.2 The ^1H NMR chemical shifts of to the most shielded protons corresponding to the bridging unit (the central methylene units) and the bent benzene ring.

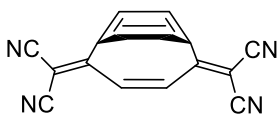
$[n]$ paracyclophane	central methylene proton (ppm) (multiplicity, no. of H)	aromatic proton (ppm) (multiplicity, no. of H)
[10]paracyclophane	+0.70 (m, 4H)	7.04 (s, 4H)
[9]paracyclophane	+0.40 (m, 4H)	7.00 (s, 4H)
[8]paracyclophane 1.25	-0.25 (m, 1H)	7.15 (m, 4H)
[7]paracyclophane 1.31	-1.40 (dd, 1H)	7.15 (d, 4H)
[6]paracyclophane	+0.33 (m, 4H)	7.17 (s, 4H)
[5]paracyclophane	+0.01 (m, 1H)	7.44 (m, 4H)
[4]paracyclophane 1.62	+5.85 (s, 2H)	7.97 (s, 2H)



1.25 CO_2H



1.31 CO_2H



1.62

about 2.0 ppm compared to a normal methylene unit (δ 1.4 ppm). This unusual shift is presumably due to the combination of ring current and the presence of an electron withdrawing group. On the other hand, the aromatic protons consistently move to lower field as the cyclophanes become more strained.

Another interesting aspect of $[n]$ paracyclophanes is the conformational processes in the bridge. Allinger and Carballeira studied the strain energy and conformational behaviour of these cyclophanes³¹ and established that $[n]$ paracyclophanes containing odd-numbered bridges prefer either C_s or C_2 symmetric conformations and the ones with even-numbered bridges prefer C_2 symmetry (Figure 1.8). This presumably has its origin in the minimization of torsional strain (favourable staggered conformations) in the bridge.

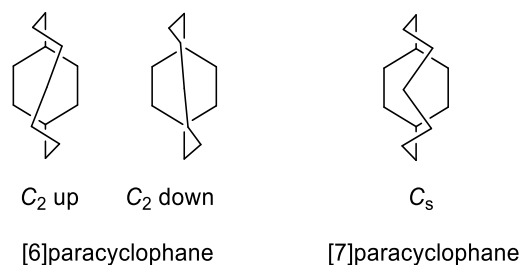


Figure 1.8 Calculated conformational structures for $[n]$ paracyclophanes ($n=6-7$).

1.2.2 $[n](2,7)$ Pyrenophanes

The next member in the ropyrene series is pyrene (**1.4**), which is probably the most well-studied PAH, due to its interesting photochemical and photophysical properties (*e.g.* formation of excimers in solution with a long excited-state half-life (410 ns) and high fluorescence quantum yield ($\phi = 0.65$)).³² Bridging pyrene at the two maximally separated positions gives rise to the $[n](2,7)$ pyrenophanes (**1.13**), which are the most populous class of pyrenophanes. The (2,7) bridging motif in pyrene is equivalent to the (1,4) or *para* motif

in benzene (**1.3**). Consequently, any deformation from planarity of the pyrene unit is distributed over the entire framework of this system. Cyclophanes containing pyrene system came into existence with Misumi's synthesis of [2.2](2,7)pyrenophanes **1.78** and **1.79** in 1975 and the first $[n](2,7)$ pyrenophane **1.80b** appeared in the literature in 1996 (Figure 1.9).^{33,34}

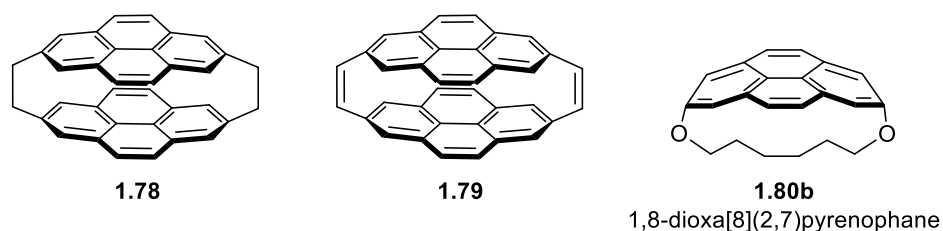


Figure 1.9 Structures of [2.2](2,7)pyrenophanes **1.78-1.79** and $[n](2,7)$ pyrenophane **1.80b**.

Having access to a series of cyclophanes containing just one aromatic unit would be valuable to meaningfully address the consequences of increasing the bend in the pyrene unit on their chemical, physical and spectroscopic properties. Thus, the Bodwell group has reported the synthesis of a variety of $[n](2,7)$ pyrenophanes over a two-decade period using

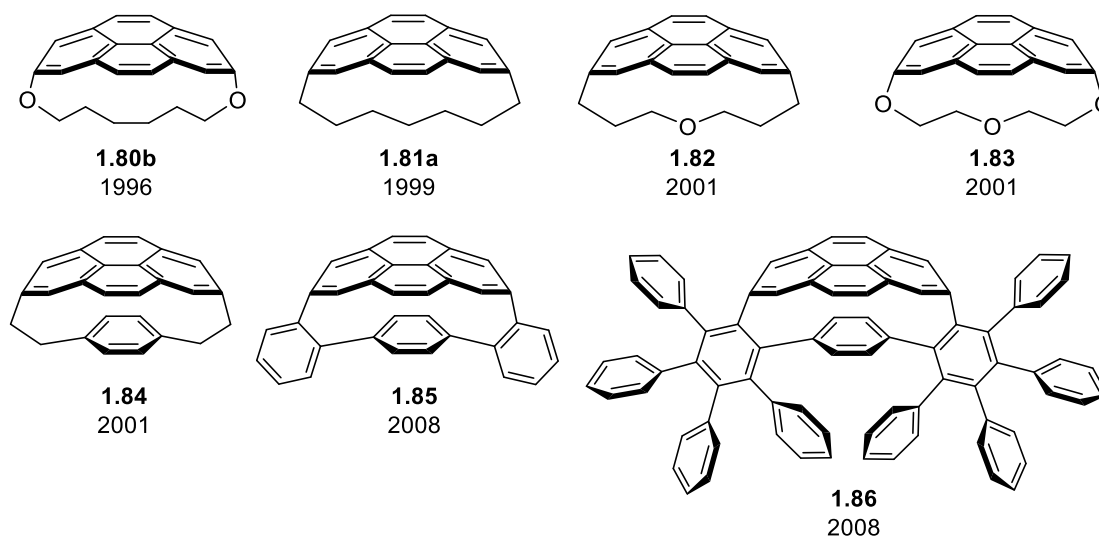
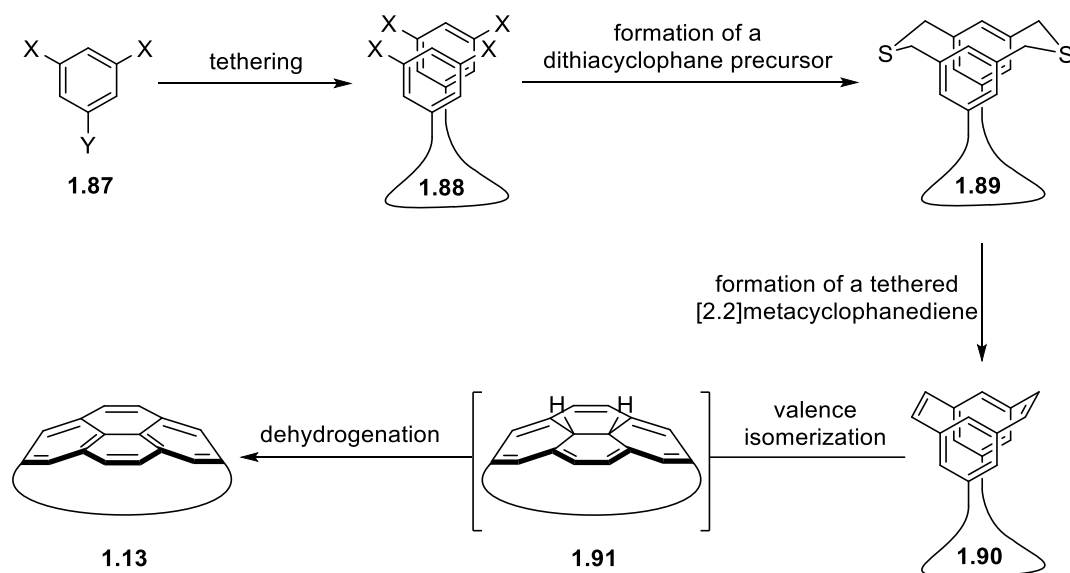


Figure 1.10 Some $[n](2,7)$ pyrenophanes reported by Bodwell.

a Type III strategy (Figure 1.10).^{35,36}

1.2.2.1 Synthesis of $[n](2,7)$ Pyrenophanes

The general strategy used for the synthesis of $[n](2,7)$ pyrenophanes (**1.13**) is outlined in Scheme 1.16. An appropriately trisubstituted aromatic compound **1.87** is tethered to afford bis(difunctionalized) species **1.88**. This is then converted into a dithia $[n.3.3]$ cyclophane **1.89**, which can then be used to form a tethered $[2.2]$ metacyclophanediene **1.90** *via* ring contraction. Heating the diene in the presence of DDQ delivers the corresponding $[n](2,7)$ pyrenophanes (**1.13**) *via* a valence isomerization/dehydrogenation (VID) reaction. The VID reaction in the synthesis of $[n](2,7)$ pyrenophanes (**1.13**) is discussed in detail in Chapter 3, but it is worth mentioning that this reaction is powerful in the generation of $[n](2,7)$ pyrenophanes due the large ASE of the pyrene system (74.6 kcal/mol),³⁷ which plays a major role in offsetting developing strain as the bent and relatively unstrained $[2.2]$ metacyclophanediene **1.90** goes through a



Scheme 1.16 General strategy for the synthesis of $[n](2,7)$ pyrenophanes (**1.13**).

cis-10*b*,10*c*-dihydropyrene **1.91** *en route* to the pyrenophane **1.13**. A specific example of Bodwell's approach is the synthesis of [7](2,7)pyrenophane (**1.81a**), which is the smallest member of the parent series to have been isolated and thus has the most highly-distorted pyrene unit (Scheme 1.17).

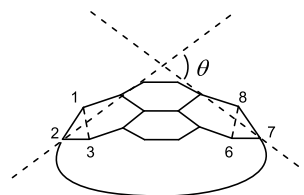
Esterification of 5-hydroxyisophthalic acid (**1.92**) gave diester **1.93**. To prepare for the installation of the tether, the phenolic oxygen was activated by triflation to give triflate **1.94**. Two benzene units were then tethered using a Sonogashira cross-coupling reaction to afford **1.95**. The alkynes in **1.95** were then hydrogenated to generate **1.96**, which has the tether in its final form (**1.96**).

To set the stage for cyclophane formation, functional group interconversion (reduction and bromination) was performed to deliver tetrabromide **1.97**. Treatment of **1.97** with Na₂S/Al₂O₃³⁸ furnished the relatively unstrained dithiacyclophane **1.98**. A four-step sequence involving *S*-methylation, thia-Stevens rearrangement, *S*-methylation and Hofmann elimination was then applied to convert dithiacyclophane **1.98** into the corresponding [2.2]metacyclophanediene **1.99**.³⁹ The VID reaction of [2.2]metacyclophanediene with DDQ in benzene at reflux delivered the target [7](2,7)pyrenophane **1.81a**. A series of [*n*](2,7)pyrenophanes **1.81a-d** (*n*=7-10),³⁵ 1,*n*-dioxo[*n*](2,7)pyrenophanes (**1.80a-f** *n* = 7-12)^{36,38} and [*m.n*]pyrenophanes **1.84-1.86** were synthesized using similar synthetic sequences (Figure 1.10).

dioxa[*n*](2,7)pyrenophanes (**1.80a-f**) are shown below. 1,7-Dioxa[7](2,7)pyrenophane (Entry 1, Table 1.3) contains the most distorted pyrene unit to have been isolated so far. This pyrenophane is the current record holder with $\theta = 109.2^\circ$, which means that the pyrene system in this cyclphane is more bent than the one that can be identified in the equator of D_{5h} C₇₀ ($\theta = 108.0^\circ$).^{35b}

Table 1.3 Bend angles (θ) of some of the [*n*](2,7)pyrenophanes synthesized in the Bodwell group and the definition of the bend angle θ .

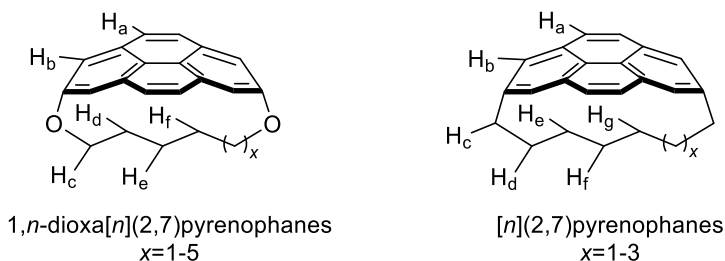
entry	bridge nature	θ_{exp}	$\theta_{\text{calculated}}$
1	–O(CH ₂) ₅ O–	109.2	113.3
2	–O(CH ₂) ₆ O–	87.8	94.9
3	–O(CH ₂) ₇ O–	72.9	77.8
4	–O(CH ₂) ₈ O–	57.7	61.2
5	–O(CH ₂) ₉ O–	39.9	42.2
6	–O(CH ₂) ₁₀ O–	34.6	33.1
7	–(CH ₂) ₇ –	-	104.6
8	–(CH ₂) ₈ –	80.8	87.0
9	–(CH ₂) ₉ –	62.4	70.3
10	–(CH ₂) ₁₀ –	46.4	54.4



The aromaticity of the pyrenophanes was measured by geometric (the harmonic oscillator model of aromaticity or HOMA), magnetic (the nucleus-independent chemical shift or NICS) and energetic (the aromatic stabilization energy or ASE) criteria. The most important conclusion from the study of these compounds was that the aromaticity of pyrene unit is only weakly affected by deformation from planarity (the retention of aromaticity is well over 90%).^{35a,41} It should be noted that the loss of aromaticity becomes more

significant as the pyrene system becomes substantially distorted, but even the most distorted system retains 64-81% of its aromatic character (depending upon the criterion used to measure). The ^1H NMR spectra of $[n](2,7)$ pyrenophanes **1.81a-c** and 1, n -dioxan[n](2,7)pyrenophanes (**1.80a-f**) show consistent upfield shifts of the aromatic protons with shortening of bridge but, not such a constant change was observed for aliphatic protons (Table 1.4).

Table 1.4 The ^1H NMR data for some $[n](2,7)$ pyrenophanes and 1, n -dioxan[n](2,7)pyrenophanes.

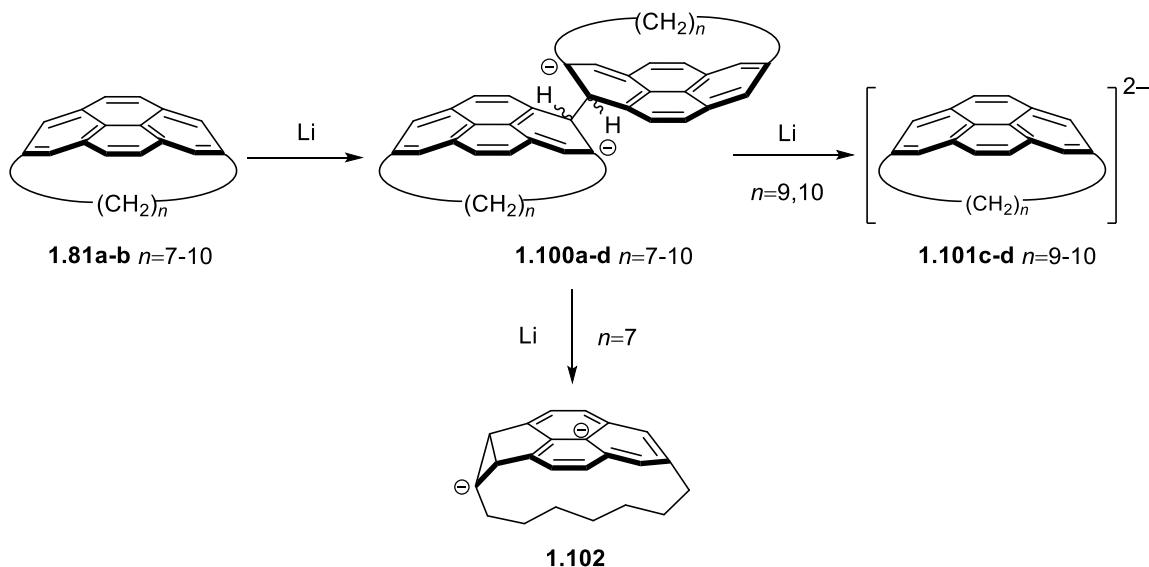


entry	bridge nature	H _a	H _b	H _c	H _d	H _e	H _f	H _g
1	–O(CH ₂) ₅ O–	7.72	7.22	3.31	–0.04	–2.10	-	-
2	–O(CH ₂) ₆ O–	7.84	7.44	3.59	0.10	–1.46	-	-
3	–O(CH ₂) ₇ O–	7.91	7.64	3.76	0.71	–1.89	–0.73	-
4	–O(CH ₂) ₈ O–	7.92	7.72	4.02	0.93	–1.17	–0.67	-
5	–O(CH ₂) ₉ O–	7.98	7.83	4.19	1.2	–0.27	–0.64	–1.04
6	–O(CH ₂) ₁₀ O–	7.96	7.85	4.31	1.4	–0.14	–0.14	–0.63
7	–(CH ₂) ₇ –	7.67	7.34	2.30	0.45	–1.38	–1.38	-
8	–(CH ₂) ₈ –	7.84	7.59	2.59	0.88	–0.69	–1.45	-
9	–(CH ₂) ₉ –	7.91	7.75	2.84	1.10	0.05	–0.94	–2.08

In contrast to what was observed for the benzene ring protons in $[n]$ paracyclophanes, the aromatic protons in the pyrene system (H_a and H_b) moved upfield

with increasing bend. In the electronic absorption spectra, no significant shift in the longest wavelength signals (the π bonds) was observed over the full range of bend.

In the case of chemical reactivity, $[n](2,7)$ pyrenophanes **1.81a-d** showed different behaviour upon reduction with alkali metal in going from $[7]$ - to $[10](2,7)$ pyrenophanes. Reduction of $[n](2,7)$ pyrenophane **1.81a-d** ($x=7-10$) with lithium metal furnished dimers **1.100a-d** ($n=7-10$) resulting from coupling of radical anions (Scheme 1.18).^{34b,42} For the two least strained systems, further reduction with lithium metal afforded antiaromatic dianions **1.101c-d** ($n=9-10$). The situation was then observed to change as the bridge became shorter. The further reduction of the next smaller member, $[8](2,7)$ pyrenophanes (**1.81b**), did not occur due to the unfavourability of forming a strained antiaromatic system (**1.101b**, $n=7$).

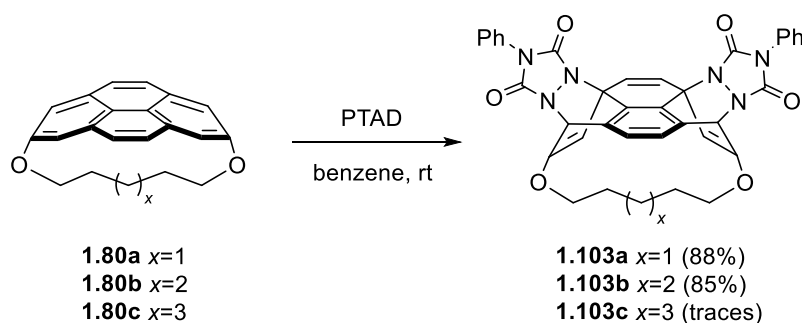


Scheme 1.18 Reduction of $[n](2,7)$ pyrenophanes **1.81a-d**.

The formation of **1.101a** ($n=7$) was expected to be even more unfavourable. Indeed, $[7](2,7)$ pyrenophane, the most highly-strained member of the series, underwent a further

rearrangement reaction to deliver the bicyclo[3.1.0]hexane structure **1.102**. It seems very likely that the higher amount of strain relief was the driving force for this unusual escape from strained antiaromaticity. Therefore, it can be concluded that dianioin **1.101b** ($n=8$) was not strained enough for this escape route (rearrangement).

A limited amount of chemistry has been performed on the $1,n$ -dioxan[n](2,7)pyrenophanes. Some of the more strained $1,n$ -dioxan[n](2,7)pyrenophanes (**1.80a-c** $x=1-3$) were found to undergo Diels-Alder reactions on positions 1 and 3a of pyrene unit with 4-phenyl-1,2,4-triazoline-3,5-dione (PTAD) as a reactive dienophile to afford adducts **1.103a-b** (Scheme 1.19).^{34a,35b} 1,9-Dioxan[9](2,7)pyrenophane (**1.80c** $x=3$) remained unreactive under the same conditions, which suggests that a particular amount of strain relief is necessary to counterbalance the loss in ASE.



Scheme 1.19 Diels-Alder reactions of $1,n$ -dioxan[n](2,7)pyrenophanes (**1.80a-c**) with PTAD.

Electrophilic aromatic substitution reactions of both series of $[n]$ (2,7)pyrenophanes **1.81a-d** ($n=7-10$) and $1,n$ -dioxan[n](2,7)pyrenophanes (**1.80a-f** $n=5-10$) could be useful starting points for the synthesis of larger aromatic systems, but only unsuccessful attempts of electrophilic bromination reaction of 1,8-dioxan[8](2,7)pyrenophane (**1.80d**) have been reported, which delivered either addition or bridge-cleaved products.^{34a}

1.2.3 $[n](2,9)$ Peropyrenophanes

Peropyrene (**1.5**) is the third member of ropyrenes. Bridging the two most remote positions of peropyrene gives rise to the $[n](2,9)$ peropyrenophanes (**1.14**), none of which has been synthesized. [2]Metacyclo[2](1,3)peropyrenopane **1.104** is the only peropyrenophane that has been obtained and this was as a byproduct of Misumi's synthesis of teropyrene (Figure 1.12).³³

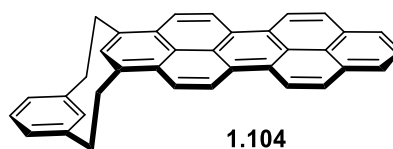


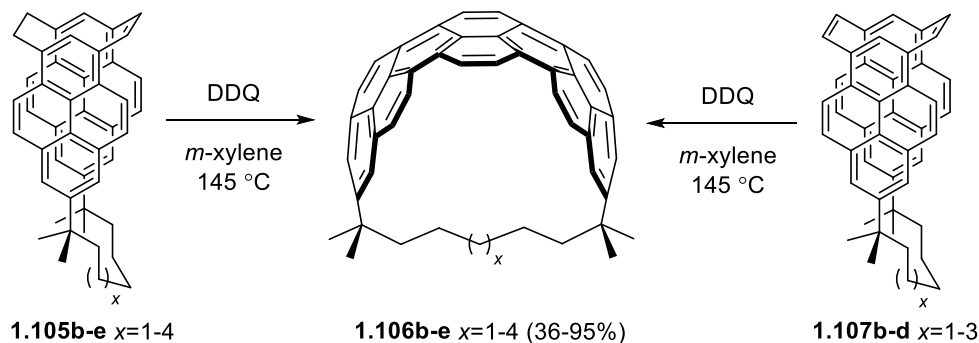
Figure 1.12 (1,3)Peropyrenophane **1.104** – the only reported peropyrenophane.

1.2.4 $[n](2,11)$ Teropyrenophanes

1.2.4.1 Synthesis of $[n](2,11)$ Teropyrenophanes

Teropyrene (**1.6**) follows peropyrene in the ropyrenes series and the $[n](2,11)$ teropyrenophanes (**1.15**) are the $[n]$ cyclophanes that arise from bridging the two most remote sites in teropyrene. Two different approaches (double-McMurry and Wurtz-McMurry) have been developed by the Bodwell group to synthesize a series of 1,1, n , n -tetramethyl $[n](2,11)$ teropyrenophanes **1.106b-e** ($n=7-10$).⁴³ These synthetic routes, which are discussed in detail in Chapter 2 involve a Type III strategy, similar to the one used for the synthesis of $[n](2,7)$ pyrenophanes (**1.13**). Application of the powerful VID methodology in the cyclophane-forming step furnished the target $[n](2,11)$ teropyrenophanes (**1.106b-e**) from tethered pyrenophanemonoene **1.105b-e** and pyrenophanediene **1.107b-d** upon reaction with DDQ (Scheme 1.20). In comparison to the larger homologues **1.106c-e**, **1.106b** ($n=7$), took a longer time to form and required the use

of more equivalents of oxidant, which is a reflection of the higher strain energy of this cyclophane.



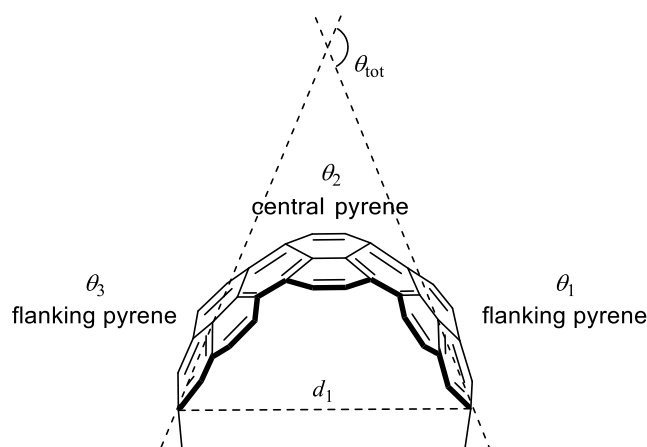
Scheme 1.20 Synthesis of 1,1,*n,n*-tetramethyl[*n*](2,11)teropyrenophanes **1.106b-e** (*n*=7-10).

1.2.4.2 Consequences of Bending the Teropyrene System in [*n*](2,11)Teropyrenophanes

Teropyrene (C₃₆), is significantly larger than pyrene (C₁₆), but the length of the bridges in the [*n*](2,11)teropyrenophanes **1.106b-e** is the same as those in the [*n*](2,7)pyrenophanes **1.81b-d**. Thus, the end-to-end bend of the aromatic unit in **1.106b-e** is much greater than that in **1.81b-d**. Three pyrene substructures can be identified in the teropyrene structure, hence individual θ values (θ_1 , θ_2 , θ_3) can be measured for each of them. The central pyrene system has the largest θ value in all cases and the largest value ($\theta_2=102.3^{\circ}$ for **1.106b**) falls well short of the largest θ value for a [*n*](2,7)pyrenophane (109.2° for **1.80a**). But the overall total bend angle (θ_{tot}) in [*n*](2,11)teropyrenophanes is defined as the smallest angle between the two terminal planes formed by three carbon atoms in the teropyrene system (Table 1.5). There is a good agreement between calculated end-to-end bend (θ_{tot}) in the teropyrene systems (**1.106b**: 178.7° , **1.106c**: 169.0° , **1.106d**: 156.6°) with experimental (X-ray) values (**1.106b**: 177.8° , **1.106c**: 167.0° , **1.106d**: 154.3°).

The distance between the two bridgehead carbon atoms (d_1) is another parameter, which becomes important when it comes to the study of armchair single-walled carbon nanotubes (SWCNT), because $[n](2,11)$ teropyrenophanes can be viewed as the segments of SWCNT, in which diameter is a key factor.

Table 1.5 Definition of the total bend angle (θ_{tot}), other bend angles θ_1 , θ_2 , θ_3 and distance between the two terminal carbons (d_1).

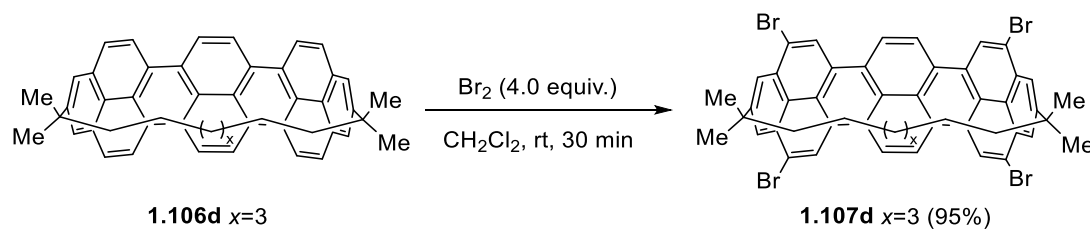


Entry	$n=6$ (calcd)	$n=7$ (calcd)	$n=7$ (exp)	$n=8$ (calcd)	$n=8$ (exp)	$n=9$ (calcd)	$n=9$ (exp)
θ_1	78.7	74.9	72.6	70.9	67.8	66.5	63.8
θ_2	109.5	101.3	102.3	92.8	94.4	84.4	90.2
θ_3	78.7	74.9	73.6	70.9	70.1	66.5	62.1
θ_{tot}	192.4	178.7	177.9	169.0	167.0	156.6	154.3
d_1 (Å)	7.21	8.18	8.08	9.16	9.10	10.12	9.80
SE (kcal/mol)	80.2	68.3	-	60.7	-	51.2	-

As the degree of bend of the teropyrene system increases, the ^1H NMR chemical shifts of the aryl protons move to higher field. In contrast, the ^{13}C NMR data of **1.106b-e** are very similar to one another and no major trends were observed as the teropyrene system

becomes more distorted. The longest wavelength absorption (λ_{max}) in the absorption and emission spectra for $[n](2,11)$ teropyrenophanes **1.106b-d** (λ_{max} = 484, 489, and 494 nm respectively) show a small blue shift with increasing bend in the teropyrene system. This is in contrast to the $[n]$ paracyclophanes, where a red shift is observed as the benzene ring becomes more bent (Section 1.2.1.2). By comparison, the $[n](2,7)$ pyrenophanes show virtually no change in the position of longest wavelength absorption.^{34c}

Due to low solubility of the parent cyclophane (**1.6**), the only reported characterization of teropyrene was a UV-Vis spectrum.³³ Hence, any investigation of its chemical reactivity was not possible. The incorporation of teropyrene into a $[n]$ cyclophane enhanced the solubility and provided the opportunity to study its electrophilic aromatic substitution chemistry, in particular bromination. Treatment of $[9](2,11)$ teropyrenophane **1.106d** with Br_2 (4.0 equiv.) at room temperature exclusively afforded the tetrabromide **1.107d** in 95% yield (Scheme 1.21).⁴⁴ It is worth mentioning that the overall bend of the teropyrene system in tetrabromide **1.107d** ($\theta_{\text{tot}}=157.4^\circ$) is somewhat larger than that of $[9]$ teropyrenophane **1.106d** ($\theta_{\text{tot}}=154.3^\circ$). Bromination of the less strained 1,1,10,10-tetramethyl $[10](2,11)$ teropyrenophane (**1.106e**) with Br_2 (4.0 equiv.) proceeded smoothly and the tetrabromide **1.107e** ($x=4$) was obtained as the only product. Upon moving to the



Scheme 1.21 Bromination of 1,1,9,9-tetramethyl $[9](2,11)$ teropyrenophane (**1.106d**).

more strained homologues, 1,1,8,8-tetramethyl[8](2,11)teropyrenophane (**1.106c**) and 1,1,7,7-tetramethyl[7](2,11)teropyrenophane (**1.106b**), the reaction with 4.0 equivalents of Br₂ afforded a 70:30 and 60:40 mixture of tetrabromide and pentabromide, respectively.

Another appealing feature of these belt-shaped molecules is the presence of a sizeable cavity, which could conceivably be occupied by molecules and ions to form host-guest complexes. Indeed, it has recently been reported that **1.106d** forms metal complexes with K⁺, Rb⁺ and Cs⁺ in the gas phase.⁴⁵ According to infrared multiphoton dissociation spectra, there are red-shifted C-H stretching bands in the gas-phase vibrational spectra of these ionic complexes. This is due the interaction between the metal cation inside the cavity and some of the bridge C-H bonds. Therefore, it was concluded the high population of complex is where the metal cation is inside the cavity of [9](2,11)teropyrenophane **1.106d** (*endo*).

1.3 Summary

Bridging the two maximally separated positions of each member of the ropyrenes series of PAHs (benzene (**1.3**), pyrene (**1.4**), peropyrene (**1.5**) and teropyrene (**1.6**)) gives rise to a series of [n]cyclophanes: [n]paracyclophanes, [n](2,7)pyrenophanes, [n](2,9)peropyrenophanes and [n](2,11)teropyrenophanes. The chemistry and properties of these cyclophanes is affected by altering the degree of bend in aromatic systems. A large amount of chemistry has been performed on the [n]paracyclophanes, but considerably less has been done with the [n](2,7)pyrenophanes and [n](2,11)teropyrenophanes. With regard to the latter, opportunities for the further study of the chemistry of these cyclophanes and their use in the construction of more highly bent aromatic systems.

1.4 References and Notes

1. Brown, C. J.; Farthing, A. C. *Nature* **1949**, *164*, 915–916.
2. Cram, D. J.; Steinberg, H. *J. Am. Chem. Soc.* **1951**, *73*, 5691–5704.
3. Pellegrin's synthesis of *anti* [2.2]metacyclophane in 1899 and Parekh and Guha's synthesis of 1,2,9,10-tetrathia[2.2]paracyclophane in 1934 precede the original works given in references 1 and 2, however, the concept of cyclophanes as bridged aromatic systems was defined decades after.
4. a) Ghods Ghasemabadi, P.; Yao, T.; Bodwell, G. J. *Chem. Soc. Rev.* **2015**, *44*, 6494–6518. b) Gleiter, R.; Hopt, H. *Modern Cyclophane Chemistry*, ed. New York, 2004.
5. a) Cram, D. J.; Cram, J. M. *Acc. Chem. Res.* **1971**, *4*, 204–213. b) Bickelhaupt, F. *Pure. Appl. Chem.* **1990**, *62*, 373–382. c) Tsuji, M.; Ohkita, M.; Nishida, S. *J. Am. Chem. Soc.* **1993**, *115*, 5284–5285. d) Tsuji, M.; Ohkita, M.; Konno, T.; Nishida, S. *J. Am. Chem. Soc.* **1997**, *119*, 8425–8431. e) Kawai, H.; Suzuki, T.; Ohkita, M.; Tsuji, T. *Chem. Eur. J.* **2003**, *6*, 4177–4187.
6. Bodwell, G. J.; Ernst, L.; Hanenel, M.; Hopf, H. *Angew. Chem. Int. Ed.* **1989**, *28*, 455–456.
7. Bodwell, G. J.; Ernst, L.; Hopf, H. *Chem. Ber.* **1989**, *122*, 1013–1016.
8. Semmelheck, M. F.; Harrison, J. J.; Young, D. C.; Gutierrez, A.; Rafii, S.; Clardy, J. *J. Am. Chem. Soc.* **1985**, *107*, 7508–7514.
9. a) Jenneskens, L. W.; de Kanter, F. J. J.; Kraakman, P. A.; Turkenburg, L. A. M.; Koolhaas, W. E.; de Wolf, W. H.; Bickelhaupt, F.; Tobe, Y.; Kakiuchi, K.; Odaira,

- Y. *J. Am. Chem. Soc.* **1985**, *107*, 3716–3717. b) Novoselov, K. S.; Geim, A. K.; Morozov, S. V.; Jiang, D.; Zhang, Y.; Dubonos, S. V.; Grigorieva and I. V.; Firsov, A. A. *Science* **2004**, *306*, 666–669.
10. a) Yang, W.; Monterio, J. H. S. K.; de Bettencourt-Dias, A. Chalifoux, W. A. *Can. J. Chem.* **2017**, *95*, 341–345. 14. b) Unikela, K. S.; Merner, B. L.; Ghods Ghasemabadi, P.; Warford, C. C.; Qiu, C.; Dawe, L. N.; Zhao, Y.; Bodwell, G. J. manuscript in preparation. Chalifoux and co-workers suggested the name “pyrenacenes” while Bodwell and co-workers suggested the term “ropyrènes” because it is consistent with the name of the rylenes series, which is named after the common ending of the individual compound names (perylene, terrylene...).
11. Rumi, M.; Zerbi, G.; Müllen, K. *J. Chem. Phys.* **1998**, *108*, 8662–8670.
12. Vögtle, F. *Top. Curr. Chem.* **1983**, *115*, 157. b) Vögtle, F.; Schröder, A.; Karbach, D. *Angew. Chem. Int. Ed.* **1991**, *30*, 575–579. c) Schröder, A.; Karbach, D.; Guthier, R.; Vögtle, F. *Chem. Ber.* **1992**, *125*, 1881–1887. d) Breidenbach, S.; Ohren, S. Vögtle, F. *Chem. Eur. J.* **1996**, *2*, 832–837.
13. a) Cram, D. J.; Allinger, N. L.; Steinberg, H. *J. Am. Chem. Soc.* **1954**, *76*, 2743–2752. b) Cram, D. J.; Antar, F. M. *J. Am. Chem. Soc.* **1958**, *80*, 3103–3109.
14. Tobe, Y.; Kakiuchi, K.; Odaira, Y.; Hoskai, T.; Kai, Y.; Kasai, N. *J. Am. Chem. Soc.* **1983**, *105*, 1376–1377.
15. a) Tsuji, T.; Okuyama, M.; Ohkita, M.; Kawai, H.; Suzuki, T. *J. Am. Chem. Soc.* **2003**, *125*, 951–961. b) Ma, B.; Sulzbach, H. M.; Reminton, R. B.; Schaefer III, H. F. *J. Am. Chem. Soc.* **1995**, *117*, 8392–8400. c) Schleyer, P. V. R.; Maeker, C.;

- Dransfeld, A.; Jiao, H.; van Eikema Hommes, N. J. R. *J. Am. Chem. Soc.* **1996**, *118*, 6317–6318.
16. Kostermans, G. B. M.; Bobeldijk, M.; de Wolf, W. H.; Bickelhaupt, F. *J. Am. Chem. Soc.* **1987**, *109*, 2471–2475.
 17. Chenung, Y. S.; Wang, C. K.; Li, W. K. *J. Mol. Struct.* **1998**, *454*, 17–24.
 18. Krygowski, T. M.; Cyrański, M. K. *Chem. Rev.* **2001**, *101*, 1385–1419.
 19. Allinger, N. L.; Freiberg, L. A.; Hermann, R. B.; Miller, M. A. *J. Am. Chem. Soc.* **1963**, *85*, 1171–1176.
 20. Cram, D. J.; Antar, M. F. *Organic Chemistry, Volume 2*, 1964.
 21. Allinger, N. L.; Walter, T. J. *J. Am. Chem. Soc.* **1972**, *94*, 9267–9268.
 22. Otsubo, T.; Misumi, S. *Synth. Commun.* **1978**, *8*, 285–289.
 23. Cram, D. J.; Daeniker, H. U. *J. Am. Chem. Soc.* **1954**, *76*, 2743–2752.
 24. Ueda, T.; Kanomata, N.; Machida, H. *Org. Lett.* **2005**, *7*, 2365–2368.
 25. Tobe, Y.; Kaneda, T.; Kakiuchi, K.; Odaira, Y. *Chem. Lett.* **1985**, 1301–1304.
 26. Kostermans, G. B. M.; de Wolf, W. H.; Bickelhaupt, F. *Tetrahedron* **1987**, *43*, 2955–2966.
 27. Okuyama, M.; Tsuji, T. *Angew. Chem. Int. Ed.* **1997**, *36*, 1085–1088.
 28. Tsuji, T.; Komiya, Z.; Nashida, S. *Tetrahedron Lett.* **1980**, *21*, 3583–3586.
 29. a) Tsuji, T.; Nishida, S. *J. Am. Chem. Soc.* **1989**, *111*, 368–369. b) Tobe, Y.; Takemura, A.; Jimbo, M.; Takahashi, T.; Kobiro, K.; Kakiuchi, K. *J. Am. Chem. Soc.* **1992**, *114*, 3479–3491.

30. Allinger, N. L.; Walter, T. J.; Newton, M. G. *J. Am. Chem. Soc.* **1974**, *96*, 4588–4596.
31. a) Carballera, L.; Casado, J.; González, E.; Ríos, M. A. *J. Chem. Phys.* **1982**, *77*, 5655–5663; b) Allinger, N. L.; Sprague, J. T.; Liljefors, T. *J. Am. Chem. Soc.* **1974**, *96*, 5100–5104.
32. a) Förster, T.; Kasper, K. *Z. Elektrochem* **1955**, *59*, 976–980. b) Birks, J. B. *Photophysics of Aromatic Molecules*, Wiley-Interscience. London, 1970. c) Winnik, F. M. *Chem. Rev.* **1994**, *94*, 587–614. d) Berlman, I. B. *Handbook of Fluorescence Spectra of Aromatic Molecules*, Academic Press. New York, 1971; e) Karupannan, S.; Chambron, J.-C. *Chem. Asian J.* **2011**, *6*, 964–984.
33. Umemoto, T.; Satani, S.; Sakata, Y.; Misumi, S. *Tetrahedron Lett.* **1975**, *16*, 3159–3162.
34. a) Bodwell, G. J.; Flemming, J. J.; Mannion, M. R.; Miller, D. O. *J. Org. Chem.* **2000**, *65*, 5360–5370. b) Aprahamian, I.; Bodwell, G. J.; Fleming, J. J.; Manning, G. P.; Mannion, M. R.; Merner, B. L.; Sheradsky, T.; Vermeij, R. J.; Rabinovitz, M. *J. Am. Chem. Soc.* **2004**, *126*, 6765–6775. c) Mannion, M. R. Ph.D. Dissertation, Memorial University, 1999.
35. a) Bodwell, G. J.; Bridson, J. N.; Cyrański, M. K.; Kennedy, J. W.; Krygowski, T. M.; Mannion, M. R.; Miller, D. O. *J. Org. Chem.* **2003**, *68*, 2089–2098. b) Bodwell, G. J.; Bridson, J. N.; Houghton, T. G.; Kennedy, J. W.; Mannion, M. R. *Chem. Eur. J.* **1999**, *5*, 1823–1827.

36. Bodwell, G. J.; Bridson, J. N.; Houghton, T. J.; Kennedy, J. W.; Mannion, M. R. *Angew. Chem. Int. Ed.* **1996**, *35*, 1320–1321.
37. Nakamura, E.; Tahara, K.; Matsuo, Y.; Sawamura, M. *J. Am. Chem. Soc.* **2003**, *125*, 2834–2835.
38. Bodwell, G. J.; Houghton, T. J.; Koury, H. E.; Yarlagadda, B. *Synlett* **1995**, 751–752.
39. Mitchell, R. H.; Ward, T. R.; Wang, Y. *Heterocycles* **2001**, *54*, 249–257.
40. Bodwell, G. J.; Fleming, J. J.; Miller, D. O. *Tetrahedron* **2001**, *57*, 3577–3585.
41. Dobrowolski, M. A.; Cyranski, M. K.; Merner, B. L.; Bodwell, G. J.; Wu, J.; Scheyer, P. V. R. *J. Org. Chem.* **2008**, *73*, 8001–8009.
42. a) Aprahamian, I.; Bodwell, G. J.; Fleming, J. J.; Manning, G. P.; Mannion, M. R.; Sheradsky, T.; Vermeij, R. J.; Rabinovitz, M. *J. Am. Chem. Soc.*, **2003**, *125*, 1720–1721. b) Aprahamian, I.; Bodwell, G. J.; Fleming, J. J.; Manning, G. P.; Mannion, M. R.; Sheradsky, T.; Vermeij, R. J.; Rabinovitz, M. *Angew. Chem. Int. Ed.* **2003**, *42*, 2547–2550.
43. a) Merner, B. L.; Dawe, L. N.; Bodwell, G. J. *Angew. Chem. Int. Ed.*, **2009**, *48*, 5487–5491. b) Merner, B. L.; Unikela, K. S.; Dawe, L. N.; Thompson, D. V.; Bodwell, G. J. *Chem. Commun.* **2013**, *49*, 5930–5932.
44. Unikela, K. S.; Roemmele, T. L.; Houska, V.; McGrath, K. E.; Tobin, D. M.; Dawe, L. N.; Boéré, R. T.; Bodwell, G. J. *Angew. Chem. Int. Ed.* **2018**, *57*, 1707–1711.
45. Chen, Y.; Jami-Alahmadi, Y.; Unikela, K. S.; Bodwell, G. J.; Fridgen, T. D. *ChemPhysChem* **2018**, *19*, 2194–2199.

CHAPTER 2: Attempted Synthesis of 1,1,6,6-Tetramethyl[6](2,11)teropyrenophane

2.1 Introduction

As for any $[n]$ cyclophane (a cyclophane consisting of just one aromatic system and one bridge), the $[n](2,11)$ teropyrenophanes (**2.1**) offer the opportunity to study how the chemical and physical properties of the aromatic system (teropyrene) change with incremental changes in structure. The teropyrene system is of interest because it represents a 36-carbon segment of graphene nanoribbons (**2.2**), armchair SWCNTs (**2.3**) and also Vögtle belts (**2.4**).¹

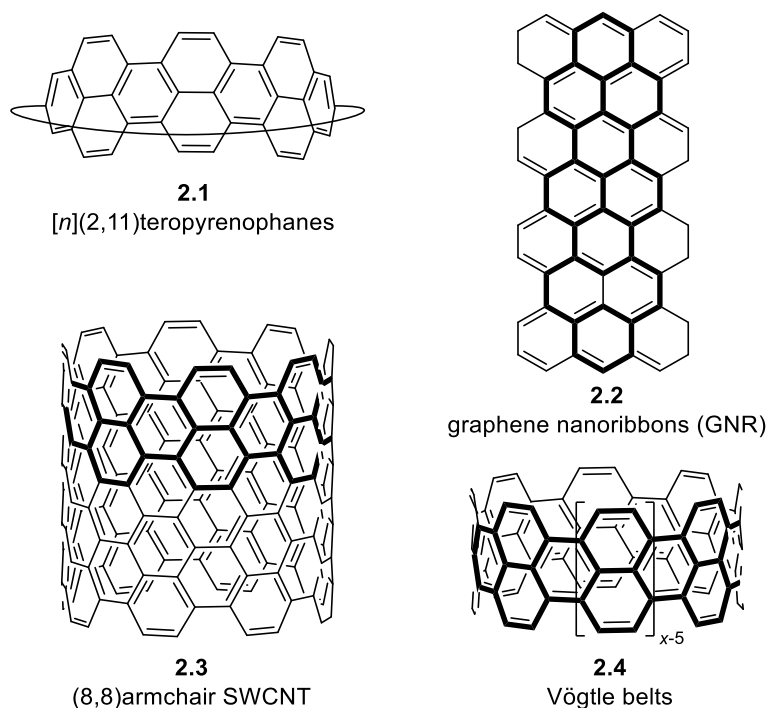


Figure 2.1 $[n](2,11)$ Teropyrenophanes (**2.1**), graphene nanoribbons (**2.2**), (8,8) armchair SWCNTs (**2.3**) and Vögtle belts (**2.4**). The teropyrene structures in **2.2-2.4** are highlighted.

As described in Chapter 1, the only reported synthesis of the parent teropyrene (**2.5**) was by Misumi in 1975 (Figure 2.2).² Due to very low solubility, the only reported characterization was a UV-Vis spectrum.

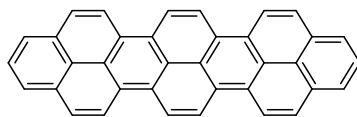


Figure 2.2 Teropyrene (**2.5**).

In contrast, 1,1,*n,n*-tetramethyl[*n*](2,11)teropyrenophanes **2.6b-e** exhibit good solubility in common organic solvents, which provided the opportunity to initiate the investigation of the chemistry and spectroscopic properties of the teropyrene system.^{3,4} For example, the bromination chemistry of [*n*](2,11)teropyrenophanes **2.6b-e** was studied (Figure 2.3, see Chapter 1 for details).⁵

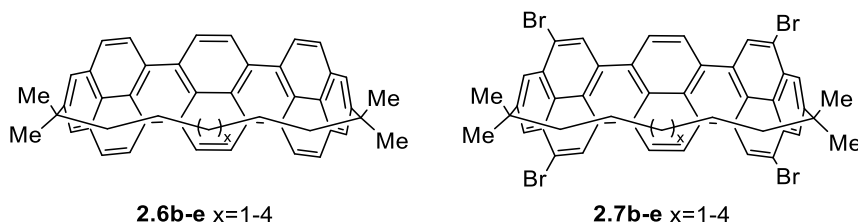
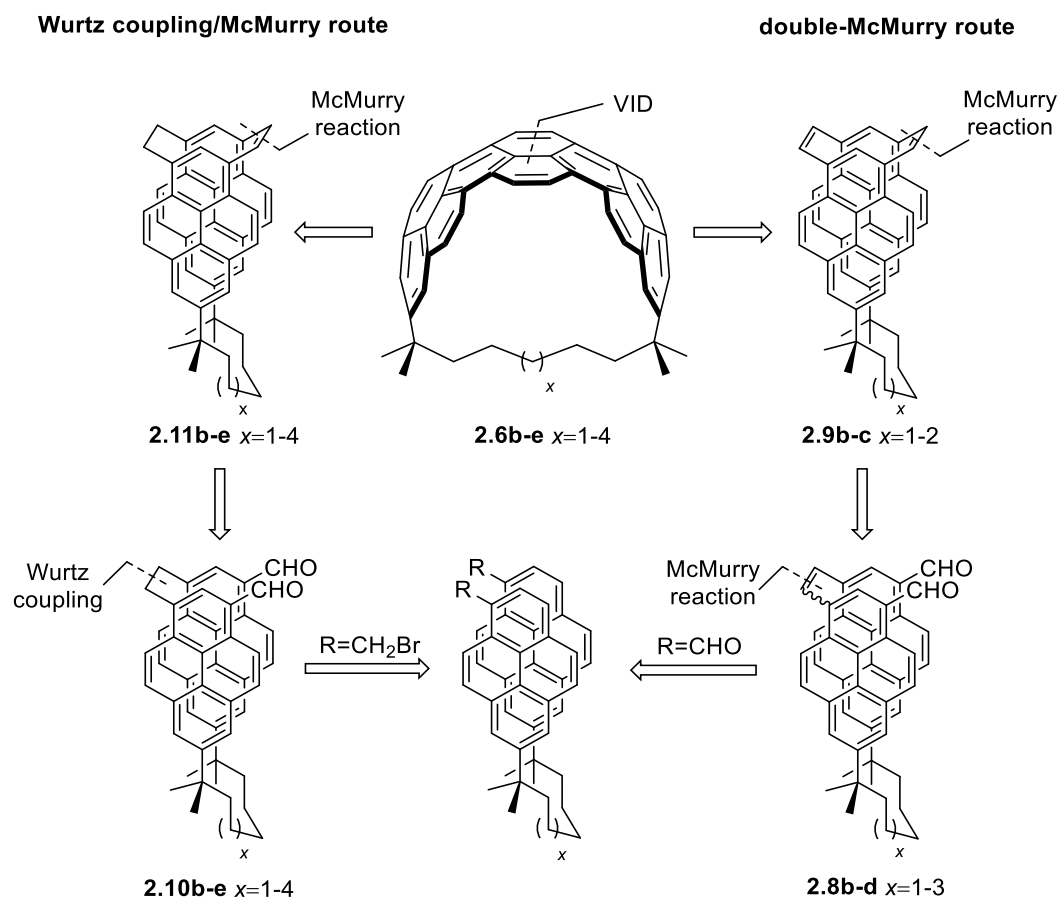


Figure 2.3 [*n*](2,11)Teropyrenophanes **2.6b-e** and synthesized tetrabromides **2.7b-e**.

In addition, the presence of a sizeable cavity raises the possibility of host-guest chemistry. In fact, it has recently been shown that **2.6d** forms metal complexes with K^+ , Rb^+ and Cs^+ in the gas phase (see Chapter 1, Section 1.2.4.2).⁶ No molecule-molecule host-guest complexes have yet been observed in solution, but work aimed at achieving this goal is underway in collaboration with Prof. Brian Wagner, UPEI.

2.2 Previously Reported Synthesis of a Homologous Series of 1,1,*n,n*-Tetramethyl[*n*](2,11)teropyrenophanes

The retrosynthetic analysis of a homologous series of 1,1,*n,n*-tetramethyl[*n*](2,11)teropyrenophanes **2.6b-e** is shown in Scheme 2.1.³ Two different approaches have been reported for the synthesis of these [*n*](2,11)teropyrenophanes. The two routes, which both fall under the Type III strategy (Chapter 1), are closely related and differ only in the methods used to install the two two-atom bridges in the [*n*.2.2]pyrenophanediene **2.9b-c** and [*n*.2.2]pyrenophanemonoenes **2.11b-e**, which serve as direct synthetic precursors to the [*n*](2,11)teropyrenophanes **2.6b-e**.



Scheme 2.1 Retrosynthetic analysis of teropyrenophane targets **2.6b-e**.

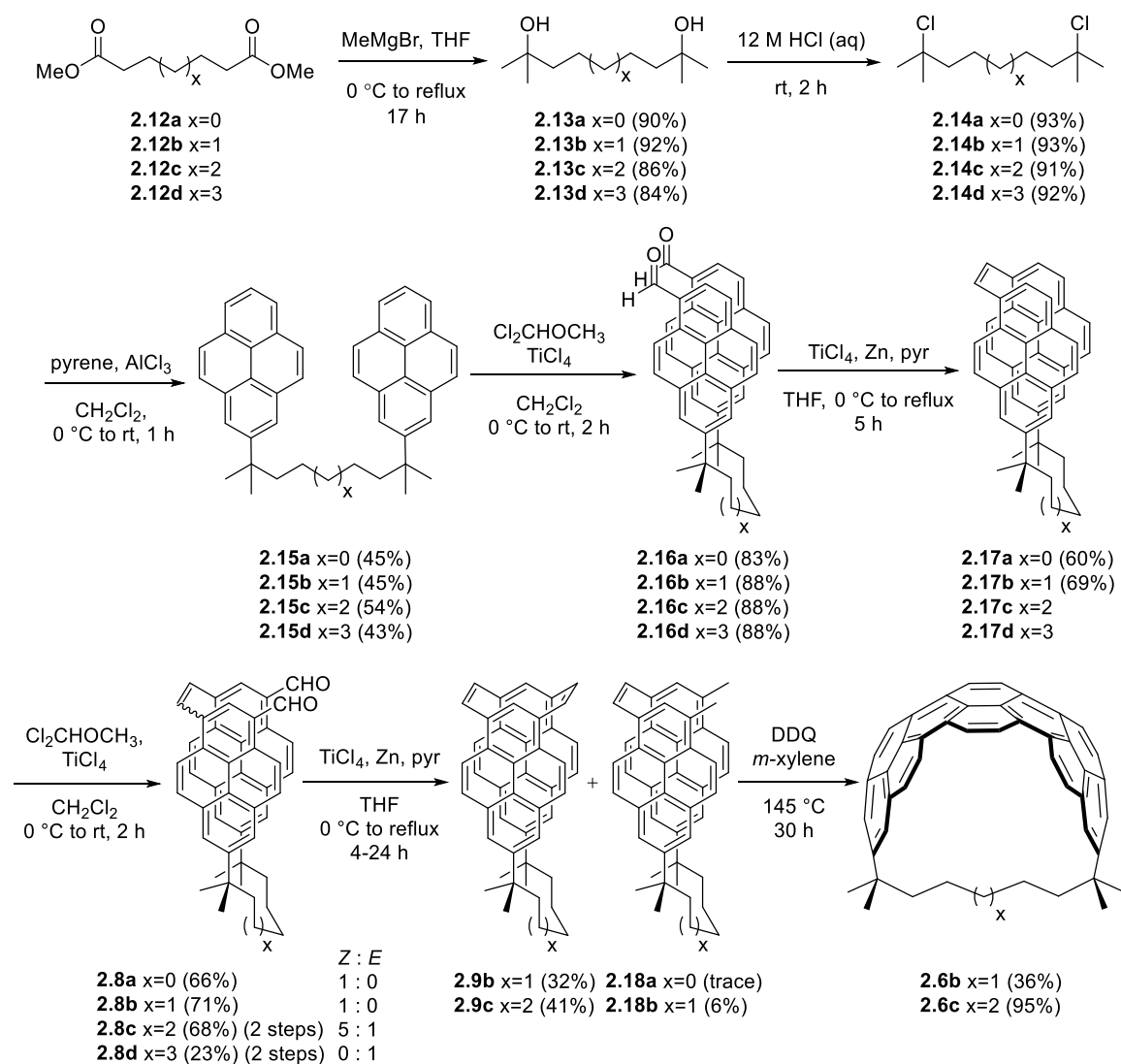
2.2.1 Synthesis of 1,1,*n,n*-Tetramethyl[*n*](2,11)teropyrenophanes **2.6b,c** via a Double-McMurry Route

1,1,8,8-Tetramethyl[8](2,11)teropyrenophane **2.6c** ($x=2$) was the first member of this family to be synthesized, and this was achieved using a “double-McMurry” approach.³ 1,1,7,7-tetramethyl[7](2,11)teropyrenophane **2.2b** was later delivered in a similar way (Scheme 2.2).

The Grignard reaction of a series of commercially available diesters, dimethyl adipate (**2.12a**), dimethyl pimelate (**2.12b**), dimethyl suberate (**2.12c**) and dimethyl azelate (**2.12d**) with methylmagnesium bromide furnished tertiary diols **2.13a-d** in excellent yields. Treatment of **2.13a-d** with concentrated HCl generated dichloride **2.14a-d** (91-93%). Subsequent reaction of **2.14a-d** with pyrene under Friedel-Crafts alkylation conditions led to the formation of dipyren-2-ylalkanes **2.15a-d** (43-54%).

The use of tertiary alkyl chlorides was a key element of the synthetic plan. It was known⁷ that the selective substitution of the 2 and 7 positions of pyrene occurs in Friedel-Crafts *tert*-alkylation reactions due to the steric interactions between the bulky electrophile and the adjacent *peri*-protons. Furthermore, once installed, the substituents sterically encumber the adjacent positions and thus enable subsequent functionalization to occur exclusively at the other end of the pyrene system. Thus, Rieche formylation of **2.15a-d** provided dialdehydes **2.16a-d** (83-88%) with complete regioselectivity. Intramolecular McMurry reaction of **2.16a-d** resulted in reductive coupling of the two aldehyde groups to afford **2.17a-d**. At this point, **2.17a-b** were obtained exclusively as their *Z* isomers and **2.17c** was formed as a chromatographically inseparable mixture of diastereomers. This mixture was formylated without characterization and a separable mixture of (*E*)- and (*Z*)-

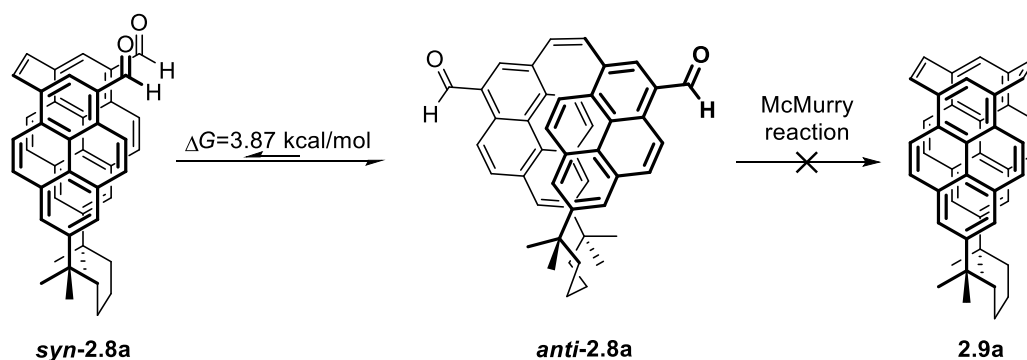
2.8c was obtained. The geometry of the double-bond in **2.17d** was exclusively *E*, which led to (*E*)-**2.8d** (not suitable for the next Intramolecular McMurry reaction). Thus, progress could only be made with **2.8a-c**. Their McMurry reaction afforded **2.9b-c** (32-41%) along with the reduction products **2.18a** (trace by LCMS analysis) and **2.18b** (6%). Compounds **2.9b-c** were successfully converted into the corresponding $[n](2,11)$ teropyrenophanes **2.6b-c** (36-95%) upon heating in *m*-xylene in the presence of DDQ.



Scheme 2.2 Synthesis of 1,1,*n,n*-tetramethyl $[n](2,11)$ teropyrenophanes (**2.6b-c**) using a double-McMurry strategy.

The McMurry reaction featured prominently in the synthesis of **2.8b-c**. Indeed, its use in the formation of cyclophanedienes **2.9b-c** was a daring tactic. The success of these McMurry reactions was remarkable because numerous earlier attempts to employ the McMurry reaction to construct [2.2]metacyclophanediene systems proceeded very poorly ($\leq 4.3\%$).⁸ Possible π - π interactions between the two pyrene systems in the starting dialdehydes **2.16a-d** and **2.8b-d** and/or increased preorganization due to the presence of two bridges instead of one were the reasons put forward for the success of the McMurry reactions.

The double-McMurry strategy failed at the stage of the second bridge-forming reaction for both **2.8a** and **2.8d**, but for different reasons. In the case of **2.8d** (9-atom bridge), the *E*-configured alkene is not suited to the intramolecular McMurry reaction. For the smallest homologue **2.8a**, the bridging alkene is correctly configured, but the *anti* conformation of the pyrenophane was observed to be highly populated by ¹H NMR. In this conformation, the two formyl groups are too far from one another to undergo reductive coupling (Scheme 2.3).^{9,10}



Scheme 2.3 Failure of McMurry reaction in the synthesis of cyclophanediene **2.9a**.

The calculated ΔG (at the B3LYP/6-31G(d) level of theory at standard conditions) for *anti/syn* isomerization of **2.8a** in the gas phase was 3.87 kcal/mol, which would correspond to a 709:1 equilibrium ratio of *anti:syn*. Thus, the double-McMurry strategy was only able to deliver [7]- and [8](2,11)teropyrenophanes (**2.6b-c**).

To investigate the change in chemical and physical properties of the teropyrene system with the change in degree of distortion from planarity (length of the chain) and also to address the stereochemistry and conformational problems during the formation of the first and second vinylene bridges, respectively, the higher and lower homologues of **2.6b-c** were approached using a different method.

2.2.2 Synthesis of 1,1,*n,n*-Tetramethyl[*n*](2,11)teropyrenophanes **2.6b-e** via a Wurtz coupling/McMurry Route

The potential solution to “upper limit” problem (longer bridges) was replacement of the first double bond with a saturated carbon-carbon bond. Particularly, this involved replacing the first McMurry reaction of the double-McMurry route with a Wurtz coupling. This reaction was chosen because it had a history of successful application in the synthesis of [2.2]metacyclophanes.¹¹ As before, the second two-atom (unsaturated) bridge was installed with a Rieche formylation followed by a McMurry reaction to furnish [*n*.2.2]pyronphanemonoenes **2.11b-e**, which like the corresponding dienes **2.9b-c** still have a 6 π -electron system suitable for the VID reaction leading to teropyrenophanes **2.6b-e** (Scheme 2.4).¹²

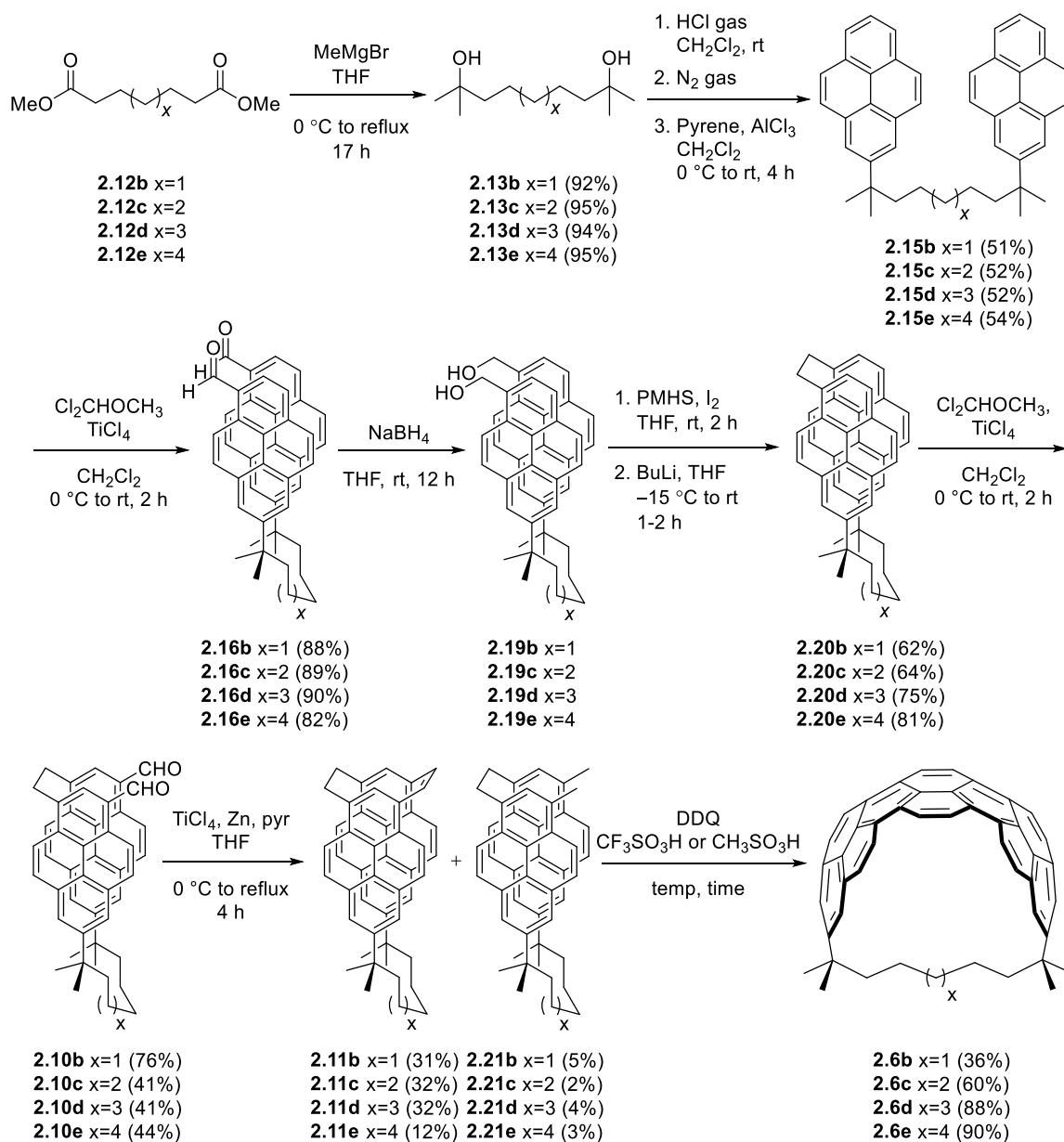
[*n*](2,11)Teropyrenophanes **2.6b-e** were originally synthesized on a small scale,^{3,9} and this was followed by the development of a modified large-scale synthesis.^{10,13} This

commenced with a two-fold Grignard reaction of commercially available diesters **2.12b-e** with methylmagnesium bromide to afford diols **2.10b-e** (35-40 g). HCl gas (generated from the dropwise addition of conc. HCl to conc. H₂SO₄) in dichloromethane was then employed instead of conc. aqueous HCl to generate dichlorides **2.14b-e**, which were used immediately in a Friedel-Crafts alkylation of pyrene to deliver dipyren-2-ylalkanes **2.15b-e** over two steps in moderate yields (51-54%, 30-59 g).

Regioselective formylation of **2.15b-e** produced dialdehydes **2.16b-e** (82-90%, 30-55 g). To prepare for the key Wurtz-coupling reaction, dialdehydes **2.16b-e** were reduced with sodium borohydride and the resulting crude diols were converted into the corresponding diiodides upon reaction with polymethylhydrosiloxane (PMHS) and iodine in dry THF.¹⁰ Once the formation of diiodides (not shown) was complete (TLC analysis), the reaction mixture was diluted with THF (to promote intramolecular Wurtz coupling) and BuLi was added dropwise at -15 °C. This afforded [*n*.2](7,1)pyrenophanes **2.20b-e** (62-81%, 3 steps, 8-22.5 g).

Rieche formylation of **2.20b-e** furnished dialdehydes **2.10b-e** (41-76%). The low yields were due to losses during chromatographic separation of minor regioisomeric dialdehydes. Intramolecular McMurry reaction of **2.10b-e** delivered [*n*.2.2](7,1,3)pyrenophanes **2.11b-e** (12-32%, 3-11.6 g) and reduction products **2.21b-e** (2-5%). The yields are comparable to those of the second McMurry reaction in the double-McMurry approach. In the case of the large-scale VID reactions, two major problems were encountered. First, removal of relatively large amounts of the high-boiling solvent (*m*-xylene) and second, the competing insertion of DDQ into the benzylic C-H bond of

methylated aromatic solvents at high temperatures (>110 °C).¹⁴ To address these issues, modified conditions¹⁵ were developed for the conversion of [n.2.2]pyrenophanemonoenes **2.11b-e** into [n](2,11)teropyrenophanes **2.6b-e** (52-90%). Unfortunately, different conditions were required for each substrate: **2.6b** (DDQ, CH₃SO₃H, 40 °C, 30 min), **2.6c** (DDQ, CF₃SO₃H, rt, 30 min) and **2.2d-e** (DDQ, CH₃SO₃H, rt, 10 min).



Scheme 2.4 Synthesis of [n](2,11)teropyrenophanes **2.6b-e** using a Wurtz/McMurry route.

2.3 Toward the Synthesis of 1,1,6,6-Tetramethyl[6](2,11)teropyrenophane

As described in Section 2.2.1, the double-McMurry approach, which was investigated by a previous graduate student (Kiran Sagar Unikela) in the Bodwell group, turned out to be unsuccessful due to the preference for the *anti*-conformation of dialdehyde **2.8a** ($x=0$) (Scheme 2.3). After a failed attempt to achieve the synthesis of **2.9a** using the double-McMurry route, it was decided to pursue the synthesis of [6](2,11)teropyrenophane (**2.6a**) via the Wurtz/McMurry route. Before going into results of this work, it would be informative to consider the importance of the synthesis of this challenging target.

2.3.1 1,1,6,6-Tetramethyl[6](2,11)teropyrenophane: A Lower Limit to These Highly Distorted π -Systems or Current Synthetic Route?

Shortening of the tether in the series of $[n](2,11)$ teropyrenophanes increases the calculated end-to-end bend (θ_{ot} , Chapter 1) in the teropyrene systems (**2.6b**: 178.7° , **2.6c**: 169.0° , **2.6d**: 156.6°)¹⁰. The calculated values are in a good agreement with the experimental values (**2.6b**: 177.9° , **2.6c**: 167.0° , **2.6d**: 154.3°)¹⁰ and the agreement becomes slightly better as the teropyrenophane becomes smaller.⁹ Decreasing the bridge by another carbon atom (to $n=6$) increases the calculated bend in the teropyrene system to 192.4° . Thus, investigation of the capability of the VID methodology to deliver this more highly strained target (SE=80.2 kcal/mol for **2.6a**, SE=68.3 kcal/mol for **2.6b**)¹⁰ becomes important as the success or failure of this work will provide information about the limits of both the ability of the synthetic methodology to deliver bent teropyrenophanes and the stability of the smaller teropyrenophanes under the conditions of their formation. This knowledge will underpin decisions about when to abandon the current approaches and

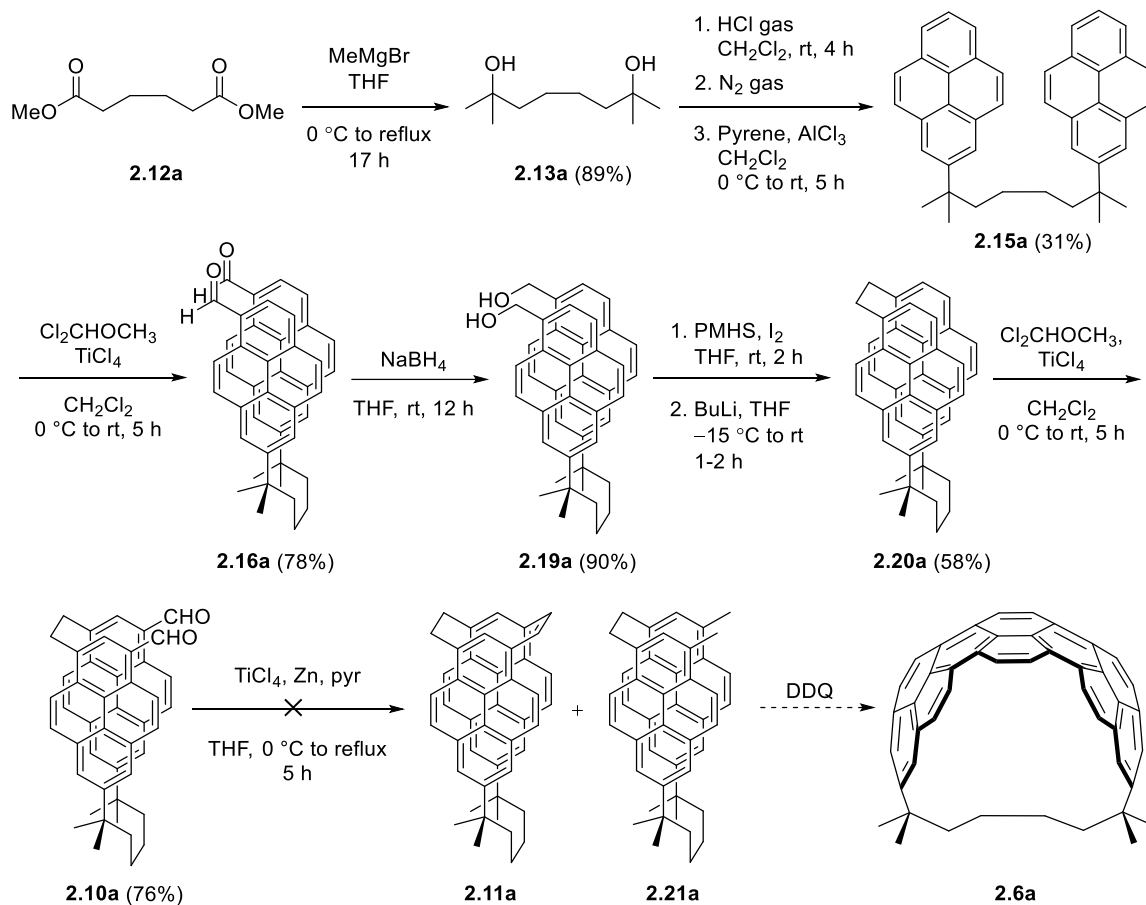
pursue the development of new synthetic routes to 1,1,*n,n*-tetramethyl[*n*](2,11)teropyrenophanes. The clear starting point to probe the “lower limit” of the synthetic approach was to apply the Wurtz coupling/McMurry route to the synthesis of 1,1,6,6-tetramethyl[6](2,11)teropyrenophane (**2.6a**).

2.4 Results and Discussion

2.4.1 Attempted Synthesis of 1,1,6,6-Tetramethyl[6](2,11)teropyrenophane (**2.6a**) via a Wurtz/McMurry Route

Work aimed at the synthesis of **2.6a** commenced with a two-fold Grignard reaction of commercial dimethyl adipate (**2.12a**) with methylmagnesium bromide to produce diol **2.13a** in 89% yield (Scheme 2.5). HCl gas (generated from the dropwise addition of conc. HCl to conc. H₂SO₄) was then bubbled into a solution of diol **2.13a** in dichloromethane. The HCl stream was removed and the reaction mixture was first purged with nitrogen gas (to remove excess HCl) and then used immediately in a Friedel-Crafts alkylation of pyrene. As expected, the pyrene system showed complete regioselectivity for the 2 positions, giving dipyren-2-ylalkane **2.15a** in 31% yield. The *tert*-alkyl substituents at the 2 positions provided enough steric bulk to disfavour subsequent electrophilic aromatic substitution at the adjacent positions. Thus, Rieche formylation of **2.15a** furnished 11,21-diformyl-1,1,6,6-tetramethyl[6,2](7,1)pyrenophane (**2.16a**) with complete regioselectivity in 78% yield. The dialdehyde **2.16a** was reduced smoothly using NaBH₄ to afford diol **2.19a** in high yield. The diol **2.19a** was then subjected to the iodination/Wurtz coupling sequence and cyclophane **2.20a** was obtained in 58% yield. At this stage, attempted intramolecular

McMurry reaction of **2.10a** failed to afford cyclophane **2.11a** or even the reduced product **2.21a** (LCMS and ^1H NMR analysis).¹⁶



Scheme 2.5 Attempted synthesis of 1,1,6,6-tetramethyl[6](2,11)terpyrenophanes (**2.6a**) using a Wurtz coupling/McMurry route.

Knowing that the double-McMurry route failed at the second McMurry reaction due to an unfavourable conformation of dialdehyde **2.16a**, it seemed likely that the failure of **2.10a** was attributable to the same phenomenon. To obtain information about the conformational preference of dialdehyde **2.10a**, the ^1H NMR spectrum of pyrenophanedialdehyde **2.10a** was compared to those of the higher homologues **2.10b-d** of

the series (Figure 2.4). The first three members of the series (**2.10a-c**) show high field signals that correspond to the aryl protons located on the edge of the pyrene system across from the one bearing the formyl group (H_{A-C} , Figure 2.4). Therefore, it can be concluded that **2.10a-c** have highly populated *anti* conformations. In the *anti* conformations these protons lie over the other pyrene system and thus would be expected to be strongly shielded.

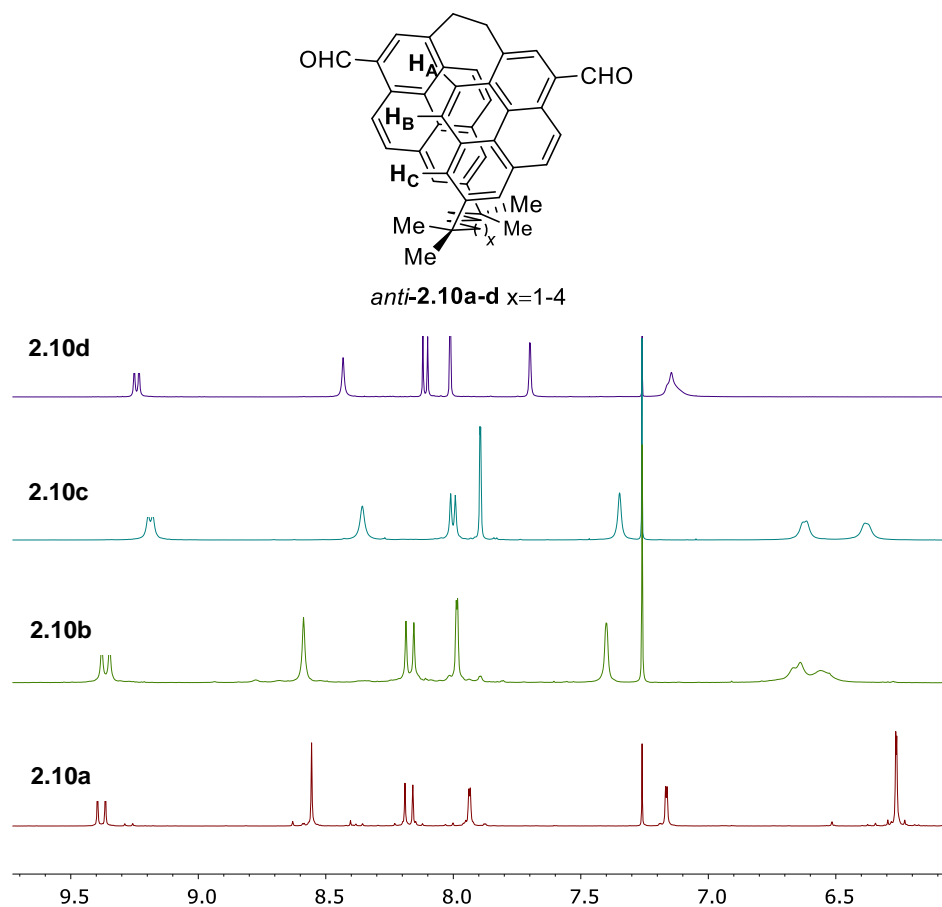


Figure 2.4 Aromatic region of the 1H NMR spectra of dialdehydes **2.10a-d**.

In Figure 2.5, a linked set of ring flipping processes of [6.2](7,1)pyrenophane **2.10a** that connect the *syn*, *anti*, *syn'* and *anti'* conformations is shown, which can be generalized to higher homologues **2.10b-d**. Even though **2.10b-d** appear to have highly populations of

anti conformations, the broad signals in **2.10b-d** (which undergo successful intramolecular McMurry reactions) suggest relatively easy *anti/anti'* interconversion (Figure 2.4). This interconversion has to pass through a *syn* or *syn'* conformation and thus the *syn* conformation must be accessible at room temperature and would be expected to be even more populated at the higher temperature of the McMurry reaction. In contrast, the sharper highfield signals in the spectrum of **2.10a** (which undergoes unsuccessful intramolecular McMurry reaction) points to a less accessible *syn* conformation. Consequently, intramolecular McMurry reaction of **2.10a** could not occur, because in the *anti* conformation, the two formyl groups are too far away from one another to undergo reductive coupling. It is worth mentioning that the highest homologue **2.10d**, shows the least populated *anti* conformation among the other homologous series.

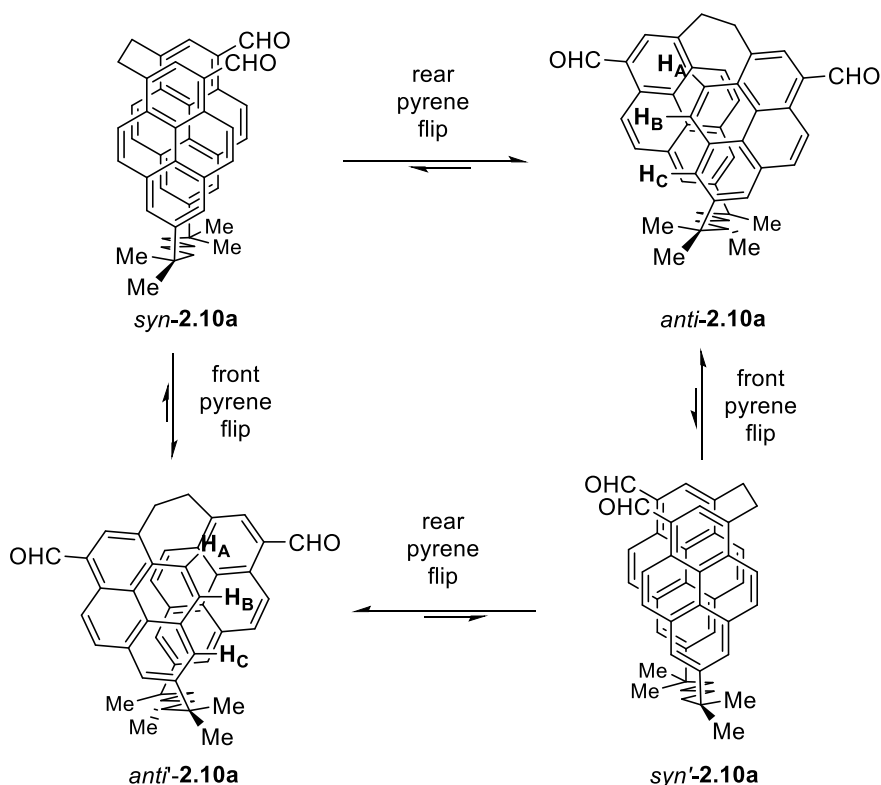


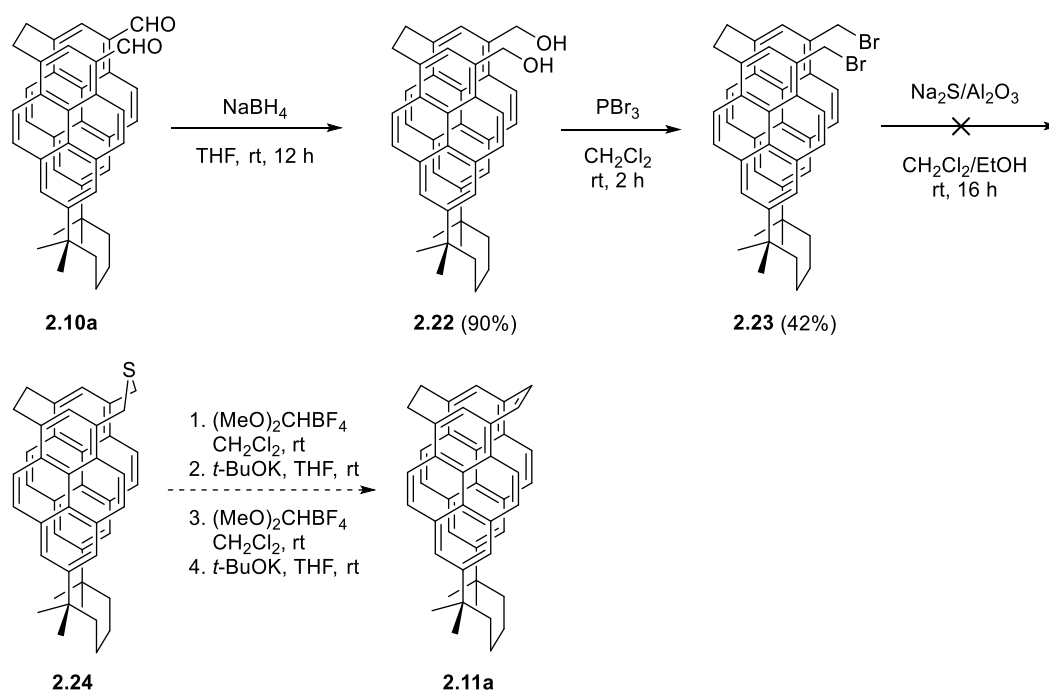
Figure 2.5 Conformational ring flip of pyrenophane **2.10a**.

2.4.2 Attempted Synthesis of 1,1,6,6-Tetramethyl[6](2,11)teropyrenophane through the Thiacyclophane-based Pathway A

Most of the reported pyrenophane syntheses proceed through a dithiacyclophane intermediate that is prepared from a tetrakis(bromomethyl) precursor. As such, they can be classified as Type I strategies (Chapter 1). In all of these cases, the dithiacyclophane was converted into the corresponding cyclophanedienes by a four-step sequence consisting of *S*-methylation, thia-Stevens rearrangement, *S*-methylation and Hofmann elimination. The use of this approach in the synthesis of teropyrenophanes had not been attempted because more direct methods for forming the two-carbon bridges (McMurry reactions and Wurtz coupling) had been discovered. The failure of the **2.8a** and **2.10a** to undergo an intermolecular McMurry reaction prompted the investigation of using a thiacyclophane-based approach (Scheme 2.6). Accordingly, dialdehyde **2.10a** was reduced using NaBH₄ to afford diol **2.22** in 90% yield. The crude diol¹⁷ was treated with PBr₃ in dichloromethane to give dibromide **2.23** (42%). Purification of this dibromide was problematic, presumably due to hydrolysis of the labile benzylic bromides during extraction and chromatography. To avoid this problem, crude dibromide **2.23** was reacted with Na₂S/Al₂O₃.¹⁸

According to TLC analysis, a new compound was obtained. The bright blue fluorescence of the new spot suggests that there are no bromides present. The aromatic region of the ¹H NMR spectrum of this compound, like all of the other [6.2]pyrenophanes, shows high field chemical shifts for one of the protons and very high field chemical shifts for the *K*-region protons (AB system). These aspects of the ¹H NMR spectrum are very similar to crude dibromide **2.23** and even dialdehyde **2.10a**, which suggests that it is an unclosed compound but not clearly the alcohol (because it is not mobile on column

chromatography, while the unknown compound was purified chromatographically). LCMS analysis indicates a signal at $m/z=637$, which corresponds to a compound with a molar mass of 636 g/mol. This does not match any of the conceivable products of this reaction. Therefore, the exact nature of substituents at this point of time is unclear and the compound identity could not be determined.



Scheme 2.6 Attempted synthesis of 1,1,6,6-tetramethyl[6](2,11)teropyrenophane (**2.6a**) through a thiacyclopentane-based pathway A.

The only difference between **2.10a** and **2.23** is the nature of the substituents. It thus appears as though the general conformational preference of the cyclophane skeleton is responsible for the failure of **2.10a** and **2.23** to afford [*n*.2.2](7,1,3)cyclophanes. To confirm that the crude dibromide **2.23** also has a strong preference for the *anti* conformation, the ¹H

NMR spectrum was investigated. Since the isolation of dibromide **2.23** in pure form was problematic, it seemed reasonable to conduct a study of cyclophane **2.20a** instead.

2.4.3 VT-NMR Spectra and Conformational Behaviours of $[n.2](7,1)$ Pyrenophanes **2.20a** and **2.20b**

The conformational behavior of cyclophanes has been of interest for several decades and the main tool for investigating such processes is ^1H NMR spectroscopy.¹⁹ To address the issues in both synthetic routes, the ^1H NMR spectrum of cyclophane **2.20a** was investigated in detail and compared to that of the higher homologue **2.20b** (Figure 2.6).

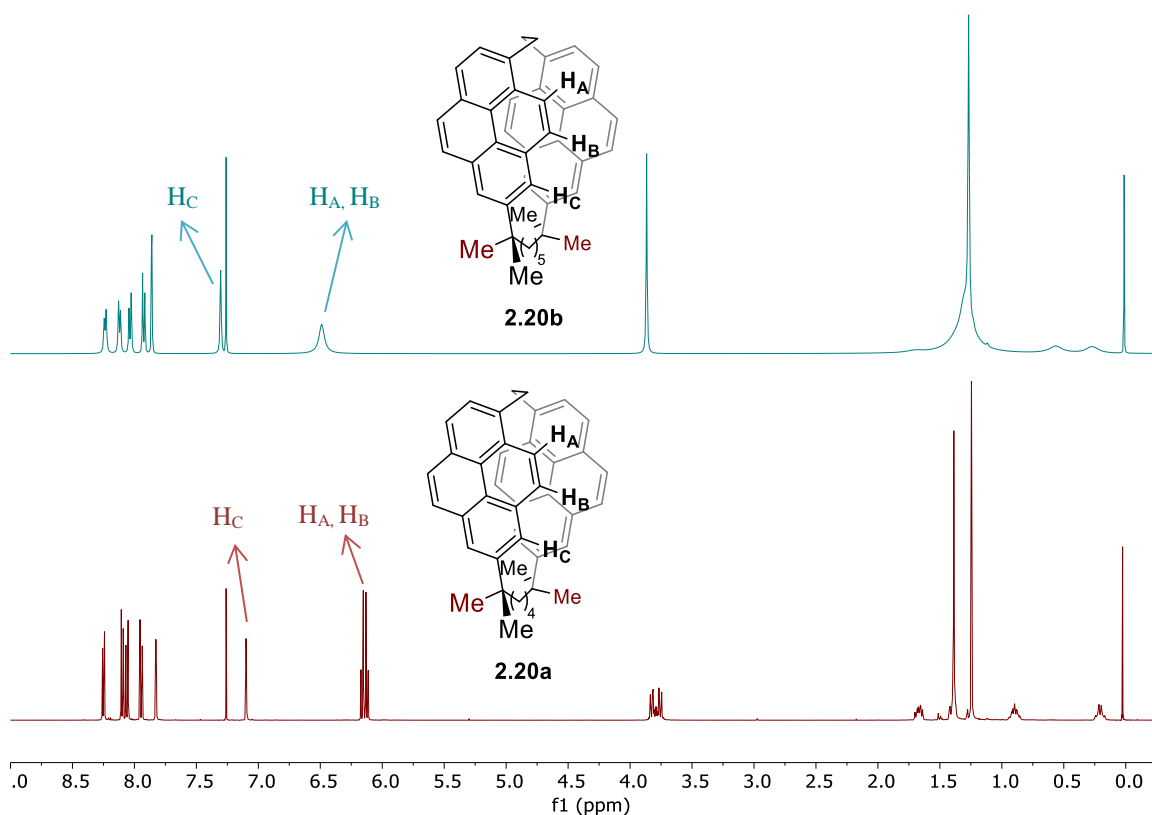


Figure 2.6 The ^1H NMR spectra of $[n.2](7,1)$ pyrenophanes **2.20a** and **2.20b**.

All of the signals in the ^1H NMR spectrum of cyclophane **2.20b** are broad, especially those in the aliphatic region and the highest field aromatic protons, which are due to *K*-region protons closest to the two-atom bridge. Clearly room temperature is not very far from the temperature of coalescence. The energy barrier (ΔG^\ddagger) for the *anti/anti'* interconversion was determined using a VT-NMR experiment (Figure 2.7).

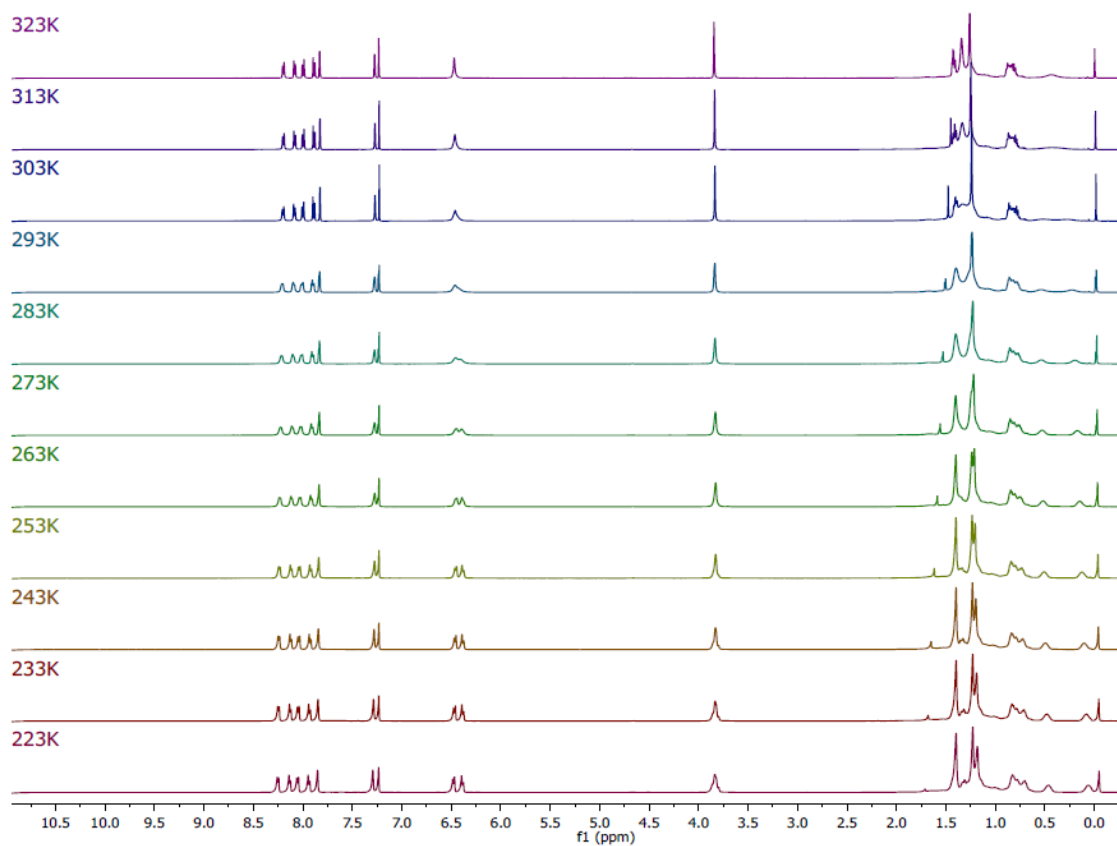


Figure 2.7 500 MHz VT-NMR spectrum of [7.2](7,1)pyrenophane **2.20b**.

At $-50\text{ }^\circ\text{C}$ (223 K), the aliphatic region of the spectrum of **2.20b** contained two signals for methyl groups (δ 1.25, 1.21) and one somewhat broad singlet (δ 3.86) for the bridging unit. The *K*-region protons appeared as a somewhat broad AB system (δ 6.51-

6.40). Upon heating, the methyl signals broadened and ultimately coalesced at 10 °C ($T_c=283$ K, $\Delta G^\ddagger=14.3$ kcal/mol).

In contrast to **2.20b**, the ^1H NMR spectrum of **2.20a** is very-well resolved at room temperature. At 95 °C (368 K), the two methyl signals had broadened, but were clearly not close to coalescence (Figure 2.8). The shape of these signals resembled those of **2.20b** at -50 °C (223 K), *i.e.* 60 K below the T_c . Assuming that the spectrum of **2.20a** is also 60 K below T_c , then T_c for **2.20a** would be 155 °C (428 K), and $\Delta G^\ddagger=20.8$ kcal/mol.

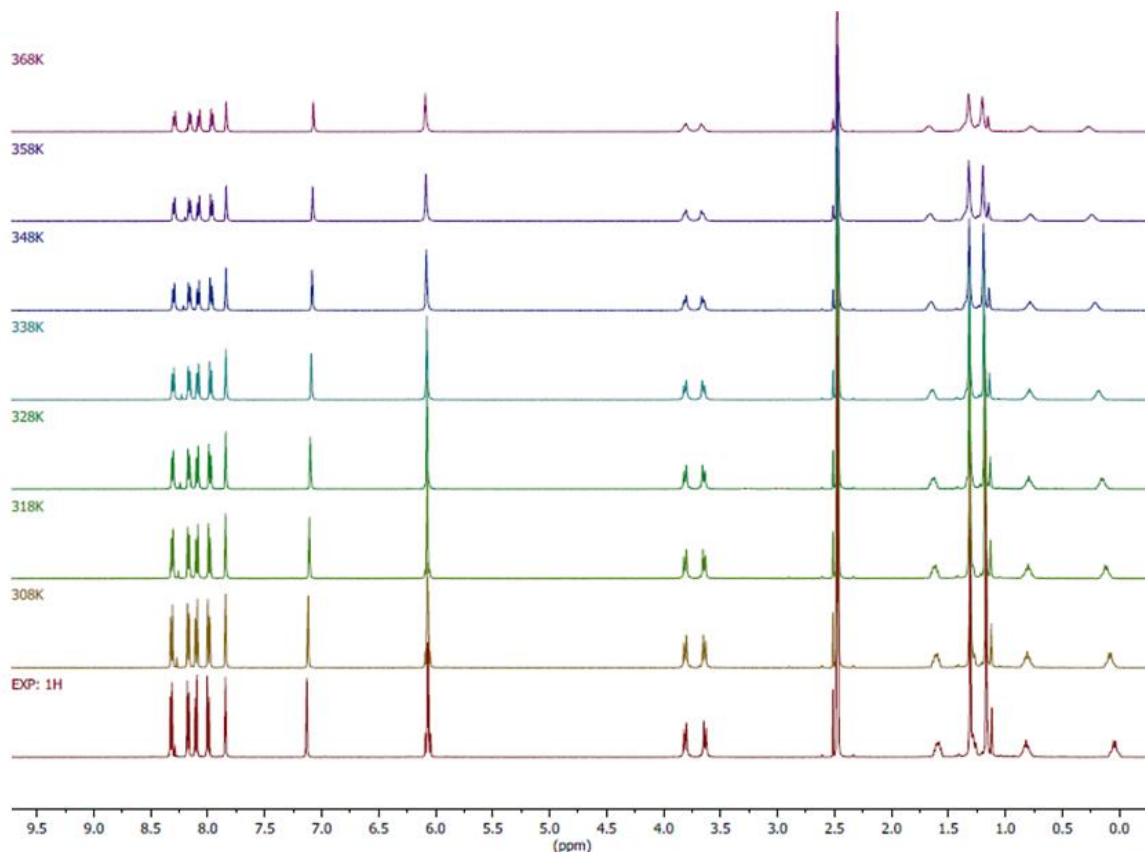


Figure 2.8 500 MHz VT-NMR spectrum of **2.20a**.

From previous work and work described above, it is clear that moving from a seven-

carbon bridge to a six-carbon bridge in both the $[n.2](7,1)$ cyclophane and $[n.2](7,1)$ cyclophanemonoene series has dire consequences for the formation of the final two-carbon bridge. Experimental and computational results both support the conclusion that a strong preference for an *anti* conformation that places key functional groups too far away from one another to undergo coupling is the main issue. The definitive identification of the underlying reasons for the observed behaviour is a challenging prospect because of the flexibility of the long bridge and the large number of conformations that are available to it. Nevertheless, some insight can be gained from what is known about the conformational behaviour of small cyclophanes.²⁰ Recognizing that the 1,7-substituent pattern in the pyrene system orients the bonds to the substituents at a 120° angle, comparisons to cyclophanes with meta-substituted benzene rings (metacyclophanes) are appropriate (Figure 2.9).

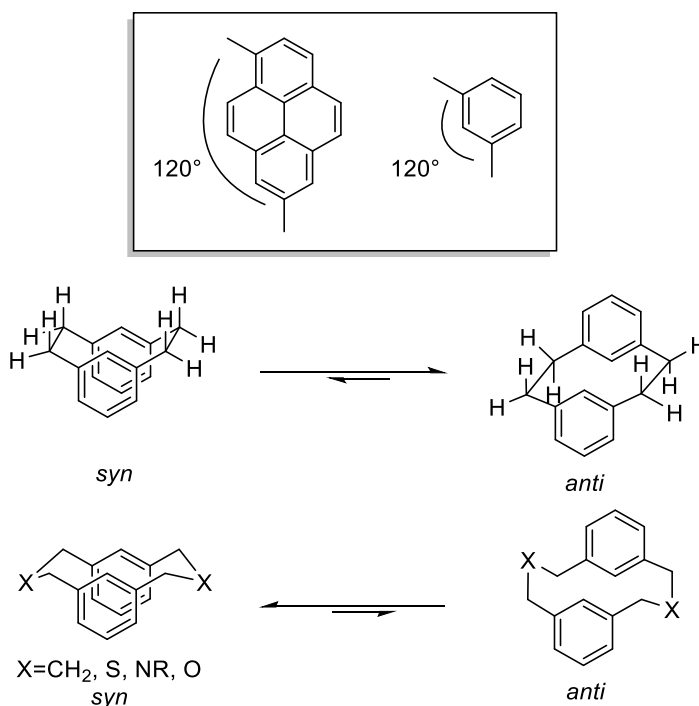


Figure 2.9 Conformational preference in $[n.n]$ metacyclophanes.

It is known that [*n.n*]metacyclophanes exhibit a clear preference for either the *anti* or *syn* conformation depending upon whether the value of *n* is odd or even. [2.2]Metacyclophane shows strong preference for the *anti* conformation (*ca.* 10 kcal/mol)^{21a} and this is attributable to the conformation of the bridges. In the *anti* conformer, the ethano bridges are staggered, whereas those in the *syn* conformer are eclipsed.^{21b} In contrast, the *syn* conformer of [3.3]metacyclophane (and various hetero[3.3]metacyclophanes) has fully staggered bridges and is the preferred conformation. Torsional strain (eclipsing) in the corresponding *anti* conformation is unavoidable. The odd-even trend continues in the [4.4]metacyclophane and [5.5]metacyclophane and the origin of the effect can be traced back to the preference of the aliphatic bridges for maximally staggered conformations.

The problematic pyrenophane systems were the [6.2](7,1)pyrenophanes and the [6.2](7,1)pyrenophanemonoenes. In both cases, both bridges have even numbers of carbon atoms. Provided that the trends in the metacyclophanes are transferable to the [*n.2*](7,1)pyrenophanes, one would expect a preference for the *anti* conformation for [6.2](7,1)pyrenophane **2.20a**. As discussed above, this is indeed the case. Upon moving to [7.2](7,1)pyrenophane **2.20b**, the bridges are odd and even, which would lead to the prediction of a less pronounced preference for the *anti* conformation. In fact, the ¹H NMR data show lower field chemical shifts for H_A, H_B, and H_C than for **2.20a** (see Figure 2.6 and Figure 2.10), which may indicate a somewhat more populated *syn* conformation. The extra carbon in the long bridge also introduced easier conformational mobility, as evidenced by the VT-NMR experiment. In the case of dialdehydes **2.10a-d**, it appeared as though *anti* conformers were dominant for **2.10a-c** (and possibly even for **2.10d**). This suggests that it

is the two-atom bridge that more heavily influences the *syn/anti* isomerism than the long bridge in the $[n.2](7,1)$ pyrenophanes and that change in reactivity (in going from $n=7$ to $n=6$) is mainly due to a big change in the energy barrier to critical *anti/anti'* interconversion (which passes through *syn/syn'*) and not necessarily the innate *syn/anti* preference. Having identified the two-atom bridge in the $[n.2](7,1)$ pyrenophanes as the main reason for the failure of the synthetic work aimed at 1,1,6,6-tetramethyl[6](2,11)teropyrenophane, it was decided to replace this bridge with a three-atom bridge with the intention of favouring the *syn* conformation at the point where the third bridge was to be installed.

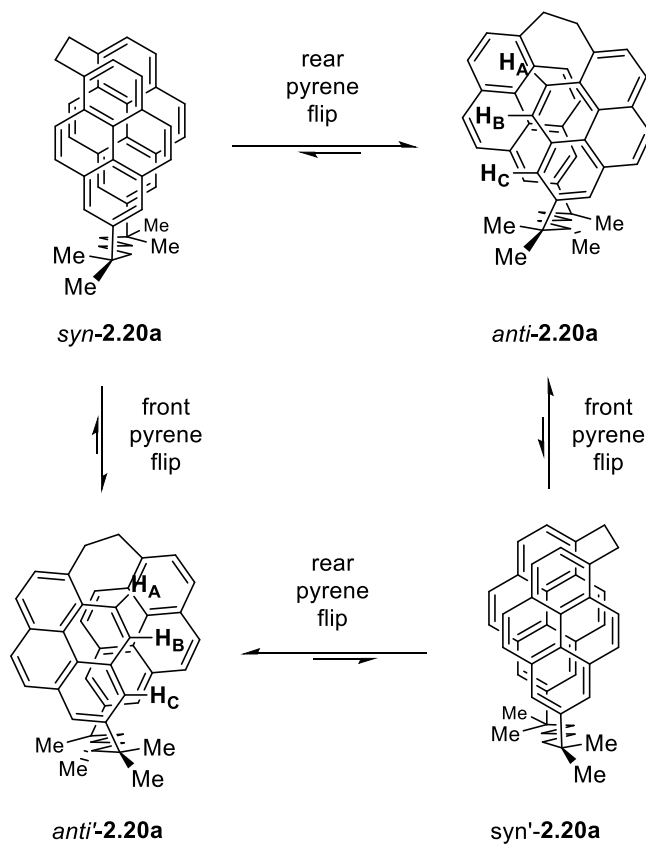
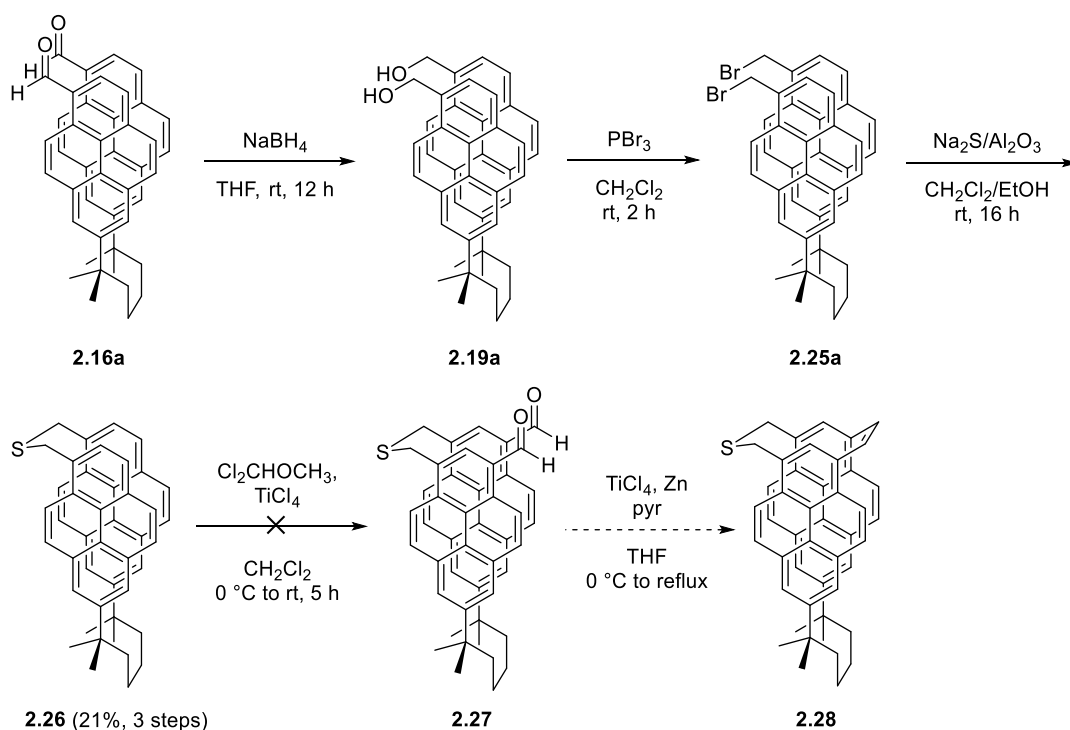


Figure 2.10 Conformational ring flip of [6.2](7,1)pyrenophane **2.20a**.

2.4.4 Attempted Synthesis of 1,1,6,6-Tetramethyl[6](2,11)teropyrenophane through the Thiacyclophane-based Pathway B

The first choice for a three-atom bridge was CH_2SCH_2 because of the tremendous amount of precedent for its use in cyclophane chemistry as a precursor to a CH_2CH_2 or $\text{CH}=\text{CH}$ bridge (Scheme 2.7).^{9,21a} Accordingly, dialdehyde **2.16a** (3 steps from dimethyl adipate, Scheme 2.5) was converted into diol **2.19a** using NaBH_4 . The crude product was of good purity (^1H NMR analysis) and was used without chromatographic purification. Reaction of **2.19a** with PBr_3 afforded dibromide **2.25a**, which was also used without chromatographic purification to avoid hydrolysis back to **2.19a**. Treatment of crude **2.25a** with $\text{Na}_2\text{S}/\text{Al}_2\text{O}_3$ furnished thiacyclophane **2.26** in 21% yield over 3 steps.



Scheme 2.7 Attempted synthesis of 1,1,6,6-tetramethyl[6](2,11)teropyrenophane (**2.6a**) through the thiacyclophane-based pathway B.

The ^1H NMR spectrum of **2.26** (Figure 2.11) contains relatively sharp singlets at δ 1.45 (12H) and 4.35 (4H) for the methyl protons and the CH_2SCH_2 protons, respectively. This indicates that, **2.26** undergoes a rapid conformational process at room temperature, which exchanges the environment of the diastereotopic CH_2S and $(\text{CH}_3)_2\text{C}$ protons. A sharp AB system is observed at δ 6.60 and 6.36 ($J=9.3$ Hz) for H_A and H_B , and a doublet δ 7.44 ($J=1.7$ Hz) for H_C . These high field chemical shift are similar to those for **2.20a**, which strongly suggests that the *anti* conformation is highly populated. Thus, the introduction of

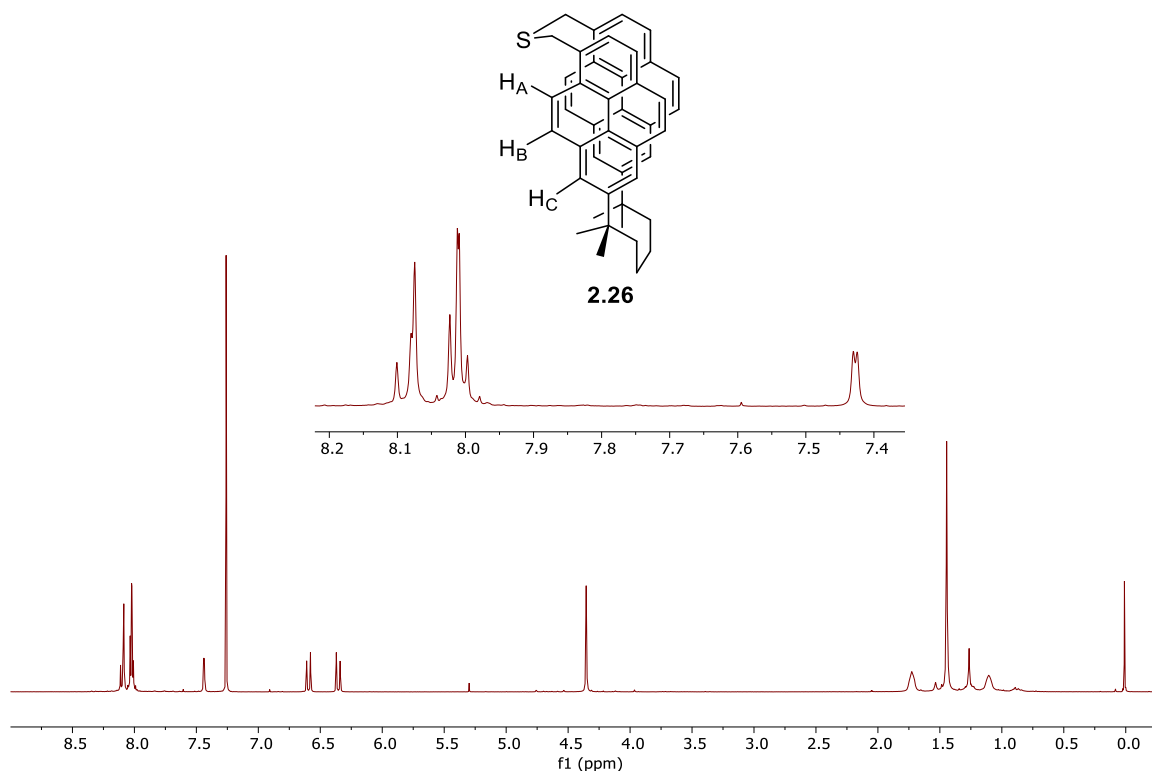


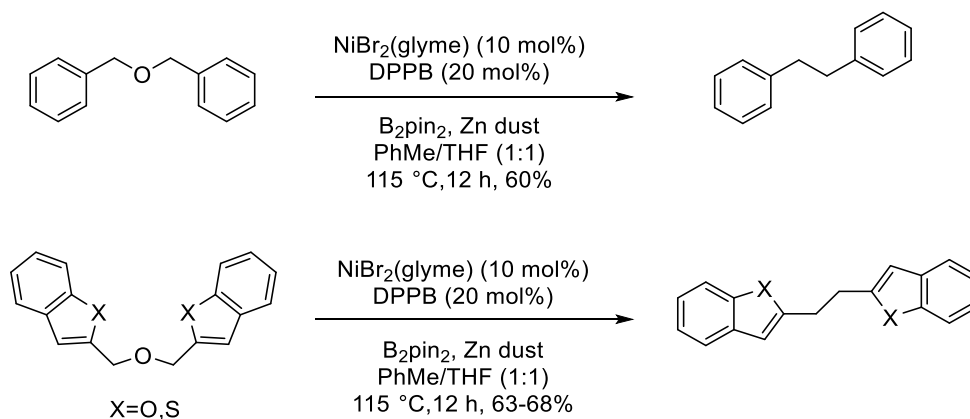
Figure 2.11 The ^1H NMR spectrum of thiacyclophane **2.26**.

the three-atom CH_2SCH_2 bridge did not appear to have led to the expected preference for the *syn* conformation. However, the expansion of the two-atom bridge in **2.20a** to a three-

atom bridge in **2.26** did lower the barrier to *anti/anti'* interconversion significantly. Based on the observation that the ^1H NMR spectrum of **2.26** is sharp and that of [7.2](7,1)pyrenophane **2.20b** is broad, it appears as though the conformational process in **2.26** has an even lower energy barrier than **2.20b**. This means that the *syn* conformers suitable for McMurry reaction should be accessible. Since the dialdehyde **2.10b** derived from **2.20b** undergoes successful intramolecular McMurry reaction, it was expected that dialdehyde **2.27** would do same. However, despite several attempts, Rieche formylation of **2.26** was unsuccessful. It seems very likely that the thioether bridge in **2.26** was cleaved during Rieche formylation. Therefore, it was decided to replace the thioether bridge (CH_2SCH_2) with an ether bridge (CH_2OCH_2) with the aim of providing better chemical stability during the formylation. Importantly, methodology is available for the deoxygenation of ethers to give an alkane (see below).

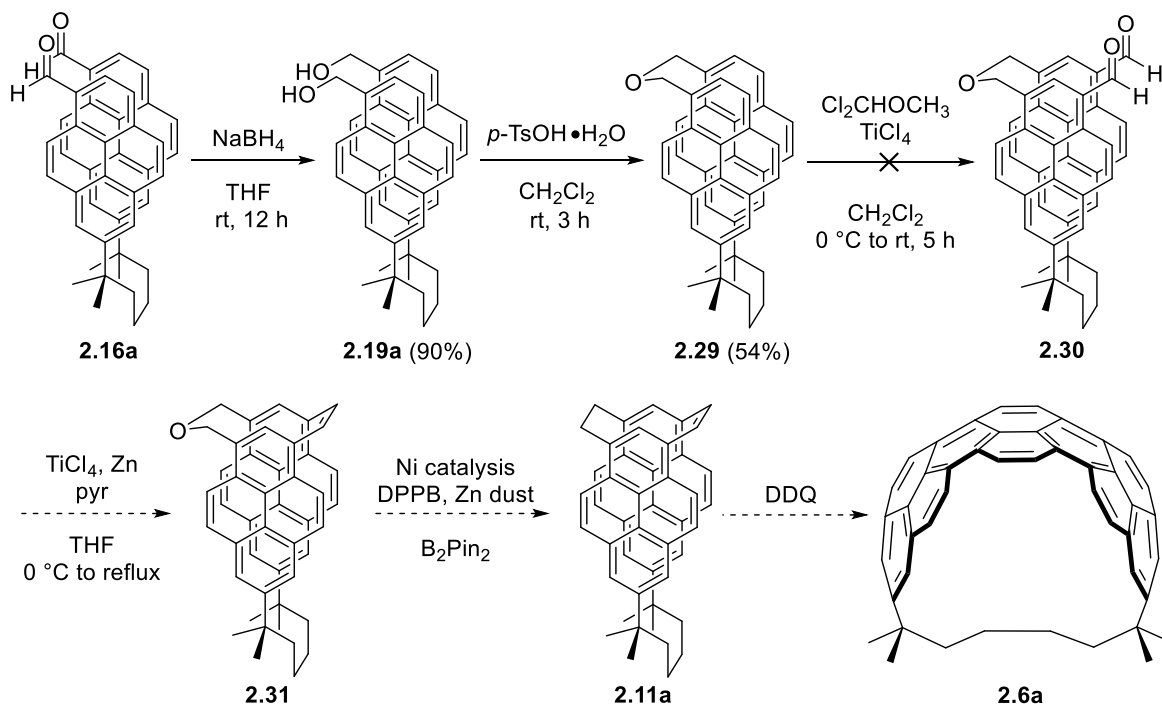
2.4.5 Attempted Synthesis of 1,1,6,6-Tetramethyl[6](2,11)teropyrenophane through an Oxacyclophane-based Pathway A

Cao and Shi reported the synthesis of 1,2-diarylethanes *via* direct deoxygenation of diaryl ethers to form carbon-carbon bonds in the presence of a Ni catalyst, 1,4-bis(diphenylphosphino)butane (DPPB) and Zn dust at 115 °C (Scheme 2.8).²² These conditions could be used as a means for the deoxygenation of an oxacyclophane intermediate to form a $\text{CH}_2\text{--CH}_2$ bridge. With this knowledge, a different synthetic plan was designed to synthesize [6](2,11)teropyrenophane **2.6a** (Scheme 2.9).



Scheme 2.8 Reductive deoxygenation of diaryl ethers reported by Cao and Shi.

Dialdehyde **2.16a** was reduced with NaBH_4 to furnish diol **2.19a** in 90% yield. It was found that **2.19a** could be converted into oxacyclophane **2.29** in 54% yield upon reaction with *p*-toluenesulfonic acid in dichloromethane. As with thiacyclophane **2.26**, all



Scheme 2.9 Attempted synthesis of 1,1,6,6-tetramethyl[6](2,11)teropyrenophane (**2.6a**) through an oxacyclophane-based pathway A.

attempts to produce dialdehyde **2.30** via Rieche formylation failed. Again, all of the starting material was consumed. Only a bright yellow spot on the baseline was observed by TLC analysis. The ^1H NMR spectrum of oxacyclophane **2.29** (Figure 2.12) is very similar to that of thiacyclophane **2.26**, which suggests that it also has a highly populated *anti* conformation (δ 7.46 (d, J =1.6 Hz), δ 6.86 (d, J =9.2 Hz), δ 6.37 (d, J =9.3 Hz)) and is conformationally mobile at room temperature (δ 5.23 (s, 4H), δ 1.44 (s, 4H)).

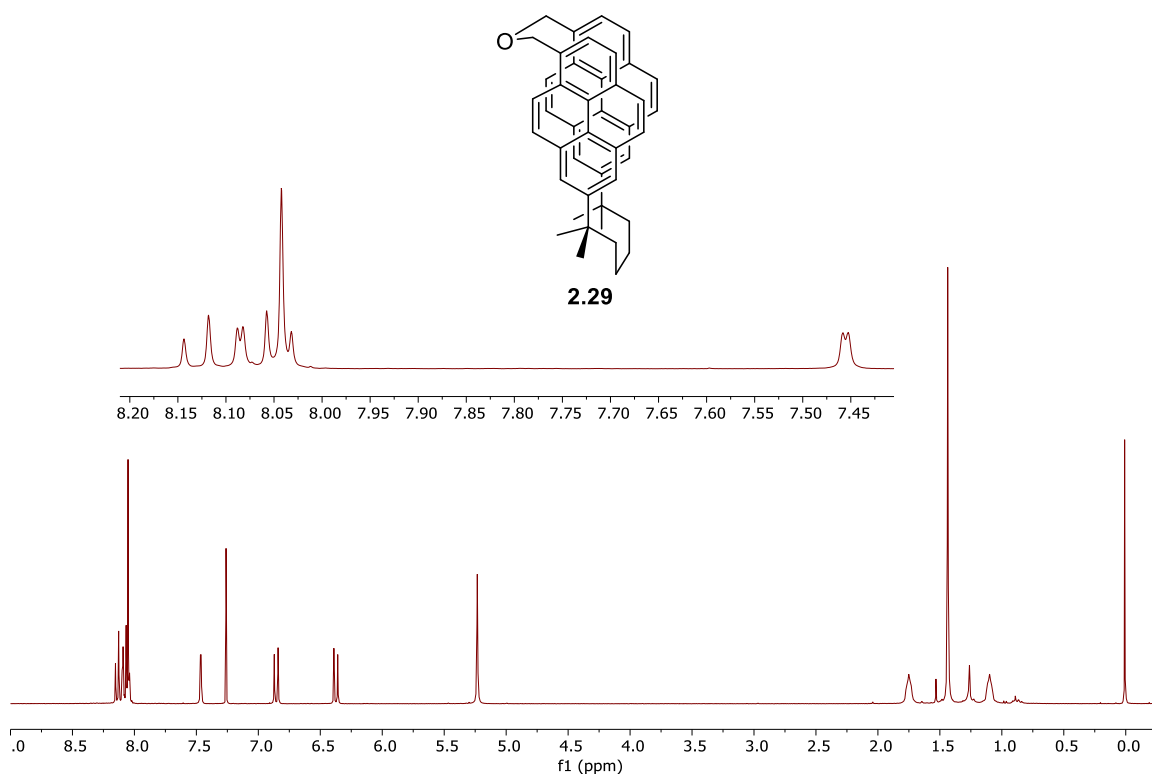
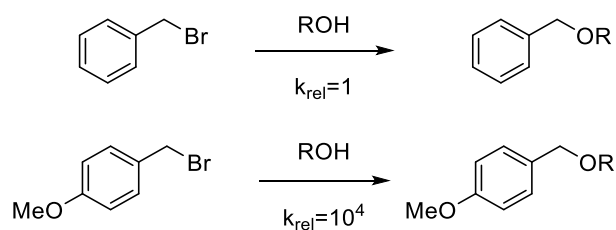


Figure 2.12 The ^1H NMR spectrum of oxacyclophane **2.29**.

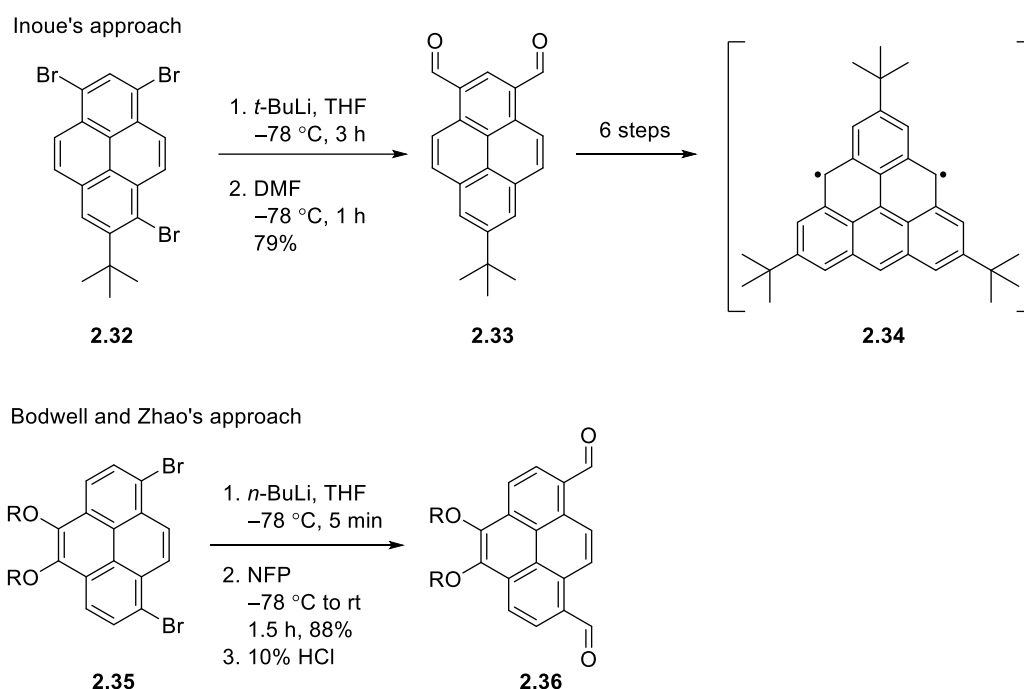
Rieche formylation had been found to be the most reliable reaction to afford dialdehydes **2.16a-d** and **2.10a-d** in short reaction times, but it failed to deliver dialdehydes **2.27** and **2.30** most likely due to cleavage of their three-atom bridges. Ethers and thioethers are normally compatible with Rieche formylation conditions,^{23a} so it would appear that the

ether and thioether functionalities in **2.26** and **2.29** are unusually reactive. The large orbital coefficient (high electron density) of pyrene at the 1,3,6,8-positions, which contributes strongly to the preference for electrophilic aromatic substitution at these positions, would also be expected to provide strong stabilization for developing positive charge at carbon atoms attached to these positions. As such, any atom that could function as a leaving group would be more prone to leaving than at a normal benzylic site, especially in the presence of a Lewis acid such as TiCl_4 . In this regard, it has been observed previously in the Bodwell group and during the course of this investigation that 1-(bromomethyl)pyrene derivatives undergo facile hydrolysis to the corresponding 1-(hydroxymethyl)pyrene derivatives during aqueous workup and even column chromatography. This is comparable to benzyl bromide and 4-methoxybenzyl bromide, the latter of which undergoes solvolysis (hydrolysis) $\sim 10^4$ times faster than the former due to stabilization of development positive charge as the leaving group leaves (Scheme 2.10).^{23b} Thus, for **2.26** and **2.29** the observation of a bright yellow spot on the baseline of the TLC is consistent with formylation of the pyrene system and the observation that they cannot be induced to move off the baseline is consistent with ether/thioether cleavage to leave polar functionality. The vanishingly low solubility of the products prevented the determination of exactly what these functionalities are.



Scheme 2.10 Solvolysis rate of benzyl bromide and 4-methoxybenzyl bromide.

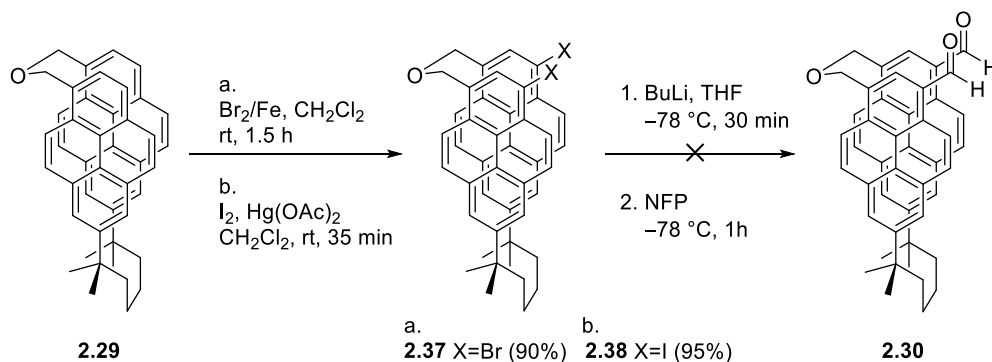
To avoid problematic Rieche formylation, an alternative approach was sought. Bromination by electrophilic aromatic substitution by a halogen-metal exchange/formylation protocol is a well-established method for introducing one or more formyl groups to an aromatic system including pyrene. For example, Inoue²⁴ *et al.* reported the synthesis of dialdehyde **2.33** from tribromide **2.32** and Bodwell and Zhao²⁵ reported the synthesis of ether-containing dialdehyde **2.36** in 88% yield (Scheme 2.11).



Scheme 2.11 Inoue's synthesis of dialdehyde **2.33** and Bodwell's synthesis of dialdehyde **2.36**.

To test the halogenation/formylation approach, **2.29** was reacted with Br₂/Fe in dichloromethane to furnish the dibromo oxacyclophane **2.37** in 90% yield, while the reaction of **2.29** with I₂ in the presence of mercury(II) acetate in the same solvent afforded diiodo oxacyclophane **2.38** in 95% yield. Reaction of both compounds (**2.37** and **2.38**) with BuLi followed by *N*-formylpiperidine (NFP) failed to deliver the desired dialdehyde **2.30**.

TLC analysis showed that after the addition of NFP one immobile spot on the baseline was formed, which is again consistent with a bridge-cleavage reaction. This could happen through two conceivable ways including a simple S_N2 opening reaction in the presence of Bu^- as the nucleophile or a Wittig ring-contraction reaction. Unfortunately, the poor solubility of isolated compound prevented the determination of what exactly was obtained.



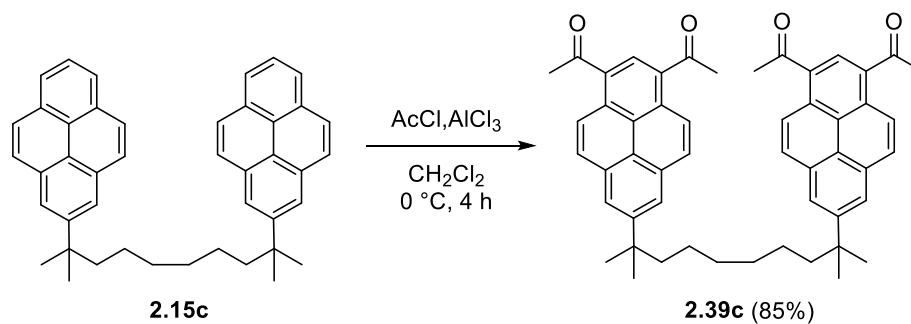
Scheme 2.12 Attempted synthesis of 1,1,6,6-tetramethyl[6](2,11)teropyrenophane (**2.6a**) through an oxacyclophane-based pathway B.

Since, installation of the requisite formyl groups proved to be unsuccessful a different synthetic approach to construct the bridges was necessitated at this stage. In the final attempt to synthesize the [6](2,11)teropyrenophane (**2.6a**), tetrafunctionalization of the dipyrenylalkane **2.15a** was investigated.

2.4.6 Attempted Synthesis of 1,1,6,6-Tetramethyl[6](2,11)teropyrenophane through a Fourfold Functionalization-based Approach

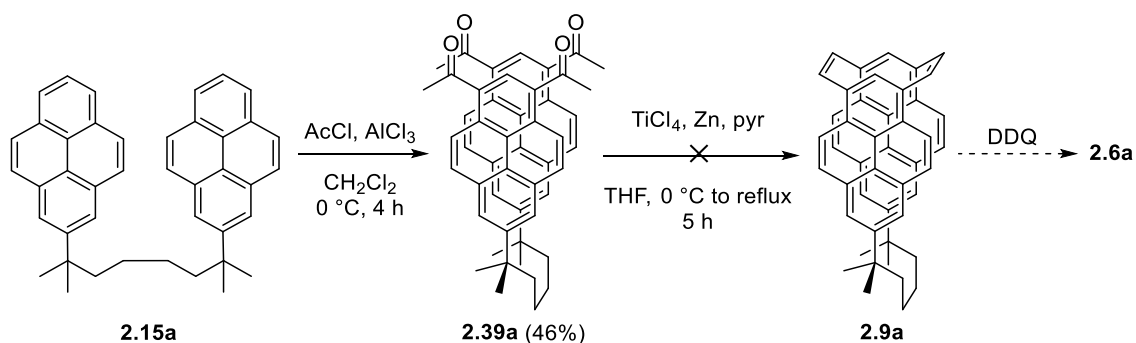
As discussed in Section 2.2.1, the bulky *tert*-alkyl substituents block or reduce the reactivity of the adjacent positions of each pyrene unit in the dipyren-2-ylalkanes **2.15a-d** and thus direct functionalization to occur at the other end of the pyrene systems. Previous

attempts to tetrafunctionalize **2.15a** and **2.15c** using halomethylation, bromination, Rieche formylation and most Friedel-Crafts acylations were unsuccessful owing to various combinations of poor product solubility, over reaction, incomplete reaction and separation issues.⁹ The only exception was the Friedel-Crafts acylation of dipyrren-2-ylalkane **2.15c** with acetyl chloride/ AlCl_3 , which afforded tetraketone **2.39c** in 85% yield (Scheme 2.13).



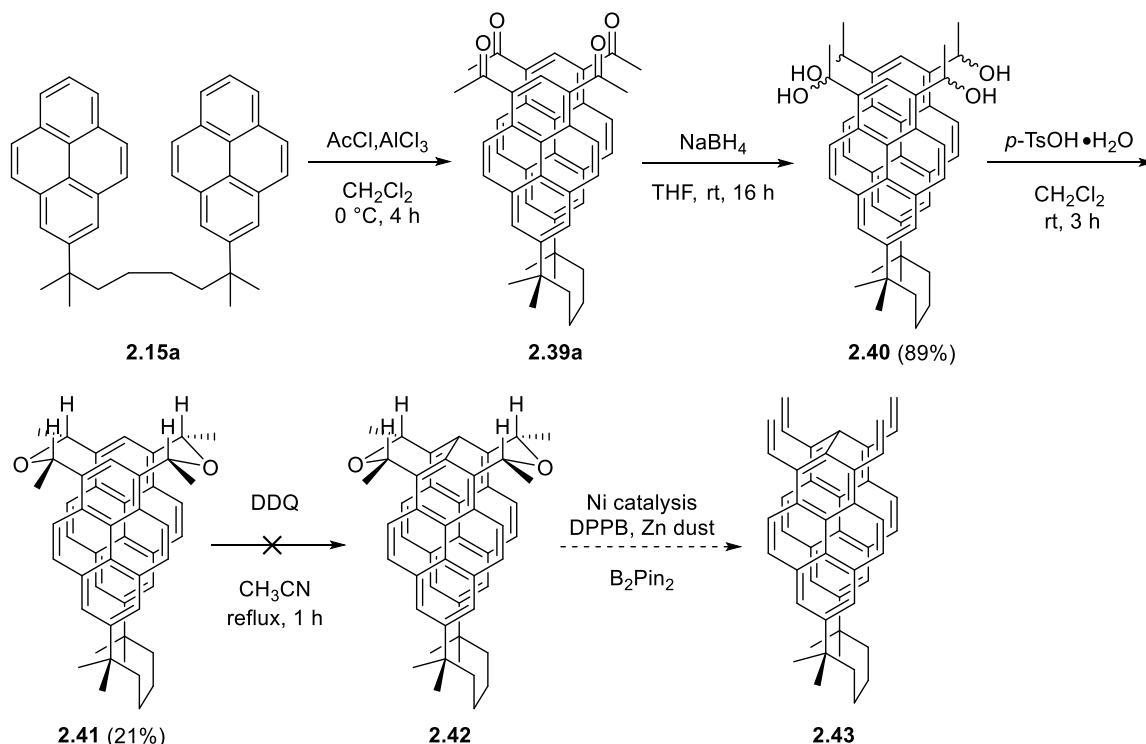
Scheme 2.13 Merner's synthesis of **2.39c** via Friedel-Crafts acylation.

Although this chemistry provided access to a very useful-looking tetraketone system, all attempts to convert it into the corresponding tetraacid (*e.g.* haloform reactions) were unsuccessful. Similarly, the use of other acid chlorides in the Friedel-Crafts acylation did not afford related tetraketones. Interestingly no attempted McMurry reaction to afford [*n.2.2*]pyrenophanediene **2.9c** was reported. To investigate whether tetrafunctionalization would be a viable approach to 1,1,6,6-tetramethyl[6](2,11)teropyrenophane, dipyrren-2-ylalkane **2.15a** was used in a Friedel-Crafts acylation with acetyl chloride/ AlCl_3 . This afforded tetraketone **2.39a** in 46% yield. McMurry reaction of this compound resulted in the formation of mixture of products (TLC analysis), from which no identifiable compound could be isolated (Scheme 2.14). Even if diene **2.9a** or teropyrenophane **2.6a** was formed, the yield would be very low. This being the case, a different approach was investigated.



Scheme 2.14 Failure of McMurry reaction to afford **2.6a**.

In view of the successful formation of oxacyclophane **2.29** from diol **2.19a**, it was decided to reduce **2.39a** with NaBH_4 (Scheme 2.15). This furnished the corresponding tetraol **2.40**, presumably as a mixture of diastereomers, in 89% yield. This polar intermediate was subjected without purification to reaction with *p*-toluenesulfonic acid in



Scheme 2.15 Attempted synthesis of 1,1,6,6-tetramethyl[6](2,11)teropyrenophane through the fourfold functionalization-based approach.

dichloromethane to give dioxacyclophane **2.41** (21%). Although the yield was modest, it is the first cyclophane in the pyrenophane family generated directly from a tetrafunctionalized precursor. The ^1H NMR spectrum of **2.41** has four signals in the aromatic region (1:2:2:2), as well as a single AX_3 system at δ 5.76 (q, $J=6.5$ Hz) and 1.82 ppm (d, $J=6.5$ Hz), which means that a single, highly symmetric diastereoisomer was formed (Figure 2.13). As in the case of simple [3.3]metacyclophanes (Figure 2.14), the CH_2OCH_2 bridges in **2.41** can adapt either *pseudo*-chair or *pseudo*-boat conformations.²⁰

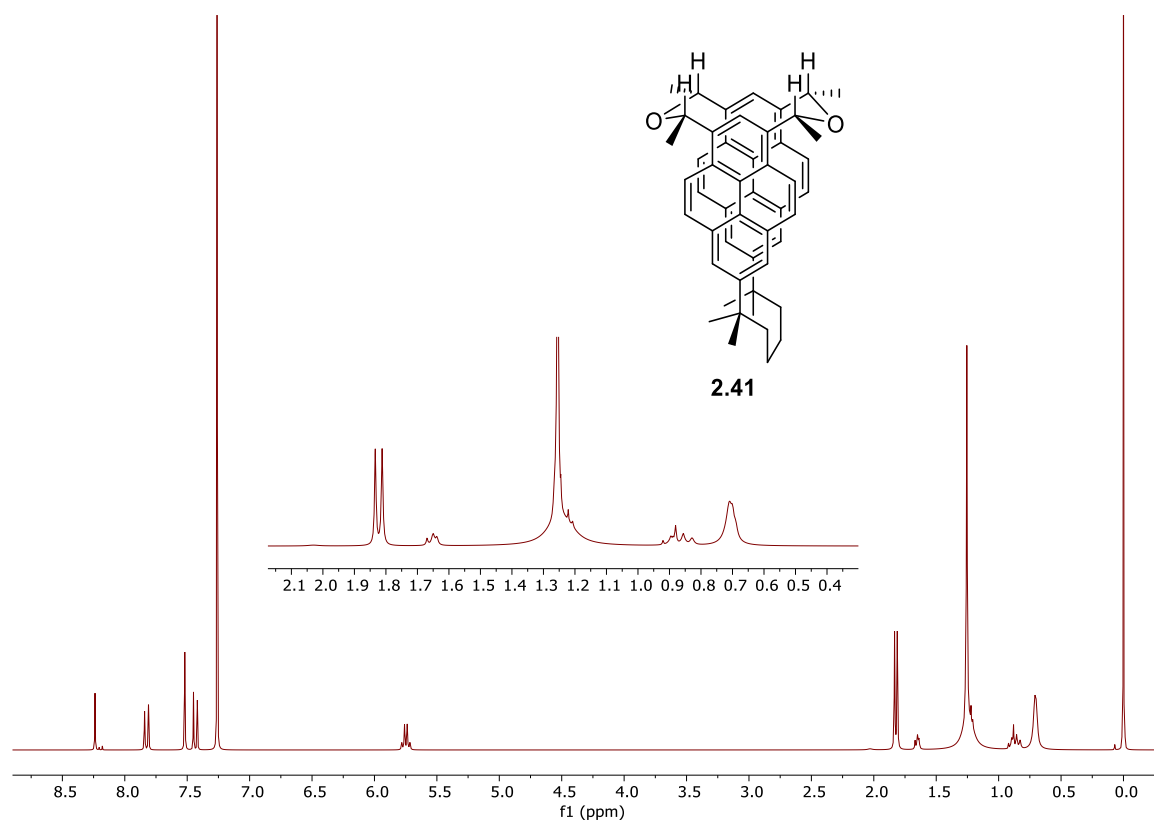


Figure 2.13 The ^1H NMR spectrum of dioxacyclophane **2.41**.

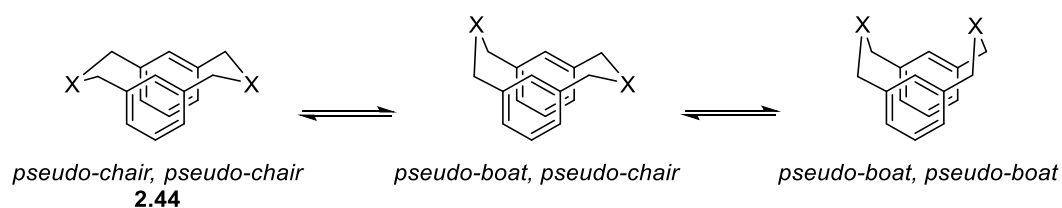


Figure 2.14 Conformational bridge flips in [3.3]metacyclophanes **2.44** (X = CH₂, S, O, NR).

The observation of high symmetry in the ¹H NMR spectrum of **2.41** means that the methyl groups are all symmetry related and that both ether bridges have the same bridge conformation. This limits the possible structures of **2.41** to four possibilities, **2.41A-D** (Figure 2.15). Conformers **2.41A** and **2.41B** can be interconverted by a bridge flip of both ether bridges, and the same is true for **2.41C** and **2.41D**. Based on the examination of molecular models, **2.41B** and **2.41C** appear to have unfavourable steric clashes between

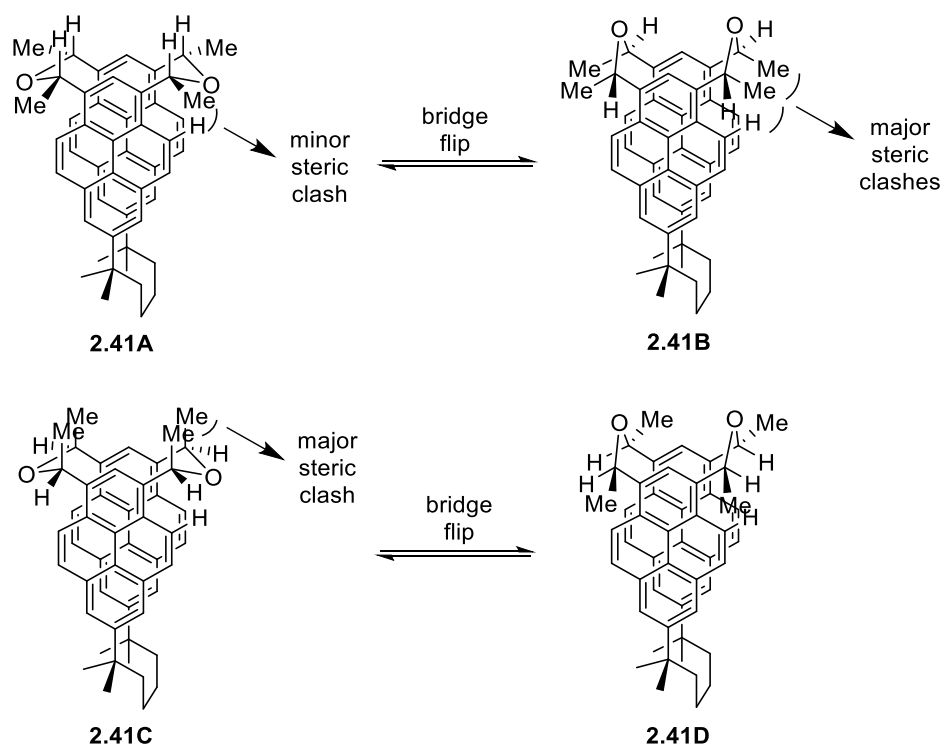


Figure 2.15 Conformational bridge flips in dioxacyclophane **2.41**.

neighbouring groups. Additionally, for **2.41B**, there looks to be an additional unfavourable interaction between the methyl groups and the nearest *K*-region proton. Unfavourable methyl-methyl interactions are not present in **2.41A** and **2.41D**, but it appears as though there may be a small steric interaction in **2.41A** between the methyl groups and the nearest *K*-region proton. At this stage, **2.41D** seemed to be the most likely structure for **2.41**. Structures of **2.41A-2.41D** were calculated at the B3LYP/6-31G(d) level of theory (calculations performed by Prof. Yuming Zhao, Memorial University) and **2.41D** was found to be 7.95 kcal/mol lower in energy than **2.41A**, and far lower in energy than **2.41C** (17.73 kcal/mol) and **2.41B** (39.51 kcal/mol) (Figure 2.16).

The formation of **2.41** as a single isomer deserves some comments. Tetraol **2.40** is

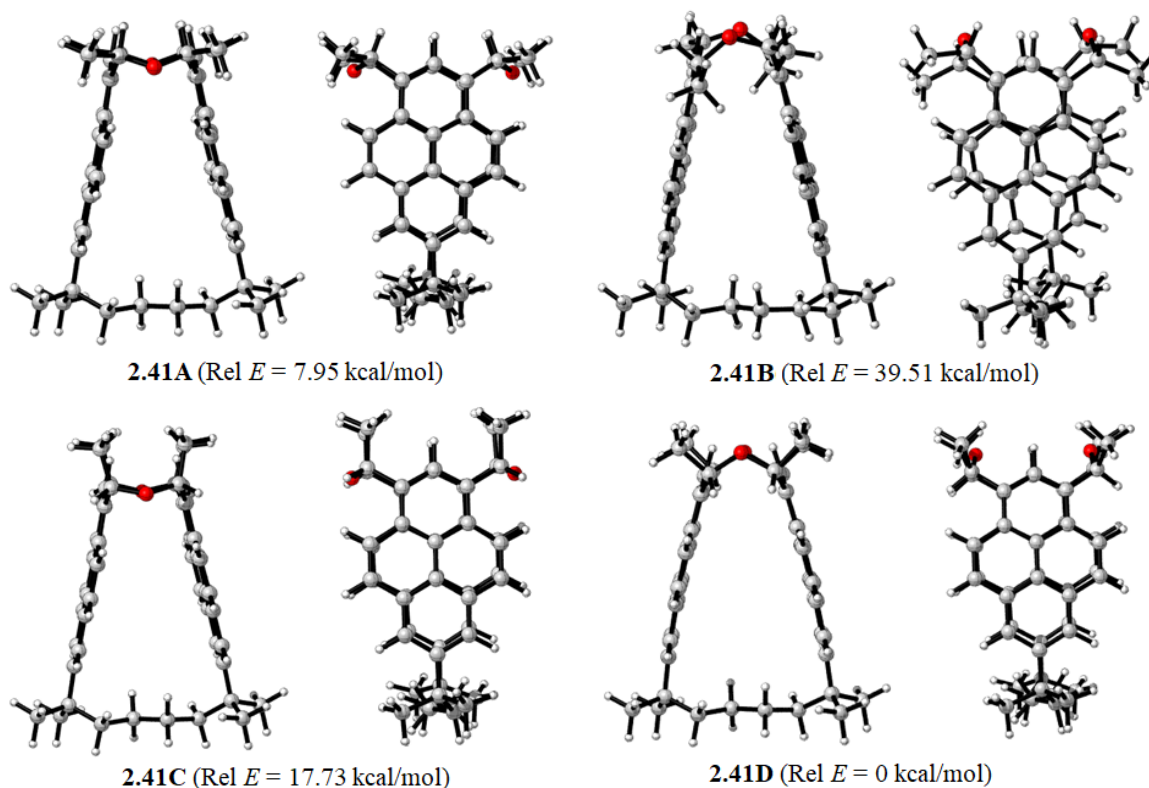
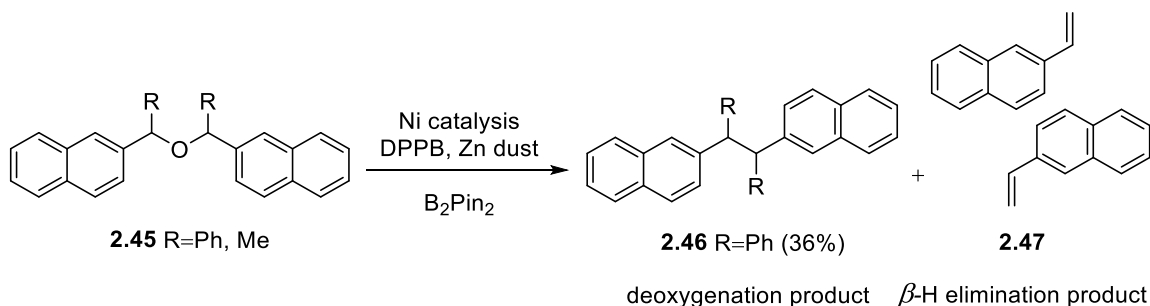


Figure 2.16 Relative energies of **2.41A-2.41D**, calculated at B3LYP/6-31G(d) level of theory.

presumably a mixture of four diastereomers, but only a single diastereomer of **2.41** was found. The low yield of **2.41** (21%) may mean that only the correctly configured isomer of **2.40** leads to **2.41** but another possibility exists. Unlike most cyclophane bridge-forming reactions, which go through an S_N2 mechanism (*e.g.* thiolate-bromide coupling), the acid-catalyzed ether formation leading to **2.41** almost certainly goes through an S_N1 mechanism. As mentioned earlier, the pyrene system should provide strong stabilization to developing positive charge at the benzylic positions, which are now secondary benzylic positions. The intermediacy of benzylic carbocations (destruction of the stereogenic centre), would mean that any of the isomers of **2.40** could lead to **2.41**. This could also mean that other isomers of **2.41** form, but that the stereochemistry is “corrected” through an S_N1 -type equilibration.

The synthesis of **2.41** was a very positive development, but the prospects for the deoxygenation of **2.41** using the Cao and Shi methodology²² were not very good. Cao reported that diether **2.45** (with methyl groups at the α -position of ether) afford the β -H elimination product **2.47** (Scheme 2.16).

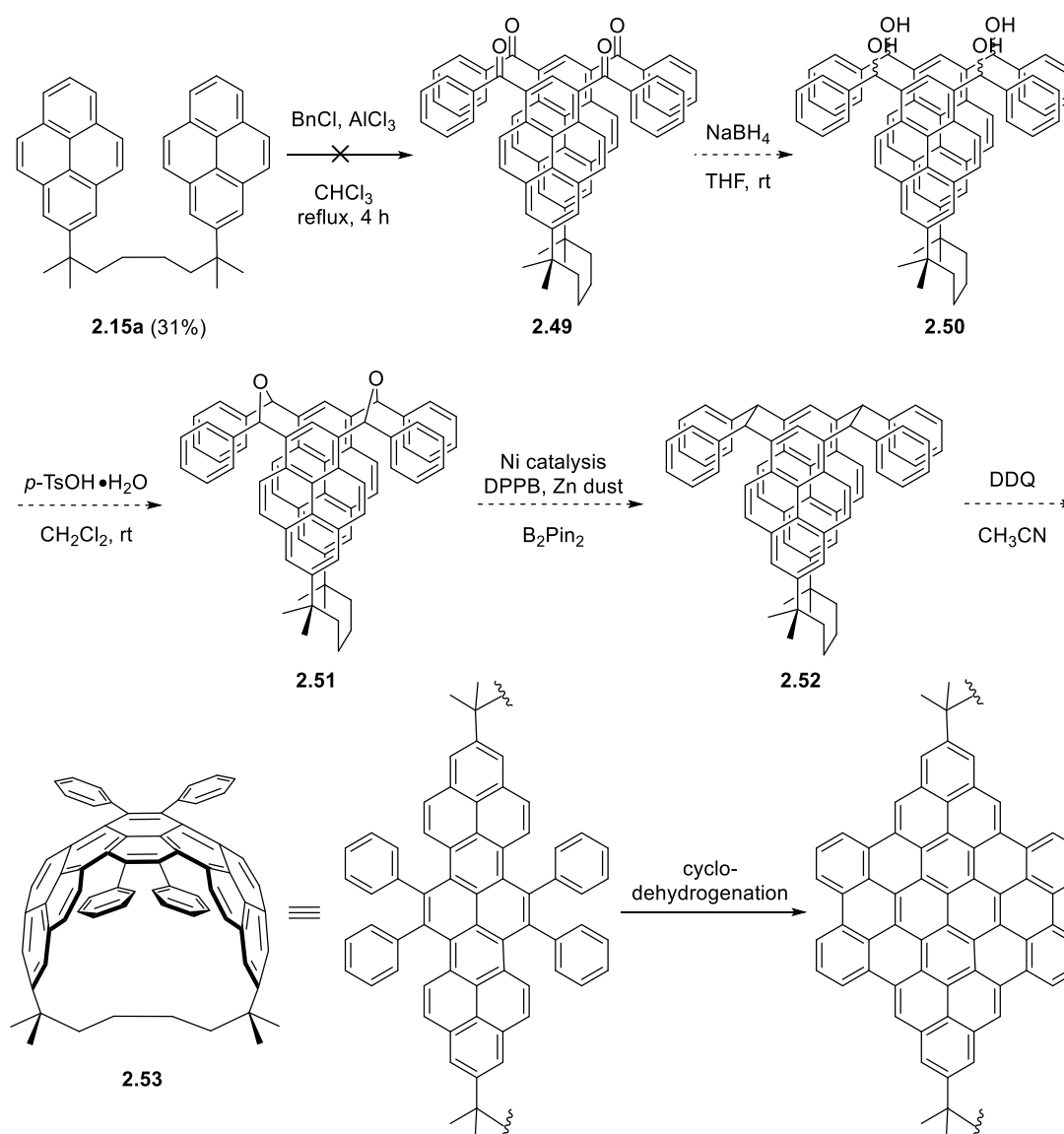


Scheme 2.16 β -H Elimination in the presence of methyl groups at the α -position of ether.

In an attempt to side-step this problem, it was decided to try and form a bond between two pyrene units in **2.41** prior to deoxygenation (Scheme 2.15). If successful, the

application of Cao's deoxygenation to cyclophane **2.42** could still be productive, even if it gave tetravinyl species **2.43**. The enforced proximity of the vinyl groups would suggest that ring closing metathesis (RCM) reaction would have good chances of success to afford **2.6a**. However, reaction of **2.41** with DDQ in CH₃CN (see Chapter 3 for a discussion of the choice of solvent) did not lead to the formation of **2.42**.²⁵ The failure of deoxygenation of diether **2.41** and the expectation that it would undergo elimination upon deoxygenation prompted the investigation of a modified approach.

In an effort to avoid the anticipated elimination reaction leading to tetravinyl **2.43**, the Friedel-Crafts acylation of **2.15a** using benzoyl chloride/AlCl₃ was attempted to afford tetraketone **2.49** (Scheme 2.17). The absence of β -H atoms would prevent the undesired elimination during deoxygenation and carrying this compound through the same synthetic pathway would lead to teropyrenophane **2.53** that contains four phenyl groups. If successful, this synthetic route would not only be shorter than the original double-McMurry route, but also deliver a tetra substituted teropyrenophane, in which the four phenyl groups could conceivably be used to grow the aromatic system. Unfortunately, work aimed at the synthesis of **2.53** failed at the first step as the Friedel-Crafts acylation of **2.15a** with benzoylchloride/AlCl₃ resulted in the formation of a mixture of products (TLC analysis), from which no distinguishable compound could be isolated.



Scheme 2.17 Attempted synthesis of **2.53** through the fourfold functionalization-based approach.

2.5 Summary

The main objective of the work described in this Chapter was to synthesize a 1,1,6,6-tetramethyl[6](2,11)teropyrenophane (**2.6a**), which would have been the new smallest member of the series. The double-McMurry and Wurtz coupling/McMurry that had been successfully applied to higher homologues were found to be unsuitable due to

unfavourable conformational behaviour (strong preference for the *anti* conformation), which prevented the formation of the key third bridge of the direct synthetic precursors to the target teropyrenophane. Therefore, it was decided to replace the two-atom bridge in the [6.2](7,1)pyrenophane **2.20a** (the main reason for the failure of original synthetic routes) with a three-atom bridge with the intention of favouring the *syn* conformation. The two choices for the three-atom bridge were thioether and ether bridges. The expansion of the bridge did not lead to the expected preference for the *syn* conformation, but it did lower the barrier to *anti/anti'* interconversion significantly, which means that the *syn* conformers suitable for McMurry reaction to install the essential third bridge should be accessible. However, thia- and oxacyclophane-based pathways failed in the Rieche formylation step most likely due to cleavage of their three-atom bridges. Application of a milder Lewis acid and the use of a halogenation/formylation approach were also unsuccessful.

To avoid the problematic formylation step, an alternative approach using the fourfold functionalization-based intermediate was sought. Friedel-Crafts acylation of dipyren-2-ylalkane **2.15a** with acetyl chloride/ AlCl_3 provided access to the tetraketone **2.39a**, which was converted into a dioxacyclophane system as a single diastereomer (**2.41D**). This dioxacyclophane, is the first cyclophane in the pyrenophane family, which is generated directly from a tetrafunctionalized precursor. The synthesis of dioxacyclophane **2.41** was a very positive development, but the prospects for the synthesis of the target teropyrenophane through the Scholl reaction and deoxygenation failed due to the ether bridge cleavage in the dioxacyclophane intermediate.

The synthesis of 1,1,6,6-tetramethyl[6](2,11)teropyrenophane (**2.6a**) remained as an unsolved challenge. Despite its relatively high calculated strain energy (80.2 kcal/mol),

all hope for achieving its synthesis should not be abandoned. Future work aimed at the synthesis of **2.6a** will, however, require the development of new synthesis pathways that avoid and/or overcome the problems encountered here.

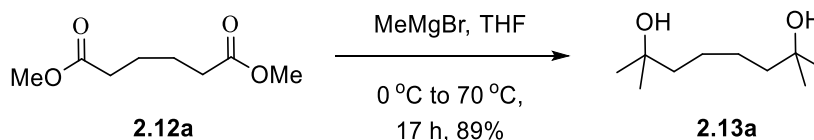
General Experimental Details

All starting materials and reagents were used as received from commercial chemical suppliers (Aldrich, Alfa Aesar, TCI and Fischer Scientific) without further purification. Reactions involving moisture sensitive catalysts and reagents were performed under an inert atmosphere of nitrogen gas using standard Schlenk technique. Either ACS grade or dry (solvent purification system) dichloromethane and tetrahydrofuran were used and hexanes were distilled before use in column chromatography. Organic solvents were removed under reduced pressure by the use of a rotary evaporator and Silica column chromatography was performed using ZEOChem 60 eco 40-63 μm . Compounds on TLC plates were visualized using UV light (254 and 365 nm) and chemical staining methods (phosphomolybdic acid and iodine).

Melting points measured using Mettler automatic digital melting point apparatus. ^1H NMR and ^{13}C NMR spectra recorded on a Bruker AVANCE 500MHz and Bruker AVANCE III 300MHz instruments (CDCl_3 , unless otherwise indicated). Chemical shifts are reported relative to internal standards: $(\text{CH}_3)_4\text{Si}$ (δ 0.00 ppm) and CDCl_3 (δ_{H} 7.26 and δ_{C} 77.16 ppm). High-resolution mass spectrometric data (HRMS) were obtained using Waters Micromass[®] GCT PremierTM instrument. Absorption and fluorescence spectra were recorded on Agilent HP8453A UV-Visible absorbance spectrophotometer and PTI QuantaMaster 6000 spectrofluorometer, respectively. Microwave reactions performed on a CEM discoverer SP microwave synthesizer equipped with explorer-12 hybrid.

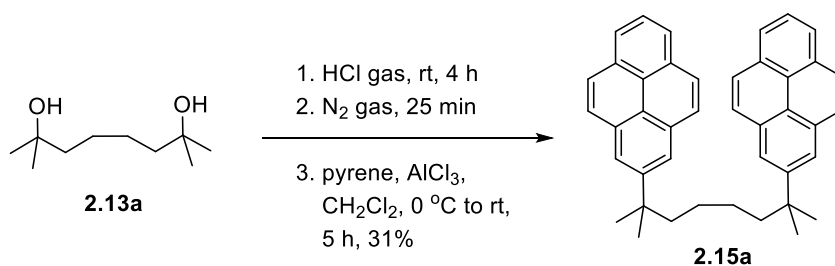
2.6 Experimental Procedures and Characterization Data

2,7-Dimethyl-2,7-octanediol (2.13a)



A solution of dimethyl adipate (**2.12a**) (10.4 g, 59.7 mmol) in anhydrous THF (1000 mL) was added dropwise over a period of 30 min to a stirred 0 °C solution of methylmagnesium bromide (3.0 M in Et₂O, 90 mL, 0.27 mol) under a nitrogen atmosphere (3 L 3-neck round-bottomed flask). After the addition was complete, the reaction mixture was heated at reflux for 17 h. The reaction mixture was cooled to 0 °C. The white cake was then neutralized by the slow addition of saturated ammonium chloride solution (200 mL). Most of the THF was removed under reduced pressure. Ether (500 mL) was added to the resulting mixture. The layers were separated, and the aqueous layer was extracted with ether (2×200 mL). The combined organic layers were washed with brine (200 mL), dried over Na₂SO₄, gravity filtered and concentrated under reduced pressure to afford a white solid, which was recrystallized from hexane to yield compound **2.13a** as a white powder (9.30 g, 89%); *R*_f=0.10 (50% ethyl acetate/hexanes); m.p. 62–63 °C (hexane); ¹H NMR (300 MHz, CDCl₃) δ 1.21 (s, 12H), 1.34–1.37 (m, 4H), 1.47 (s, 2H), 1.46–1.49 (m, 4H); ¹³C NMR (75 MHz, CDCl₃) δ 25.02, 29.30, 44.10, 71.16; HRMS (APPI) calculated for C₁₀H₂₃O₂ [M+H]⁺ 175.1698, found 175.1693.

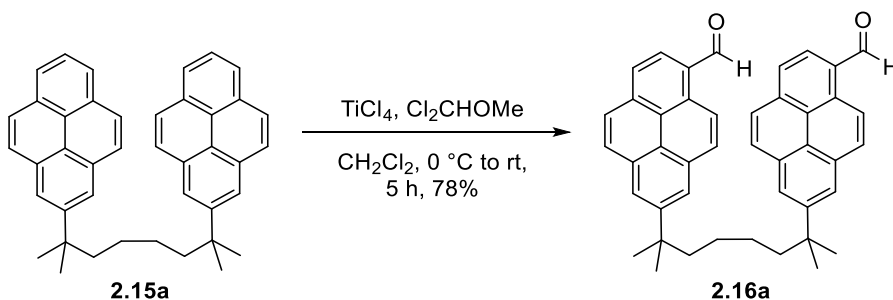
2,7-Dimethyl-2,7-bis(2-pyrenyl)octane (**2.15a**)



Diol **2.13a** (10.1 g, 57.9 mmol) was dissolved in dry dichloromethane (1000 mL, 2 L 3-neck round-bottomed flask) and HCl gas (generated by the dropwise addition of concentrated HCl into 98% sulfuric acid, 2 L 3-neck round-bottomed flask) was purged into the solution for a period of 4 h (complete conversion was monitored by TLC analysis using a PMA stain). Nitrogen was purged into the reaction mixture for 25 min to remove the excess HCl. The solution was then cooled to 0 °C followed by the addition of pyrene (117.2 g, 579.3 mmol) and aluminium chloride (16.98 g, 127.4 mmol). The ice bath was removed, and the resulting dark brown mixture was stirred at room temperature for 5 h. The reaction mixture was poured into ice-cold water (300 mL) and extracted with dichloromethane (2×100 mL). The combined organic layers were washed with brine solution (1×100 mL), dried over sodium sulfate and solvents were removed under reduced pressure. The solid brownish orange residue was subjected to column chromatography (25×12 cm; 8% chloroform/hexanes) to afford **2.15a** as an off-white solid (9.74 g, 31%): R_f =0.32 (10% chloroform/hexanes); m.p. 205–206 °C; ¹H NMR (500 MHz, CDCl₃) δ 8.14 (d, J =7.6 Hz, 4H), 8.08 (s, 4H), 8.04–7.94 (m, 10H), 1.75–1.70 (m, 4H), 1.48 (s, 12H), 1.04–0.99 (m, 4H); ¹³C NMR (75 MHz, CDCl₃) δ 147.58, 130.96, 130.86, 127.62, 127.16, 125.49, 124.71, 122.80, 45.17, 38.20, 29.49, 25.62 (a fewer-than-expected number of

aromatic signals was observed, presumably due to overlap); HRMS (APPI) calculated for $C_{42}H_{38}$ $[M]^+$ 542.2974, found 542.2971.

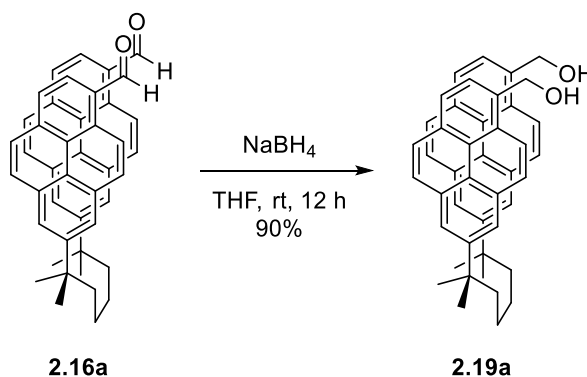
2,7-Bis(6-formylpyren-2-yl)-2,7-dimethyloctane (2.16a)



2,7-Bis(2-pyrenyl)-2,7-dimethyloctane (**2.15a**) (2.01 g, 3.68 mmol) was dissolved in dry dichloromethane (90 mL) and dichloromethylmethyl ether (2.96 g, 25.8 mmol), titanium(IV) chloride (4.89 g, 25.7 mmol) was added at $0\text{ }^{\circ}C$ under a nitrogen atmosphere. The ice bath was removed and the deep purple reaction mixture was stirred at room temperature for 5 h. The reaction mixture was slowly poured (exothermic) into ice-cold water (150 mL). The layers were separated, and the aqueous layer was extracted with dichloromethane (2×50 mL). The combined organic layers were washed with brine (50 mL), dried over Na_2SO_4 and the solvent was removed under reduced pressure. The light brown residue was subjected to column chromatography (20×5.0 cm; dichloromethane) to afford **2.16a** as a bright yellow solid (1.72 g, 78%): $R_f=0.23$ (dichloromethane); m.p. $130\text{--}132\text{ }^{\circ}C$ (dichloromethane); 1H NMR (500 MHz, $CDCl_3$) δ 10.75 (s, 2H), 9.35 (d, $J=9.3$ Hz, 2H), 8.39 (d, $J=8.0$ Hz, 2H), 8.23–8.17 (m, 6H), 8.11 (d, $J=8.9$ Hz, 2H) 8.01 (d, $J=8.9$ Hz, 2H), 1.77–1.72 (m, 4H), 1.50 (s, 12H), 1.05–1.00 (m, 4H); ^{13}C NMR (125.77 MHz, $CDCl_3$)

δ 193.20, 148.54, 135.44 131.18, 131.11, 131.01, 130.95, 130.89, 130.34, 127.38, 127.11, 124.93, 124.74, 124.62, 124.43, 122.98, 122.69, 45.31, 38.46, 29.56, 25.82; HRMS (APPI) calculated for $C_{44}H_{38}O_2$ $[M]^+$ 598.2872, found 598.2871.

2,7-Bis[6-(hydroxymethyl)pyren-2-yl]-2,7-dimethyloctane (2.19a**)**

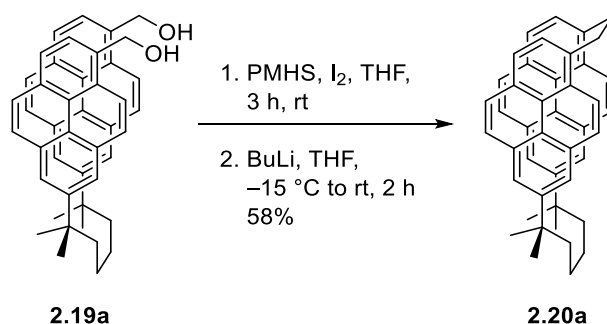


Sodium borohydride (0.265 g, 7.02 mmol) was added to a stirred solution of 2,7-bis(6-formylpyren-2-yl)-2,7-dimethyloctane (**2.16a**) (0.602 g, 1.01 mmol) in THF (30 mL). The reaction mixture was stirred at room temperature for 12 h and then cooled to 0 °C. The reaction mixture was neutralized using a 5.0 M aqueous HCl solution. Most of the THF was removed under reduced pressure. Dichloromethane (300 mL) was added to the resulting mixture. The layers were separated, and the aqueous layer was extracted with dichloromethane (2×100 mL). The combined organic layers were washed with brine (70 mL), dried over Na_2SO_4 , gravity filtered and concentrated under reduced pressure to afford compound **2.19a** as a fluffy white solid (0.500 g, 90%): R_f =0.10 (50% ethyl acetate/hexanes); m.p. 102.8-103.5 °C (dichloromethane); 1H NMR (300 MHz, $CDCl_3$) δ 8.26 (d, J =9.3 Hz, 2H), 8.11–7.96 (m, 12H), 5.36 (s, 4H), 1.93 (s, 2H), 1.72-1.70 (m, 4H),

1.47(s, 12H), 1.03–1.00 (m, 4H); ^{13}C NMR (75 MHz, CDCl_3) δ 147.72, 133.59, 131.13, 130.53, 128.63, 127.72, 127.15, 125.73, 124.48, 123.19, 123.07, 122.94, 122.79, 63.91, 45.07, 38.21, 29.75, 29.44, 25.60 (a fewer-than-expected number of aromatic signals was observed, presumably due to overlap); HRMS (APPI) calculated for $\text{C}_{44}\text{H}_{41}\text{O}_2$ $[\text{M}+\text{H}-\text{H}_2\text{O}]^+$ 585.3152, found 585.3166.

1,1,6,6-Tetramethyl[6.2](7,1)pyrenophane (**2.20a**)

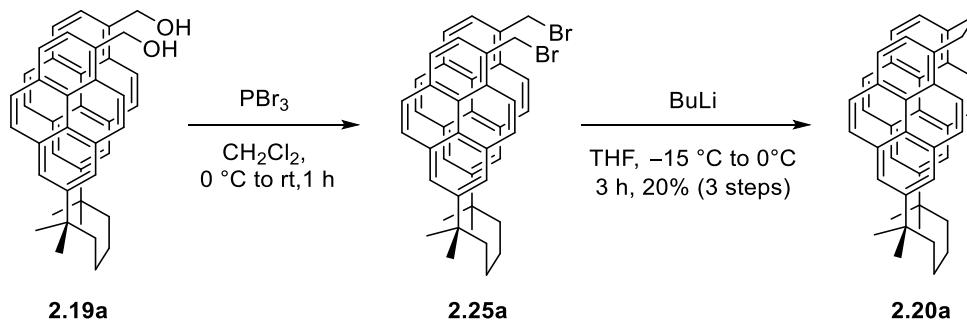
Method A.



Diol **2.19a** (0.500 g, 0.830 mmol) was dissolved in THF (20 mL, 100 mL 3-neck round-bottomed flask) and PMHS (0.106 g, 1.77 mmol) and then iodine (0.31 g, 1.2 mmol) were added under a nitrogen atmosphere. The reaction mixture was stirred at room temperature until the starting material was completely consumed (*ca.* 3 h, TLC analysis). The reaction mixture was diluted with THF (30 mL) and cooled to -15°C . BuLi (1.5 M, 2.9 mL, 4.4 mmol) was added gradually over a period of 5 min and left to stir for 2 h during which the brown solution turned to pale yellow. The solution was cooled to 0°C (ice bath) and quenched with ice-cold water, the reaction mixture was neutralized using 5.0 M aqueous HCl. Most of the THF was removed under reduced pressure and dichloromethane

(100 mL) was added to the resulting mixture. The layers were separated, and the aqueous layer was extracted with dichloromethane (2×100 mL). The combined organic layers were washed with brine (50 mL), dried over Na₂SO₄, gravity filtered and concentrated under reduced pressure. The yellow residue was subjected to column chromatography (20×4 cm; 10% chloroform/hexanes) to afford compound **2.20a** (0.273 g, 58%) as a fluffy white solid. See below for characterization.

Method B.

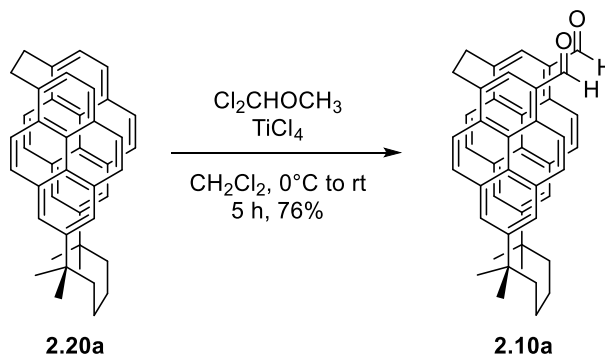


Crude diol **2.19a** (0.500 mg, 0.830 mmol) was dissolved in dichloromethane (50 mL) and the solution was cooled to 0 °C. Phosphorous tribromide (0.330 mg, 1.21 mmol) was added and the reaction mixture was stirred at 0 °C for 1 h. The reaction mixture was poured into ice-cold water and the layers of the resulting mixture were separated. The aqueous layer was extracted with dichloromethane (2×10 mL). The combined organic layers were washed with brine (25 mL), dried over Na₂SO₄, gravity filtered and concentrated under reduced pressure to afford dibromide **2.25a** (0.326 g) as a pale yellow solid: *R*_f=0.60 (20% ethyl acetate/hexanes); m.p. 197-198 °C (dichloromethane); ¹H NMR (500 MHz, CDCl₃) δ 8.32 (d, *J*=9.2 Hz, 2H), 8.14 (d, *J*=9.0 Hz, 2H), 8.13 (d, *J*=1.2 Hz,

2H), 8.10 (d, $J=1.7$ Hz, 2H), 8.06 (d, $J=7.8$ Hz, 2H), 7.99 (d, $J=8.8$ Hz, 2H), 7.97 (d, $J=7.7$ Hz, 2H), 7.96 (d, $J=8.9$ Hz, 2H), 5.25 (s, 4H), 1.77–1.68 (m, 4H), 1.49 (s, 12H), 1.04–0.98 (m, 4H); ^{13}C NMR (125 MHz, CDCl_3) δ 148.35, 132.14, 131.32, 130.88, 130.70, 129.24, 128.80, 128.61, 127.69, 127.44, 125.39, 124.96, 123.82, 123.79, 123.15, 122.99, 45.46, 38.55, 32.66, 29.76, 25.95; HRMS (APPI) calculated for $\text{C}_{44}\text{H}_{40}^{79}\text{Br}_2$ $[\text{M}]^+$ 726.1496, found 726.1513. Crude dibromide **2.25a** (0.326 g, 0.449 mmol) was dissolved in anhydrous THF (30 mL) and the solution was cooled to 0 °C under a nitrogen atmosphere. BuLi (1.05 M, 0.43 mL, 0.45 mmol) was added dropwise over a period of 20 min. The reaction mixture was then quenched with ice-cold water (10 mL) and most of the THF was removed under reduced pressure. Dichloromethane was added to the resulting mixture. The layers were separated, and the aqueous layer was extracted with dichloromethane (2×5 mL). The combined organic layers were washed with brine (10 mL), dried over Na_2SO_4 , filtered and concentrated under reduced pressure. The pale yellow residue was subjected to column chromatography (20×4.0 cm; 12% chloroform/hexanes) to afford pyrenophane **2.20a** (0.120 g, 20% over three steps) as a fluffy white solid: $R_f=0.32$ (25% dichloromethane/hexanes); m.p. 210.1–212.8 °C (dichloromethane); ^1H NMR (500 MHz, CDCl_3) δ 8.25 (d, $J=7.7$ Hz, 2H), 8.10 (d, $J=7.7$ Hz, 2H), 8.06 (d, $J=8.8$ Hz, 2H), 7.94 (d, $J=8.8$ Hz, 2H), 7.82 (d, $J=1.7$ Hz, 2H), 7.09 (d, $J=1.7$ Hz, 2H), 6.16 (d, $J=9.2$ Hz, 2H), 6.12 (d, $J=9.2$ Hz, 2H), 3.88–3.72 (AA'BB' spectrum, 4H), 1.70–1.63 (m, 2H), 1.38 (s, 6H), 1.40–1.32 (m, 2H), 1.24 (s, 6H), 0.92–0.88 (m, 2H), 0.26–0.15 (m, 2H); ^{13}C NMR (125 MHz, CDCl_3) δ 146.37, 136.76, 132.14, 131.32, 130.88, 130.70, 129.24, 128.80, 128.61,

127.69, 127.44, 125.39, 124.96, 123.82, 123.79, 123.15, 122.99, 45.46, 38.55, 32.66, 29.76, 25.95; HRMS (APPI) calculated for $C_{44}H_{40}$ $[M]^+$ 568.3130, found 568.3145.

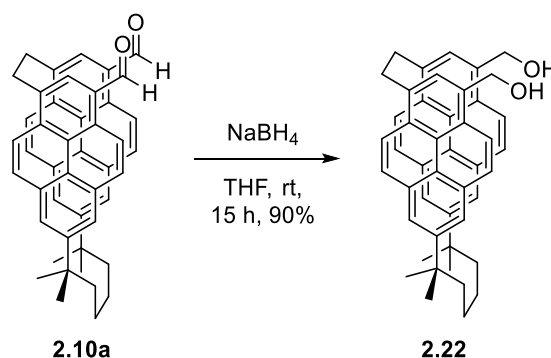
11,21-Diformyl-1,1,6,6-tetramethyl[6.2](7,1)pyrenophane (2.10a)



Pyrenophane **2.20a** (0.119 g, 0.209 mmol) was dissolved in dry dichloromethane (20 mL) and the solution was cooled to $0^\circ C$ under a nitrogen atmosphere. Titanium(IV) chloride (0.79 g, 4.2 mmol) and dichloromethyl methyl ether (0.48 g, 4.2 mmol) were added and the resulting deep purple solution was stirred at room temperature for 4 h. The reaction mixture was slowly poured (exothermic) into ice-cold water (20 mL). The layers were separated, and the aqueous layer was extracted with dichloromethane (2×10 mL). The combined organic layers were washed with brine (20 mL), dried over Na_2SO_4 and the solvent was removed under reduced pressure. The yellow residue was subjected to column chromatography (12×7 cm; 40% dichloromethane/hexanes) to afford pyrenophane dialdehyde **2.10a** (0.095 g, 76%) as a yellow solid: $R_f=0.13$ (dichloromethane); m.p. $>300^\circ C$ (dichloromethane); 1H NMR (500 MHz, $CDCl_3$) δ 10.95 (s, 2H), 9.38 (d, $J=9.2$ Hz, 2H), 8.56 (s, 2H), 8.17 (d, $J=9.5$ Hz, 2H), 7.93 (d, $J=1.8$ Hz, 2H), 7.16 (d, $J=1.8$ Hz, 2H), 6.28

(d, $J=9.2$ Hz, 2H), 6.25 (d, $J=9.2$ Hz, 2H), 3.95–3.73 (AA'BB' spectrum, 4H), 1.77–1.68 (m, 2H), 1.45–1.38 (m, 2H), 1.36 (s, 6H), 1.24 (s, 6H), 0.88–0.78 (m, 2H), 0.30–0.20 (m, 2H); ^{13}C NMR (75 MHz, CDCl_3) δ 193.47, 147.51, 136.02, 134.85, 132.92, 130.06, 130.01, 129.84, 128.13, 127.72, 124.96, 124.42, 123.79, 122.46, 122.43, 121.72, 121.52, 45.54, 38.44, 36.61, 30.71, 28.89, 26.66; HRMS (APPI) calculated for $\text{C}_{46}\text{H}_{40}\text{O}_2$ $[\text{M}+\text{H}]^+$ 625.3029, found 625.3039.

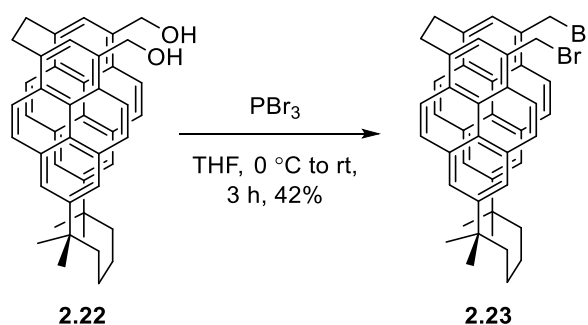
Diol 2.22



Sodium borohydride (0.076 g, 0.21 mmol) was added to a stirred solution of 11,21-diformyl-1,1,6,6-tetramethyl[6.2](7,1)pyrenophane (**2.10a**) (0.171 g, 0.272 mmol) in THF (15 mL). The reaction mixture was stirred at room temperature over a period of 15 h and then cooled to 0 °C (ice bath). The reaction mixture was neutralized using 5.0 M aqueous HCl. Most of the THF was removed under reduced pressure. Dichloromethane (20 mL) was added to the resulting mixture. The layers were separated, and aqueous layer was extracted with dichloromethane (2×15 mL). The combined organic layers were washed with brine (15 mL), dried over Na_2SO_4 , gravity filtered and concentrated under reduced

pressure to afford compound **2.22** as a fluffy white solid (0.154 g, 90%): $R_f=0.10$ (30% ethyl acetate/hexane); m.p. $>300\text{ }^{\circ}\text{C}$ (dichloromethane); HRMS (APPI) for $\text{C}_{46}\text{H}_{44}\text{O}_2$ $[\text{M}+\text{H}-\text{H}_2\text{O}]^+$ 611.3308, found 611.3331. ^1H and ^{13}C NMR analysis of diol **2.22** were not possible due to the very low solubility of **2.22** in most common organic solvents. This compound was taken to the next step without further purification.

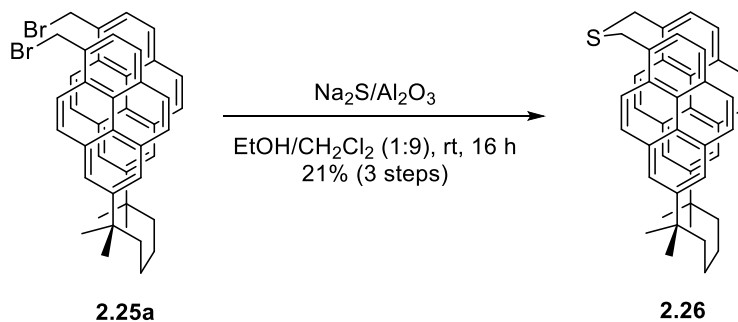
Dibromide **2.23a**



Crude diol **2.22** (0.71 mg, 0.11 mmol) was dissolved in dry dichloromethane (12 mL) and the solution was cooled to $0\text{ }^{\circ}\text{C}$. Phosphorous tribromide (0.35 mg, 0.13 mmol) was added and the reaction mixture was stirred at $0\text{ }^{\circ}\text{C}$ for 3 h (under a nitrogen atmosphere). The reaction mixture was poured into ice-cold water and the layers of the resulting mixture were separated. The aqueous layer was extracted with dichloromethane (2×10 mL). The combined organic layers were washed with brine (20 mL), dried over Na_2SO_4 , gravity filtered and concentrated under reduced pressure to afford dibromide **2.23** (0.35 g, 42%) as a pale yellow solid: $R_f=0.50$ (20% ethyl acetate/hexanes); m.p. $>300\text{ }^{\circ}\text{C}$ (dichloromethane); ^1H NMR (500 MHz, CDCl_3) δ 8.34 (d, $J=9.1\text{ Hz}$, 2H), 8.14 (s, 2H), 8.05 (d, $J=9.2\text{ Hz}$, 2H), 7.83 (d, $J=1.7\text{ Hz}$, 2H), 7.10 (d, $J=1.7\text{ Hz}$, 2H), 6.22 (d, $J=9.3\text{ Hz}$,

2H), 6.18 (d, $J=9.2$ Hz, 2H), 5.43 (d, $J=10.3$ Hz, 2H), 5.37 (d, $J=10.3$ Hz, 2H), 3.80–3.72 (AA'BB' spectrum, 4H), 1.76–1.71 (m, 2H), 1.32 (s, 6H), 1.32 (s, 6H), 0.90–0.88 (m, 2H), 0.78–0.76 (m, 2H), 0.34–0.29 (m, 2H); ^{13}C NMR (75 MHz, CDCl_3) δ 146.18, 136.58, 130.53, 130.10, 129.86, 127.56, 127.03, 125.14, 124.46, 122.73, 122.11, 121.47, 45.56, 38.23, 36.81, 31.27, 27.93, 26.45 (a fewer-than-expected number of signals was observed, presumably due to overlap); HRMS (APPI) calculated for $\text{C}_{46}\text{H}_{42}^{79}\text{Br}_2$ $[\text{M}]^+$ 752.1697, found 752.1704.

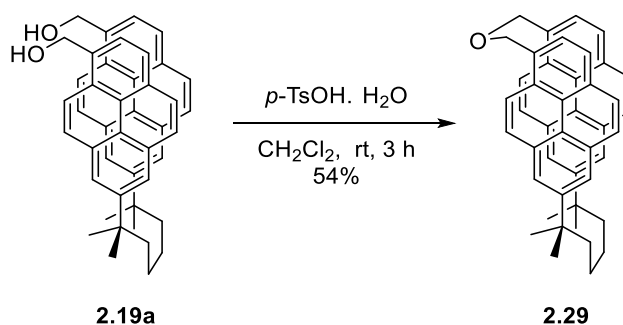
1,1,6,6-Tetramethyl-18-thia[6.3](7,1)pyrenophane (2.26)



$\text{Na}_2\text{S}/\text{Al}_2\text{O}_3$ (0.166 g, 1.09 mmol) was added in four equal portions to a stirred room temperature solution of **2.25a** (0.100 g, 0.137 mmol) in 1:9 (v/v) EtOH/dichloromethane (150 mL) over a 20 min period. The resulting slurry was stirred vigorously for 16 h and the reaction mixture was suction filtered through a plug of celite. The filtrate was concentrated under reduced pressure and the residue was subjected to column chromatography (30×3.0 cm; 40% dichloromethane/hexanes) to afford 1,1,6,6-tetramethyl-18-thia[6.3](7,1)pyrenophane (**2.26**) (0.421 g, 21%, 3 steps) as a yellow oil: $R_f=0.60$ (40 % dichloromethane/hexanes); ^1H NMR (300 MHz, CDCl_3) δ 8.08 (d, $J=7.8$ Hz, 2H),

8.08–8.07 (m, 2H), 8.01 (d, $J=7.8$ Hz, 2H), 8.01–8.00 (m, 4H), 7.44 (d, $J=1.7$ Hz, 2H), 6.60 (d, $J=9.3$ Hz, 2H), 6.36 (d, $J=9.3$ Hz, 2H), 4.35 (s, 4H), 1.73–1.71 (m, 4H), 1.44 (s, 12H), 1.11–1.10 (m, 4H); ^{13}C NMR (75 MHz, CDCl_3) δ 146.94, 131.17, 130.92, 130.86, 130.43, 128.91, 127.67, 127.59, 127.24, 126.83, 125.24, 124.07, 123.30, 122.86, 122.71, 122.60, 43.96, 38.74, 33.07, 29.67, 26.34; HRMS (APPI) calculated for $\text{C}_{44}\text{H}_{40}\text{S}$ $[\text{M}]^+$ 600.2826, found 600.2829.

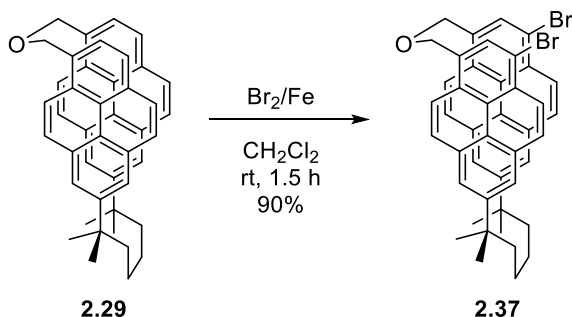
1,1,6,6-Tetramethyl-18-oxa[6.3](7,1)pyrenophane (**2.29**)



A solution of diol **2.19a** (0.500 g, 0.830 mmol) in dichloromethane (100 mL) was added dropwise over a period of 30 min to a stirred room temperature solution of *p*-toluenesulfonic acid monohydrate in dichloromethane (0.0158 g, 0.0229 mmol, 200 mL). After the addition was complete, the reaction mixture was stirred at room temperature for 2 h and it was then quenched with water (100 mL). The layers were separated, and the aqueous layer was extracted with dichloromethane (2×100 mL). The combined organic layers were washed with brine (100 mL), dried over Na_2SO_4 , gravity filtered and concentrated under reduced pressure. The yellow residue was subjected to column chromatography (15×4.0 cm; 40% dichloromethane/hexanes) to afford 1,1,6,6-

tetramethyl-18-oxa[6.3](7,1)pyrenophane (**2.29**) (0.269 g, 54%) as a white solid: R_f =0.31 (50 % dichloromethane/hexanes); m.p. 228.4–229.5 °C (dichloromethane); NMR (300 MHz, CDCl_3) δ 8.14 (d, J =7.7 Hz, 2H), 8.09 (d, J =1.7 Hz, 2H), 8.05 (d, J =7.7 Hz, 2H), 8.04 (s, 4H), 7.46 (d, J =1.6 Hz, 2H), 6.85 (d, J =9.2 Hz, 2H), 6.37 (d, J =9.3 Hz, 2H), 5.23 (s, 4H), 1.76–1.74 (m, 4H), 1.44 (s, 12H), 1.11–1.08 (m, 4H); ^{13}C NMR (75 MHz, CDCl_3) δ 146.94, 131.72, 131.31, 130.94, 130.52, 130.26, 128.28, 127.96, 127.21, 126.78, 123.91, 123.67, 123.12, 122.79, 69.81, 43.84, 38.85, 26.52 (a fewer-than-expected number of signals was observed, presumably due to overlap); HRMS (APPI) calculated for $\text{C}_{44}\text{H}_{40}\text{O}$ $[\text{M}+\text{H}]^+$ 585.3254, found 585.3268.

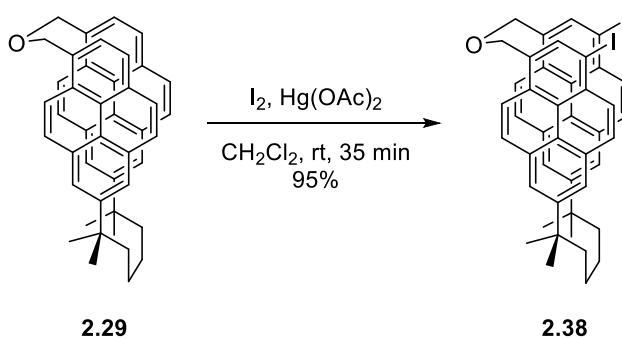
Dibromo oxacyclophane **2.37**



1,1,6,6-Tetramethyl-18-oxa[6.3](7,1)pyrenophane (**2.29**) (0.080 g, 0.133 mmol) was dissolved in dichloromethane (2 mL). Iron filings (0.002 g, 0.039 mmol) and bromine (0.053 g, 0.332 mmol) were added and the resulting solution was stirred at room temperature for 90 min. The reaction mixture was then poured into water (5 mL). The layers were separated, and the aqueous layer was extracted with dichloromethane (2×5 mL). The combined organic layers were washed with brine (10 mL), dried over Na_2SO_4 ,

gravity filtered and concentrated under reduced pressure. The yellow residue was subjected to column chromatography (10×3.0 cm; 5% ethylacetate/hexanes) to afford dibromo oxacyclophane **2.37** (0.090 g, 90%) as a pale yellow solid: R_f =0.43 (10% ethylacetate/hexanes); m.p. 203.8–205.5 °C (dichloromethane); LCMS, ^1H and ^{13}C NMR analysis were not possible due to the very low solubility of dibromo oxacyclophane **2.37** in most organic solvents. The compound was partially dissolved in $\text{DMSO}-d_6$ by heating, but a precipitate formed during the process of acquisition. In contrast, diiodo oxacyclophane **2.38** was quite soluble in CDCl_3 .

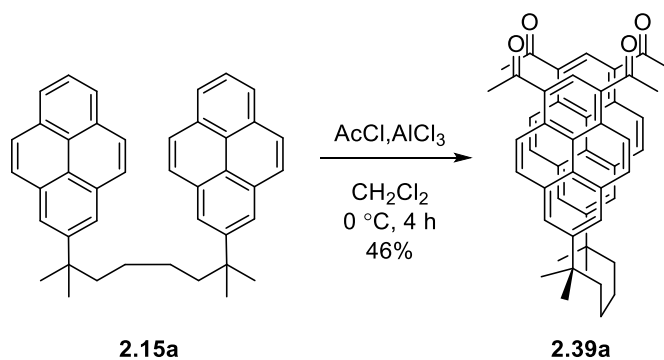
Diiodo oxacyclophane **2.38**



1,1,6,6-Tetramethyl-18-oxa[6.3](7,1)pyrenophane (**2.29**) (0.095 g, 0.16 mmol) was dissolved in dichloromethane (7 mL). Mercury(II) acetate (0.16 g, 0.48 mmol) and iodine (0.123 g, 0.487 mmol) were added and the resulting burgundy solution was stirred at room temperature for 35 min. The reaction mixture was then suction filtered through a plug of celite and poured into water (5 mL). The layers were separated, and the aqueous layer was extracted with dichloromethane (2×10 mL). The combined organic layers were washed with brine (10 mL), dried over Na_2SO_4 , gravity filtered and concentrated under reduced

pressure. The yellow residue was subjected to column chromatography (12×3.0 cm; 25% dichloromethane/hexanes) to afford diiodo oxacyclophane **2.38** (0.13 g, 95%) as a pale yellow solid: $R_f=0.6$ (50% dichloromethane/hexanes); m.p. 243.7–245.6 °C (dichloromethane); NMR (300 MHz, CDCl_3) δ 8.49 (s, 2H), 8.18 (d, $J=9.2$ Hz, 2H), 8.09 (d, $J=1.5$ Hz, 2H), 8.05 (d, $J=9.2$ Hz, 2H), 7.48 (d, $J=1.5$ Hz, 2H), 7.03 (d, $J=9.2$ Hz, 2H), 6.54 (d, $J=9.3$ Hz, 2H), 5.18 (s, 2H), 1.76–1.74 (m, 4H), 1.54 (s, 12H), 1.42 (s, 6H), 1.06–1.05 (m, 4H); ^{13}C NMR (75 MHz, CDCl_3) δ 147.44, 138.35, 132.76, 132.18, 130.62, 130.55, 130.18, 130.07, 129.71, 127.07, 125.31, 123.66, 123.40, 121.67, 95.01, 69.56, 43.60, 38.68, 30.25, 26.43 (a fewer-than-expected number of aromatic signals was observed, presumably due to overlap); HRMS (APPI) calculated for $\text{C}_{44}\text{H}_{38}^{126.9}\text{I}_2\text{O}$ $[\text{M}+\text{H}-\text{I}]^+$ 710.2158, found 710.2166.

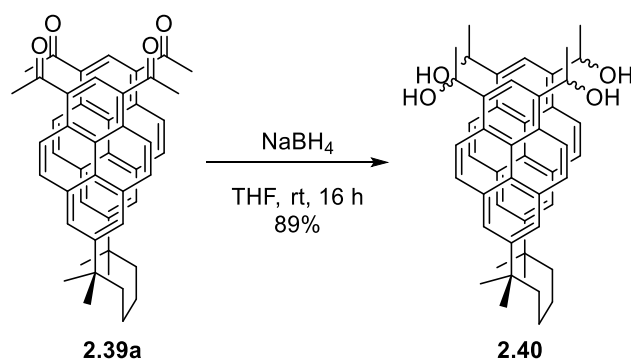
2,7-Bis(6,8-diacetylpyren-2-yl)-2,7-dimethyldecane (**2.39a**)



Aluminum chloride (0.216 g, 1.61 mmol) was added to a stirred $0\text{ }^\circ\text{C}$ solution of acetylchloride (0.60 g, 0.77 mmol) and 2,7-bis(2-pyrenyl)-2,7-dimethyloctane (**2.15a**) (0.100 g, 0.184 mmol) in dry dichloromethane (5 mL). The deep orange reaction mixture

was kept at 0 °C (ice bath) and stirred for 4 h, after which it was poured into ice-cold water (10 mL). The layers were separated, and the aqueous layer was extracted with dichloromethane (2×10 mL). The combined organic layers were washed with brine (10mL), dried over Na₂SO₄ and the solvent was removed under reduced pressure. The light orange mass isolated was subjected to recrystallization from acetone to afford tetraketone **2.39a** as a bright yellow solid (0.60 g, 46%): *R*_f = 0.22 (30% ethylacetate/hexanes); m.p. 218–219 °C (acetone); ¹H NMR (300 MHz, CDCl₃) δ 8.95 (d, *J*=9.4 Hz, 4H), 8.68 (s, 2H), 8.21 (d, *J*=9.3 Hz, 4H), 8.20 (s, 4H), 2.94 (s, 12H), 1.76–1.71 (m, 4H), 1.49 (s, 12H), 0.98–1.04 (m, 4H); ¹³C NMR (75 MHz, CDCl₃) δ 201.69, 148.96, 132.12, 131.82, 131.15, 130.39, 127.79, 125.45, 124.54, 38.39, 30.67, 29.42, 25.70 (a fewer-than-expected number of signals was observed, presumably due to overlap); HRMS (APPI) calculated for C₅₀H₄₆O₄ [M]⁺ 710.3383, found 710.3401.

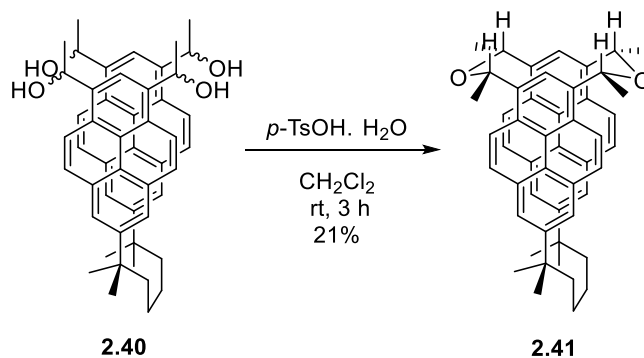
Tetraol **2.40**



Sodium borohydride (0.064 g, 1.7 mmol) was added to a stirred solution of 2,7-bis(6,8-diacetylpyren-2-yl)-2,7-dimethyldecane (**2.39a**) (0.030 g, 0.042 mmol) in THF (5 mL). The reaction mixture was stirred at room temperature over a period of 16 h and then

cooled to 0 °C (ice bath). The reaction mixture was neutralized using 5.0 M aqueous HCl. Most of the THF was removed under reduced pressure. Dichloromethane (10 mL) was added to the resulting mixture. The layers were separated, and aqueous layer was extracted with dichloromethane (2×10 mL). The combined organic layers were washed with brine (15 mL), dried over Na₂SO₄, gravity filtered and concentrated under reduced pressure to afford compound **2.40** as a white solid (0.027 g, 89%): *R*_f=0.10 (60% ethyl acetate/hexanes); m.p. >300 °C (dichloromethane); HRMS (APPI) calculated for C₅₀H₅₄O₄ [M+H–2H₂O]⁺ 683.2997, found 683.3101; ¹H and ¹³C NMR analysis of tetraol **2.40**, which conceivably exists as a mixture of isomers were not possible due to the poor solubility of **2.40** in most common organic solvents. Compound **2.40** was taken to the next step without further purification.

Dioxacyclophane **2.41**



A solution of crude tetraol **2.40** (0.100 g, 0.139 mmol) in dichloromethane (150 mL) was added dropwise over a period of 30 min to a stirred room temperature solution of *p*-toluenesulfonic acid monohydrate in dichloromethane (0.11 g, 0.40 mmol, 50 mL). After

the addition was complete, the reaction mixture was stirred at room temperature for 3 h and it was then quenched with water (50 mL). The layers were separated, and the aqueous layer was extracted with dichloromethane (2×50 mL). The combined organic layers were washed with brine (100 mL), dried over Na₂SO₄, gravity filtered and concentrated under reduced pressure. The pale yellow residue was subjected to column chromatography (12×4.0 cm; 5% ethylacetate/hexanes) to afford dioxacyclophane **2.41** (0.0199 g, 21%) as a white solid: R_f = 0.26 (60 % dichloromethane/hexanes); m.p. >300 °C (dichloromethane); ¹H NMR (300 MHz, CDCl₃) δ 8.24 (s, 2H), 7.82 (d, J =9.4 Hz, 4H), 7.52 (s, 2H), 7.43(d, J =9.3 Hz, 4H), 5.76 (q, J =6.5 Hz, 4H), 1.82 ppm (d, J =6.5 Hz, 12H), 1.67–1.65 (m, 2H), 1.25 (s, 12H), 1.25–1.22 (m, 2H), 0.89–0.82 (m, 2H), 0.71–0.68 (m, 2H); ¹³C NMR (75 MHz, CDCl₃) δ 145.49, 136.05, 129.55, 126.65, 125.89, 125.36, 122.95, 122.10, 120.66, 74.58, 45.56, 38.11, 29.86, 29.75, 26.52, 24.55; HRMS (APPI) calculated for C₅₀H₅₀O₂ [M+H–H₂O]⁺ 665.3911, found 665.3915.

2.7 References and Notes

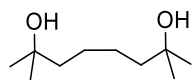
1. a) Yang, W.; Monterio, J. H. S. K.; de Bettencourt-Dias, A. Chalifoux, W. A. *Can. J. Chem.* **2017**, *95*, 341–345. 14. b) Vögtle, F. *Top. Curr. Chem.* **1983**, *115*, 157–159. c) Lewis, S. E. *Chem. Soc. Rev.* **2015**, *44*, 2221–2304. d) Darzi, E. R.; Jasti, R. *Chem. Soc. Rev.* **2015**, *44*, 6401–6410.
2. Umemoto, T.; Kawashima, T.; Sakata, Y.; Misumi, S. *Tetrahedron Lett.* **1975**, *16*, 1005–1006.
3. Merner, B. L.; Dawe, L. N.; Bodwell, G. J. *Angew. Chem. Int. Ed.* **2009**, *48*, 5487–5491.
4. Mannion, M. R. Ph.D. Dissertation, Memorial University, 1999.
5. Unikela, K. S.; Roemmele, T. L.; Houska, V.; McGrath, K. E.; Tobin, D. M.; Dawe, L. N.; Boere, R. T.; Bodwell, G. J. *Angew. Chem. Int. Ed.* **2018**, *57*, 1707–1711.
6. Chen, Y.; Jami-Alahmadi, Y.; Unikela, K. S.; Bodwell, G. J.; Fridgen, T. D. *ChemPhysChem* **2018**, *19*, 2194–2199.
7. a) Dewar, M. J. S.; Dennington, R. D. *J. Am. Chem. Soc.*, **1989**, *111*, 3804–3808. b) Casas-Solvas, J. M.; Howgego, J. D.; Davis, A. P. *Org. Biomol. Chem.* **2014**, *12*, 212–232. c) Ogino, K.; Iwashima, S.; Inokuchi, H.; Harada, Y. *Bull. Chem. Soc. Jpn.* **1965**, *38*, 473–477.
8. a) Bodwell, G. J.; Nandaluru, P. R. *Isr. J. Chem.* **2012**, *52*, 105–138. b) Yamato, T.; Hironaka, T.; Saisyō, T.; Manabe, T. Okuyama, K. *J. Chem. Res.* **2003**, 277–288.
9. Merner, B. L. Ph.D. Dissertation, Memorial University, 2010.
10. Unikela, K. S. Ph.D. Dissertation, Memorial University, 2014.

11. a) Yamato, T.; Miyamoto, S.; Saisyo, T.; Manabe, T.; Okuyama, K. *J. Chem. Res. (S)*, **2003**, 63–65; b) Tsuge, A.; Nago, H.; Mataka, S.; Tashiro, M. *J. Chem. Soc. Perkin Trans. 1*, **1992**, 1179–1185; c) Paioni, R.; Jenny, W. *Helv. Chim. Acta*, **1969**, 52, 2041–2054.
12. a) Arnold, D. R.; Abraitys, V. Y.; McLeod, D. Jr. *Can. J. Chem.* **1971**, 49, 923–935; b) Koch, T. H.; Brown, D. A. *J. Org. Chem.* **1971**, 36, 1934–1937; c) Baird, N. C.; Draper, A. M.; Mayo, P. D. *Can. J. Chem.* **1988**, 66, 1579–1588.
13. Merner, B. L.; Unikela, K. S.; Dawe, L. N.; Thompson, D. V.; Bodwell, G. J. *Chem. Commun.* **2013**, 49, 5930–5932.
14. Batista, V. S.; Crabtree, R. H.; Konezny, S. J.; Luca, O. R.; Praetorius, J. M. *New J. Chem.* **2012**, 36, 1141–1144.
15. Zhai, L.; Shukla, R.; Rathore, R. *Org. Lett.* **2009**, 11, 3474–3477.
16. TLC analysis of the reaction mixture showed the presence of three mobile spots, which were separated by column chromatography. ¹H NMR and LCMS analysis of these compounds did not match in any way what was expected for **2.11a** or even the reduced product **2.21a**. The structures of these compounds have not been determined.
17. Compound **2.22** was taken to the next step without further purification.
18. Na₂S/Al₂O₃ reagent reference: Bodwell, G. J.; Houghton, T. J.; Koury, H. E.; Yarlagadda, B. *Synlett* **1995**, 751–752.
19. a) Inouye, M.; Fujimoto, K.; Furusyo, M.; Nakazumi, H. *J. Am. Chem. Soc.* **1999**, 121, 1452–1458. b) Hayashi, H. *J. Chem. Res.* **2004**, 599–601. c) Bodwell, G. J.;

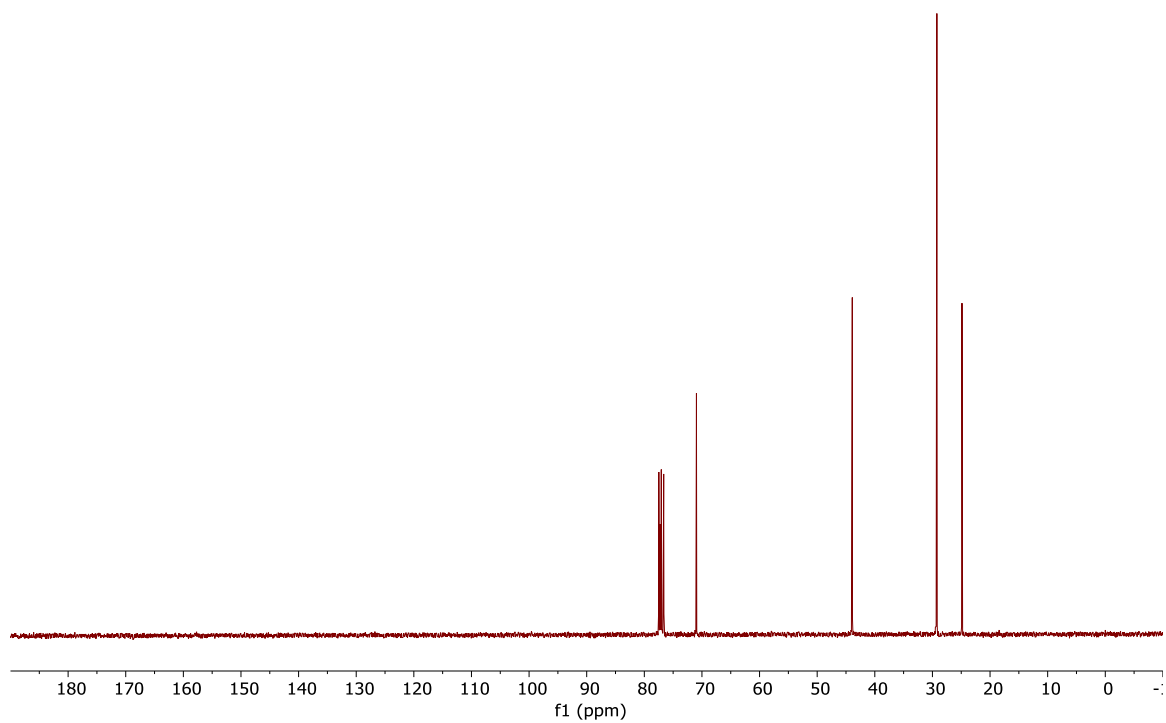
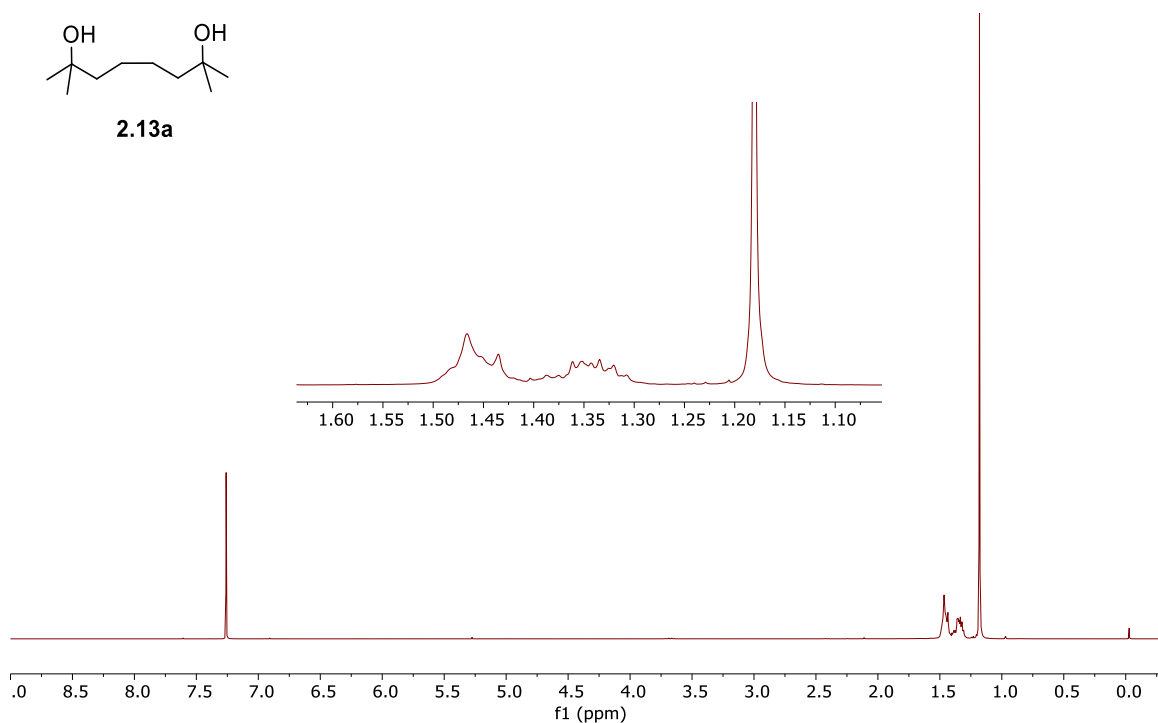
- Fleming, J. J.; Miller, D. O. *Tetrahedron* **2001**, *57*, 3577–3585. d). Yang, Y.; Mannion, M. R.; Dawe, L. N.; Kraml, C. M.; Pascal, R. A.; Bodwell, G. J. *J. Org. chem.* **2012**, *77*, 57–67. e) Halling, M. D.; Unikela, K. S.; Bodwell, G. J.; Grant, D.M.; Pugmire, R. J. *J. Phys. Chem. A*. **2012**, *116*, 5193–5198. f) Franz, D.; Robbins, S. T. Boéré, R. T.; Dibble, P. W. *J. Org. Chem.* **2009**, *74*, 7544–7547. g) Tsuge, A.; Otsuka, M.; Moriguchi, T.; Sakata, K. *Org. Biomol. Chem.* **2005**, *3*, 3590–3593. h) Paudel, A. *J. Chem. Res.* **2008**, 731–734.
20. Mitchell, R. H. Keehn, P.; Rosenfeld, S. *Nuclear Magnetic Resonance Properties and Conformational Behaviour of Cyclophanes, Chapter 4*; Academic press, 1983, 239–310.
21. a) Mitchell, R. H.; Vinod, T. K.; Bushnell, G. W. *J. Am. Chem. Soc.* **1990**, *112*, 3487–3497. b) A scissoring motion can relieve some of the torsional strain in perfect face-to-face orientation.
22. Cao, Z.; Shi, Z. *J. Am. Chem. Soc.* **2017**, *139*, 6546–6549.
23. a) Ramos-Tomillero, I.; Paradis-Bas, M.; de Pinho Ribeiro Moreira, I.; Maria Bofill, J.; Nicolás, E.; Albericio, F. *Molecules* **2015**, *20*, 5409–5422. b) Liu, K. -T.; Duanna, Y. -F.; Hou, S. -J. *J. Chem. Soc., Perkin Trans. 2*, **1998**, 2181–2185.
24. Inoue, J.; Fukui, K.; Kubo, T.; Nakazawa, S.; Sato, K.; Shiomi, D.; Morita, Y.; Yamamoto, K.; Takui, T.; Nakasuji, K. *J. Am. Chem. Soc.* **2001**, *123*, 12702–12703.
25. Khadem, M.; Walsh, J. C.; Bodwell, G. J. Zhao, Y. *Org. Lett.* **2016**, *18*, 2403–2406.
26. Starting material (**2.41**) was completely consumed and one immobile spot on the baseline formed. LCMS and ¹H NMR analysis were not possible due to the very low

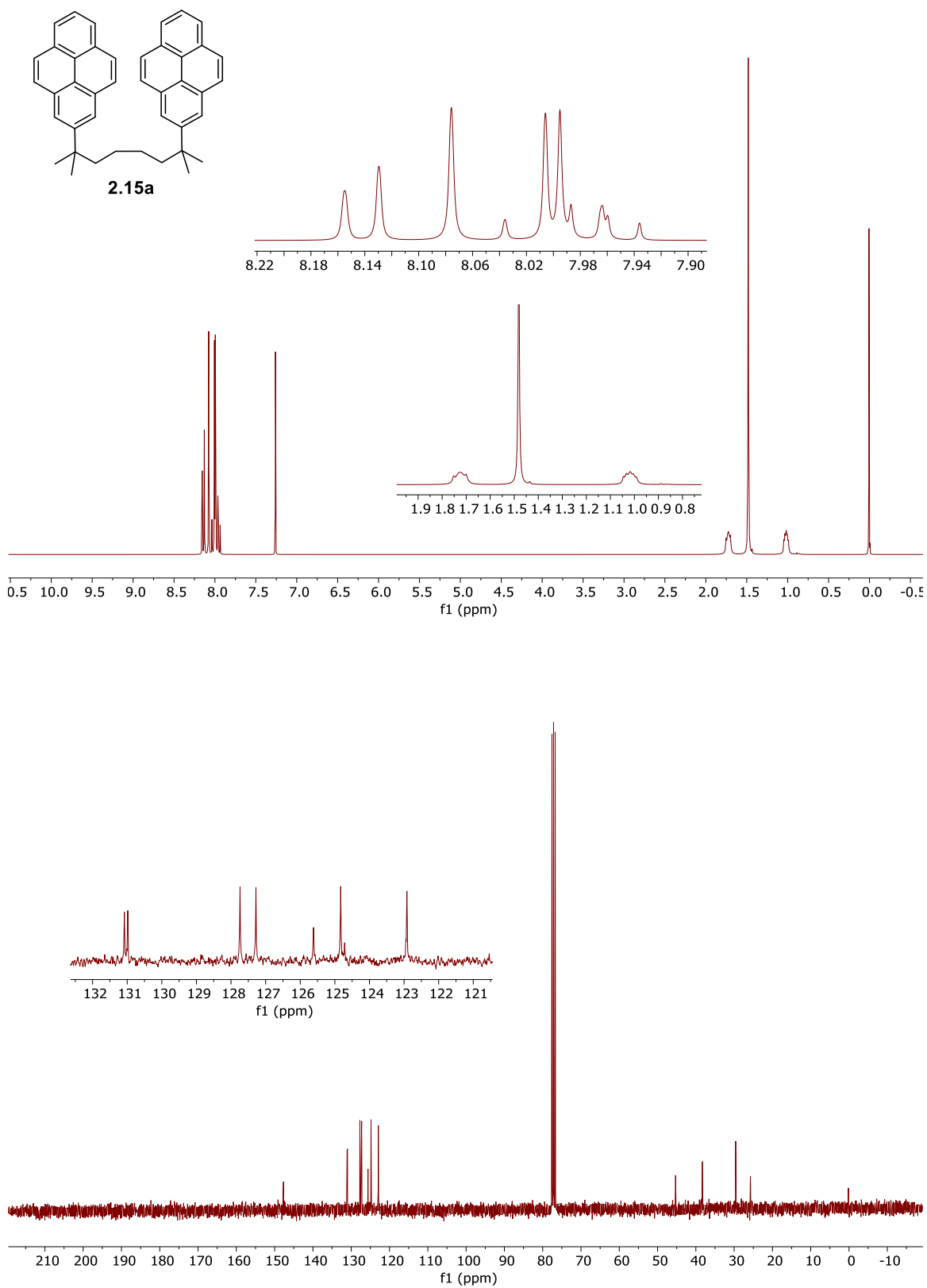
solubility of reaction mixture in most common organic solvents. The application of a milder conditions ($\text{Ac}_2\text{O}/\text{ZnCl}_2$) to afford diketone instead of dialdehyde provided the same result.

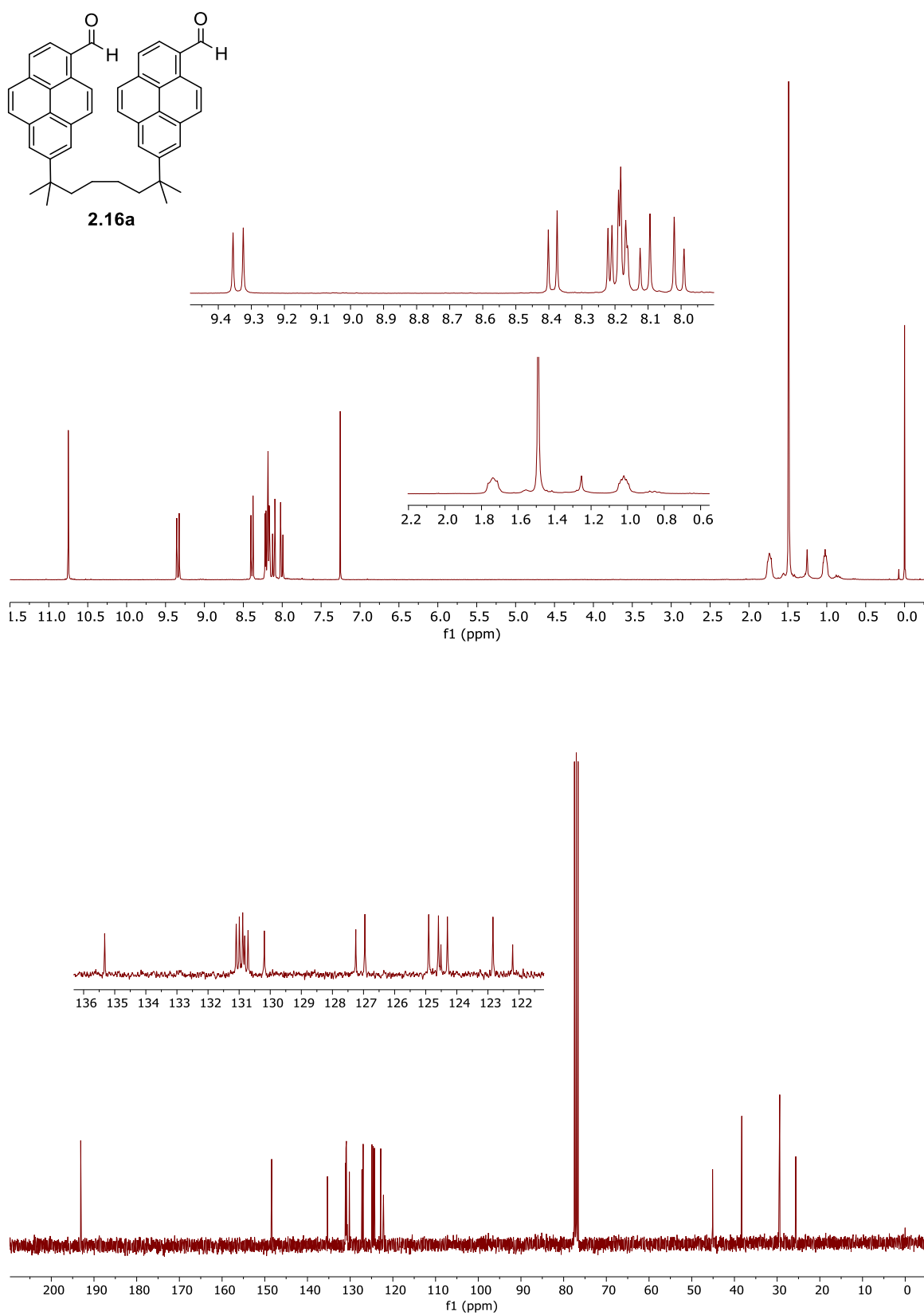
APPENDIX 1

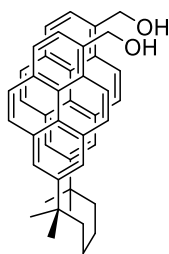


2.13a

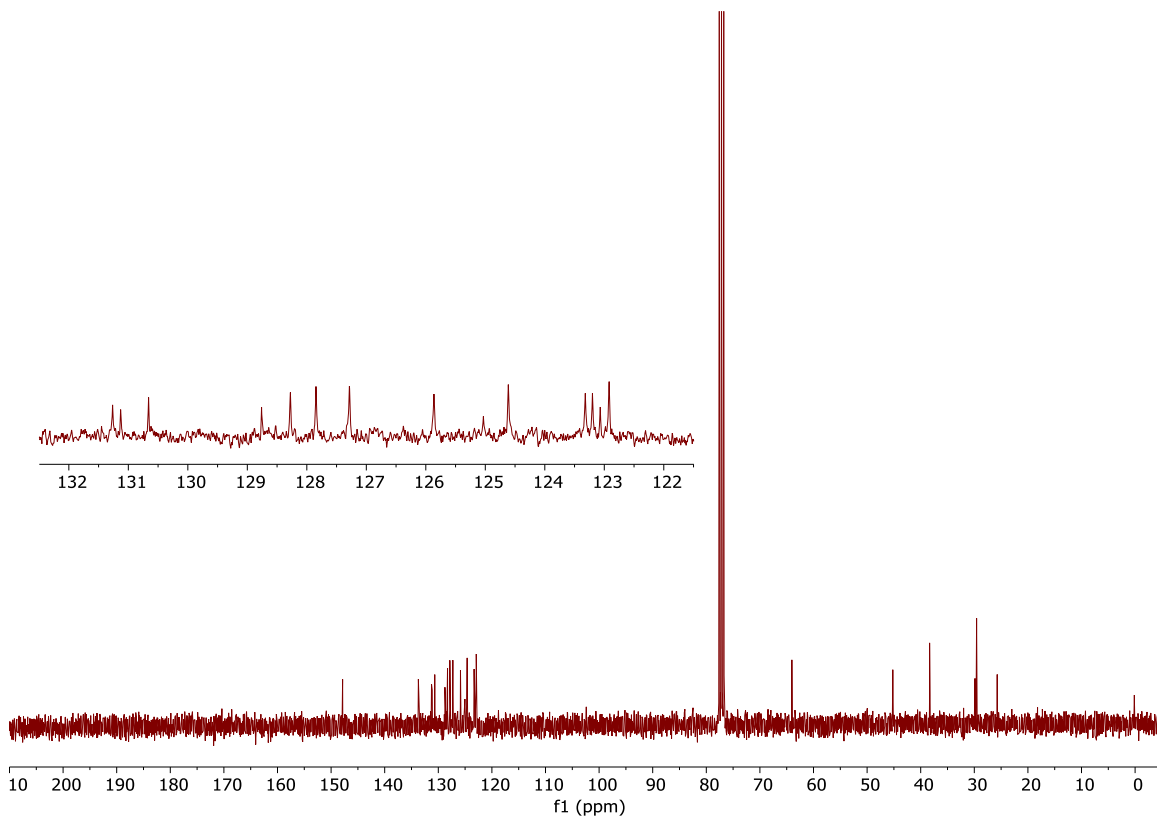
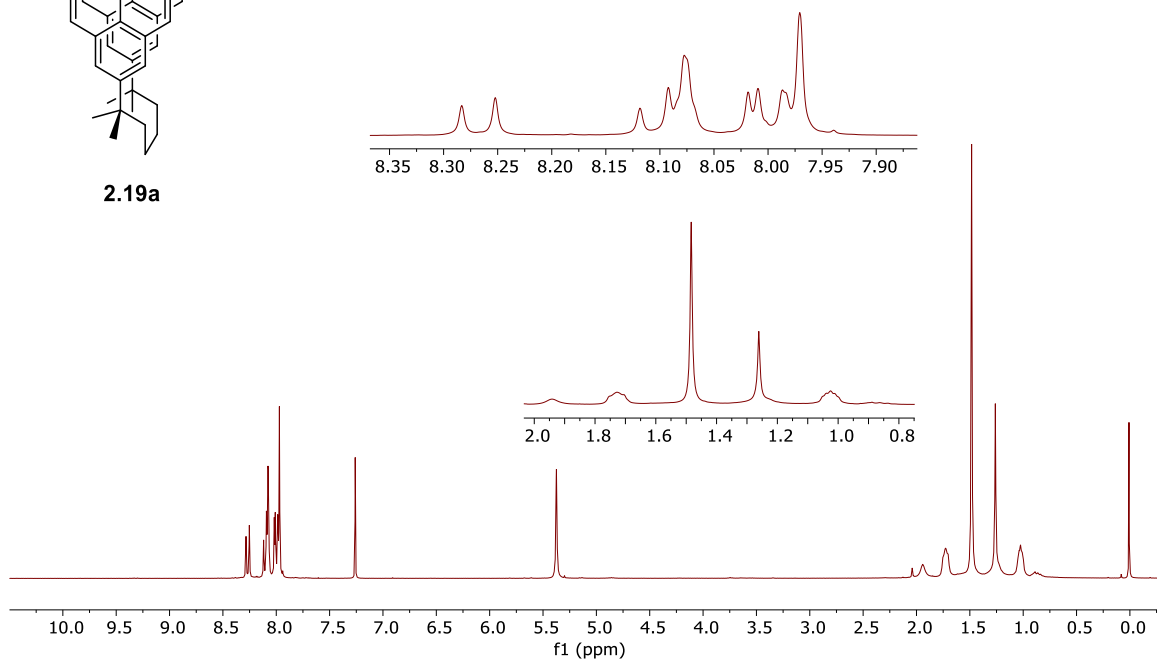


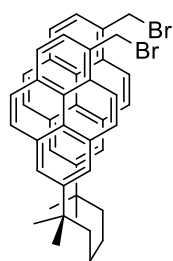




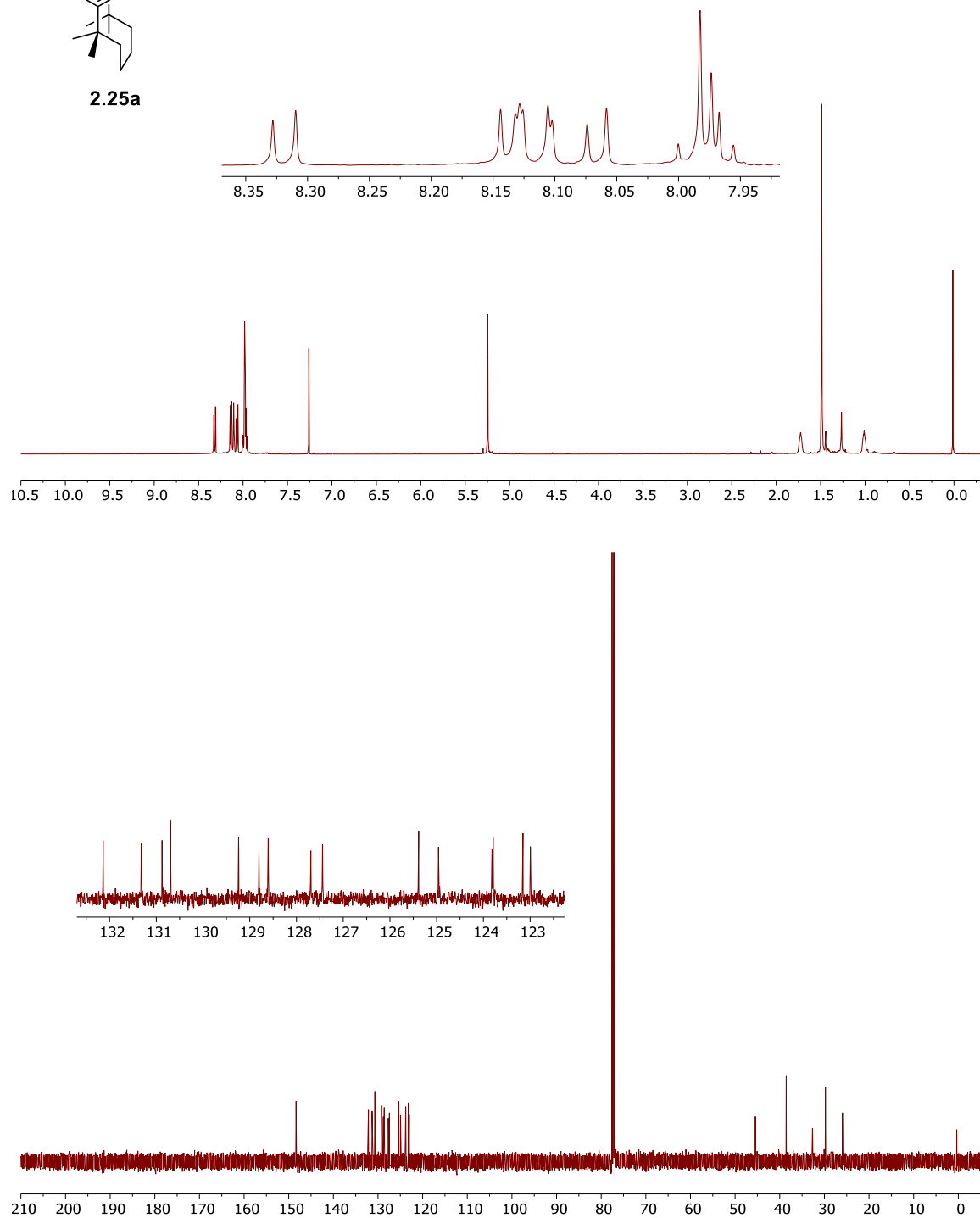


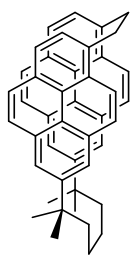
2.19a



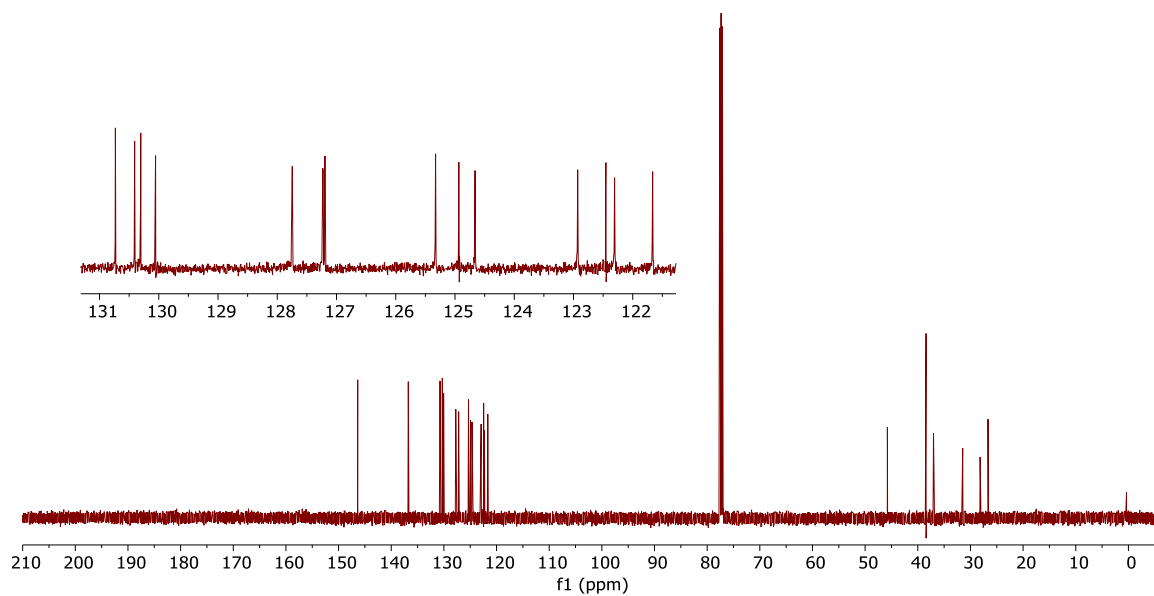
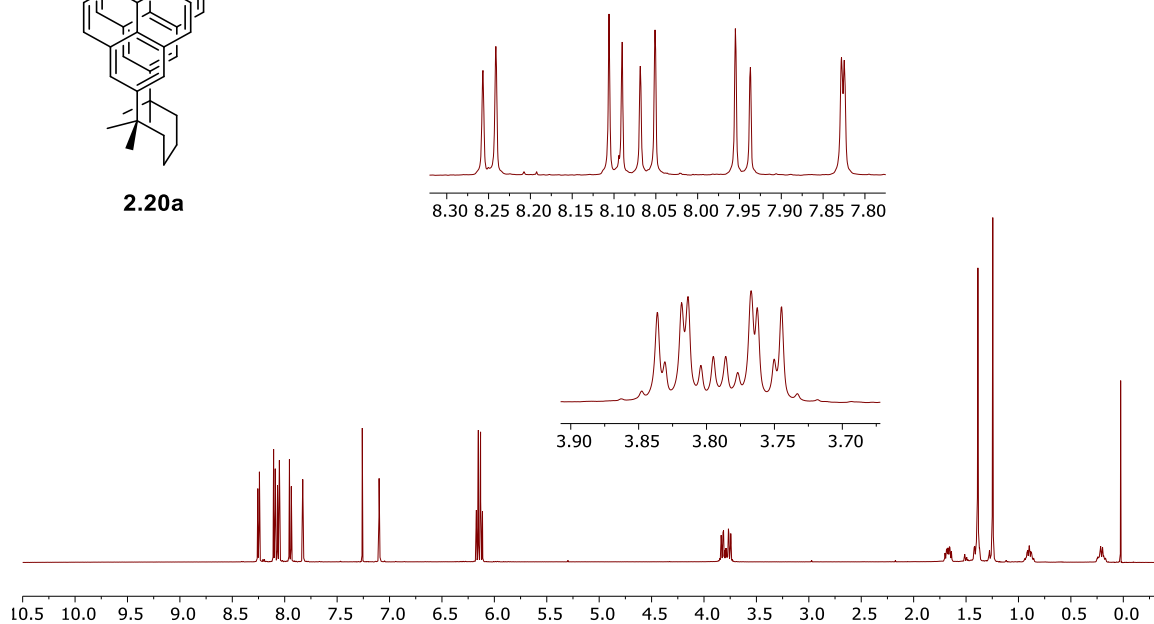


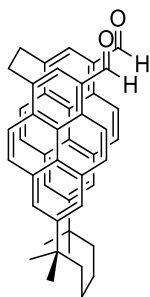
2.25a



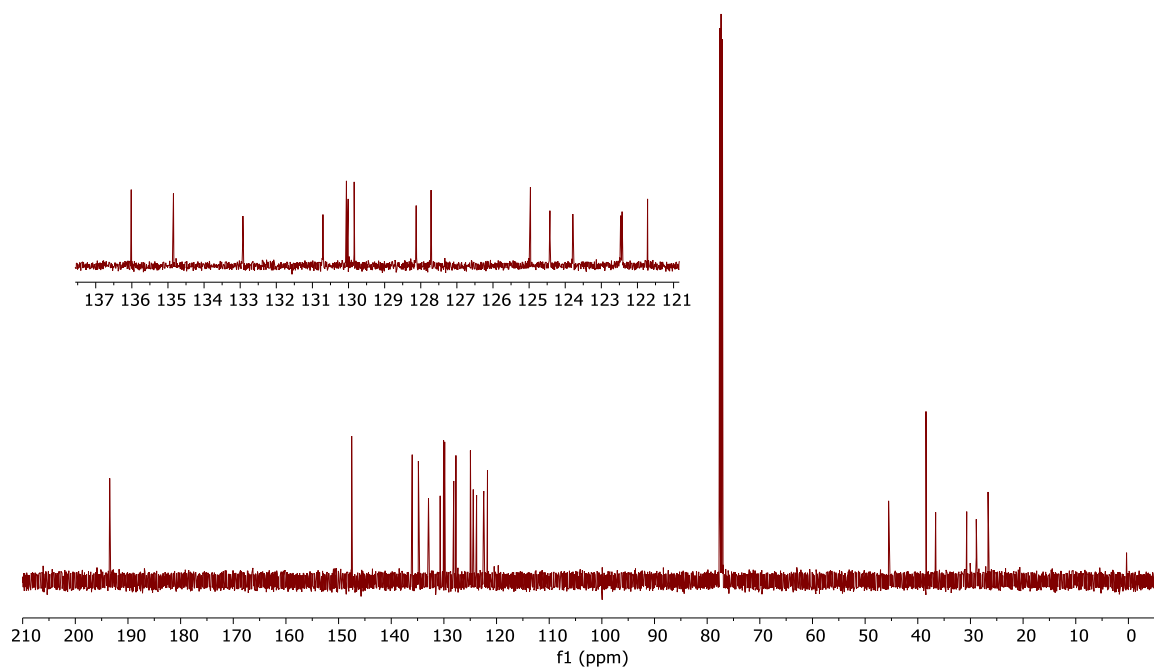
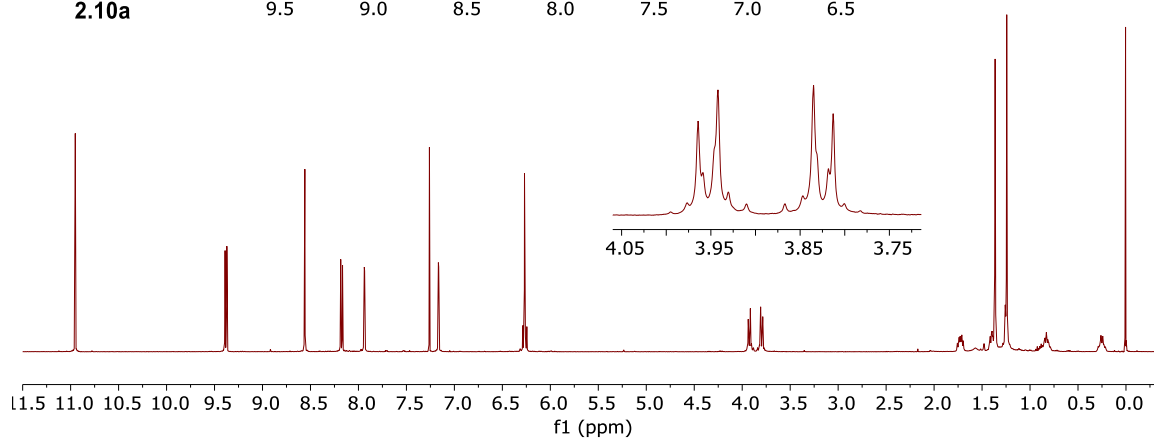
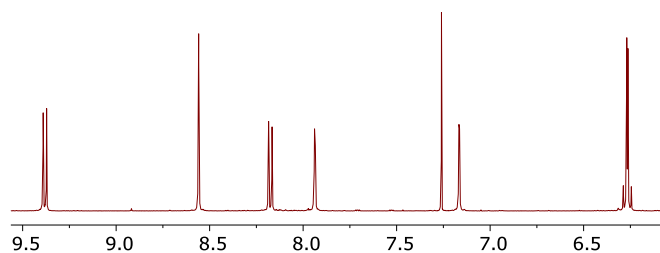


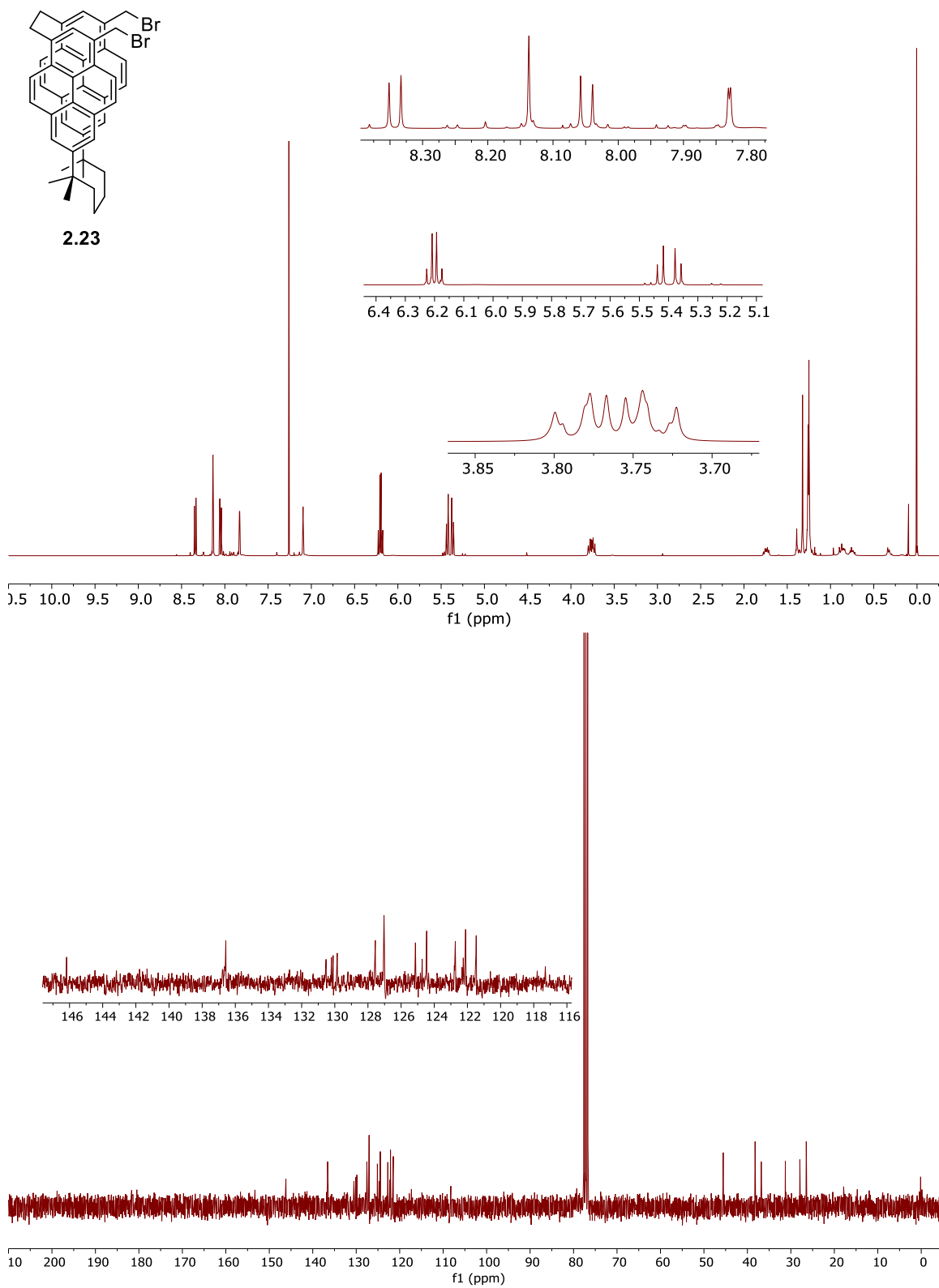
2.20a

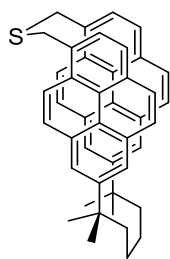




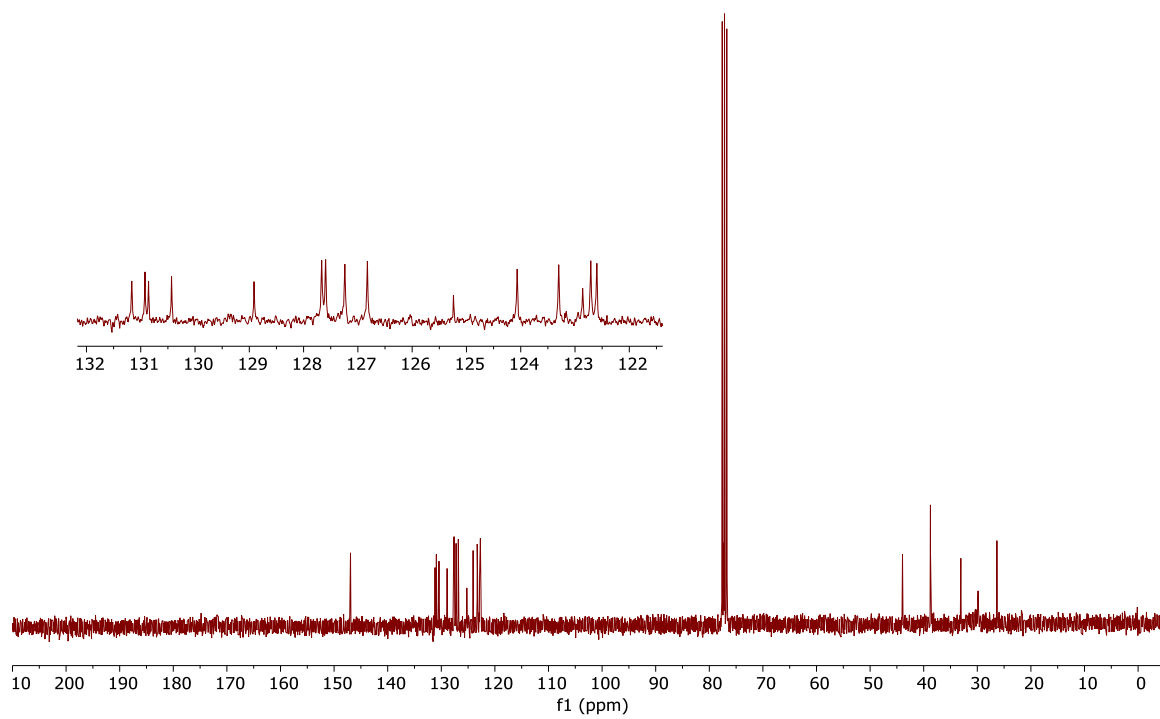
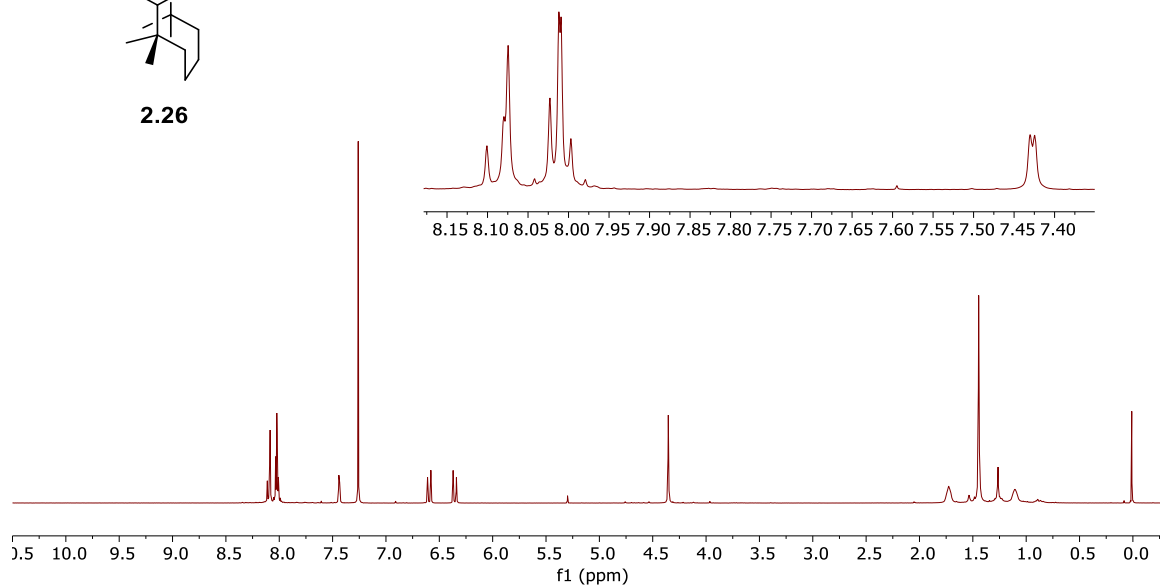
2.10a

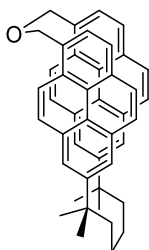




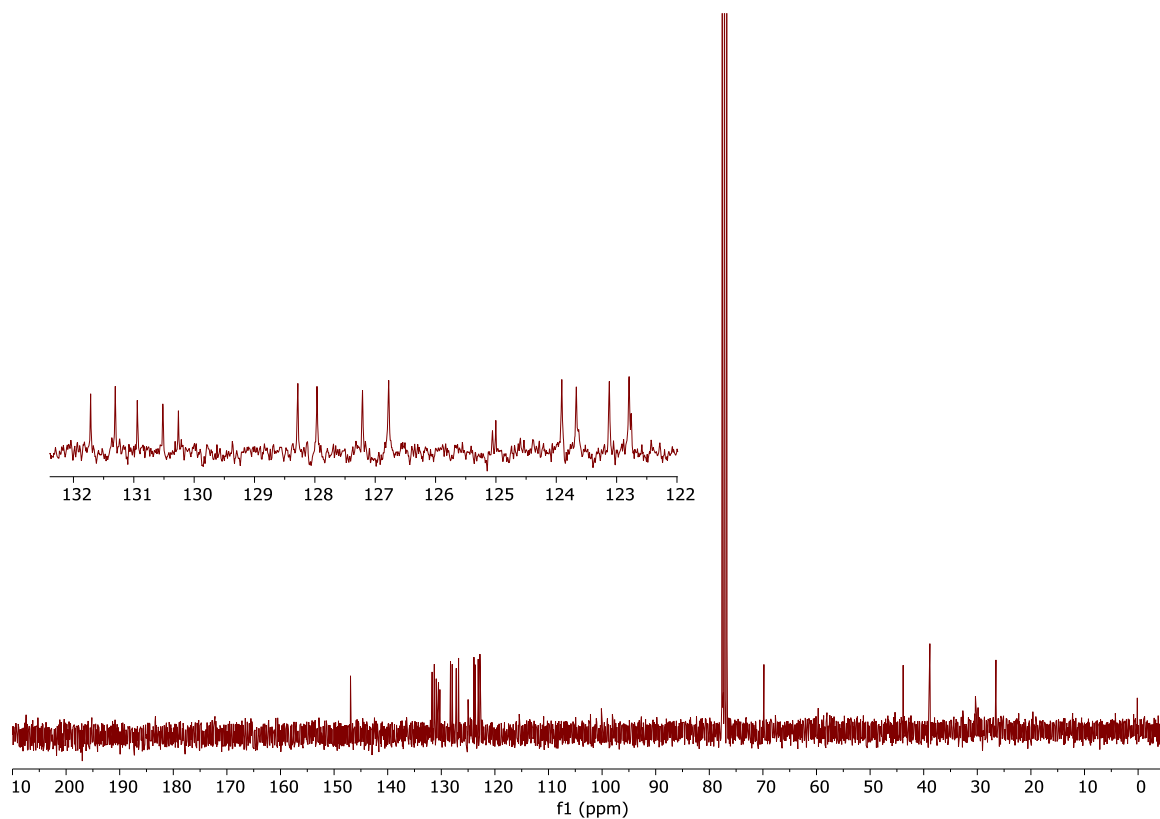
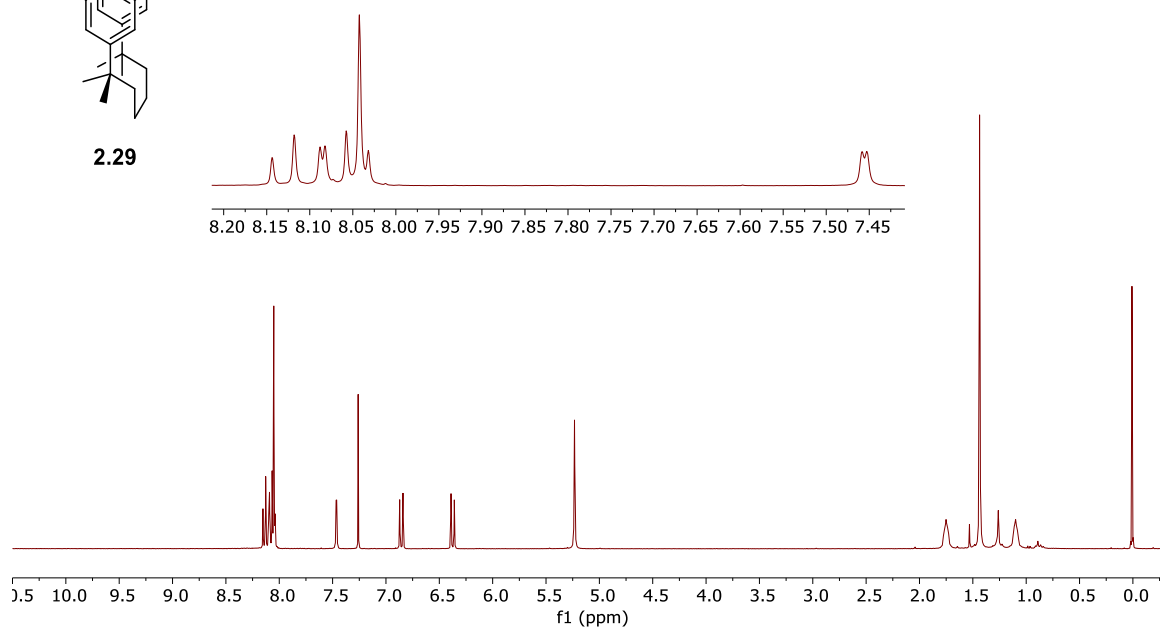


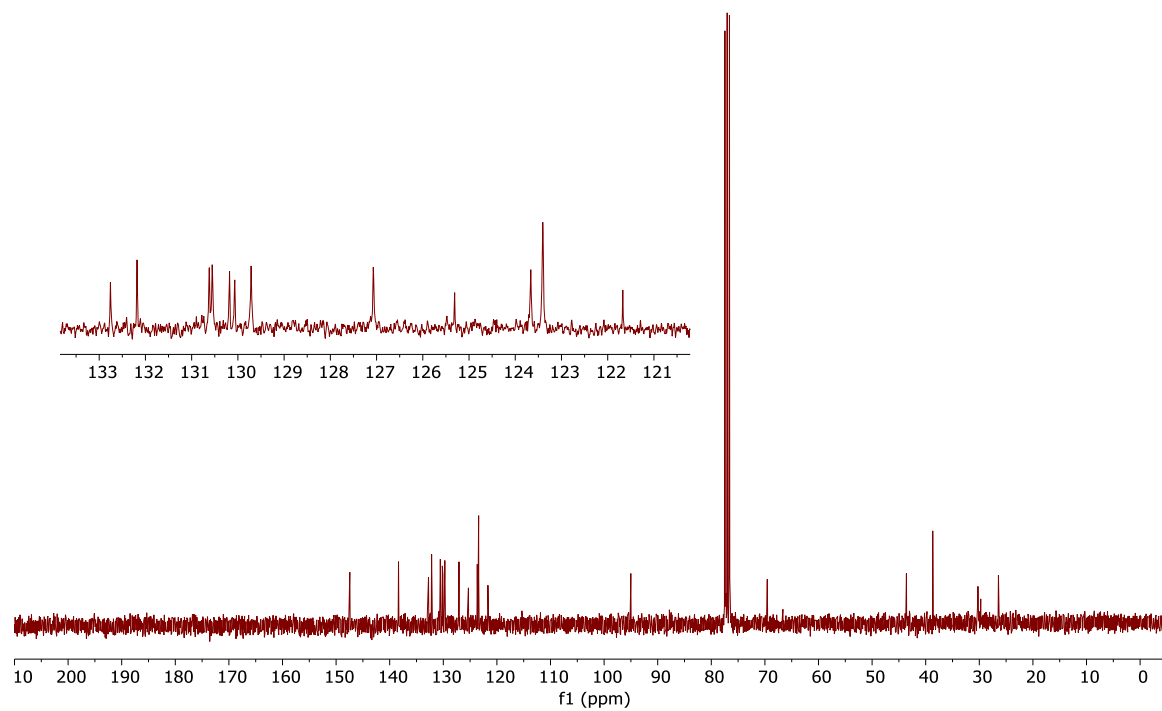
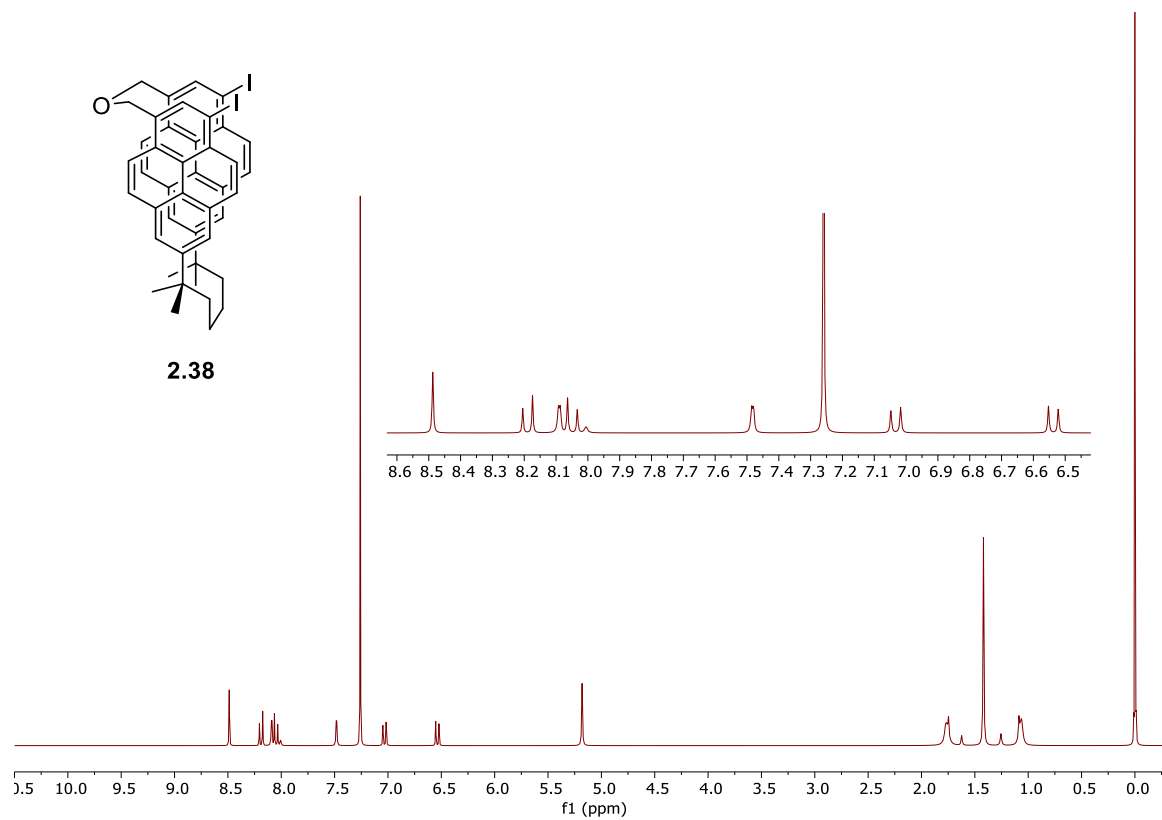
2.26

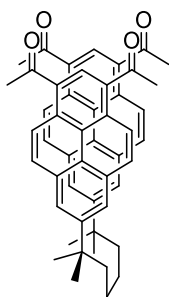




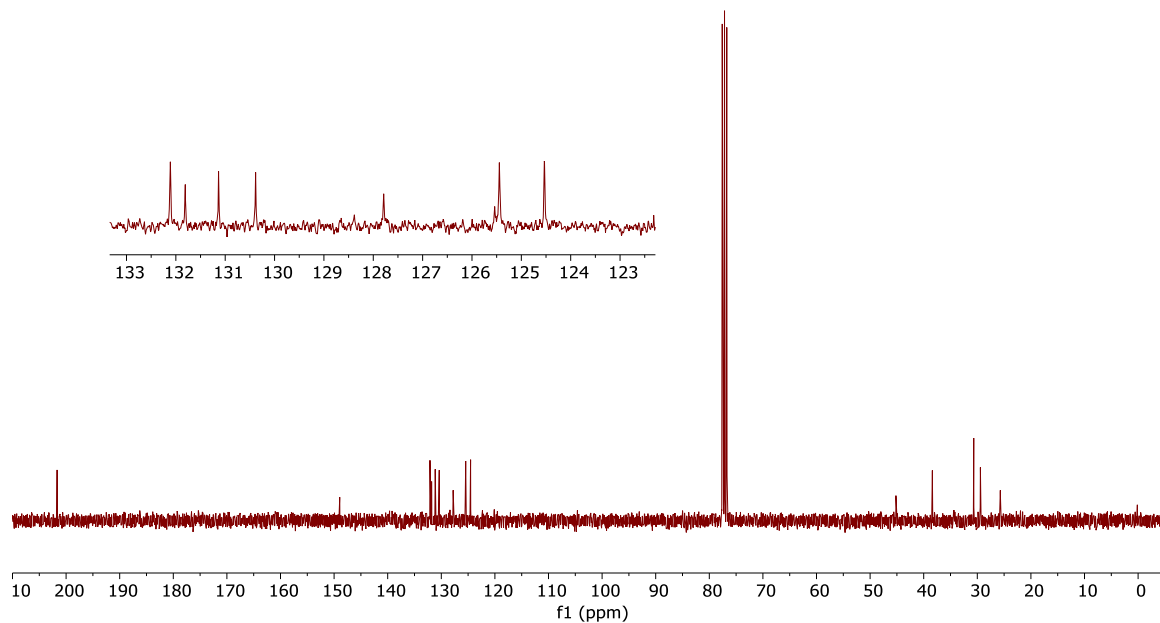
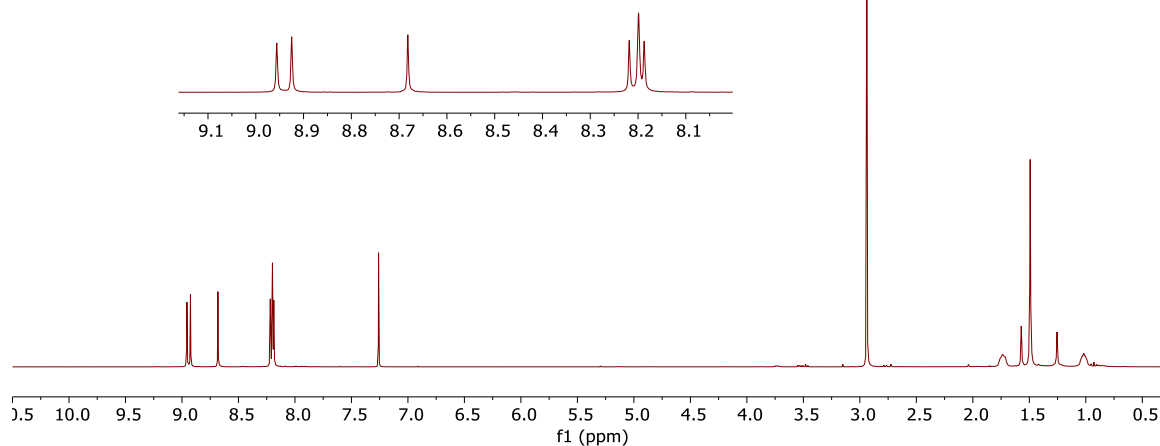
2.29

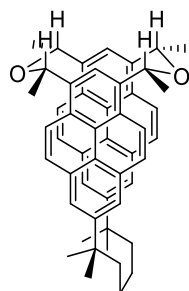




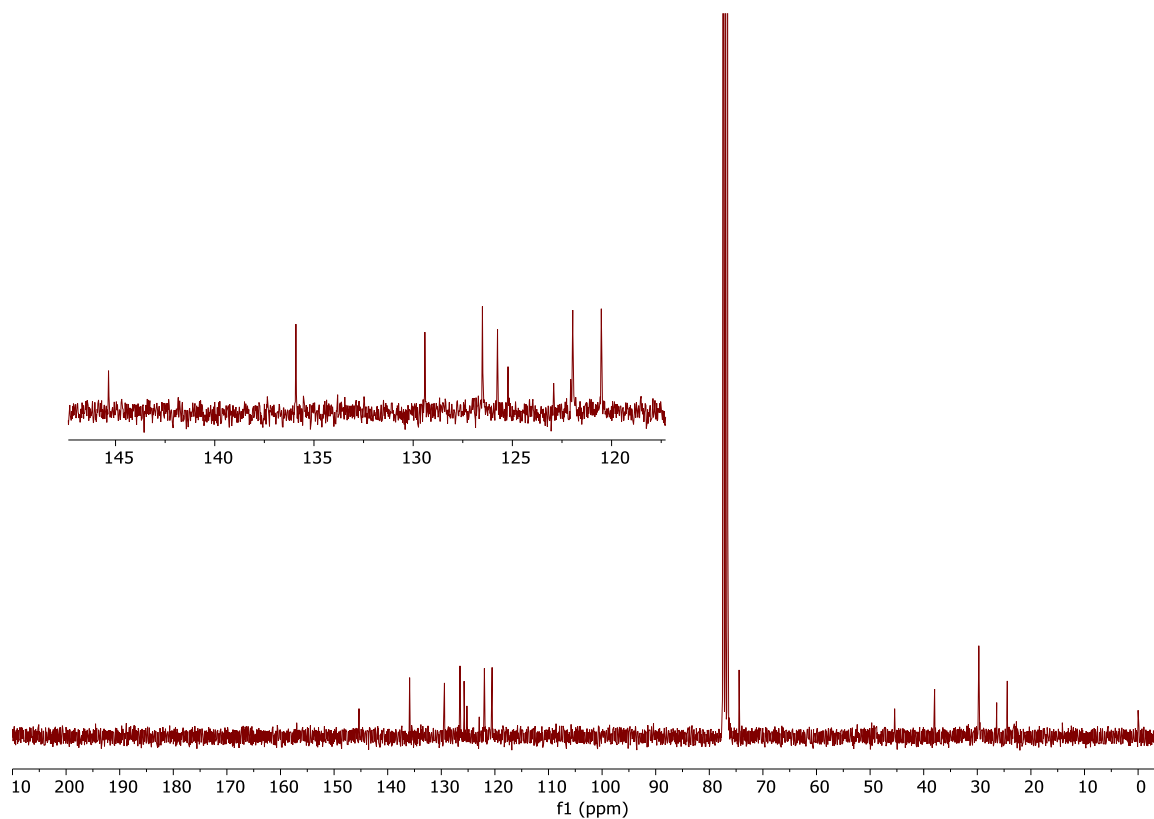
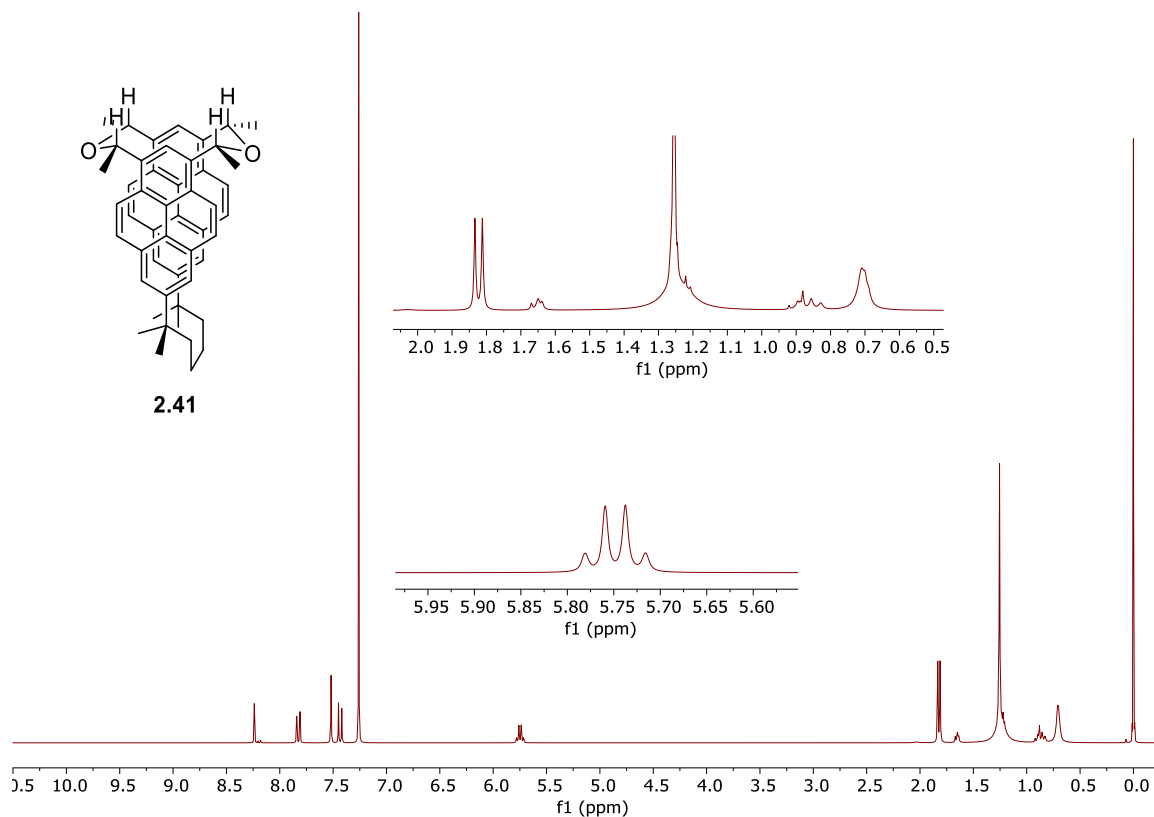


2.39a





2.41



CHAPTER 3: Optimization of the Valence

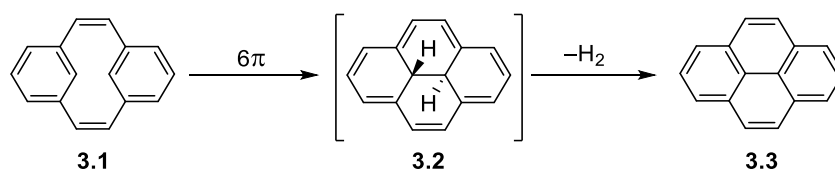
Isomerization/Dehydrogenation (VID) Reaction in the Synthesis of 1,1,*n,n*-Tetramethyl[*n*](2,11)teropyrenophanes and Further Exploration of the Chemistry of These Aromatic Half-Belts

3.1 Introduction

3.1.1 Application of the Valence Isomerization/Dehydrogenation (VID) reaction in the Synthesis of (2,7)Pyrenophanes

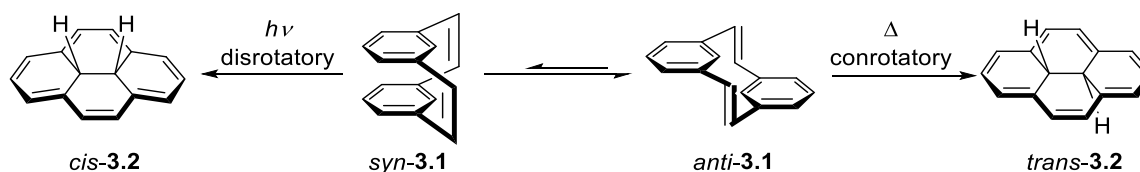
As described in Chapter 1, Type III strategies for cyclophane formation involve the generation of the aromatic system directly in a nonplanar conformation and they are the best-suited ones for the synthesis of more highly-strained cyclophanes.¹ In such cases, the formation of the arene from the bridged pre-arene is accompanied by the gain of a considerable amount of aromatic stabilization energy (ASE), which serves to counterbalance the developing strain.

One of the most powerful among cyclophane-forming reactions is known as the valence isomerization/dehydrogenation (VID) reaction (Scheme 3.1). It is based on an observation by Mitchell and Boekelheide.² The valence isomerization is a 6π electrocyclic ring closure of a [2.2]metacyclophane-1,9-diene (**3.1**), which leads to the formation of a 10b,10c-dihydropyrene (**3.2**).



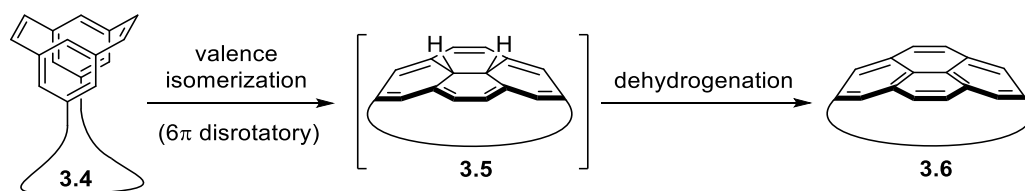
Scheme 3.1 A valence isomerization/dehydrogenation (VID) reaction.

According to the rules of the conservation of orbital symmetry,³ the valence isomerization of *anti*-[2.2]metacyclophanediene (*anti*-**3.1**), which affords *trans*-**3.2** via an antarafacial, conrotatory process, is thermally forbidden/photochemically allowed (Scheme 3.2). In contrast, the valence isomerization of *syn*-[2.2]metacyclophanediene (*syn*-**3.1**) is a suprafacial, disrotatory process, which affords *cis*-dihydropyrene (*cis*-**3.2**) by way of a thermally allowed/photochemically forbidden pathway. Unlike *trans*-dihydropyrene **3.2**, which has a planar carbon skeleton, *cis*-dihydropyrene **3.2** is saucer-shaped due to the eclipsed central C–C bond. The application of this chemistry to the synthesis of the [n](2,7)pyrenophanes **3.6** involved the installation of a chain (tether) to hold the [2.2]metacyclophanediene unit in **3.4** in the *syn* conformation (Scheme 3.3).



Scheme 3.2 *Syn* and *anti* conformers of **3.1** and their valence isomerisation reaction.

The valence isomerization step shapes the nonplanar pyrene framework, first through the formation of dihydropyrene **3.5** and then by dehydrogenation to afford the fully aromatized system (Scheme 3.3). In the cases with a smaller chain, the *cis*-10b,10c-dihydropyrenophane **3.5** would be expected to be distorted from its lowest energy saucer-shaped geometry, but not drastically, so only a relatively small amount of strain is introduced in this step. The dehydrogenation step is where most of the strain arises, but this is offset to a large extent by the gain of a significant amount of aromatic stabilization energy (ASE for pyrene = 74.6 kcal/mol).⁴ The loss of a small amount of torsional strain from the



Scheme 3.3 VID strategy for constructing nonplanar pyrenes.

removal of the two eclipsed C–H bonds may also help to promote the reaction. The first pyrenophane to be synthesized by the Bodwell group using the VID reaction was the 1,8-dioxapyrenophane **3.7** (Figure 3.1).

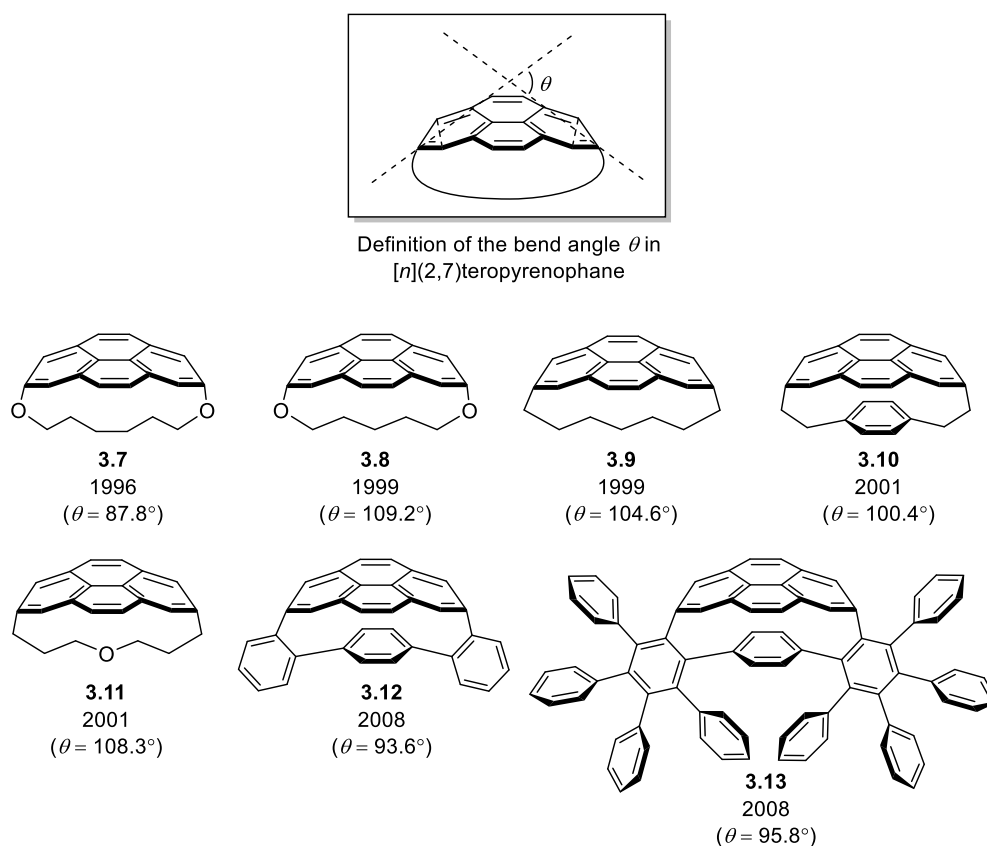
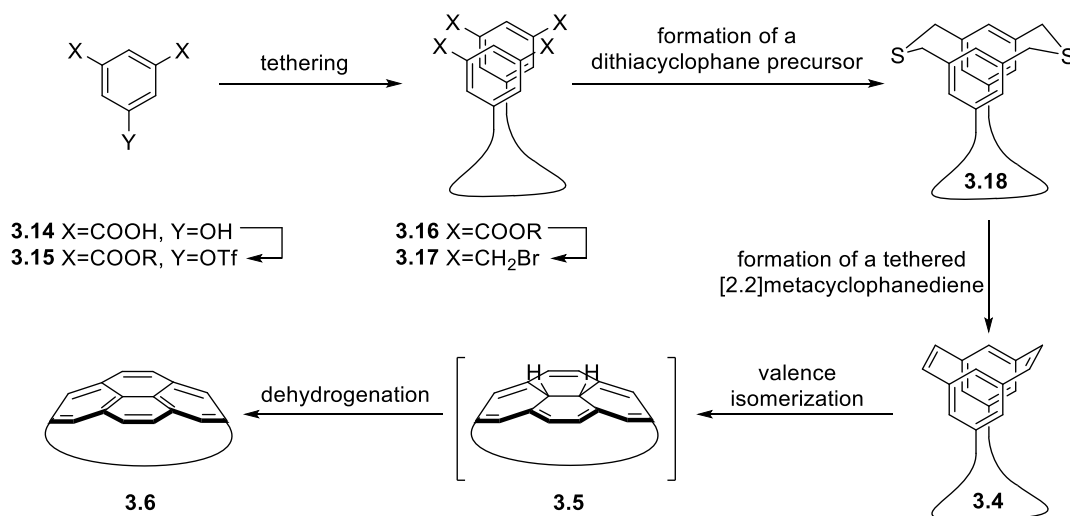


Figure 3.1 Examples of $[n](2,7)$ pyrenophanes synthesized by the Bodwell group.

This pyrenophane and a selection of other examples contain a highly distorted pyrene core. The nonplanarity of the pyrene system is quantified by the bend angle, θ . The

most bent pyrene that has been isolated and characterized using crystallography is the one in pyrenophane **3.8** ($\theta = 109.2^\circ$).

The general approach toward the synthesis of these pyrenophanes can be exemplified by the synthesis of the parent $[n](2,7)$ pyrenophanes. It starts with a 1,3,5-trisubstituted benzene, *i.e.* 5-hydroxyisophthalic acid **3.14** (Scheme 3.4). To prepare for the installation of the tether, the acid groups of **3.14** are esterified and the OH group is activated by triflation to give triflate **3.15**. Two benzene units are then tethered using a Sonogashira cross-coupling reaction to afford **3.16**. The alkynes in **3.16** are then hydrogenated to generate the tether in its final form. To set the stage for cyclophane formation, functional group interconversion (reduction and bromination) is performed to deliver tetrabromide **3.17**. Treatment of **3.17** with $\text{Na}_2\text{S}/\text{Al}_2\text{O}_3$ ⁵ furnishes the low-strain dithiacyclophane **3.18**. A four-step sequence involving *S*-methylation, thia-Stevens rearrangement, *S*-methylation and Hofmann elimination is then applied to convert dithiacyclophane **3.18** into the corresponding tethered [2.2]metacyclophanediene **3.4**.⁶

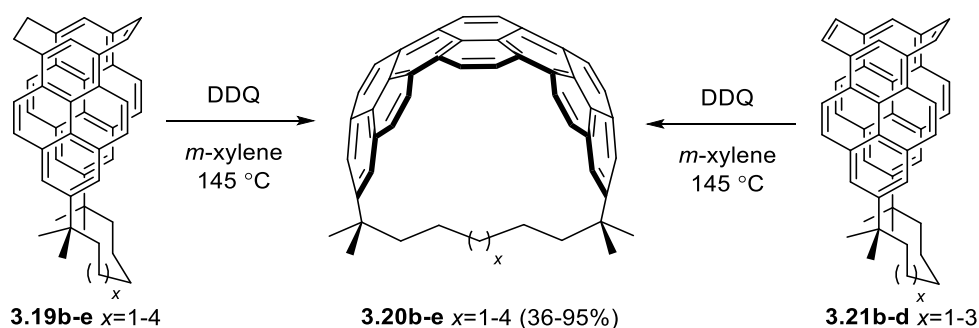


Scheme 3.4 General approach for the synthesis of different types of $[n](2,7)$ pyrenophanes.

The VID reaction of metacyclophanediene **3.4** with DDQ in benzene delivers the target $[n](2,7)$ pyrenophane **3.6**. The discovery that the VID reaction was powerful enough to furnish highly bent pyrene systems was cause for optimism that this methodology could be useful in the synthesis of larger polycyclic systems and even aromatic belts.

3.1.2 Application of the Valence Isomerization/Dehydrogenation (VID) Reaction in the Synthesis of 1,1,*n,n*-Tetramethyl $[n](2,11)$ teropyrenophanes

The extension of the VID reaction to larger aromatic systems has been successfully achieved in the synthesis of a homologous series of 1,1,*n,n*-tetramethyl $[n](2,11)$ teropyrenophanes **3.20b-e** ($n=7-10$). The $[n.2.2]$ pyrenophanemonoenes **3.19b-e** and $[n.2.2]$ pyrenophanediene **3.21b-d** (Scheme 3.5) were comparable to the parent $[2.2]$ metacyclophanediene system (**3.4**) with one significant difference, which was the size of the aromatic building blocks (benzene vs. pyrene). Heating *m*-xylene solutions of these materials (obtained from McMurry and Wurtz coupling reactions described in Chapter 2) at reflux in the presence of DDQ for 30-48 hours afforded the $[8]$ - to $[10](2,11)$ teropyrenophanes **3.20b-d** in high yield.⁸ Treatment of **3.21b-d** with DDQ in *m*-xylene also led to the corresponding teropyrenophanes and no dihydro- and tetrahydroteropyrenophanes were observed, which allayed any concerns regarding the performance of the VID reaction on a $[n.2.2]$ pyrenophanemonoene system and confirmed that the more extensive dehydrogenation involved in these reaction was not problematic.⁹ However, the VID reaction resulting in the most strained teropyrenophane **3.20b** not only required an excess amount of DDQ, but also was low-yielding and **3.19b** could not be consumed completely.



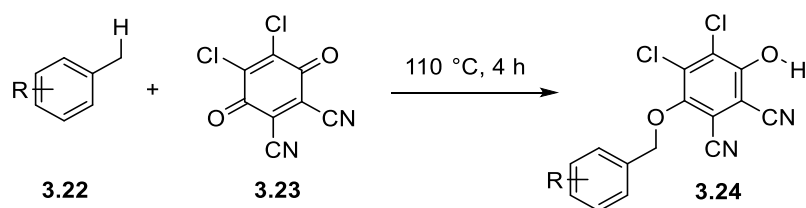
Scheme 3.5 Application of the VID reaction in the synthesis of $[n](2,11)$ teropyrenophanes **3.20b-e** ($x=1-4$).

3.1.3 Issues Associated with the VID Reaction in the Original Synthesis of 1,1, n,n -Tetramethyl $[n](2,11)$ teropyrenophanes

The initial synthetic routes afforded 5-20 mg of $[n](2,11)$ teropyrenophanes, which was only sufficient to determine their crystal structures and basic physical and spectroscopic properties. Hence, to explore their covalent and supramolecular chemistry and also study their application as starting points for the synthesis of larger aromatic systems, multigram quantities of these compounds were necessitated.

A variety of difficulties arose as the synthesis of the $[n](2,11)$ teropyrenophanes was scaled up, most of which were addressed efficiently. The biggest challenges were encountered during the VID step and this remains as the only one without a full solution.

The first issue was the use of the high-boiling solvent *m*-xylene, which was difficult to remove upon completion of the reaction on the large scale. The second major drawback was the need for a large excess of DDQ, which turned out to be due to the known reaction between this reagent and the benzylic C–H bond of methylated aromatic solvents at temperatures $>110^\circ\text{C}$ (Scheme 3.6).^{9,10}

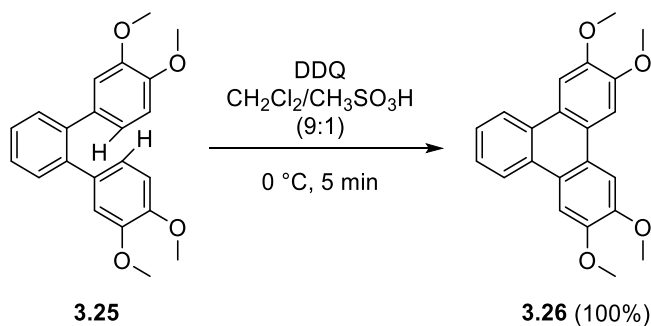


Scheme 3.6 Reaction of methylated aromatic solvents with DDQ.

To prevent the reaction between DDQ and *m*-xylene, benzene, which was originally applied for the synthesis of [8](2,11)teropyrenophane **3.20c**¹¹ was revisited. As previously observed, the reaction in this lower-boiling solvent (80 °C) was very sluggish and a need for the discovery of new conditions to achieve this transform became pressing.

3.1.4 Previous Modified Conditions for the VID Reaction in the Synthesis of 1,1,*n,n*-Tetramethyl[*n*](2,11)teropyrenophanes

The closure of the central bond in the cyclophanemonoenes **3.19b-e** could conceivably occur through a Scholl reaction rather than a valence isomerization. This being the case, Unikela decided to investigate known conditions for the Scholl reaction.⁹ Of particular interest was the report by Rathore and co-workers,¹² who described the conversion of *o*-diphenylbenzene **3.25** into tetramethoxytriphenylene **3.26** in 5 min using



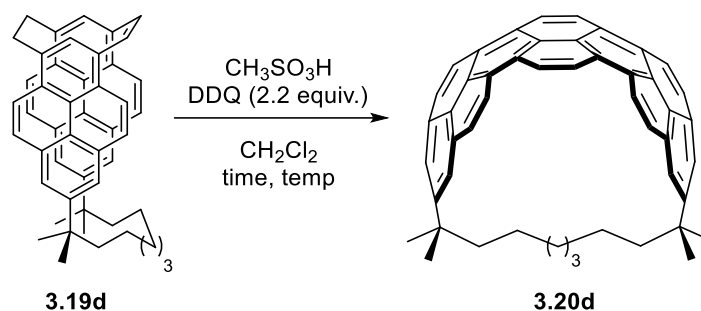
Scheme 3.7 Rathore's synthesis of tetramethoxytriphenylene **3.26** using DDQ/CH₃SO₃H.

2.0 equiv. of DDQ in 9:1 CH₂Cl₂/CH₃SO₃H at 0 °C (Scheme 3.7). Since DDQ was already being employed in the teropyrene forming reaction, it seemed to be a good starting point. Accordingly, the use of these conditions in the synthesis of [9](2,11)teropyrenophane **3.20d** were investigated (Table 1).⁹

Unikela found that the best yield was obtained when 2.2 equiv. of DDQ and 2.0 equiv. of CH₃SO₃H in CH₂Cl₂ at room temperature were used. More importantly, he was successful in scaling up the synthesis of [9](2,11)teropyrenophane to 1.85 g of product in a single experiment. Attention was then turned to the scaling up of the teropyrene-forming step of the next smaller homologue [8](2,11)teropyrenophane **3.20c** (Table 3.2), but the results were not as good, even when other acids were employed. On small scales, minor amounts of some mobile byproducts were observed and even modest scale up (to 100 mg) led to a drastic drop in the yield.

The replacement of DDQ as the oxidizing agent with the other ones such as *o*-chloranil, *p*-chloranil and benzoquinone resulted in no increase in the conversion of **3.19c** into **3.20c** even after heating the reaction for a few days. The use of toluene or ethyl acetate as the solvent resulted in no reaction.

Table 3.1 Previous optimization of the VID reaction of [n.2.2]pyrenophanemonoene **3.19d** using DDQ/CH₃SO₃H.

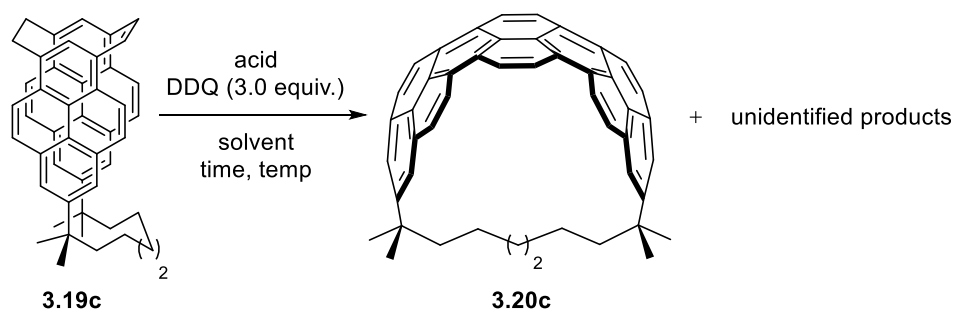


entry	3.19d (g)	CH ₃ SO ₃ H (equiv.)	t (min)	temp (°C)	3.20d (%)
1	0.01	9:1 CH ₂ Cl ₂ /CH ₃ SO ₃ H	2	0	5
2	0.01	9.5:0.5 CH ₂ Cl ₂ /CH ₃ SO ₃ H	2	0	12
3	0.01	1	120	40	75
4	0.01	2	8	rt	88
5	0.10	2	10	rt	88
6	0.50	2	10	rt	88
7	1.04	2	10	rt	85
8	2.20	2	10	rt	83

data are from reference 9

Application of the optimized conditions to form the most strained homologue [7](2,11)teropyrenophane **3.20b** was also disappointing due to the presence of substantial amounts of byproducts, partial consumption of the starting materials, time-consuming reactions and very low yields.⁹ It appeared as though the product was not stable under the conditions of its formation, possibly due to intermolecular Scholl reactions. Therefore, further research to investigate the scale up of [7]- and [8](2,11)teropyrenophanes was sorely needed.

Table 3.2 Previous optimization of the VID reaction of [*n*.2.2]pyrenophanemonoenes **3.19c**.



entry	3.19c (mg)	acid (equiv.)	solvent	t (h)	temp (°C)	3.20c (%)
1	5	CH ₃ SO ₃ H (2.0)	CH ₂ Cl ₂	0.1	rt	5
2	50	CH ₃ SO ₃ H (1.5)	CH ₂ Cl ₂	0.1	rt	22
3	50	CH ₃ SO ₃ H (1.0)	CH ₂ Cl ₂	0.15	40	52
4	50	CH ₃ SO ₃ H (0.5)	CH ₂ Cl ₂	2.5	40	38
5	50	CH ₃ SO ₃ H (0.5)	CHCl ₃	2.5	70	44
6	5	CF ₃ CO ₂ H (2.2)	CH ₂ Cl ₂	4.0	rt	5
7	5	CF ₃ CO ₂ H (4.5)	CH ₂ Cl ₂	1.5	rt	30
8	5	CF ₃ CO ₂ H (7.5)	CH ₂ Cl ₂	0.5	rt	60
9	10	CF ₃ CO ₂ H (7.5)	CH ₂ Cl ₂	0.5	rt	30
10	10	CF ₃ CO ₂ H (15.0)	CH ₂ Cl ₂	0.1	rt	53
11	10	CF ₃ CO ₂ H (35.0)	CH ₂ Cl ₂	0.1	rt	8
12	50	CF ₃ CO ₂ H (15.0)	CH ₂ Cl ₂	0.1	0	21
13	50	CF ₃ CO ₂ H (15.0)	CH ₂ Cl ₂	0.2	−30	15
14	50	CF ₃ CO ₂ H (15.0)	toluene	48.0	rt	–
15	50	CF ₃ CO ₂ H (15.0)	ethyl acetate	96.0	rt	–
16	10	CHCl ₂ CO ₂ H (15.0)	CH ₂ Cl ₂	24.0	rt	5
17	10	CHCl ₂ CO ₂ H (30.0)	CH ₂ Cl ₂	16.0	rt	10
18	10	CHCl ₂ CO ₂ H (45.0)	CH ₂ Cl ₂	16.0	rt	16
19	100	CHCl ₂ CO ₂ H (0.5 mL)	CH ₂ Cl ₂ (9.5 mL)	1.0	rt	29
20	10	CH ₃ CO ₂ H (15.0)	CH ₂ Cl ₂	24.0	rt	trace
21	10	CH ₃ CO ₂ H (0.5 mL)	CH ₂ Cl ₂ (0.5 mL)	12.0	50	10
22	10	CH ₃ CO ₂ H (0.5 mL)	–	48.0	50	–
23	10	<i>p</i> -TsOH (1.0)	CH ₂ Cl ₂	12.0	rt	trace

data are from reference 9

3.2 Results and Discussions

3.2.1 New Conditions for the VID Reaction in the Synthesis of 1,1,*n*-Tetramethyl[*n*](2,11)teropyrenophanes

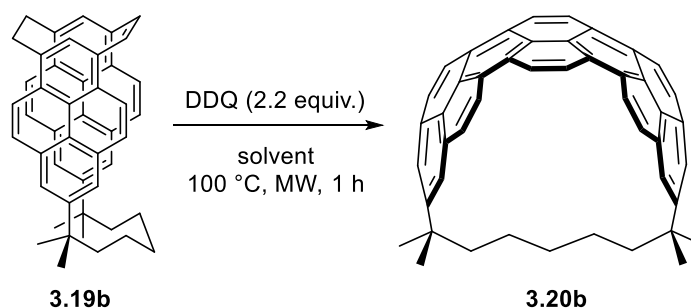
The recently modified VID methodology was only capable of delivering the least strained homologues, [*n*](2,11)teropyrenophanes **3.20d-e** in good yields and in the case of [9](2,11)teropyrenophane **3.20d**, on a gram scale. The reaction leading to the lower homologues **3.20b-c** remained problematic and scale-limited due to incomplete consumption of the starting materials and the formation of byproducts. Therefore, the development of new methodology, which could clearly afford the full series of [*n*](2,11)teropyrenophanes **3.20b-e** on a gram scale was investigated.

3.2.1.1 Application of Microwave Conditions for the VID Reaction of [7](2,11)teropyrenophane (**3.20b**)

The modification of the VID reaction to target [*n*](2,11)teropyrenophanes was started with variation of the solvent. Hence, 10 common organic solvents were selected (Table 3.3). Reactions to convert **3.19b** to the corresponding [7](2,11)teropyrenophane **3.20b** were performed on a 5 mg scale with 2.2 equiv. of DDQ in 2 mL solvent. To keep the temperature constant, microwave irradiation (100 °C) was employed and the reactions were run for 1 hour in the absence of any acid. The most efficient conversion of **3.19b** into **3.20b** occurred when 1,2-dichloroethane, acetonitrile, and chloroform were used (Table 3.3, Entries 1-3). In acetonitrile, no byproducts and only the slightest trace of starting material was observed, while in 1,2-dichloroethane or chloroform, traces of byproducts were found. In addition, a small amount of starting material remained in chloroform (TLC and ¹H NMR

analysis). Only modest conversion of **3.19b** into teropyrenophane **3.20b** occurred in ethyl acetate, *m*-xylene, and benzene (Table 3.3, Entries 4-6). Curiously, absolutely no reaction took place when hexanes, 1,4-dioxane, tetrahydrofuran, or toluene were used as the solvent (Table 3.3, Entries 7-10). Consequently, acetonitrile, which has a higher dielectric constant (ϵ) than others, was chosen as the most effective solvent. This suggests that there is a polar intermediate that is being stabilized during the VID reaction.

Table 3.3 Optimized microwave conditions for the VID reaction of [*n*.2.2]pyrenophanemonoene **3.19b**.



entry	solvent	3.20b (%)	dielectric constant (ϵ) ^c
1	1,2-dichloroethane	88 ^a	10.4
2	acetonitrile	91 ^a	36.6
3	chloroform	86 ^a	4.8
4	ethyl acetate	trace ^b	6.0
5	<i>m</i> -xylene	trace ^b	2.4
6	benzene	trace ^b	2.3
7	hexanes	0 ^b	1.9
8	1,4-dioxane	0 ^b	2.3
9	tetrahydrofuran	0 ^b	7.5
10	toluene	0 ^b	2.4

^a isolated yield

^b according to ¹H NMR and TLC analysis.

^c the values were obtained from Vogel's Practical Organic Chemistry (5th ed.).

In Figure 3.2, the aromatic region of the ^1H NMR spectra of the crude VID reactions performed in some of the mentioned solvents, are shown. The conversion of **3.19b** to **3.20b** is almost complete in 1,2-dichloroethane, chloroform and acetonitrile while no reactions occurred in toluene and tetrahydrofuran. Upon moving from toluene to ethyl acetate, the intensity of signals related to the [n.2.2]pyrenophanemonoene **3.19b** is reduced and only traces of the product (**3.20b**) signals are observed in ethyl acetate.

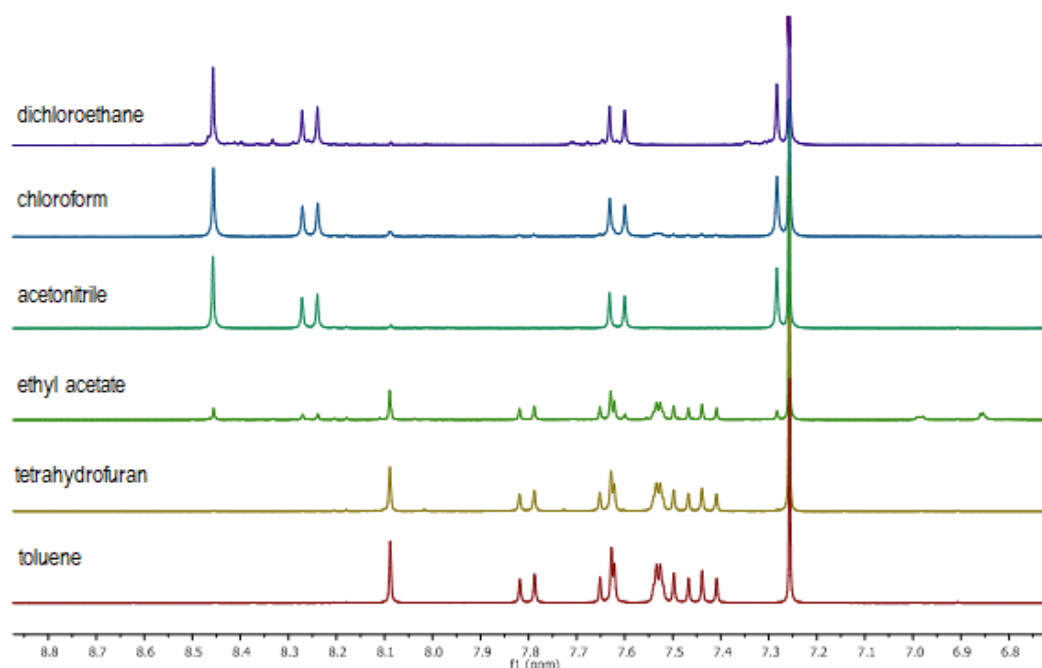


Figure 3.2 Aromatic region of the ^1H NMR spectra of the crude VID reactions of **3.19b**.

Having had remarkable success in finding a better solvent, attention was turned to the scaling up of the VID reaction. The major problem of using microwave conditions was the limit of vessels available for the large-scale reactions. Therefore, the second step of the modification was changing the microwave conditions to thermal in the preferred solvents.

3.2.1.2 Application of the Thermal Conditions for the VID Reaction of [7](2,11)Teropyrenophane (**3.20b**)

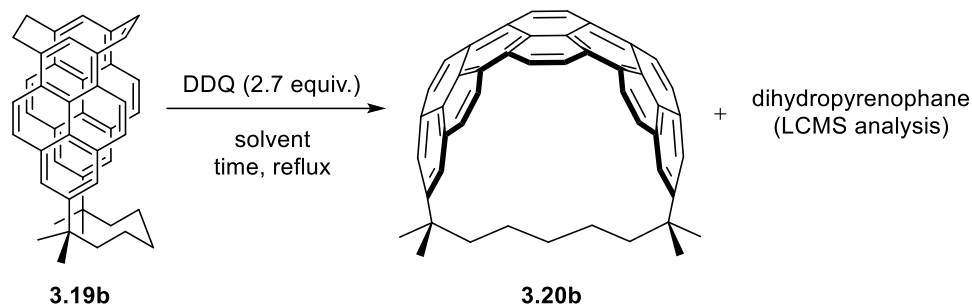
Similar to what was described in the previous Section, 2.2 equiv. of DDQ was used in 4 different solvents including 1,2-dichloroethane, chloroform, ethyl acetate and acetonitrile to afford [7](2,11)teropyrenophane **3.20b**. On a 5 mg scale, the conversion of **3.19b** into **3.20b** was incomplete in chloroform and ethyl acetate while in 1,2-dichloroethane and acetonitrile almost all starting materials were consumed (Table 3.4). Hence the reaction was scaled up to 25 mg in these two solvents. When 2.2 equiv. of DDQ was used, unlike the previous reactions, unreacted starting material and product were observed after 2.5 h at reflux (TLC analysis), thus 0.5 more equiv. of DDQ was added, which led to the consumption of the majority of remaining starting materials in less than 1 hour.

The reaction was repeated in both solvents at reflux with 2.7 equiv. of DDQ and this time only minor amounts of the starting material and dihydropyrenophane (LCMS analysis) along with product were observed (TLC analysis). Moreover, the yield of compound **3.20b** was improved to 94% (CH₃CN) and 78% (DCE). With the optimized conditions in hand (2.7 equiv. of DDQ in CH₃CN at reflux), the reaction was scaled up to 100 mg (Table 3.4, Entry 9). Although the yield dropped to 87% it was still remarkable for the most strained homologue.

The optimized conditions were then investigated on a gram scale (Table 3.4, Entry 10), which led to almost complete reaction (traces of starting material remained by TLC analysis) with high product yield (81%) after 3 hours. With these fruitful results, an attempt to scale up the less-strained homologue **3.20c** was undertaken.

Table 3.4 Optimized thermal conditions of the VID reaction of [*n*.2.2]pyrenophanemonoene

3.19b.



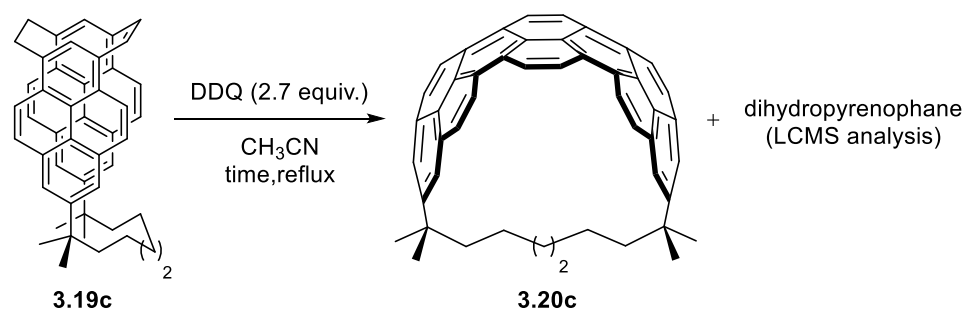
entry	3.19b (mg)	DDQ (equiv.)	solvent	time (h)	3.20b (%)
1	5	2.2	ethyl acetate	4.0	55
2	5	2.2	1,2-dichloroethane	3.5	82
3	5	2.2	acetonitrile	3.5	89
4	5	2.2	chloroform	4.0	49
5	25	2.2	1,2-dichloroethane	3.5	61
6	25	2.2	acetonitrile	3.5	71
7	25	2.7	1,2-dichloroethane	3.0	78
8	25	2.7	acetonitrile	3.0	94
9	100	2.7	acetonitrile	3.0	87
10	1020	2.7	acetonitrile	3.5	81

3.2.1.3 Application of Thermal Conditions for the VID Reaction of [8](2,11)teropyrenophane (**3.20c**)

Having had great success in addressing the problem of the large-scale VID reaction of **3.19b**, attention was turned to the less-strained homologue, [8](2,11)teropyrenophane (**3.20c**). The optimized conditions were investigated on 5 mg, 25 mg, and 1.29 g scale of **3.19c** (Table 3.5). The [*n*.2.2]pyrenophanemonoene **3.19c** was converted into

corresponding teropyrenophane **3.20c** in 2-2.5 hours with 85-90% yields. On a gram scale, only minor amounts of dihydropyrenophane was observed (LCMS analysis) while the starting material was fully consumed.

Table 3.5 Optimized thermal conditions of the VID reaction of [*n*.2.2]pyrenophanemonoene **3.19c**.



entry	3.19c (mg)	time (h)	3.20c (%)
1	5	2.0	90
2	25	2.5	88
3	1298	2.5	85

As a result, a modified and relatively mild protocol for the key teropyrene-forming step (a VID reaction) was developed and this enabled the construction of the highly-strained [7] and [8]teropyrenophanes (**3.20b-c**) on a gram-scale with excellent yields.

3.2.2 Chemistry of the 1,1,*n,n*,-Tetramethyl[*n*](2,11)teropyrenophanes

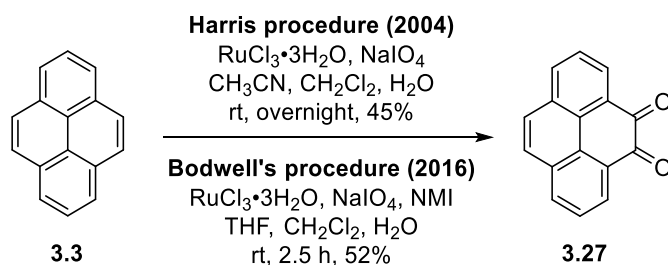
The ability of the modified conditions of the VID reaction to generate gram quantities of teropyrenophanes **3.20b-d** provided the opportunity to further explore the chemical reactivity and photophysical properties of these distorted large polynuclear

aromatic hydrocarbons (PAHs). In this regard, the direct oxidation of [7]- to [9](2,11)teropyrenophanes **3.20b-d** was studied, which not only contributed to the investigating of how systematic changes in the structure of the teropyrene unit affect its reactivity, but also could provide opportunities to convert of these *K*-region-containing PAHs into larger π -systems.

3.2.2.1 Oxidation of [7]- to [9](2,11)Teropyrenophanes to the Corresponding Diones

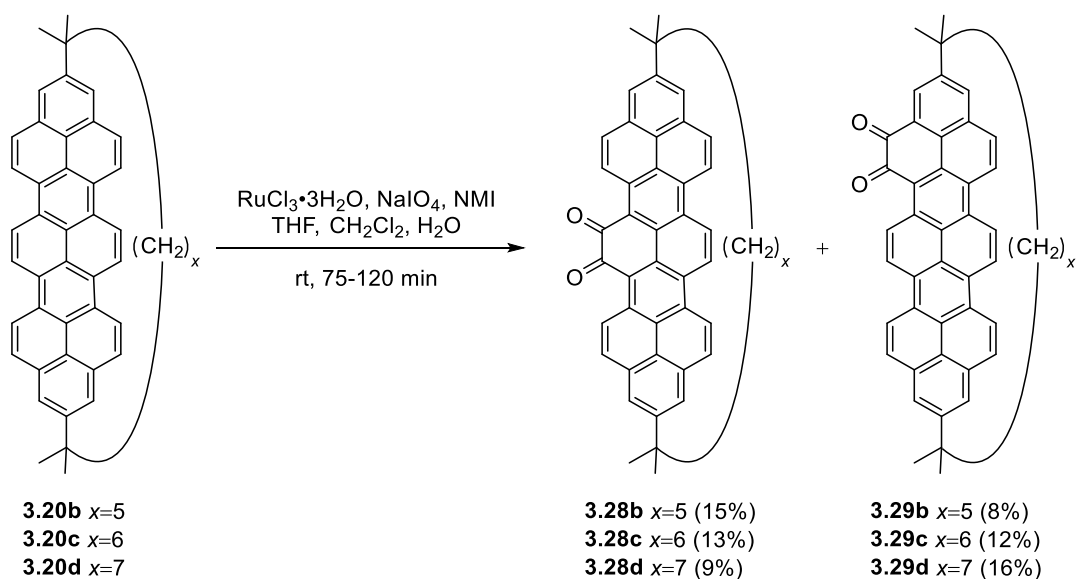
The selective oxidation of *K*-region of PAHs is a powerful method to functionalize PAHs and modify their reactivity. From a biological perspective, the resulting oxidation products are useful precursors to *K*-region oxides, which are responsible for the known carcinogenicity of PAHs and from an organic synthetic point of view, they are interesting precursors to larger π -conjugated systems.¹³

Harris and co-workers¹⁴ reported a single-step oxidation of pyrene (**3.3**) to pyrene-4,5-dione (**3.27**) utilizing catalytic amounts of ruthenium chloride in the presence of sodium metaperiodate. The major drawback of Harris's procedure was the problematic workup due to the black byproducts formed during the reaction, which preclude efficient filtration or separation. Hence, in 2016, the Bodwell group modified this procedure¹⁵ by replacing acetonitrile (one of the co-solvents) with THF and addition of *N*-methylimidazole (NMI), which allowed the reaction to be completed in 2.5 hours in 52% yield (Scheme 3.8). It was of interest to see if the optimized reaction could be exploited for oxidising larger *K*-region-containing PAHs such as [*n*](2,11)teropyrenophanes **3.20b-d** to the corresponding diones (Scheme 3.9).



Scheme 3.8 Harris' and Bodwell's oxidation of pyrene using $\text{RuCl}_3/\text{NaIO}_4$.

[7]- to [9](2,11)teropyrenophanes **3.20b-d** were subjected to oxidation reaction conditions using $\text{RuCl}_3/\text{NaIO}_4$. There are six *K*-region in **3.20b-d**, two of one type (central) and four of another (flanking). As such, two isomeric diones, **3.28b-d** (symmetric) and **3.29b-d** (unsymmetric) could conceivably form. If the reactivity of the two types of *K*-regions is the same, then a 1:2 ratio of **3.28b-d**:**3.29b-d** would be expected. The oxidation of **3.20d** afforded **3.28d** in 9% yield and **3.29d** in 16% yield. The slight deviation from the 1:2 ratio suggests that the two *K*-region have similar reactivity, the central one being slightly more reactive. In moving to **3.20c**, the yields of **3.28c** (13%) and **3.29c** (12%) are



Scheme 3.9 Oxidation of [7]- to [9](2,11)teropyrenophanes using $\text{RuCl}_3/\text{NaIO}_4$.

close to 1:1, which implies that the central *K*-region is now roughly twice as reactive as the flanking ones. This trend continues upon moving to **3.20b**, where the product ratio of **3.28b** (15%) to **3.29b** (8%) is now roughly 2:1 in favour of symmetric dione. This suggests that the central *K*-region is now about four times as reactive as the flanking ones.

The crystal structures of **3.20b-d** revealed that the most pronounced distortion from planarity in the teropyrene system is in the middle. This being the case, it seems reasonable, that this is where the greatest change in chemical reactivity would occur with increasing bend.

The absorption spectra of **3.28b-d** and **3.29b-d** consist of three sets of bands, in the ranges of 307-349 nm, 393-443 nm and 454-624 nm for **3.28b-d** and 299-375 nm, 398-463 nm and 501-704 nm for **3.29b-d**. The longest wavelength absorption maxima (λ_{max}) for the symmetrical diones are observed at 518, 511, and 504 nm for **3.28b**, **3.28c** and **3.28d**, respectively (Figure 3.3, first spectrum). The red shift that accompanies the increasing bend in the teropyrene system contrasts the blue shift that was observed for the teropyrenophanes **3.20b-d**.

Interestingly, considerably longer wavelength bands are observed for the unsymmetrical diones at 583, 593, and 603 nm for **3.29b**, **3.29c** and **3.29d**, respectively (Figure 3.3, second spectrum). The unsymmetrical diones **3.29b-d** show a blue shift with increasing bend in the teropyrene system, which is consistent with the observed trend in parent [*n*](2,11)teropyrenophanes **3.20b-d**. All six diones were found to be non-fluorescent. The contrasting trends in the absorption spectra of **3.28b-d** and **3.29b-d** were surprising and invited further scrutiny.

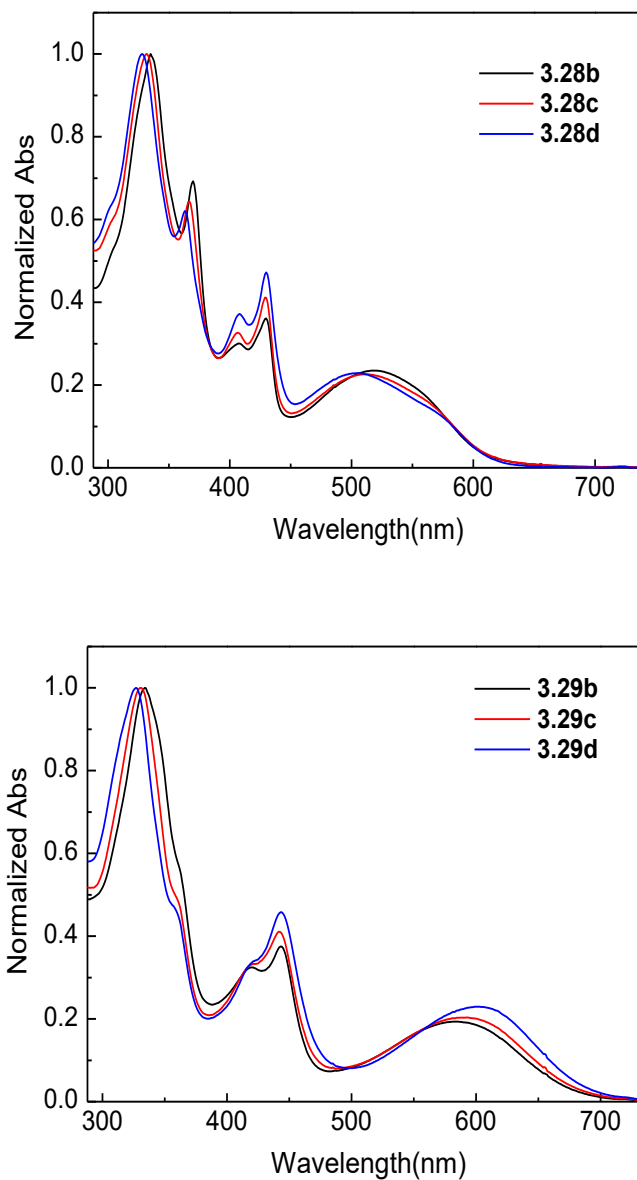


Figure 3.3 Normalized absorption spectra of diones **3.28b-d** (first spectrum) and **3.29b-d** (second spectrum) measured in CHCl_3 at room temperature.

The lowest-energy absorption bands of **3.28b-d** and **3.29b-d** all appear as broad peaks without clear vibronic features. Such spectral patterns make it difficult to precisely

determine the lowest-energy electronic transition. Deconvolution of the absorption spectra was therefore performed to gain a deeper insight into the composition of absorption bands involved in this low-energy region.[¶] As shown in Figure 3.4, the Gaussian-type functions were used to achieve very good spectral fitting outcomes, giving deconvoluted bands clearly. Now both sets of diones **3.28b-d** and **3.29a-d** show a blue shift of the longest wavelength absorption band as the teropyrene system becomes more distorted. There is also less of a difference (40-53 nm) in the position of the longest wavelength bands of symmetric and unsymmetric diones than there was in the simple inspection of the spectra (65-99 nm).

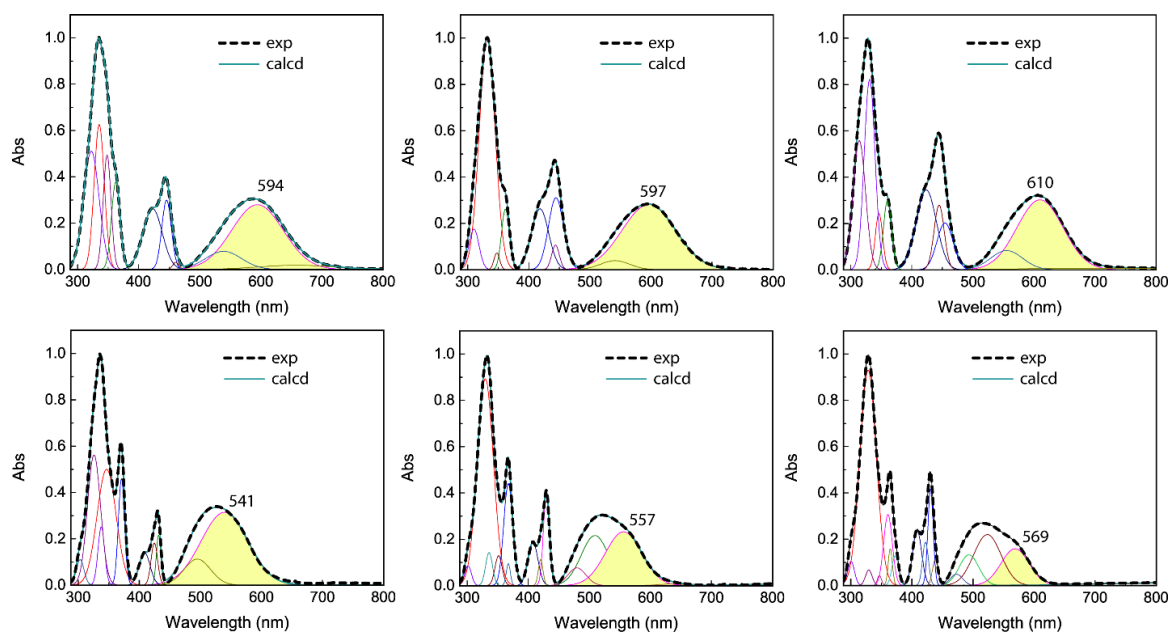


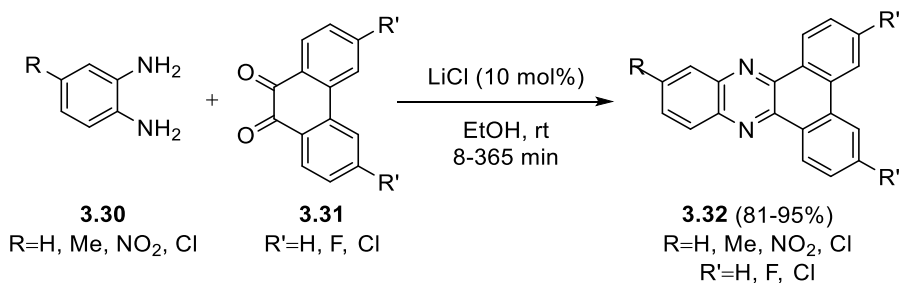
Figure 3.4 Deconvoluted UV-Vis absorption spectra of **3.29b-d** (first row, left to right) and **3.28b-d** (second row, left to right). Each spectrum was subjected to baseline correction and then fitted with Gaussian-type functions using the Fityk software package. The wavelengths of the lowest-energy peaks from the spectral fitting are highlighted.

[¶] Deconvolution were performed by Prof. Yuming Zhao, Memorial University of Newfoundland.

3.2.2.2 Teropyrenophanediones as Precursors to Larger π -Systems

Diones **3.28b-d** and **3.29b-d**, are not only potentially useful compounds for the synthesis of functionalized $[n](2,11)$ teropyrenophanes, but could also be used as starting points to grow larger systems. In this regard, it was decided to react symmetrical and unsymmetrical diones **3.28b-d** and **3.29b-d** with 1,2-aryldiamines to form 1,4-aryldiazine derivatives of teropyrenophanes (quinoxalinoteropyrenophanes). The chemistry of 1,4-aryldiazines such as quinoxalines has attracted wide interest due to their potential biological activities^{16,17} as well as their applications as building blocks for the synthesis of organic semiconductors¹⁸ and electrical and photochemical materials.^{19,20}

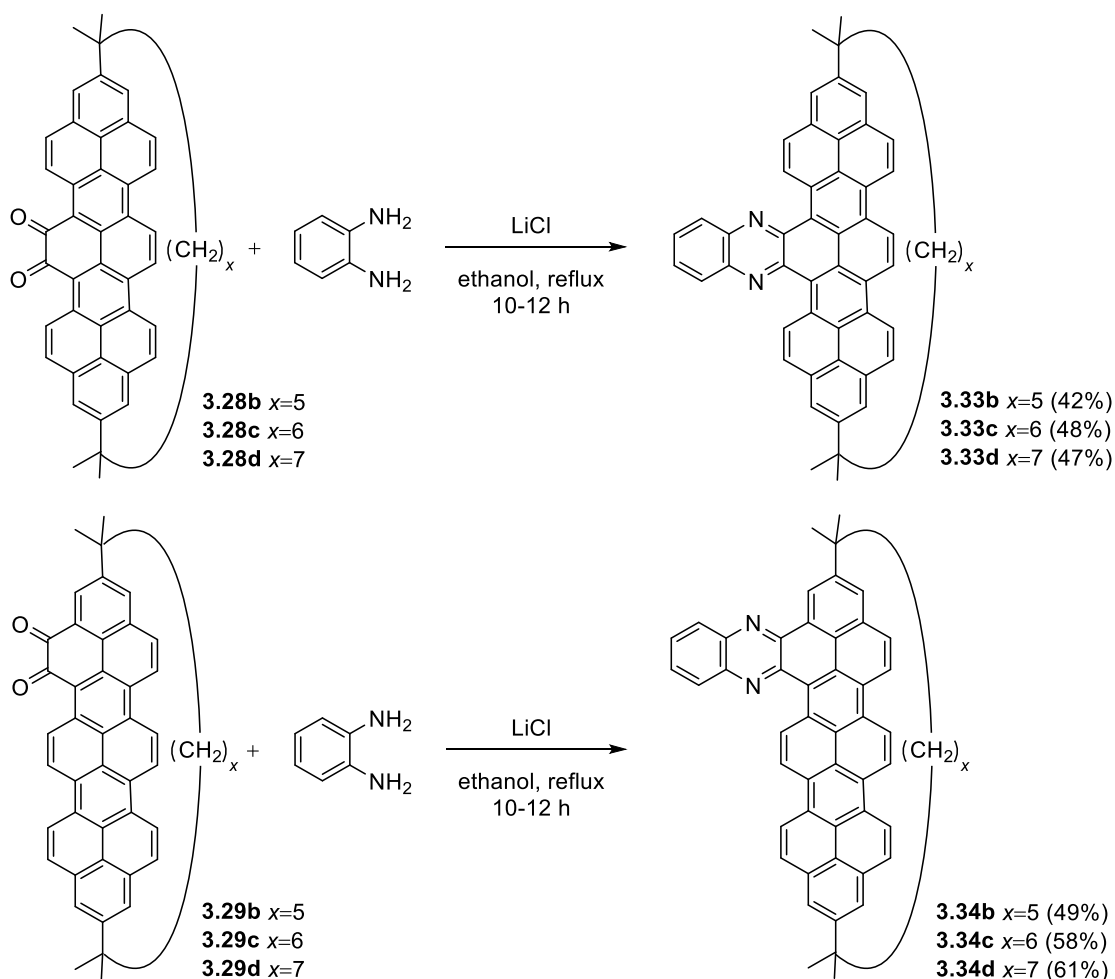
In 2012, Karami²¹ reported a simple synthetic approach to quinoxaline derivatives **3.32** *via* condensation of 1,2-dicarbonyl compounds such as **3.31** with 1,2-aryldiamines **3.30** to form 1,4-aryldiazine derivatives using lithium chloride as a heterogeneous catalyst (Scheme 3.10). Therefore, it was decided to apply these conditions as a means for the synthesis of larger π -conjugated system, *i.e.* quinoxalinoteropyrenophanes.



Scheme 3.10 Karami's synthesis of quinoxaline derivatives **3.32**.

Diones **3.28b-d** and **3.29b-d**, *o*-phenylenediamine and lithium chloride were heated in ethanol at reflux for 10-12 hours to afford two sets of products: quinoxalino[2,3-*i*]teropyrenophanes **3.33b-d** and quinoxalino[2,3-*e*]teropyrenophanes **3.34b-d** (Scheme

3.11). It should be noted that the reaction was first carried out in ethanol at room temperature by adding 10 mol% of the catalyst, but a major amount of starting material remained unreactive after 3 days. The use of excessive amounts of the catalyst was not effective. Hence, it was decided to try reflux conditions, which led to almost complete conversions.



Scheme 3.11 Synthesis of 1,4-aryldiazine derivatives of teropyrenophanes **3.33b-d** and **3.34b-d**.

The absorption spectra of **3.33b-d** and **3.34b-d** consist of four sets of bands, in the ranges of 309-356 nm, 357-472 nm, 444-509 nm and 510-647 nm for **3.33b-d**. and 307-

391 nm, 389-469 nm, 461-508 nm and 508-602 nm for **3.34b-d**. The longest wavelength absorption maxima (λ_{max}) for the symmetrical quinoxalinoteropyrenophanes are observed at 524, 533, and 534 nm for **3.33b**, **3.33c** and **3.33d**, respectively (Figure 3.5, first spectrum). The blue shift that accompanies the increasing bend in the teropyrene system is consistent with the observed trend in parent $[n](2,11)$ teropyrenophanes **3.20b-d**. Curiously,

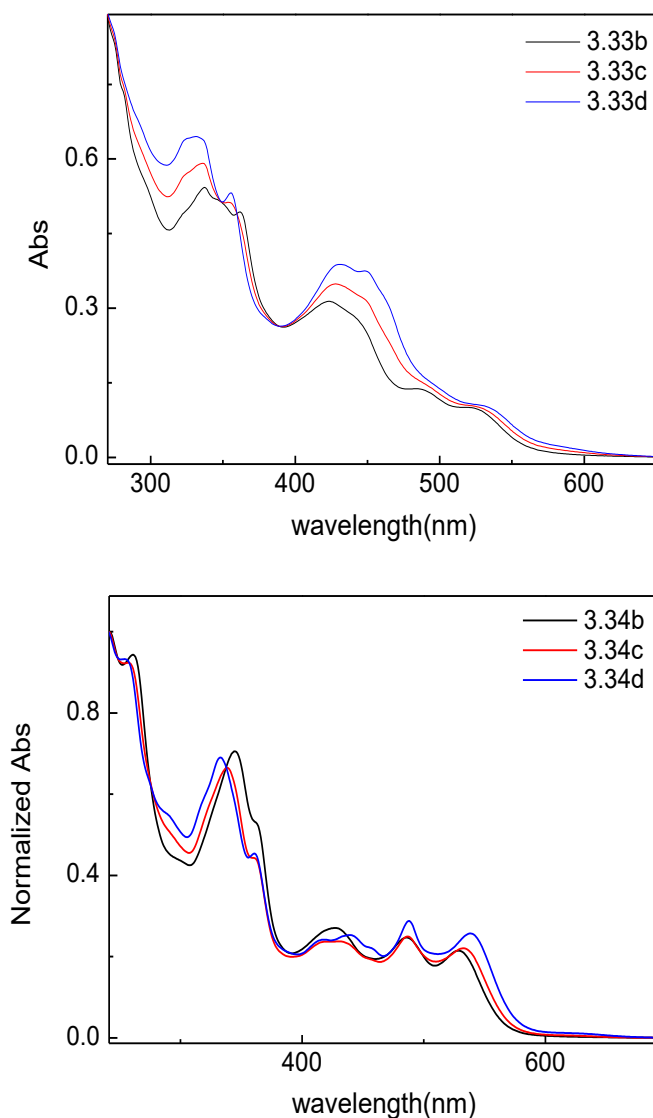


Figure 3.5 Normalized absorption spectra of quinoxalinoteropyrenophanes **3.33b-d** (first spectrum) and **3.34b-d** (second spectrum) measured in CHCl_3 at room temperature.

slightly longer wavelength bands are observed for the unsymmetrical quinoxalinoteropyrenophanes at 529, 534 and 538 nm for **3.34b**, **3.34c** and **3.34d**, respectively (Figure 3.5, second spectrum). The unsymmetrical quinoxalinoteropyrenophanes **3.34b-d** show a blue shift with increasing bend in the teropyrene system (similar to symmetrical ones), which is consistent with the observed trend in parent $[n](2,11)$ teropyrenophanes **3.20b-d**. The emission spectra for the symmetrical quinoxalinoteropyrenophanes **3.33b-d** show fluorescence bands: λ_{max} (**3.33b**) = 561 nm, λ_{max} (**3.33c**) = 570 nm, λ_{max} (**3.33d**) = 572 nm (Figure 3.6).

It should be noted that the emission spectra for unsymmetrical quinoxalinoteropyrenophanes (λ_{max} (**3.34b**) = 603 nm, λ_{max} (**3.34c**) = 604 nm, λ_{max} (**3.34d**) = 605 nm) are very similar to what was observed for symmetrical ones (**3.33b-d**), and show a blue shift upon increasing the bend in teropyrene system (Figure 3.7).

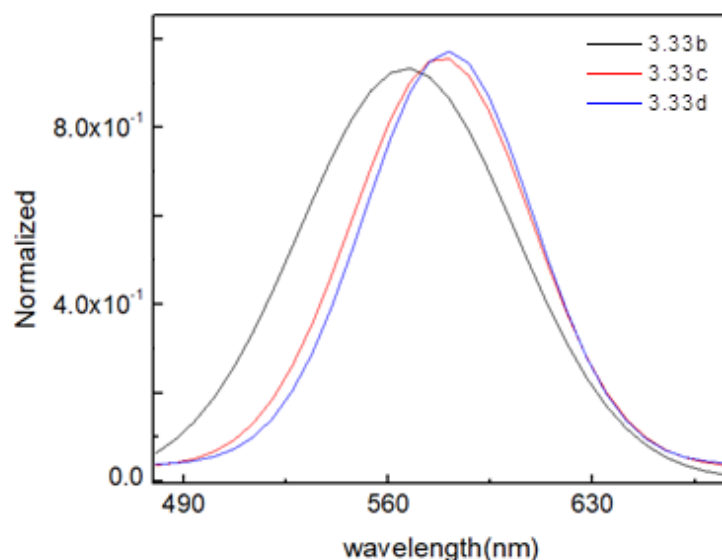


Figure 3.6 Normalized emission spectra of symmetrical quinoxalinoteropyrenophanes **3.33b-d** measured in CHCl_3 at room temperature.

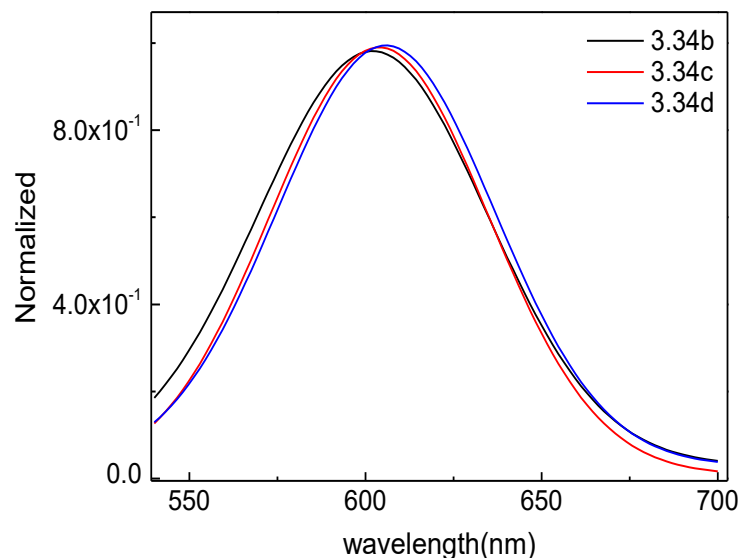


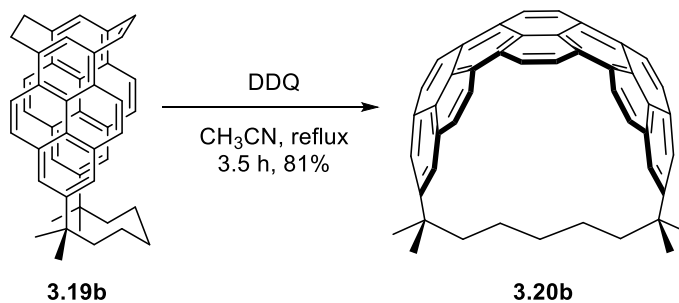
Figure 3.7 Normalized emission spectra of unsymmetrical quinoxalinoteropyrenophanes **3.34b-d** measured in CHCl_3 at room temperature.

3.3 Summary

The major challenge in the large-scale synthesis of a series of $[n](2,11)$ teropyrenophanes **3.20b-e** was the conversion of cyclophanemonoenes **3.19b-c** to teropyrenophanes **3.20b-c**. Indeed, each starting material behaved differently and required specific reaction conditions. Hence, a modified protocol for the key teropyrene-forming step (VID reaction) was developed and this enabled the synthesis of teropyrenophanes on a gram-scale. This involved the use of the CH_3CN as the solvent under thermal conditions. Having access to grams of teropyrenophanes provided the opportunity to explore new aspects of their chemistry, *i.e.* through *K*-region oxidation, which resulted in the formation of two sets of symmetrical and unsymmetrical diones. Moreover, these teropyrenophane diones were used as precursors for the synthesis of larger bent PAHs *via* reaction with *o*-phenylenediamine, which may open new avenues to construct novel aromatic half-belts.

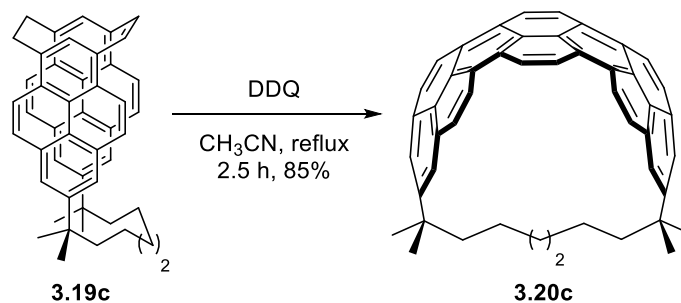
3.4 Experimental Procedures and Characterization Data

1,1,7,7-Tetramethyl[7](2,11)teropyrenophane (**3.20b**)



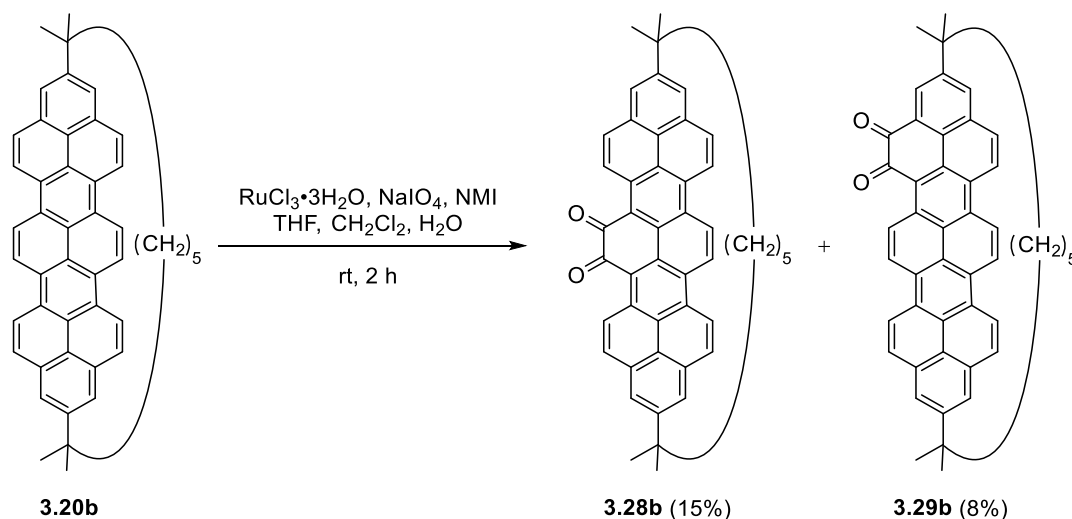
Cyclophanemonoene **3.19b** (1.02 g, 1.66 mmol) was dissolved in acetonitrile (200.0 mL) and DDQ (1.02 g, 4.49 mmol) was added. The reaction mixture was stirred at reflux for 3.5 h. Solvent was then removed and the resulting solid residue was subjected to column chromatography (10×8.0 cm; 5% ethyl acetate/hexanes) to afford teropyrenophane **3.20b** (1.01 g, 81%) as a reddish brown solid: R_f =0.29 (10% ethyl acetate /hexanes); m.p. >300 °C; ¹H NMR (500 MHz, CDCl₃) δ 8.45 (s, 4H), 8.25 (d, J =9.5 Hz, 4H), 7.61 (d, J =9.5 Hz, 4H), 7.28 (s, 4H), 1.28 (s, 12H), 0.80–0.71 (m, 4H), 0.10–0.00 (m, 2H), (–1.10)–(–1.20) (m, 4H); ¹³C NMR (75 MHz, CDCl₃) δ 144.50, 128.75, 128.41, 127.89, 126.97, 126.03, 125.44, 124.89, 124.18, 123.54, 123.18, 47.74, 38.23, 31.18, 28.42, 24.27; HRMS (APPI) calculated for C₄₇H₃₈ [M]⁺ 602.2974, found 602.2961.

1,1,8,8-Tetramethyl[8](2,11)teropyrenophane (3.20c)



Cyclophanemonoene **3.19c** (1.29 g, 2.09 mmol) was dissolved in acetonitrile (200.0 mL) and DDQ (1.28 g, 5.64 mmol) was added. The reaction mixture was stirred at reflux for 2.5 h. Solvent was then removed and the resulting solid residue was subjected to column chromatography (10×9.0 cm; 4% ethyl acetate/hexanes) to afford teropyrenophane **3.20c** (1.08 g, 85%) as a reddish orange solid: $R_f=0.33$ (10% ethyl acetate/hexanes); m.p. >300 °C; ^1H NMR (500 MHz, CDCl_3) δ 8.62 (s, 4H), 8.39 (d, $J=9.5$ Hz, 4H), 7.71 (d, $J=9.5$ Hz, 4H), 7.42 (s, 4H), 1.32 (s, 12H), 0.74–0.68 (m, 4H), –0.21–0.31 (m, 4H), (–0.60)–(–0.72) (m, 4H); ^{13}C NMR (75 MHz, CDCl_3) δ 144.92, 128.14, 127.33, 127.02, 126.95, 125.50, 124.73, 124.14, 123.26, 122.88, 123.18, 47.74, 38.23, 31.18, 28.42, 24.27; HRMS (APPI) calculated for $\text{C}_{48}\text{H}_{40}$ $[\text{M}]^+$ 616.3130, found 616.3134.

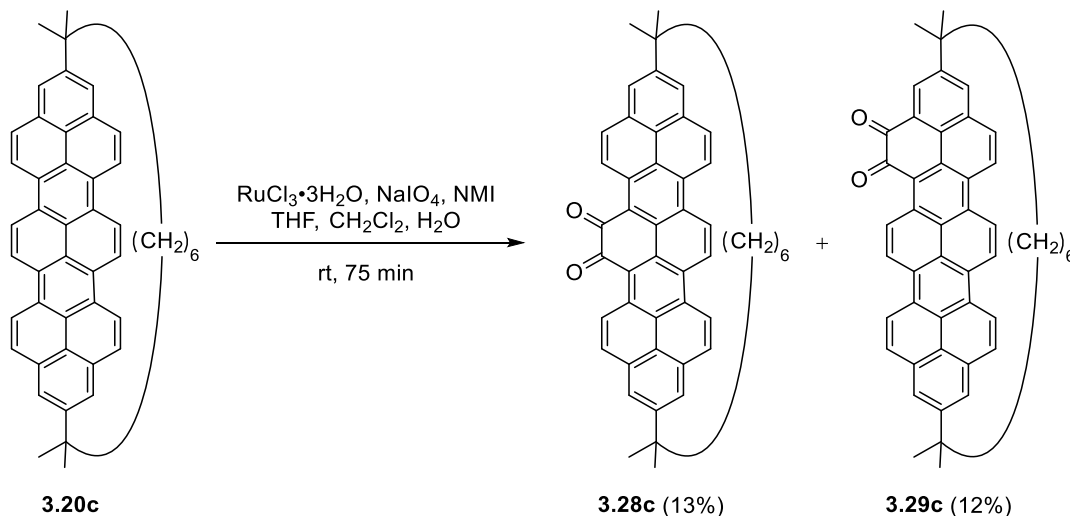
Diones **3.28b** and **3.29b**



To a solution of 1,1,7,7-tetramethyl[7](2,11)teropyrenophane (**3.28b**) (50.0 mg, 0.083 mmol) in dichloromethane (2 mL) and THF (2 mL) was added $\text{RuCl}_3 \cdot 3\text{H}_2\text{O}$ (2.1 mg, 0.0083 mmol), 1-methylimidazole (0.00033 mg, 0.0041 mmol), H_2O (3 mL) and NaIO_4 (79.9 mg, 0.373 mmol). The black solution was stirred at room temperature for 2 h. Organic solvents were removed under reduced pressure. Dichloromethane (5 mL) and H_2O (5 mL) were added and the layers separated. The aqueous layer was extracted with dichloromethane (2×5 mL). The combined organic layers were washed with brine (5 mL), dried over Na_2SO_4 , gravity filtered and concentrated under reduced pressure. The dark brown residue was subjected to column chromatography (8.0×3.0 cm; 80% dichloromethane/hexanes) to afford dione **3.28b** (7.8 mg, 15%) as a red solid: $R_f=0.28$ (80% dichloromethane/hexanes); m.p. >300 °C (dichloromethane); ^1H NMR (500 MHz, CDCl_3) δ 8.76 (d, $J=9.5$ Hz, 2H), 8.34 (s, 2H), 8.28 (d, $J=9.3$ Hz, 2H), 7.94 (d, $J=9.3$ Hz, 2H), 7.84 (d, $J=9.6$ Hz, 2H), 7.61 (d, $J=1.8$ Hz, 2H), 7.60 (d, $J=1.7$ Hz, 2H), 1.45 (s, 6H), 1.37 (s, 6H), 0.78–0.71 (m, 4H), 0.28–0.16 (m, 2H), (–0.60)–(–0.66) (m, 4H); ^{13}C NMR (75 MHz,

CDCl₃) δ 182.27, 146.05, 133.78, 132.51, 132.43, 132.08, 131.99, 130.64, 128.69, 128.31, 127.22, 125.09, 124.65, 124.57, 124.18, 122.98, 121.49, 48.56, 38.67, 32.07, 30.09, 28.55, 23.76 (a fewer-than-expected number of aromatic signals was observed, presumably due to overlap); HRMS (APPI) calculated for C₄₇H₃₆O₂ [M+H]⁺ 633.2780, found 633.2771; dione **3.29b** (4.2 mg, 8%) as a green solid: *R*_f=0.34 (80% dichloromethane/hexanes); m.p. >300 °C (dichloromethane); ¹H NMR (500 MHz, CDCl₃) δ 8.87 (d, *J*=10.1 Hz, 1H), 8.75 (d, *J*=10.0 Hz, 1H), 8.62 (d, *J*=10.2 Hz, 1H), 8.45 (d, *J*=9.4 Hz, 1H), 8.40 (d, *J*=10.1 Hz, 1H), 8.38 (d, *J*=9.4 Hz, 1H), 8.07 (d, *J*=9.4 Hz, 1H), 7.84 (d, *J*=9.4 Hz, 1H), 7.80 (d, *J*=9.5 Hz, 1H), 7.69 (s, 1H), 7.50 (s, 1H), 7.46 (d, *J*=2.3 Hz, 2H), 7.43 (d, *J*=9.5 Hz, 1H), 1.43 (s, 3H), 1.31 (s, 3H), 1.23 (s, 3H), 1.14 (s, 3H), 0.75–0.70 (m, 2H), 0.26–0.07 (m, 2H), (–0.35)–(–0.42) (m, 2H), (–0.60)–(–0.66) (m, 2H), (–0.96)–(1.01) (m, 2H); ¹³C NMR (75 MHz, CDCl₃) δ 184.15, 181.08, 148.96, 146.97, 132.14, 131.98, 130.87, 130.80, 129.91, 129.45, 129.10, 129.01, 128.89, 128.61, 128.30, 128.26, 128.19, 127.70, 127.51, 127.25, 126.49, 126.04, 124.94, 124.82, 124.49, 124.27, 123.71, 123.39, 123.21, 122.98, 122.78, 122.26, 47.69, 47.54, 38.45, 38.36, 32.08, 30.99, 30.49, 30.29, 27.88, 27.79, 25.24, 25.06, 22.85 (a fewer-than-expected number of aromatic signals was observed, presumably due to overlap and a more-than-expected number of aliphatic signals was observed, probably due to the presence of grease); HRMS (APPI) calculated for C₄₇H₃₆O₂ [M+H]⁺ 633.2761, found 633.2758.

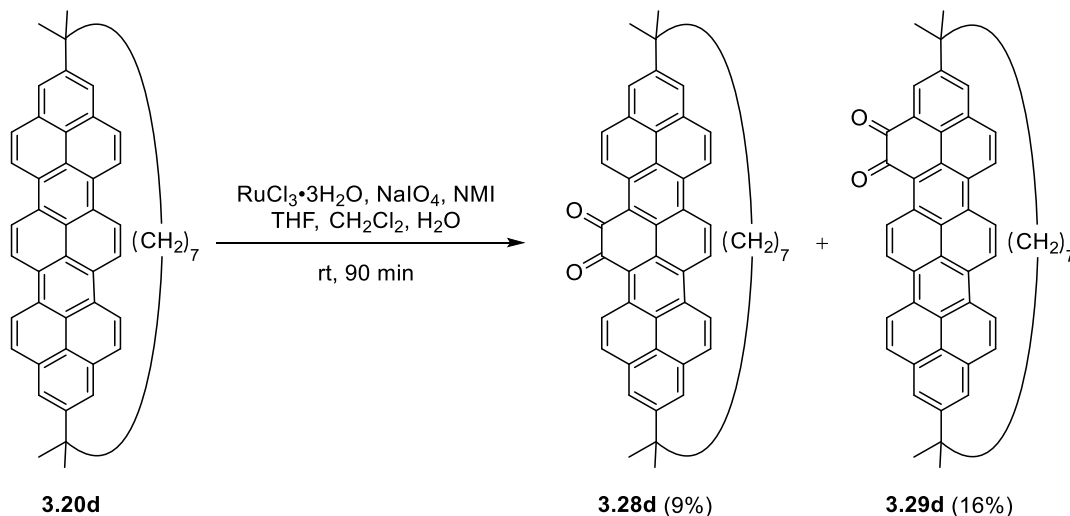
Diones **3.28c** and **3.29c**



To a solution of 1,1,8,8-tetramethyl[8](2,11)teropyrenophane (**3.20c**) (50.0 mg, 0.081 mmol) in dichloromethane (2 mL) and THF (2 mL) was added $\text{RuCl}_3 \cdot 3\text{H}_2\text{O}$ (2.1 mg, 0.0081 mmol), 1-methylimidazole (0.00032 mg, 0.0040 mmol), H_2O (3 mL) and NaIO_4 (78.1 mg, 0.365 mmol). The black solution was stirred at room temperature for 75 min. Organic solvents were removed under reduced pressure. Dichloromethane (5 mL) and H_2O (5 mL) were added and the layers separated. The aqueous layer was extracted with dichloromethane (2×5 mL). The combined organic layers were washed with brine (5 mL), dried over Na_2SO_4 , gravity filtered and concentrated under reduced pressure. The dark brown residue was subjected to column chromatography (9.0×3.0 cm; 80% dichloromethane/hexanes) to afford dione **3.28c** (6.3 mg, 12%) as a red solid: $R_f=0.29$ (80% dichloromethane/hexanes); m.p. >300 °C (dichloromethane); ^1H NMR (500 MHz, CDCl_3) δ 8.87 (d, $J=9.6$ Hz, 2H), 8.43 (s, 2H), 8.35 (d, $J=9.4$ Hz, 2H), 7.99 (d, $J=9.3$ Hz, 2H), 7.89 (d, $J=9.7$ Hz, 2H), 7.70 (d, $J=1.7$ Hz, 2H), 7.68 (d, $J=1.7$ Hz, 2H), 1.39 (s, 12H), 1.25 (s, 6H), 0.72–0.68 (m, 4H), (–0.96)–(–0.11) (m, 4H), (–0.42)–(–0.46) (m, 4H); ^{13}C

NMR (75 MHz, CDCl₃) δ 183.97, 146.87, 133.56, 132.61, 132.49, 131.64, 130.95, 128.53, 128.35, 126.51, 125.46, 125.26, 125.14, 124.85, 124.06, 123.19, 122.62, 47.70, 38.54, 32.08, 30.06, 27.52, 22.70 (a fewer-than-expected number of aromatic signals was observed, presumably due to overlap); HRMS (APPI) calculated for C₄₈H₃₈O₂ [M+H]⁺ 647.2901, found 647.2915; dione **3.29c** (6.8 g, 13%) as a green solid: *R*_f=0.35 (80% dichloromethane/hexanes); m.p. >300 °C (dichloromethane); ¹H NMR (500 MHz, CDCl₃) δ 9.09 (d, *J*=10.1 Hz, 1H), 8.90 (d, *J*=9.9 Hz, 1H), 8.77 (d, *J*=10.1 Hz, 1H), 8.56 (d, *J*=9.8 Hz, 1H), 8.50 (d, *J*=9.5 Hz, 1H), 8.20 (d, *J*=9.4 Hz, 1H), 7.91 (d, *J*=9.4 Hz, 1H), 7.90 (d, *J*=9.5 Hz, 1H), 7.80 (d, *J*=2.0 Hz, 2H), 7.62 (d, *J*=10.2 Hz, 1H), 7.51 (d, *J*=9.5 Hz, 1H), 7.43 (d, *J*=2.1 Hz, 2H), 1.44 (s, 3H), 1.43 (s, 3H), 1.35 (s, 3H), 1.18 (s, 3H), 0.72–0.68 (m, 4H), (–0.02)–(–0.08) (m, 2H), (–0.44)–(–0.53) (m, 2H), (–0.62)–(–0.73) (m, 4H); ¹³C NMR (75 MHz, CDCl₃) δ 184.45, 181.61, 148.56, 145.93, 131.58, 131.41, 131.07, 129.90, 129.71, 129.53, 129.20, 128.84, 128.88, 128.70, 128.41, 128.32, 128.29, 127.93, 127.61, 127.16, 127.10, 126.62, 126.02, 125.11, 124.87, 124.58, 124.45, 124.38, 123.86, 123.67, 123.08, 122.79, 122.63, 122.15, 47.47, 47.39, 38.49, 38.35, 37.25, 32.90, 30.95, 30.19, 29.52, 28.98, 28.79, 23.73 (a fewer-than-expected number of aromatic signals was observed, presumably due to overlap); HRMS (APPI) calculated for C₄₈H₃₈O₂ [M+H]⁺ 647.2881, found 647.2899.

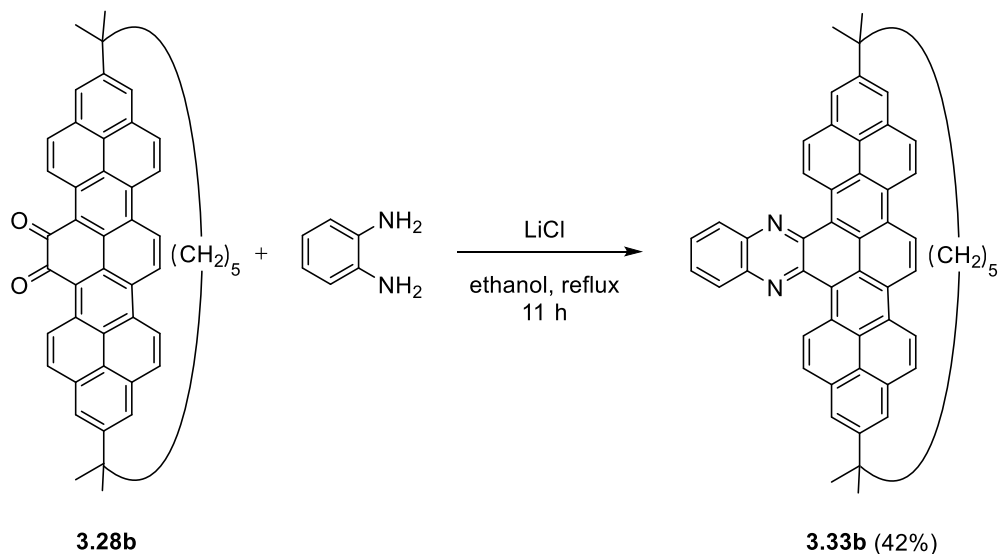
Diones **3.28d** and **3.29d**



To a solution of 1,1,9,9-tetramethyl[9](2,11)teropyrenophane (**3.20d**) (50.0 mg, 0.080 mmol) in dichloromethane (2 mL) and THF (2 mL) was added $\text{RuCl}_3 \cdot 3\text{H}_2\text{O}$ (2.1 mg, 0.0080 mmol), 1-methylimidazole (0.00032 mg, 0.0040 mmol), H_2O (3 mL) and NaIO_4 (78.1 mg, 0.365 mmol). The black solution was stirred at room temperature for 90 min. Organic solvents were removed under reduced pressure. Dichloromethane (5 mL) and H_2O (5 mL) were added and the layers separated. The aqueous layer was extracted with dichloromethane (2×5 mL). The combined organic layers were washed with brine (5 mL), dried over Na_2SO_4 , gravity filtered and concentrated under reduced pressure. The dark brown residue was subjected to column chromatography (9.0×3.0 cm; 80% dichloromethane/hexanes) to afford dione **3.28d** (4.7 mg, 9%) as a red solid: R_f =0.29 (70% dichloromethane/hexanes); m.p. >300 °C (dichloromethane); ^1H NMR (500 MHz, CDCl_3) δ 9.01 (d, J =9.6 Hz, 2H), 8.57 (s, 2H), 8.48 (d, J =9.3 Hz, 2H), 8.07 (d, J =9.3 Hz, 2H), 7.96 (d, J =9.6 Hz, 2H), 7.76 (s, 4H), 1.48 (s, 6H), 1.43 (s, 6H),), 0.71–0.68 (m, 4H), 0.28–0.26 (m, 2H), 0.15–0.11 (m, 2H), (–0.54)–(–0.56) (m, 4H), (–0.94)–(–0.10) (m, 2H); ^{13}C NMR

(75 MHz, CDCl₃) δ 184.15, 147.89, 133.78, 132.73, 132.62, 131.56, 130.97, 128.55, 128.37, 127.33, 126.75, 25.53, 125.31, 125.17, 124.89, 123.90, 123.21, 122.96, 48.42, 38.36, 30.19, 30.04, 27.26, 25.92; HRMS (APPI) calculated for C₄₉H₄₀O₂ [M+H]⁺ 661.3906, found 661.3895; dione **3.29d** (8.4 mg, 16%) as a green solid: *R*_f=0.35 (70% dichloromethane/hexanes); m.p. >300 °C (dichloromethane); 9.28 (d, *J*=10.1 Hz, 1H), 9.04 (d, *J*=9.9 Hz, 1H), 8.90 (d, *J*=10.1 Hz, 1H), 8.69 (d, *J*=9.9 Hz, 1H), 8.61 (d, *J*=9.5 Hz, 1H), 8.33 (d, *J*=9.4 Hz, 1H), 8.02 (d, *J*=9.4 Hz, 1H), 7.96 (d, *J*=9.5 Hz, 1H), 7.88 (d, *J*=2.0 Hz, 2H), 7.70 (d, *J*=10.7 Hz, 1H), 7.60 (d, *J*=9.4 Hz, 1H), 7.50 (d, *J*=2.0 Hz, 2H), 1.51 (s, 3H), 1.49 (s, 3H), 1.35 (s, 3H), 1.32 (s, 3H), 0.36–0.28 (m, 2H), 0.18–0.15 (m, 2H), 0.10–0.06 (m, 2H), (–0.11)–(–0.15) (m, 2H) (–0.21)–(–0.25) (m, 2H), (–0.46)–(–0.55) (m, 2H), (–0.81)–(–0.84) (m, 2H); ¹³C NMR (125 MHz, CDCl₃) δ 184.45, 181.48, 148.46, 145.98, 132.18, 131.98, 131.47, 129.80, 129.61, 129.50, 129.16, 128.91, 128.81, 128.71, 128.32, 128.30, 128.23, 127.83, 127.47, 127.22, 126.59, 126.04, 125.13, 124.76, 124.61, 124.47, 124.38, 123.81, 123.60, 123.05, 122.78, 122.61, 122.16, 47.48, 47.01, 38.46, 38.37, 32.08, 30.99, 30.29, 28.79, 26.24, 26.05, 25.06, 24.99, 22.86 (a fewer-than-expected number of aromatic signals was observed, presumably due to overlap); HRMS (APPI) calculated for C₄₉H₄₀O₂ [M+H]⁺ 661.3869, found 661.3881.

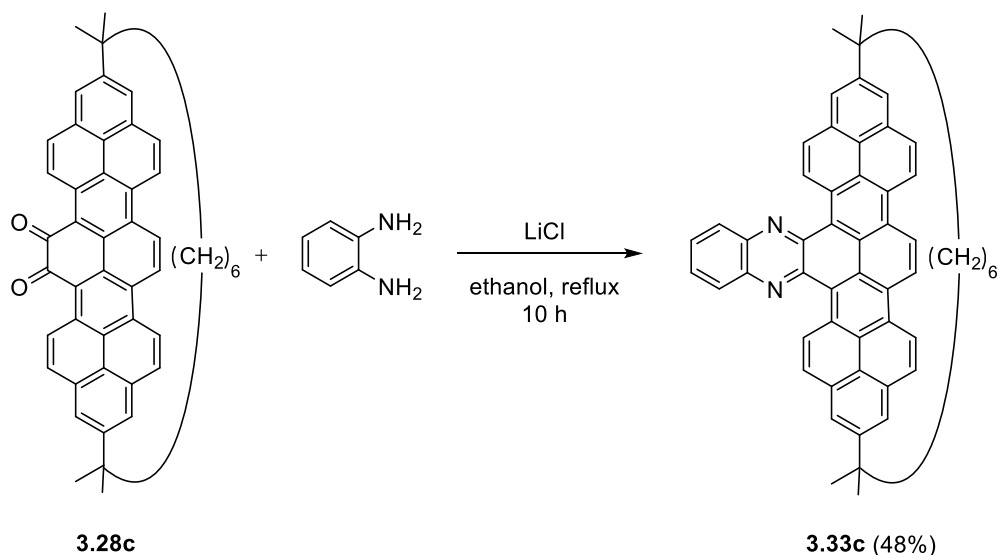
Quinoxalino[2,3-*i*]teropyrenophane **3.33b**



A mixture of dione **3.28b** (9.0 mg, 0.014 mmol), *o*-phenylenediamine (7.7 mg, 0.071 mmol) and lithium chloride (0.31 mg, 0.0071 mmol) in ethanol (2 mL) was stirred at reflux for 11 h. Organic solvent was removed under reduced pressure and the dark orange residue was subjected to column chromatography (13×4.0 cm; 7% ethyl acetate/hexanes) to afford quinoxalino[2,3-*i*]teropyrenophane **3.33b** (4.1 mg, 42%) as a dark orange solid: R_f =0.36 (20% ethyl acetate/hexanes); m.p. >300 °C (dichloromethane); ^1H NMR (500 MHz, CDCl_3) δ 9.33 (d, J =9.7 Hz, 2H), 8.50–8.47 (AA'XX' half spectrum, 2H), 8.43 (s, 2H), 8.34 (d, J =9.4 Hz, 2H), 7.96–7.94 (AA'XX' half spectrum, 2H), 7.82 (d, J =9.4 Hz, 2H), 7.66 (d, J =9.8 Hz, 2H), 7.45 (d, J =1.7 Hz, 2H), 7.39 (d, J =1.8 Hz, 2H), 1.26 (s, 6H), 1.24 (s, 6H), 0.78–0.63 (m, 4H), 0.10–(–0.02) (m, 2H), (–0.86)–(–0.80) (m, 4H); ^{13}C NMR (75 MHz, CDCl_3) δ 146.44, 141.50, 134.54, 129.84, 129.77, 129.32, 129.10, 128.33, 128.12, 128.09, 127.96, 127.75, 126.78, 126.04, 125.79, 125.08, 124.84, 124.23, 124.17, 123.82,

123.66, 47.34, 38.32, 29.98, 29.71, 23.73; HRMS (APPI) calculated for C₅₃H₄₀N₂ [M+H]⁺ 705.3285, found 705.3271.

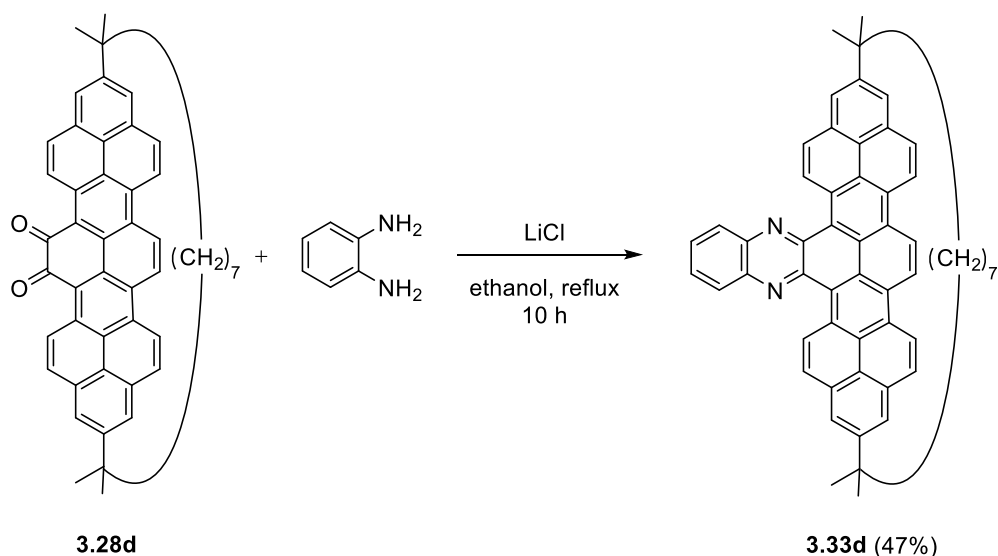
Quinoxalino[2,3-*i*]teropyrenophane **3.33c**



A mixture of dione **3.28c** (13.0 mg, 0.020 mmol), *o*-phenylenediamine (10.8 mg, 0.101 mmol) and lithium chloride (0.43 mg, 0.0010 mmol) in ethanol (2 mL) was stirred at reflux for 10 h. Organic solvent was removed under reduced pressure and the dark orange residue was subjected to column chromatography (13×4.0 cm; 5% ethyl acetate/hexanes) to afford quinoxalino[2,3-*i*]teropyrenophane **3.33c** (6.9 mg, 48%) as a dark orange solid: *R*_f=0.38 (20% ethyl acetate/hexanes); m.p. >300 °C (dichloromethane); ¹H NMR (500 MHz, CDCl₃) δ 9.57 (d, *J*=9.7 Hz, 2H), 8.58 (s, 2H), 8.52–8.50 (AA'XX' half spectrum, 2H), 8.46 (d, *J*=9.4 Hz, 2H), 7.98–7.96 (AA'XX' half spectrum, 2H), 7.91 (d, *J*=9.5 Hz, 2H), 7.76 (d, *J*=9.8 Hz, 2H), 7.60 (d, *J*=1.6 Hz, 2H), 7.53 (d, *J*=1.5 Hz, 2H), 1.49 (s, 6H), 1.40 (s, 6H), 0.62–0.55 (m, 4H), (–0.22)–(–0.20) (m, 4H), (–0.56)–(–0.59) (m, 4H); ¹³C

NMR (75 MHz, CDCl₃) δ 145.04, 142.15, 134.96, 130.08, 130.01, 129.91, 129.64, 128.47, 128.22, 128.14, 127.99, 127.76, 127.55, 126.57, 125.35, 124.79, 124.65, 124.26, 124.12, 123.70, 123.56, 47.31, 38.33, 31.99, 28.25, 23.75; HRMS (APPI) calculated for C₅₄H₄₂N₂ [M+H]⁺ 719.3445, found 719.3437.

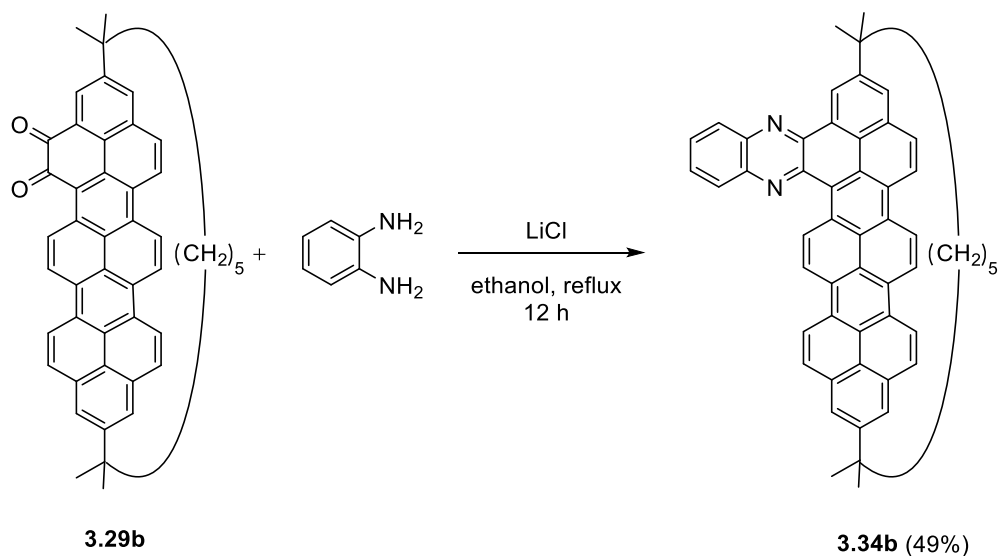
Quinoxalino[2,3-*i*]teropyrenophane **3.33d**



A mixture of dione **3.28d** (10.0 mg, 0.015 mmol), *o*-phenylenediamine (8.2 mg, 0.075 mmol) and lithium chloride (0.32 mg, 0.0075 mmol) in ethanol (2 mL) was stirred at reflux for 10 h. Organic solvent was removed under reduced pressure and the dark orange residue was subjected to column chromatography (13 × 4.0 cm; 5% ethyl acetate/hexanes) to afford quinoxalino[2,3-*i*]teropyrenophane **3.33d** (5.16 mg, 47%) as a dark orange solid: *R_f*=0.5 (20% ethyl acetate/hexanes); m.p. >300 °C (dichloromethane); ¹H NMR (500 MHz, CDCl₃) δ 9.69 (d, *J*=9.7 Hz, 2H), 8.73 (s, 2H), 8.60 (d, *J*=9.4 Hz, 2H), 8.54–8.52 (AA'XX' half spectrum, 2H), 8.00 (d, *J*=9.5 Hz, 2H), 7.99–7.97 (AA'XX' half spectrum, 2H), 7.85

(d, $J=9.8$ Hz, 2H), 7.67 (d, $J=1.7$ Hz, 2H), 7.62 (d, $J=1.7$ Hz, 2H), 1.44 (s, 6H), 1.41 (s, 6H), 0.75–0.68 (m, 4H), 0.06–0.04 (m, 4H), (–0.75)–(–0.80) (m, 4H); ^{13}C NMR (75 MHz, CDCl_3) δ 147.48, 142.51, 135.02, 129.48, 129.37, 128.95, 128.88, 128.18, 127.88, 127.45, 126.39, 126.30, 126.27, 125.41, 124.73, 124.69, 124.28, 124.14, 123.85, 123.51, 123.37, 48.09, 38.72, 38.62, 32.25, 30.01, 29.65, 28.48, 23.49 (a more-than-expected number of aliphatic signals was observed, presumably due to the presence of grease) HRMS (APPI) calculated for $\text{C}_{55}\text{H}_{44}\text{N}_2$ $[\text{M}+\text{H}]^+$ 733.3618, found 733.3602.

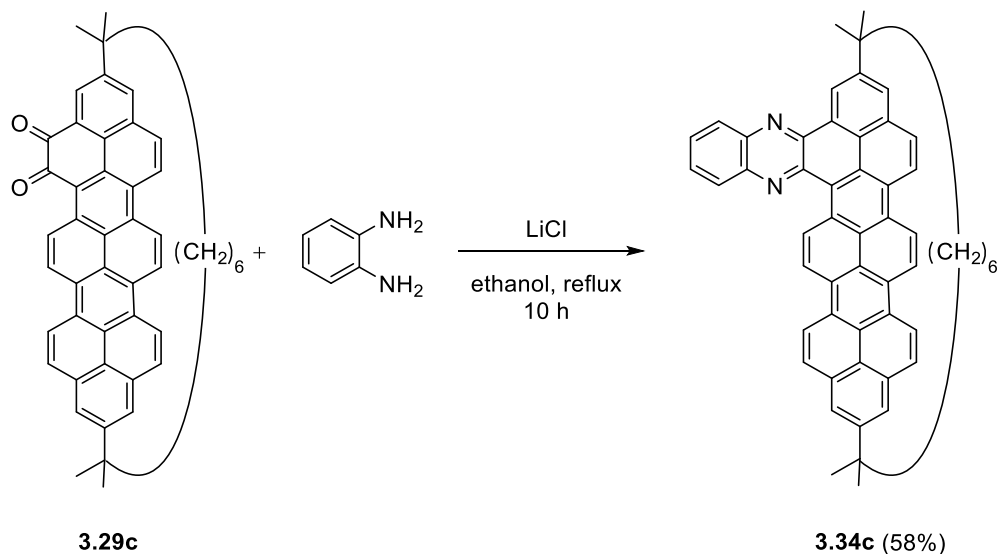
Quinoxalino[2,3-*e*]teropyrenophane **3.34b**



A mixture of dione **3.29b** (10.0 mg, 0.016 mmol), *o*-phenylenediamine (8.6 mg, 0.080 mmol) and lithium chloride (0.34 mg, 0.0081 mmol) in ethanol (2 mL) was stirred at reflux for 12 h. Organic solvent was removed under reduced pressure and the dark orange residue was subjected to column chromatography (12 \times 4.0 cm; 5% ethyl acetate/hexanes) to afford quinoxalino[2,3-*e*]teropyrenophane **3.34b** (5.5 mg, 49%) as a dark pink solid: $R_f=0.38$

(20% ethyl acetate/hexanes); m.p. >300 °C (dichloromethane); ^1H NMR (500 MHz, CDCl_3) δ 9.85 (d, $J=10.3$ Hz, 1H), 8.67 (d, $J=10.2$ Hz, 1H), 8.54 (d, $J=10.2$ Hz, 1H), 8.48 (d, $J=10.4$ Hz, 1H), 8.47–8.45 (m, 1H), 8.40 (d, $J=9.5$ Hz, 1H), 8.35 (d, $J=1.9$ Hz, 1H), 8.28–8.26 (m, 1H), 8.24 (d, $J=9.5$ Hz, 1H), 8.21 (d, $J=9.5$ Hz, 1H), 7.90 (ddd, $J=8.4, 6.9, 1.5$ Hz, 1H), 7.84 (ddd, $J=8.3, 6.9, 1.5$ Hz, 1H), 7.73 (d, $J=9.5$ Hz, 1H), 7.60 (d, $J=9.6$ Hz, 1H), 7.57 (d, $J=9.5$ Hz, 1H), 7.38–7.37 (m, 2H), 7.36 (d, $J=1.8$ Hz, 1H), 1.46 (s, 3H), 1.32 (s, 3H), 1.28 (s, 3H), 1.23 (s, 3H), 0.77–0.74 (m, 4H), 0.16–0.11 (m, 2H), (–0.59)–(0.67) (m, 4H); ^{13}C NMR (75 MHz, CDCl_3) δ 145.94, 145.24, 141.50, 141.05, 134.74, 129.60, 129.55, 129.30, 128.95, 128.91, 128.37, 128.00, 127.85, 127.69, 127.35, 127.18, 126.55, 126.39, 126.02, 125.49, 125.15, 124.17, 124.10, 123.81, 123.73, 123.55, 122.76, 122.48, 122.37, 47.35, 38.34, 38.22, 31.93, 30.05, 29.71, 29.49, 23.73, 23.50, 22.45, 22.40 (a fewer-than-expected number of aromatic signals was observed, presumably due to overlap); HRMS (APPI) calculated for $\text{C}_{53}\text{H}_{40}\text{N}_2$ $[\text{M}+\text{H}]^+$ 705.3278, found 705.3265

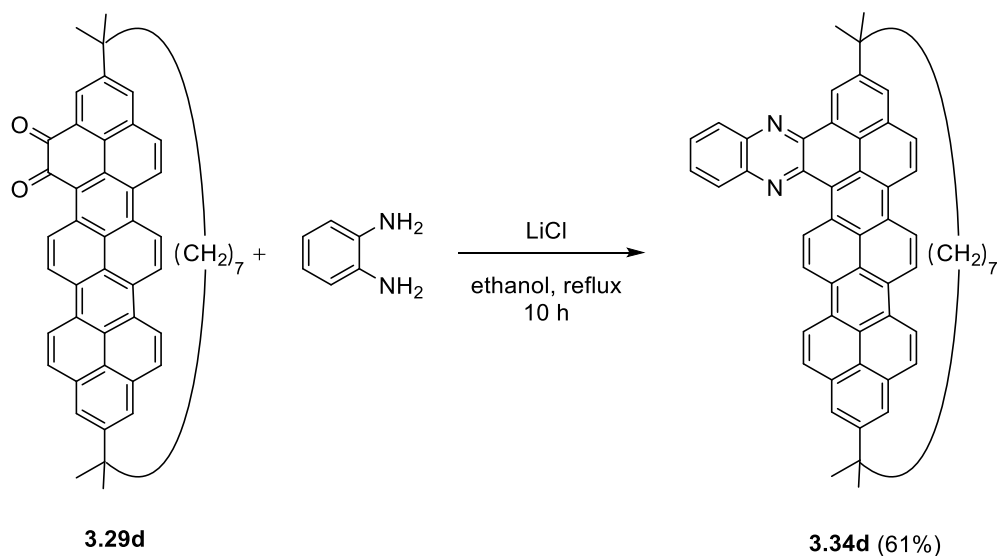
Quinoxalino[2,3-*e*]teropyrenophane **3.34c**



A mixture of dione **3.29c** (15.0 mg, 0.023 mmol), *o*-phenylenediamine (12.5 mg, 0.116 mmol) and lithium chloride (0.49 mg, 0.0012 mmol) in ethanol (2 mL) was stirred at reflux for 10 h. Organic solvent was removed under reduced pressure and the dark orange residue was subjected to column chromatography (13 × 4.0 cm; 5% ethyl acetate/hexanes) to afford quinoxalino[2,3-*e*]teropyrenophane **3.34c** (9.5 mg, 58%) as a dark pink solid: R_f = 0.4 (20% ethyl acetate/hexanes); m.p. >300 °C (dichloromethane); ^1H NMR (500 MHz, CDCl_3) δ 10.13 (d, J =10.3 Hz, 1H), 8.82 (d, J =10.0 Hz, 1H), 8.69 (d, J =10.1 Hz, 1H), 8.66 (d, J =10.4 Hz, 1H), 8.52 (d, J =9.7 Hz, 1H), 8.50–8.48 (m, 1H), 8.36 (d, J =9.5 Hz, 1H), 8.35 (d, J =9.5 Hz, 1H), 8.30–8.28 (m, 1H), 8.29–8.27 (m, 1H), 8.28 (d, J =1.7 Hz, 1H), 7.92 (ddd, J =8.4, 6.9, 1.5 Hz, 1H), 7.85 (ddd, J =8.3, 6.9, 1.5 Hz, 1H), 7.81 (d, J =9.5 Hz, 1H), 7.71 (d, J =9.5 Hz, 1H), 7.66 (d, J =9.5 Hz, 1H), 7.53 (d, J =1.7 Hz, 1H), 7.50 (d, J =1.9 Hz, 1H), 7.42 (d, J =1.8 Hz, 1H), 1.49 (s, 3H), 1.37 (s, 3H), 1.31 (s, 3H), 1.28 (s, 3H), 0.73–0.64 (m, 2H), (–0.19)–(–0.21) (m, 2H), (–0.29)–(–0.33) (m, 2H), (–0.51)–(–0.59) (m, 4H),

(−0.69)–(−0.74) (m, 2H); ^{13}C NMR (75 MHz, CDCl_3) δ 146.55, 145.24, 141.55, 141.01, 134.73, 129.61, 129.52, 129.29, 129.10, 128.35, 128.11, 128.00, 127.89, 127.70, 127.37, 127.32, 127.10, 126.64, 126.47, 126.39, 125.49, 125.14, 124.66, 124.28, 124.18, 123.79, 123.72, 123.28, 123.09, 122.75, 122.48, 122.37, 47.32, 38.32, 38.21, 31.93, 30.01, 29.41, 28.24, 27.74, 26.74, 26.39, 23.72, 23.50 (a fewer-than-expected number of aromatic signals was observed, presumably due to overlap); HRMS (APPI) calculated for $\text{C}_{54}\text{H}_{42}\text{N}_2$ $[\text{M}+\text{H}]^+$ 719.3425, found 719.3419.

Quinoxalino[2,3-*e*]teropyrenophane **3.34d**



A mixture of dione **3.29d** (14.0 mg, 0.021 mmol), *o*-phenylenediamine (11.4 mg, 0.106 mmol) and lithium chloride (0.45 mg, 0.0011 mmol) in ethanol (2 mL) was stirred at reflux for 10 h. Organic solvent was removed under reduced pressure and the dark orange residue was subjected to column chromatography (13 \times 4 cm; 5% ethyl acetate/hexanes) to afford quinoxalino[2,3-*e*]teropyrenophane **3.34d** (9.2 mg, 61%) as a dark pink solid: $R_f=0.6$

(20% ethyl acetate/hexanes); m.p. >300 °C (dichloromethane); ^1H NMR (500 MHz, CDCl_3) δ 10.39 (d, $J=10.3$ Hz, 1H), 8.98 (d, $J=10.0$ Hz, 1H), 8.84 (d, $J=10.1$ Hz, 1H), 8.82 (d, $J=10.3$ Hz, 1H), 8.66 (d, $J=9.5$ Hz, 1H), 8.60 (d, $J=2.0$ Hz, 1H), 8.54 (dd, $J=8.4, 1.5$ Hz, 1H), 8.51 (d, $J=9.5$ Hz, 1H), 8.50 (d, $J=9.5$ Hz, 1H), 8.32 (dd, $J=8.3, 1.5$ Hz, 1H), 7.94 (ddd, $J=8.4, 6.9, 1.6$ Hz, 1H), 7.92 (d, $J=9.5$ Hz, 1H), 7.88 (ddd, $J=8.4, 6.9, 1.4$ Hz, 1H), 7.80 (d, $J=9.5$ Hz, 1H), 7.75 (d, $J=9.5$ Hz, 1H), 7.59 (d, $J=1.7$ Hz, 1H), 7.58 (d, $J=1.9$ Hz, 1H), 7.55 (d, $J=1.7$ Hz, 1H), 1.54 (s, 3H), 1.42 (s, 3H), 1.37 (s, 3H), 1.35 (s, 3H), 0.78–0.70 (m, 2H), 0.27–0.16 (m, 2H), (–0.29)–(–0.33) (m, 2H), (–0.43)–(–0.47) (m, 2H), (–0.55)–(–0.61) (m, 2H), (–0.69)–(–0.73) (m, 2H), (–0.87)–(–0.90) (m, 2H); ^{13}C NMR (75 MHz, CDCl_3) δ 146.64, 145.46, 141.66, 141.21, 129.80, 129.72, 129.49, 129.32, 129.15, 128.82, 128.30, 128.21, 127.81, 127.27, 127.02, 126.74, 126.67, 126.00, 125.77, 125.39, 124.35, 124.09, 123.77, 123.58, 123.19, 123.11, 122.81, 122.51, 47.51, 47.32, 38.51, 38.35, 32.08, 30.89, 30.32, 29.52, 28.91, 28.43, 26.91, 24.97, 24.89 (a fewer-than-expected number of aromatic signals was observed, presumably due to overlap); HRMS (APPI) calculated for $\text{C}_{55}\text{H}_{44}\text{N}_2$ $[\text{M}+\text{H}]^+$ 733.3621, found 733.3604.

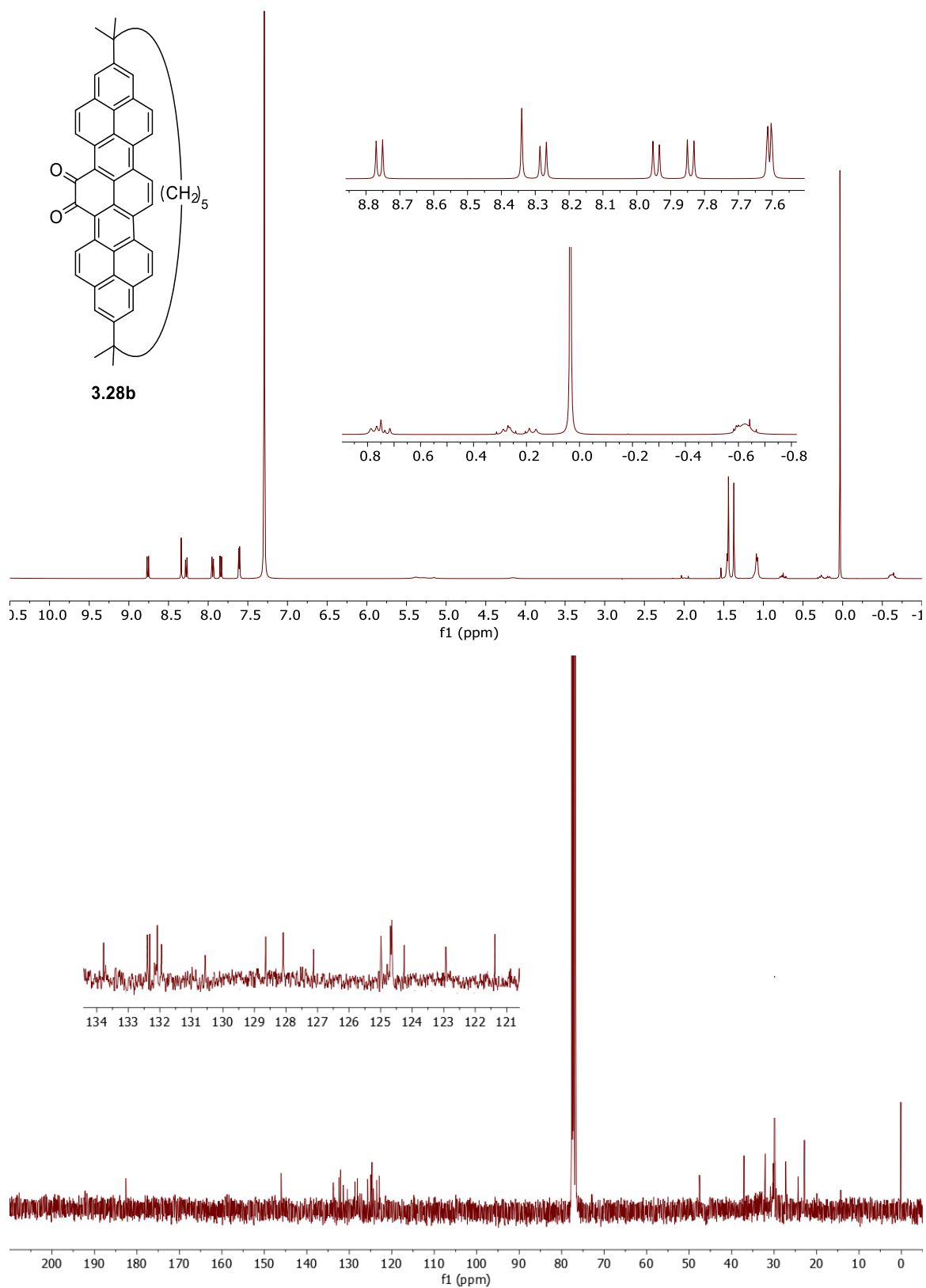
3.5 References and Notes

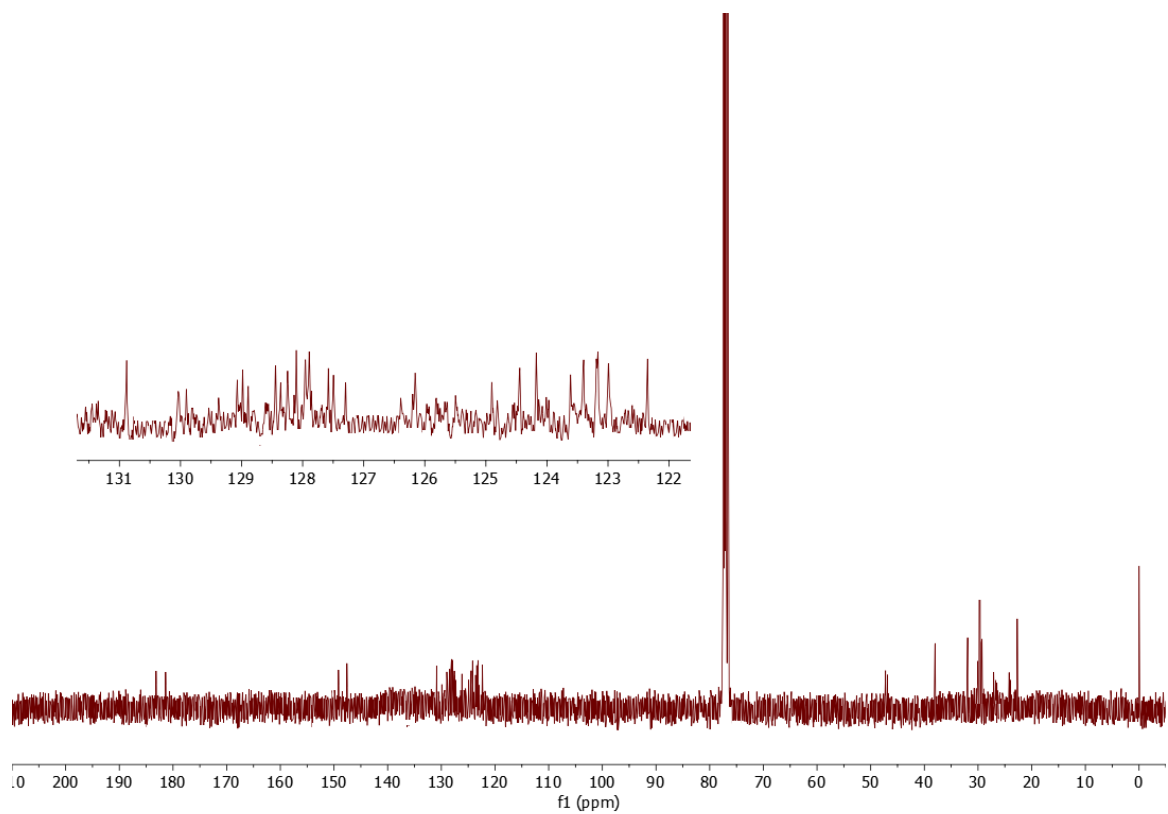
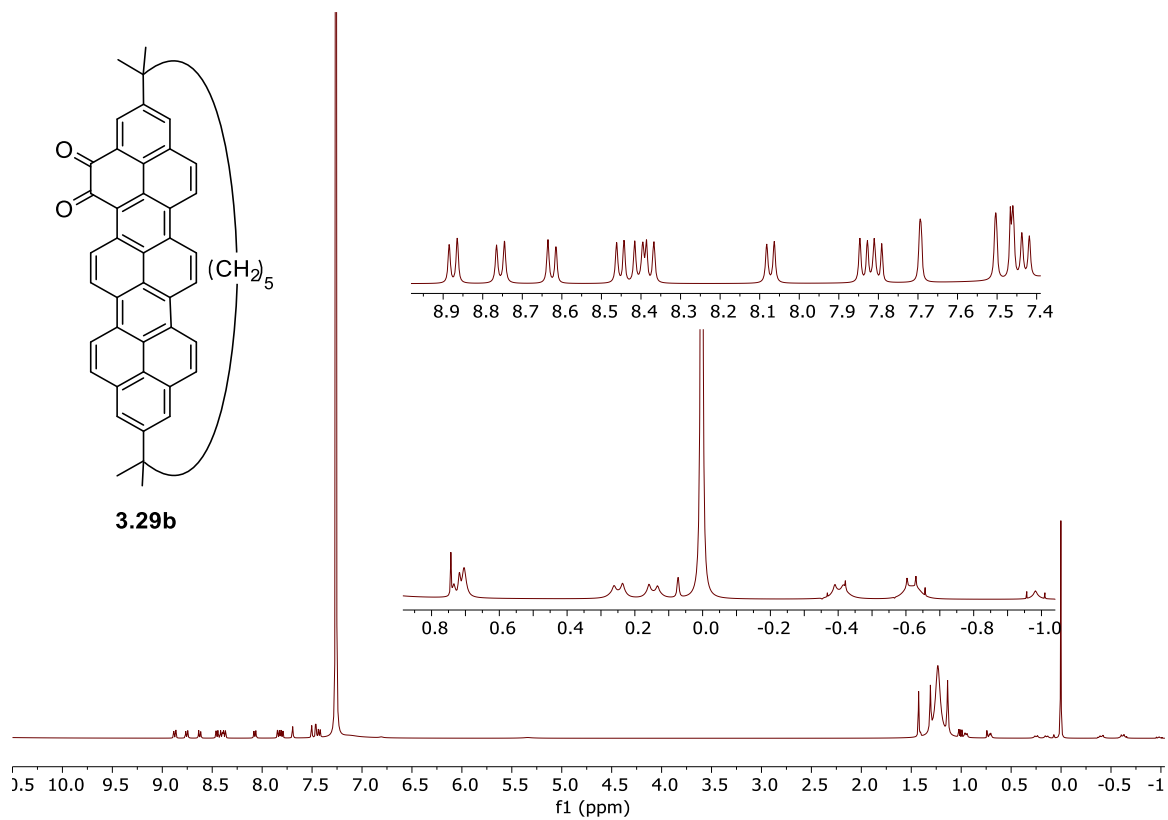
1. Jenneskens, L. W.; de Kanter, F. J. J.; Kraakman, P. A.; Turkenburg, L. A. M.; Koolhaas, W. E.; de Wolf, W. H.; Bickelhaupt, F.; Tobe, Y. Kakiuchi, K.; Odaira, Y. *J. Am. Chem. Soc.* **1985**, *107*, 3716–3717.
2. Mitchell, R. H.; Boekelheide, V. *J. Am. Chem. Soc.* **1970**, *92*, 3510–3512.
3. Woodward, R. B.; Hoffmann, R. *Angew. Chem. Int. Ed.* **1969**, *8*, 781–853.
4. Nakamura, E.; Tahara, K.; Matsuo, Y.; Sawamura, M. *J. Am. Chem. Soc.* **2003**, *125*, 2834–2835.
5. Bodwell, G. J.; Houghton, T. J.; Koury, H. E.; Yarlagadda, B. *Synlett* **1995**, 751–752.
6. Mitchell, R. H.; Ward, T. R.; Wang, Y. *Heterocycles* **2001**, *54*, 249–257.
7. a) Umemoto, T.; Kawashima, T.; Sakata, Y.; Misumi, S. *Tetrahedron Lett.* **1975**, *16*, 1005–1006. b) Sato, T.; Wakabayashi, M.; Okamura, Y. *Bull. Chem. Soc. Jpn.* **1967**, *40*, 2363–2365. c) Sato, T.; Nishiyama, K. *J. Org. Chem.* **1972**, *37*, 3254–3260. d) Allinger, N. L.; Goldon, B. J.; Hu, S. E.; Ford, R. A. *J. Org. Chem.* **1967**, *32*, 2272–2278. e) Yamato, Y.; Matsomoto, J.; Tokuhisa, K.; Sheigekuni, M.; Suehiro, K.; Tashiro, M. *J. Org. Chem.* **1993**, *57*, 395–396. f) Yamato, T.; Ide, S.; Tokuhisa, K.; Tashiro, M. *J. Org. Chem.* **1992**, *57*, 271–275.
8. Merner, B. L. Ph.D. Dissertation, Memorial University, 2010.
9. Unikela, K. S. Ph.D. Dissertation, Memorial University, 2014.

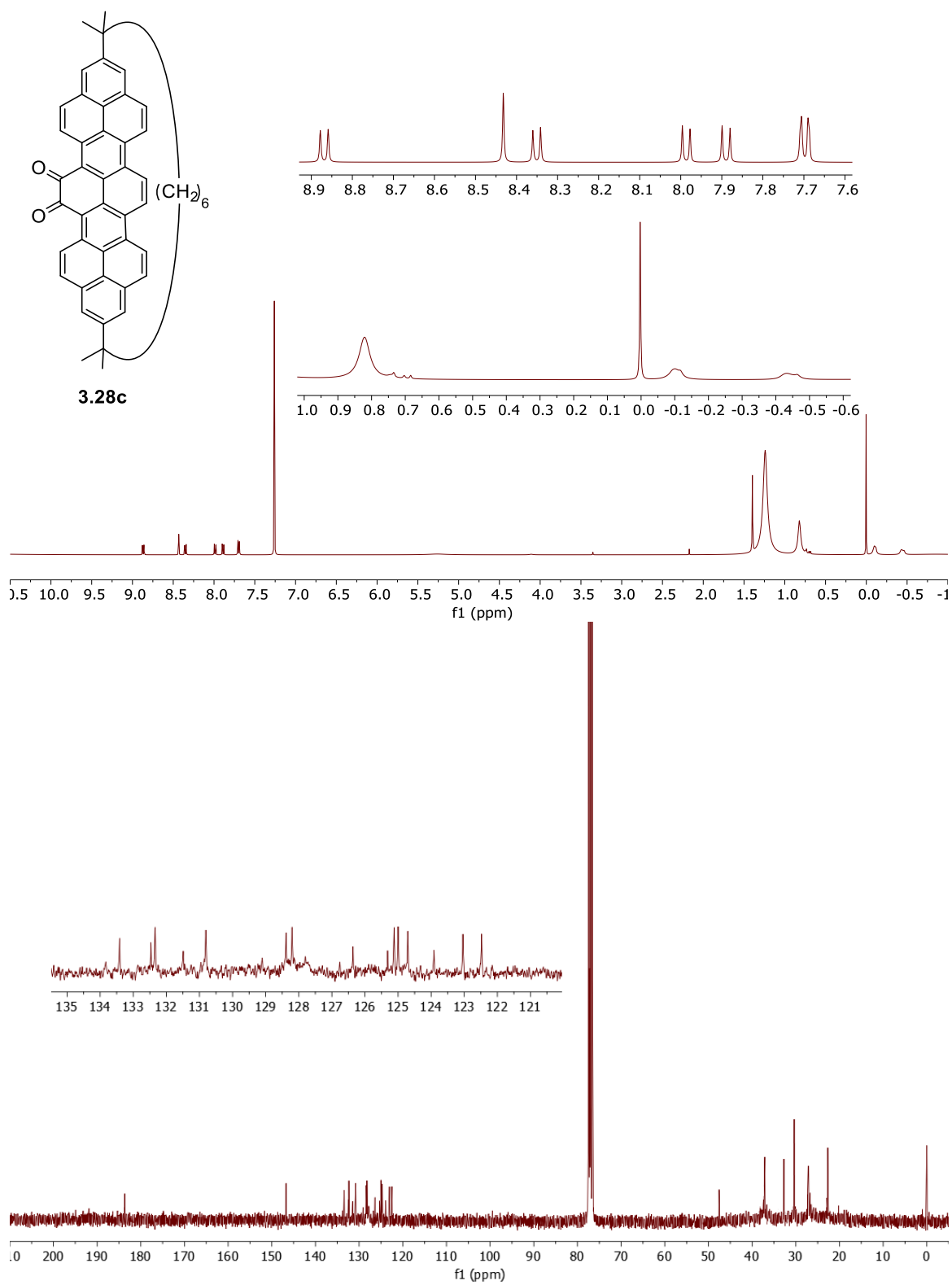
10. Batista, V. S.; Crabtree, R. H.; Konezny, S. J.; Luca, O. R.; Praetorius, J. M. *New J. Chem.* **2012**, *36*, 1141–1144.
11. Merner, B. L. Bodwell, G. J. Unpublished results.
12. Zhai, L.; Shukla, R.; Rathore, R. *Org. Lett.* **2009**, *11*, 3474–3477.
13. a) Kastler, M.; Schmidt, J.; Pisula, W.; Sebastiani, D.; Müllen, K. *J. Am. Chem. Soc.* **2006**, *128*, 9526–9534. b) Harvey, R. G. *Polycyclic Aromatic Hydrocarbons: chemistry and Carcinogenicity*. New York, 1991.
14. Hu, J.; Zhang, D.; Harris, F. W. *J. Org. Chem.*, **2005**, *70*, 707–708.
15. a) Walsh, J. C.; Williams, K. M.; Lungerich, D.; Bodwell, G. J. *Eur. J. Org. Chem.* **2016**, *36*, 5933–5936. b) Venkataramana, G.; Dongare, P.; Dawe, L.; Thompson, D.; Zhao, Y.; Bodwell, G. J. *Org. Lett.* **2011**, *13*, 2240–2243.
16. a) Zhu, W.; Dai, M.; Xu, Y.; Qian, X. *Bioorg. Med. Chem.* **2008**, *16*, 3255–3260. b) Hui, X.; Desrivot, J. Bories, C.; Loiseau, O. M.; Franck, X.; Hocquemiller, R.; Figadere, B. *Med. Chem. Lett.* **2006**, *16*, 815–820.
17. a) Corona, P.; Carta, A.; Loriga, M.; Vitale, G.; Paglietti, G. *Eur. J. Med. Chem.* **2009**, *44*, 1579–1591. b) Yamaguchi, T.; Matsumoto, S.; Watanabe, K. *Tetrahedron Lett.* **1998**, *39*, 8311–8312.
18. Dailey, S.; Feast, W. J.; Peace, R. J.; Sage, I. C.; Till, S.; Wood, E. L. *J. Mater. Chem.* **2001**, *11*, 2238–2243.
19. a) Yamamoto, T.; Sugiyama, K.; Kushida, T.; Inoue, T.; Kanabara, T. *J. Am. Chem. Soc.* **1996**, *118*, 3930–3937. b) Nurulla, I.; Yamaguchi, I.; Yamamoto, T. *Polym. Bull.* **2000**, *44*, 231–238.

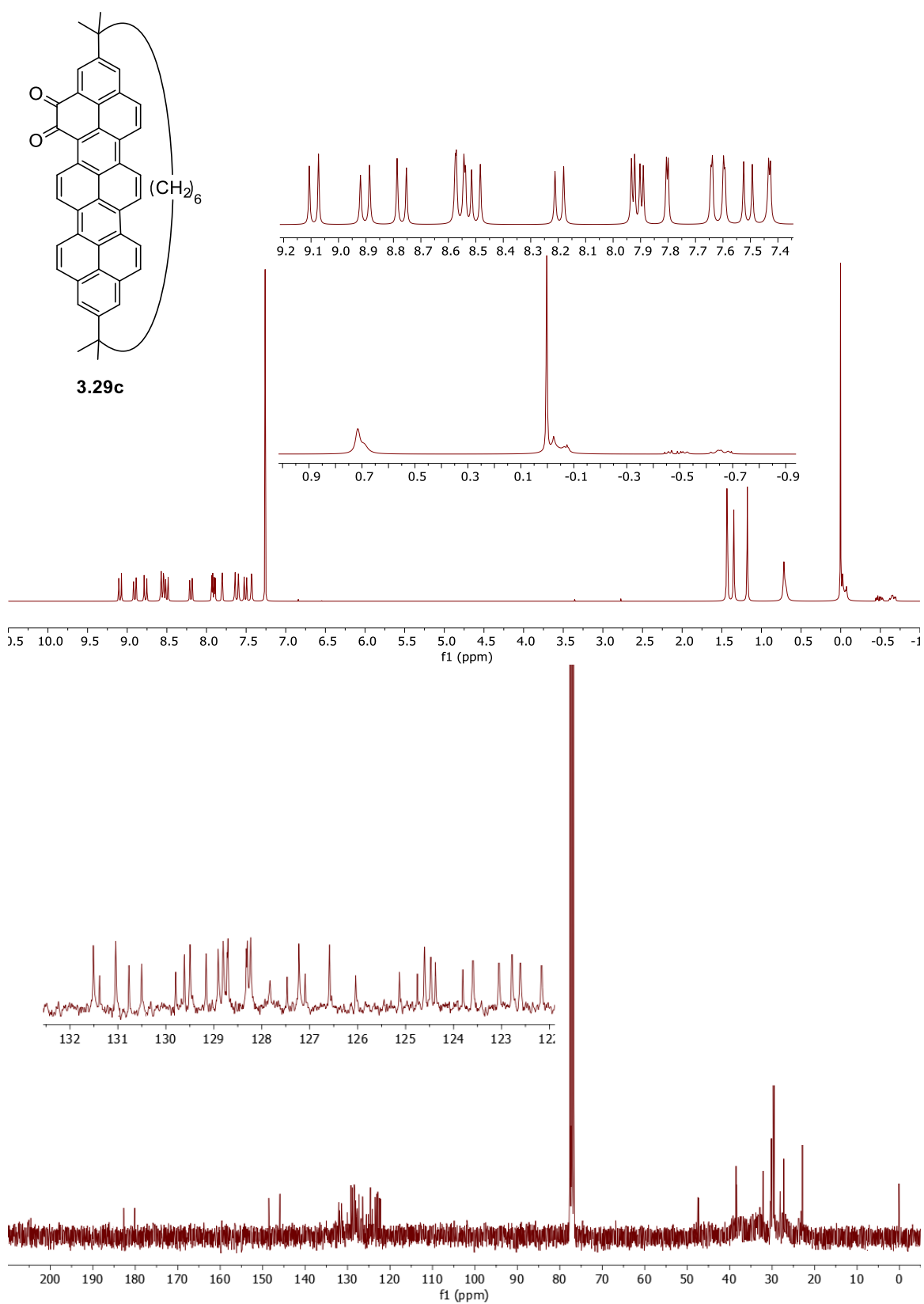
20. Yamamoto, T.; Lee, B. L.; Kokubo, H.; Kishida, H.; Hirota, K.; Wakabayashi, T.; Okamoto, H. *Macromol. Rapid. Commun.* **2003**, *24*, 440–443.
21. Karami, B.; Rooydel, R.; Khodabakhshi, S. *Acta Chim. Slov.* **2012**, *59*, 183–188.

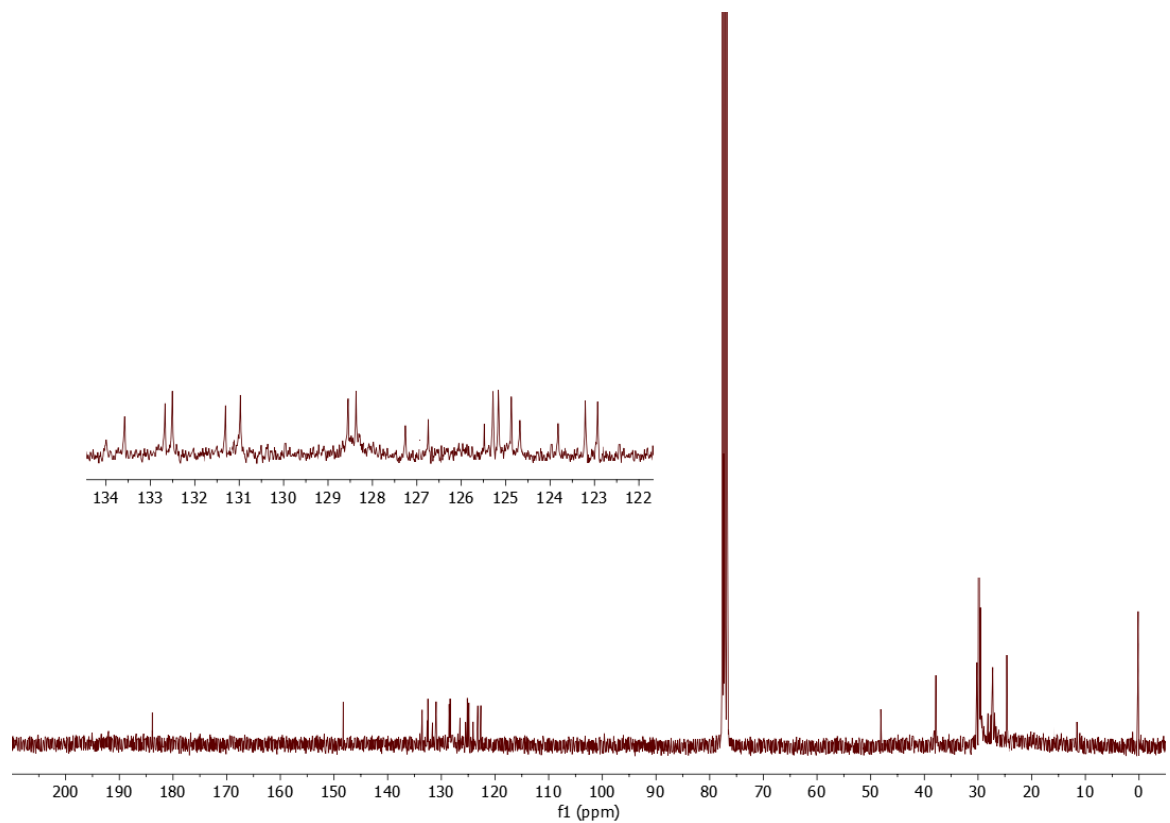
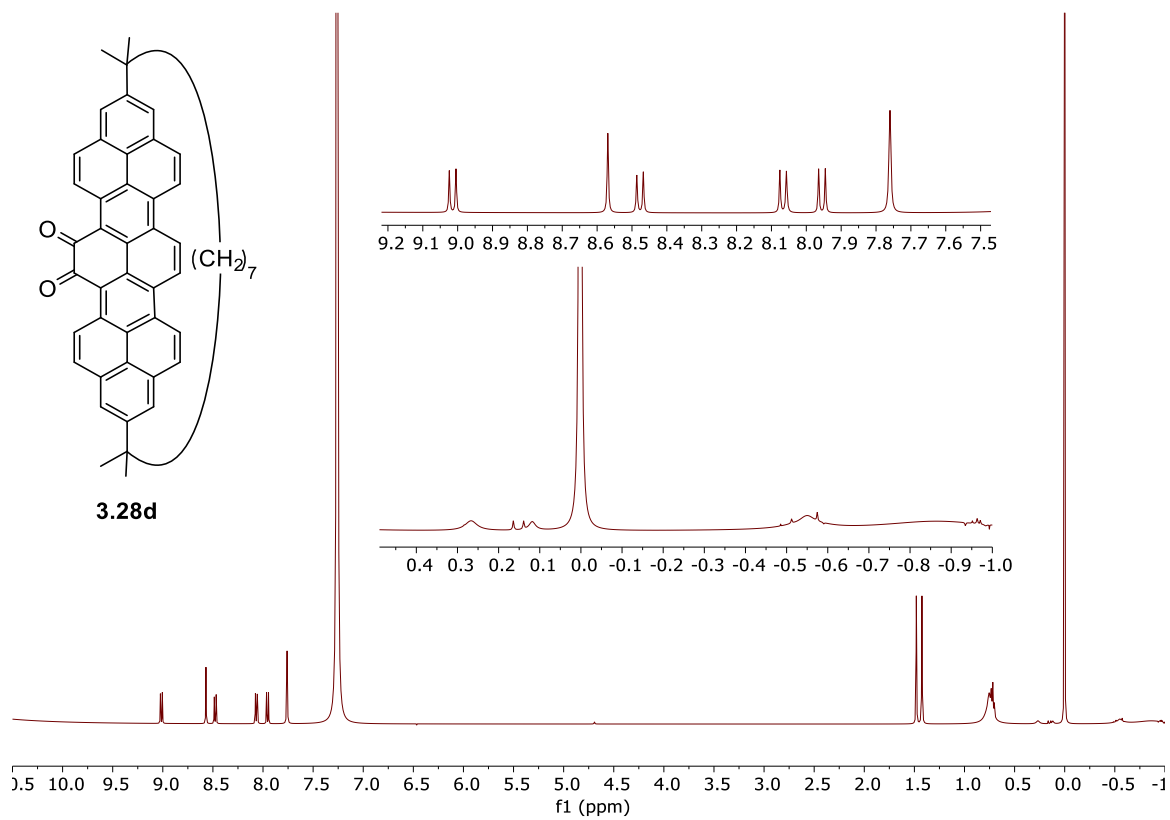
APPENDIX 2

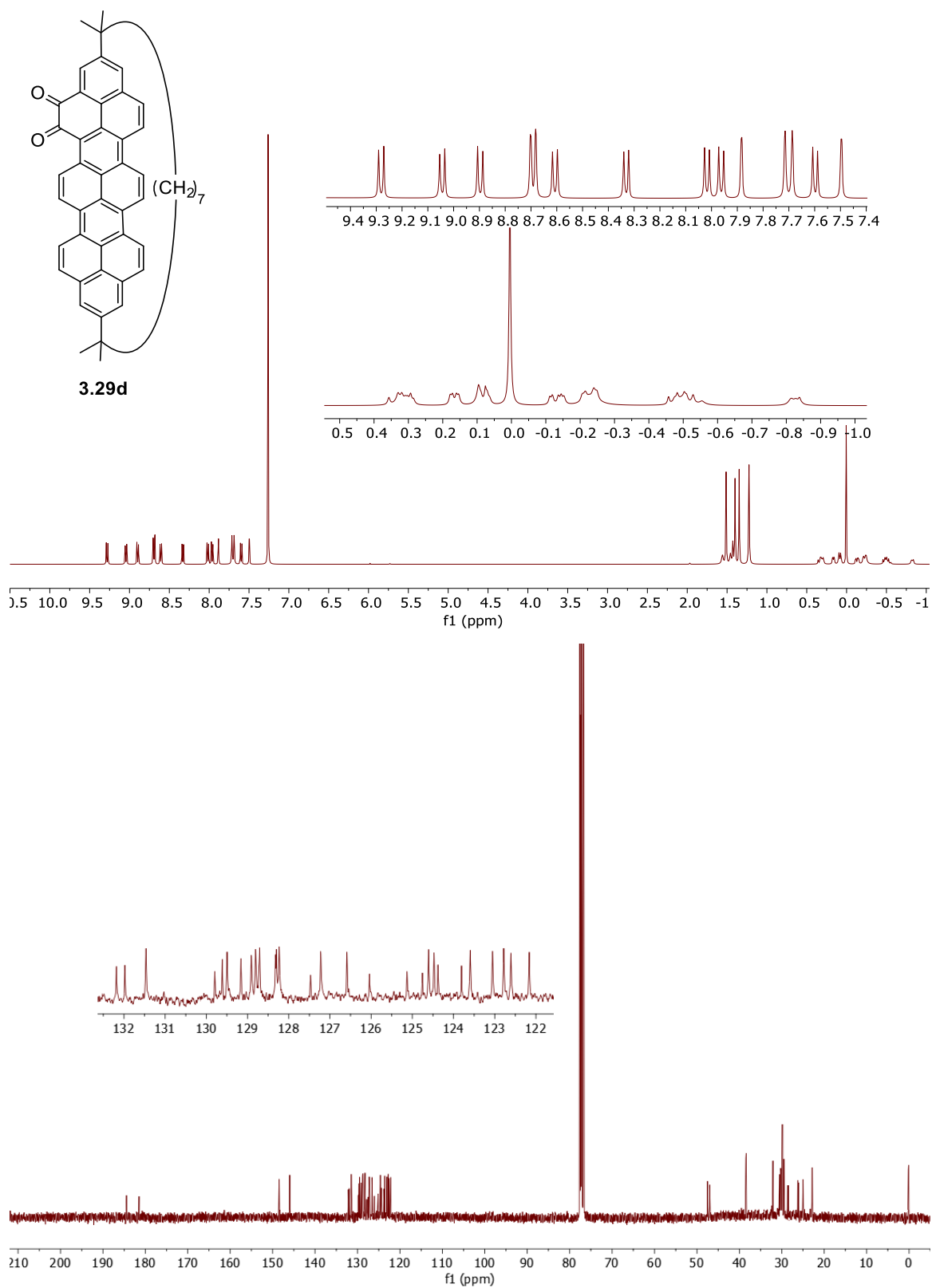


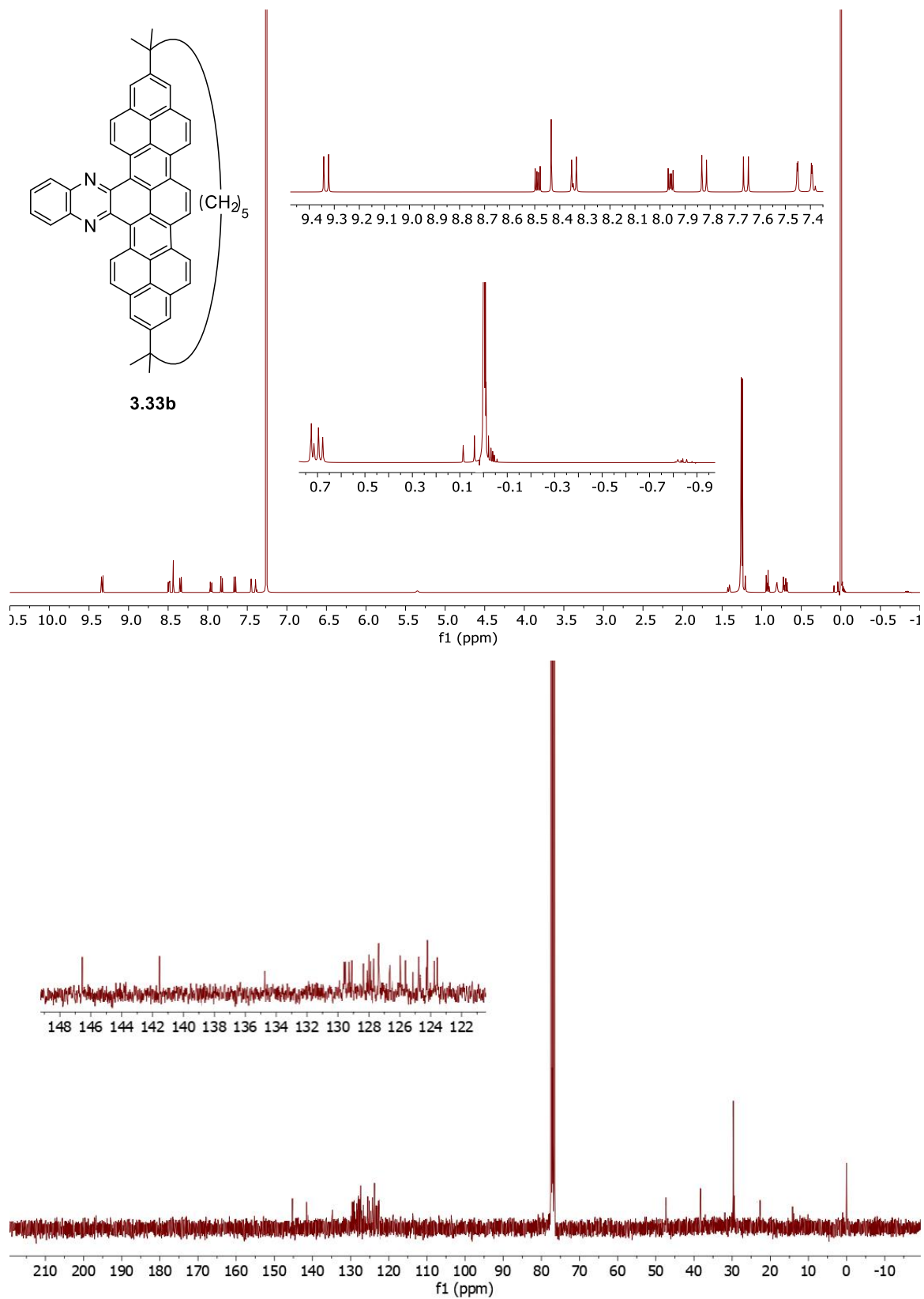


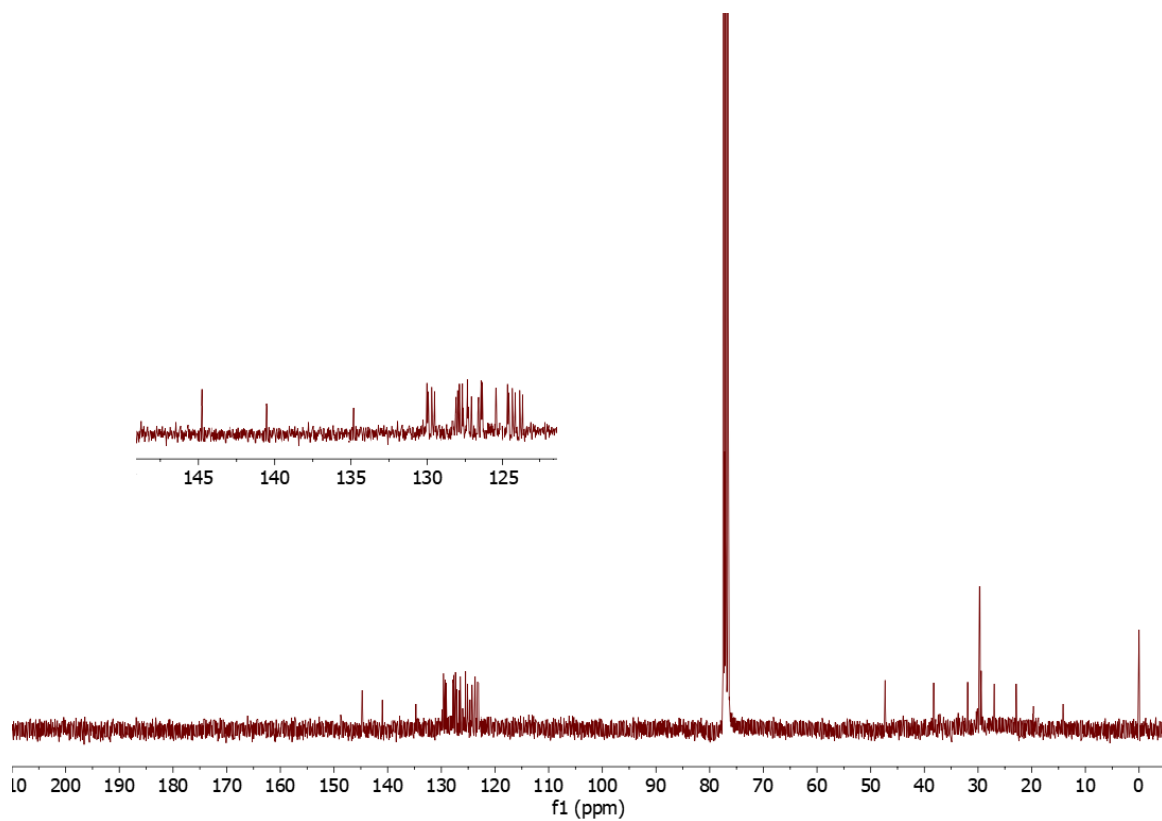
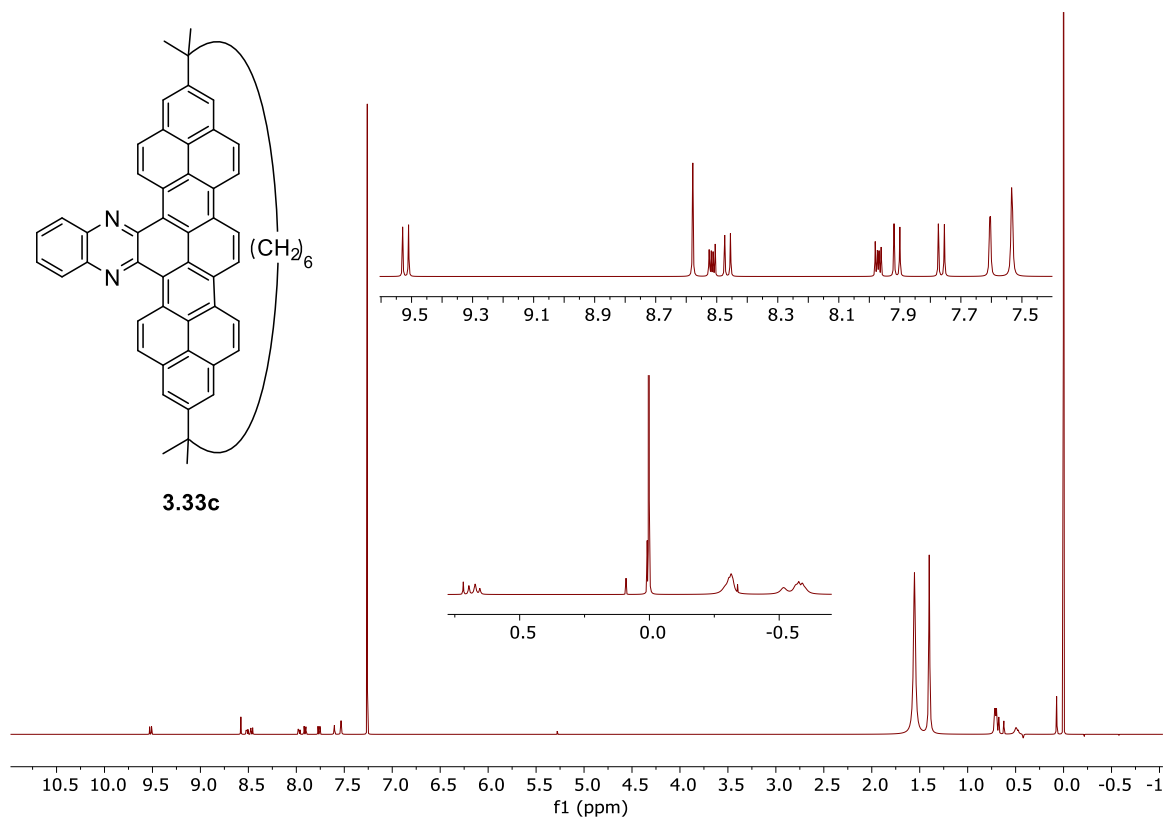


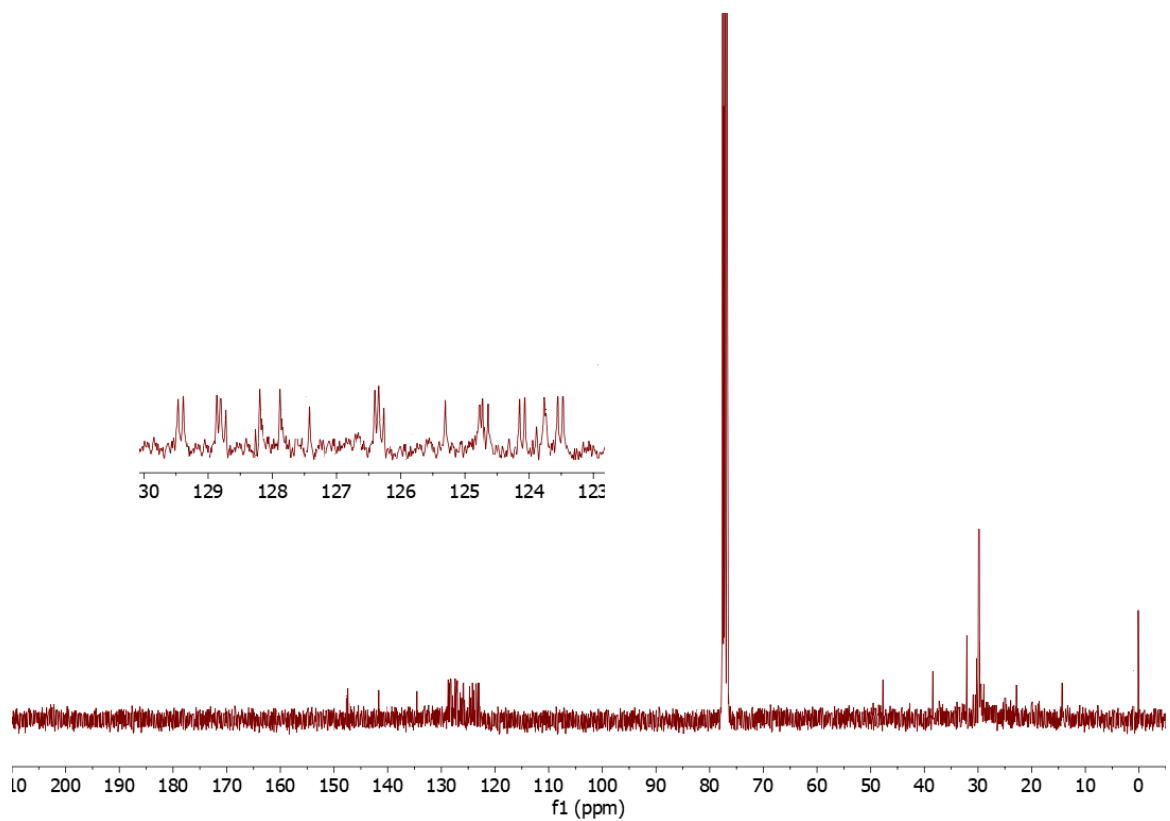
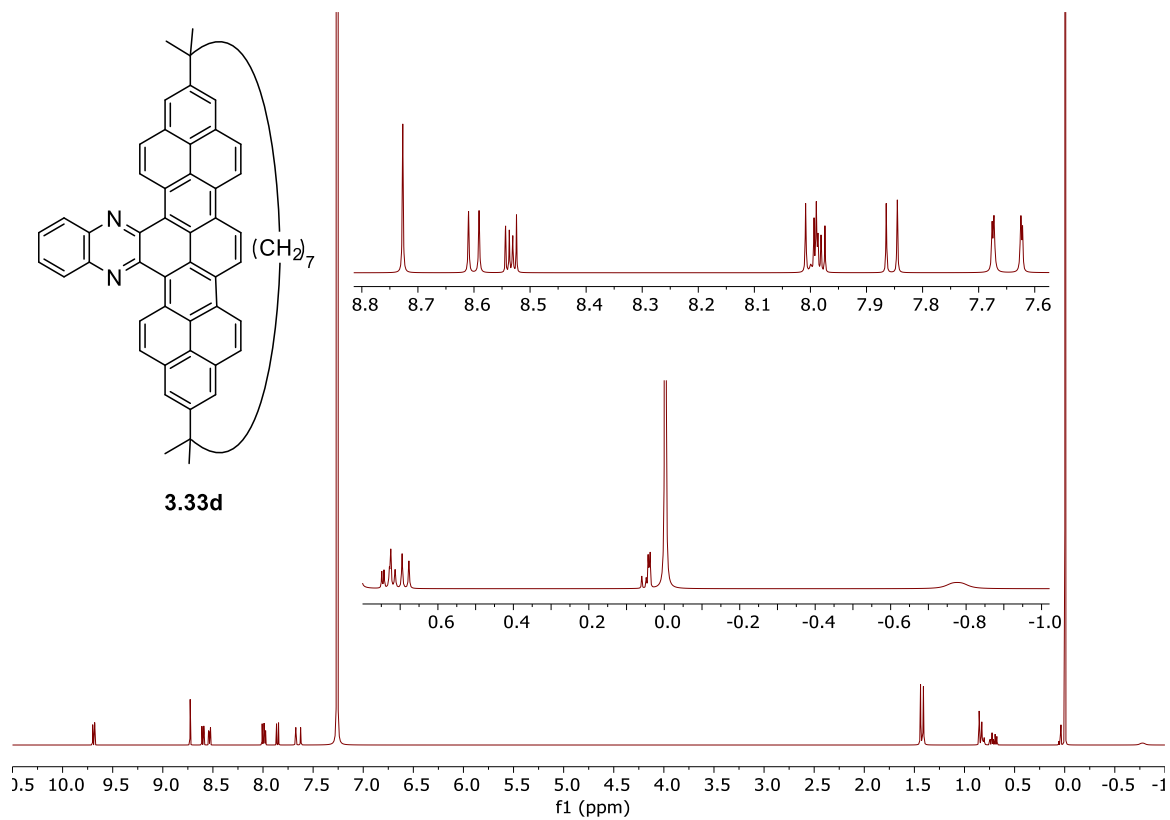


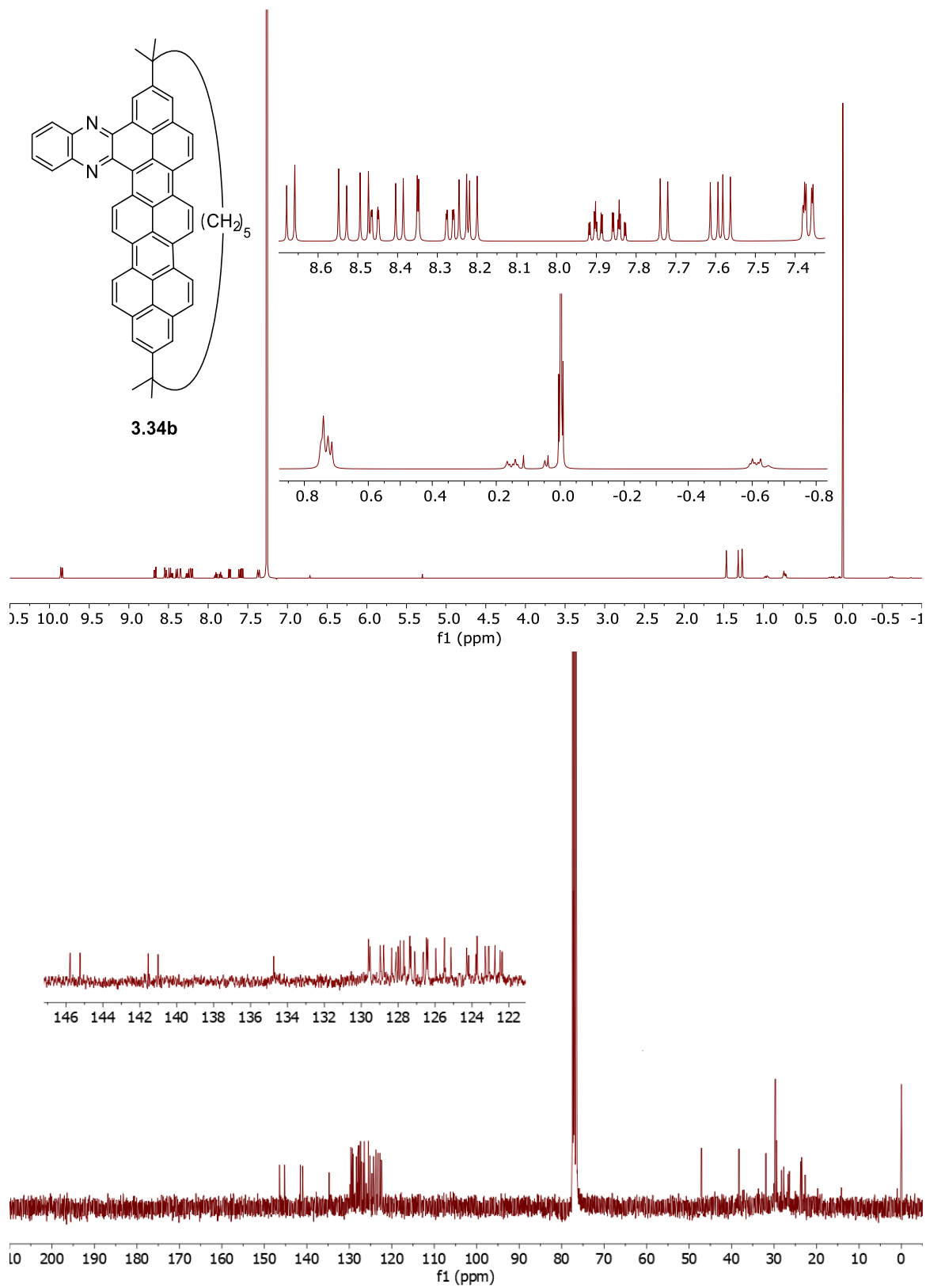


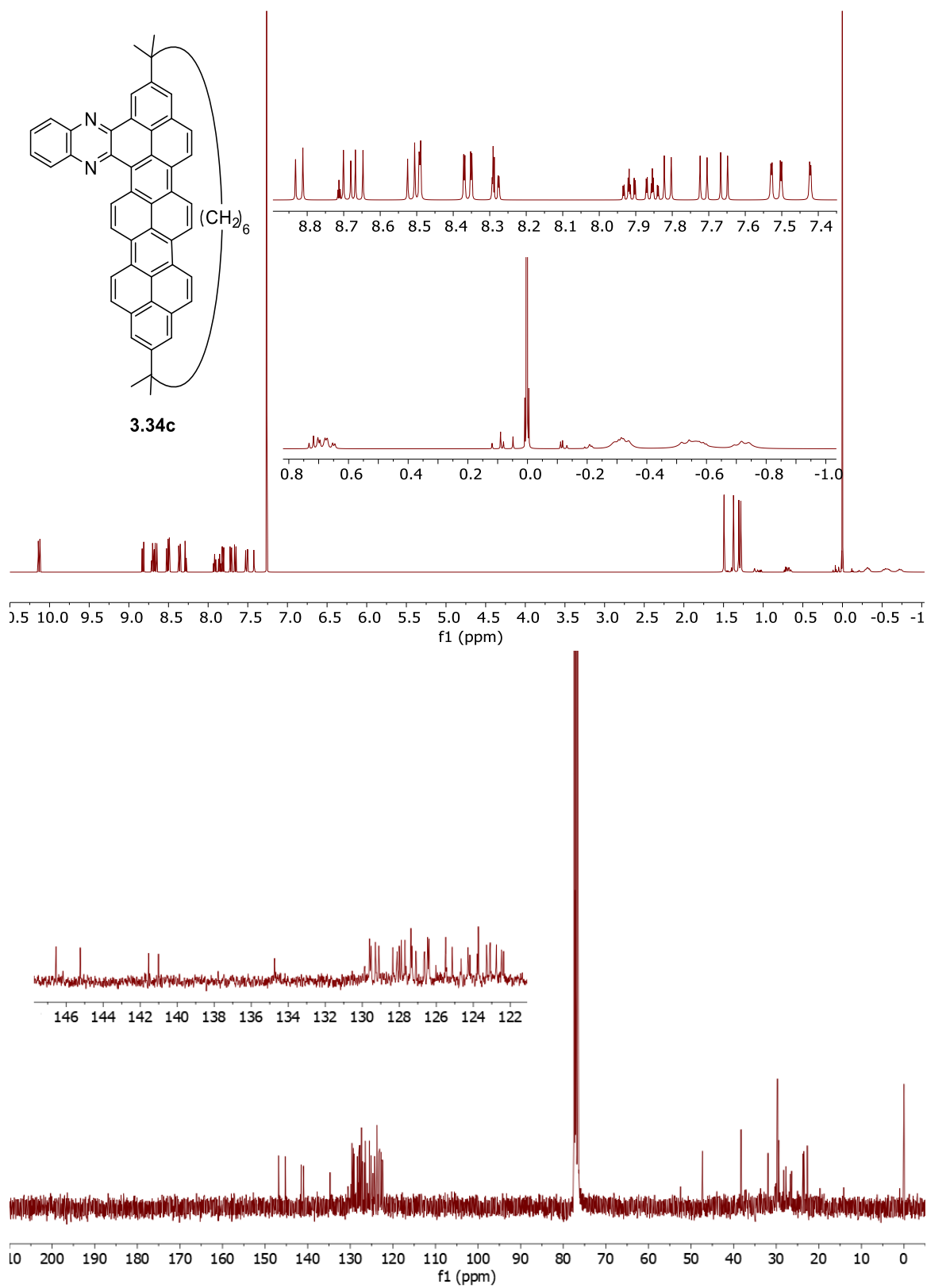


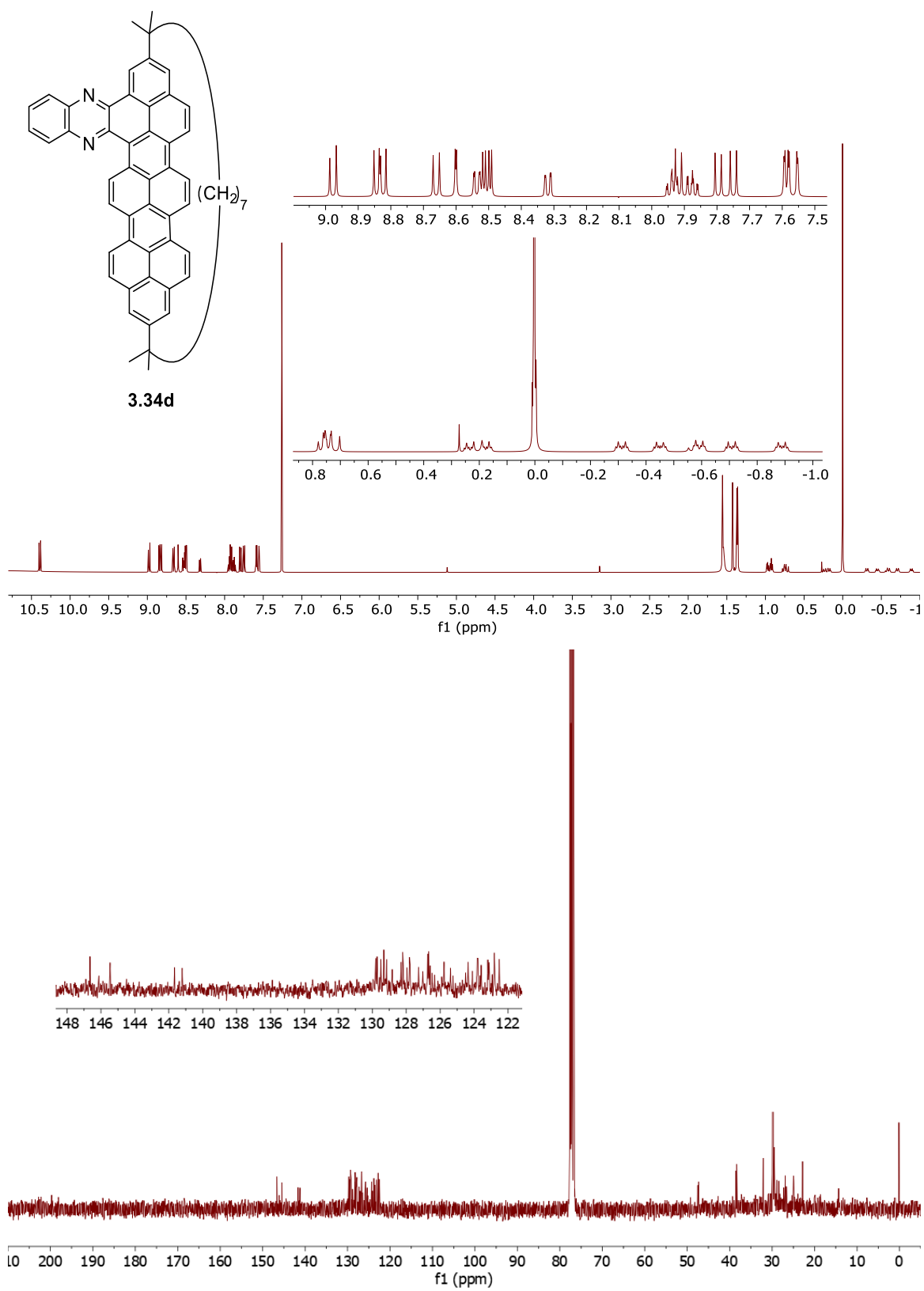












CHAPTER 4: Synthesis of Pyridine-Containing Cyclophanes

4.1 Introduction

As mentioned in Chapter 1, a cyclophane is a system in which one or more aromatic units are connected by one or more bridges at non-adjacent positions. Cyclophanes containing two aromatic systems and two bridges are an especially well-studied class of cyclophanes. They are sub-classified as symmetric $[n.n]$ cyclophanes when both the two aromatic units are identical and the two bridges are of equal length, often identical in nature (*e.g.* **4.1** and **4.2**, Figure 4.1). Unsymmetric (or mixed) $[n.n]$ cyclophanes have two different aromatic systems and two bridges of equal length (*e.g.* **4.3-4.5**).

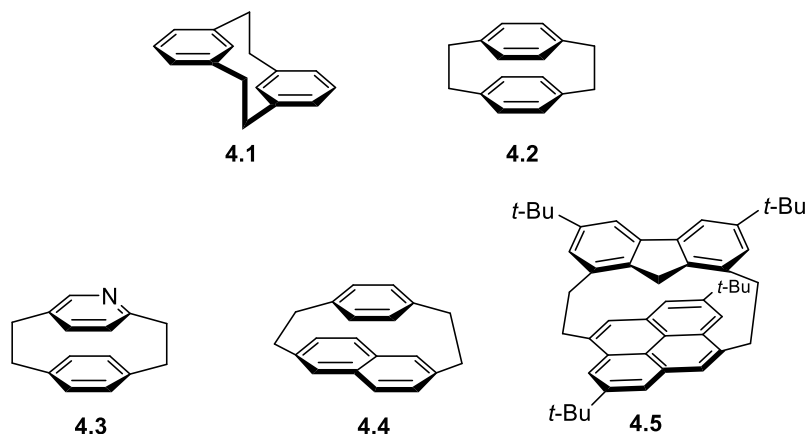


Figure 4.1 A few examples of symmetric $[n.n]$ cyclophanes **4.1-4.2** and mixed $[n.n]$ cyclophanes (**4.3-4.5**).^{1,2}

When the bridges are not of equal length, then the terms symmetric $[m.n]$ cyclophanes *e.g.* **4.6** and unsymmetric (or mixed) $[m.n]$ cyclophanes *e.g.* **4.7** apply (Figure 4.2).³ A feature of multilayered cyclophane **4.7** is transmission of electronic effects from one aromatic ring to another. Internal charge transfer is observed within donor

acceptor phanes. The bridges in cyclophanes are not limited to just aliphatic chains but can also consist of unsaturated units (usually *Z* alkenes) and even benzannulated alkenes (*o*-phenylene units). This particular type of C_2 bridge can lead to cyclophanes consisting exclusively of arylene units *e.g.* **4.8** and **4.9** (Figure 4.3).⁴ 1,3-phenylene units can also be used to build cyclophanes, *e.g.* **4.10** and there is now very strong overlap with a class of compound known as cyclic oligoarylenes.⁵

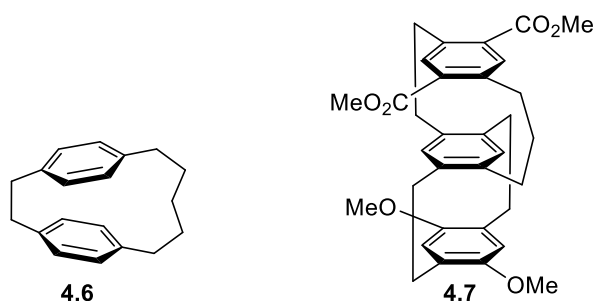


Figure 4.2 Symmetric $[m.n]$ cyclophane **4.6** and mixed $[m.n]$ cyclophane **4.7**.

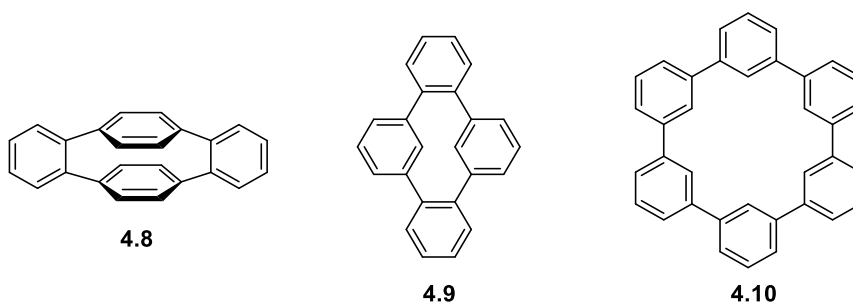
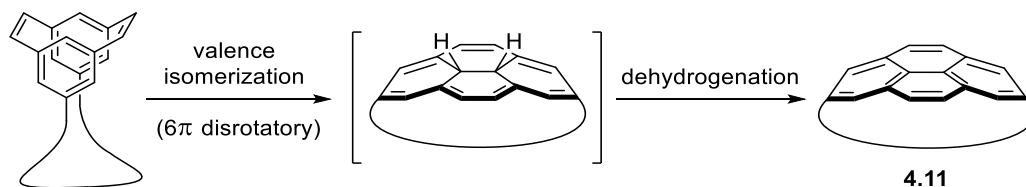


Figure 4.3 Symmetric $[n.n]$ cyclophanes **4.8-4.9** and cyclic oligoarylene **4.10**.

Unsymmetric $[n.n]$ cyclophanes are interesting because aromatic systems of different types can be held in proximity to one another and their structures can be studied. An especially interesting scenario is where the electronic character of the two arenes is large, because it raises the possibility of charge transfer interactions.

4.2 Previously Synthesized Unsymmetric $[n,n]$ Cyclophanes from the Bodwell Group

Several unsymmetric $[n,n]$ cyclophanes have been synthesized in the Bodwell group. In each case, the strategy is an extension of the general route to the $[n](2,7)$ pyrenophanes **4.12** and several analogues containing oxygen **4.13** (Scheme 4.1 and Figure 4.4).⁶⁻⁸ The lynchpin of the strategy was the conversion of a tethered *syn*-[2.2]metacyclophanediene system into the corresponding pyrenophane **4.11** by a valence isomerization/dehydrogenation (VID) protocol (Chapter 1, Section 1.2.2.1 and Chapter 3, Section 3.1.1).



Scheme 4.1 VID strategy for constructing nonplanar pyrenes.

To exploit this strategy, which meant to make progress toward the synthesis of a Vögtle belt, the aliphatic bridge of **4.12** was replaced with appropriate aromatic units (Figure 4.4). In this vein, the (2,7)pyrenophane **4.14** was the first mixed $[n,n]$ cyclophane to be synthesized by the Bodwell group in 2001.⁹ This process of incremental structural modification, which started with parent (2,7)pyrenophanes ($x=1-4$) **4.12**, progressed from [2]paracyclo[2](2,7)pyrenophane **4.14**, to its metacyclophane isomer **4.15** and then to **4.16**.¹⁰ As with the $[n](2,7)$ cyclophanes, the pyrene unit maps onto the surface of a Vögtle-type aromatic belts **4.17**.

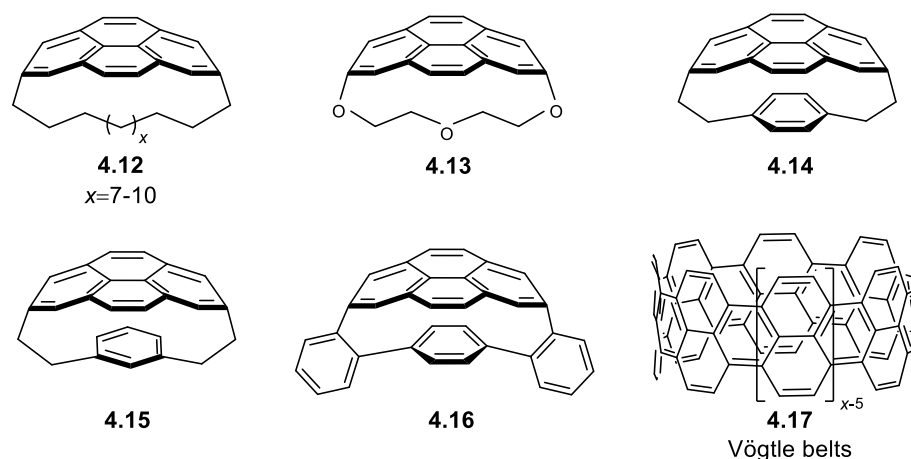
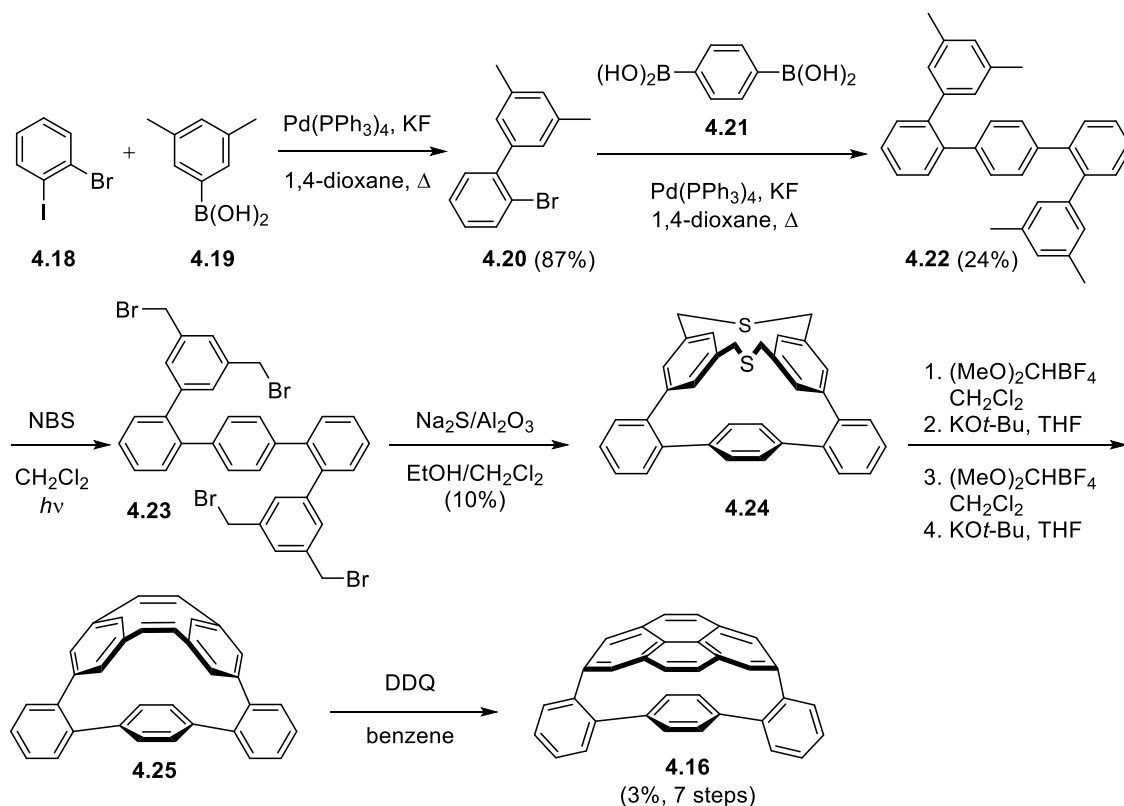


Figure 4.4 Previously reported $[n]$ pyrenophanes **4.12-4.13** and mixed $[2.2]$ cyclophanes **4.14-4.16**.

The general Sonogashira-based synthetic strategy (see Chapter 1, Section 1.2.2.1 and a later Section 4.3.2) that had been effectively applied to the syntheses of **4.12-4.15** could not be employed for **4.16** due to the absence of sp^3 -hybridized carbon atoms. The presence of the three biaryl bonds suggested a new strategy based on the Suzuki-Miyaura reaction (Scheme 4.2).

The synthesis commenced with the Suzuki-Miyaura coupling of 1-bromo-2-iodobenzene (**4.18**) with (3,5-dimethylphenyl)boronic acid (**4.19**) to furnish biphenyl **4.20** (87%). Suzuki-Miyaura coupling of **4.20** with 1,4-phenylenebis(boronic acid) (**4.21**) delivered the quinquephenyl derivative **4.22** in 24% yield. Free radical benzylic bromination of **4.22** with NBS under irradiation with visible light furnished tetrabromide **4.23** (~80%). Treatment of the crude tetrabromide **4.23** with $\text{Na}_2\text{S}/\text{Al}_2\text{O}_3$ afforded the desired dithiacyclophane **4.24**, which was carried forward without purification through a sequence of a bis(*S*-methylation) with Borch reagent, thia-Stevens rearrangement, another bis(*S*-methylation) and Hofmann elimination to furnish cyclophanediene **4.25**. This

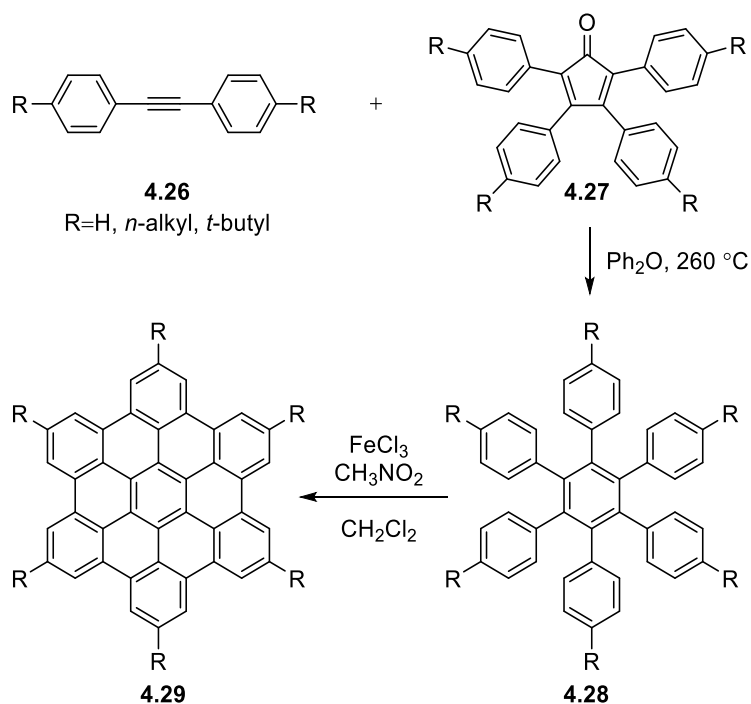
compound was not isolated in pure form. However, the treatment of the mixture with DDQ in benzene at room temperature gave **4.16** (3%, seven steps), which could be purified chromatographically. Although it was eventually successful, the synthetic approach suffered from a few drawbacks. The second Suzuki-Miyaura reaction was low-yielding and also several byproducts were produced during free-radical bromination that could not be separated from the desired product. In order to address these issues, an alternative synthesis leading to an octaphenyl derivative **4.30** was sought, which was inspired by Müllen's work on polyphenylenes and nanographenes (see Figure 4.5).¹¹



Scheme 4.2 Synthesis of pyrenophane **4.16**.

Müllen's methodology is based on a Diels-Alder reaction between diphenylacetylene **4.26** and a tetraphenylcyclopentadienone **4.27** followed by an *in-situ*

decarbonylation reaction to afford a hexaphenylbenzene derivative **4.28** (Scheme 4.3). Cyclodehydrogenation of **4.28** using an intramolecular Scholl reaction furnishes hexabenzocorenene derivative **4.29**.



Scheme 4.3 Müllen's synthesis of hexabenzocorenene derivatives **4.29**.

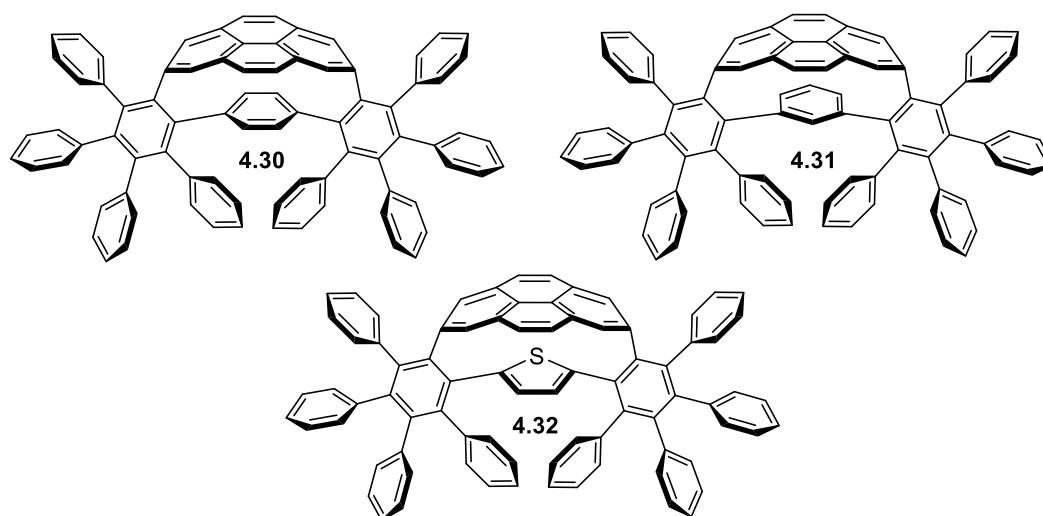
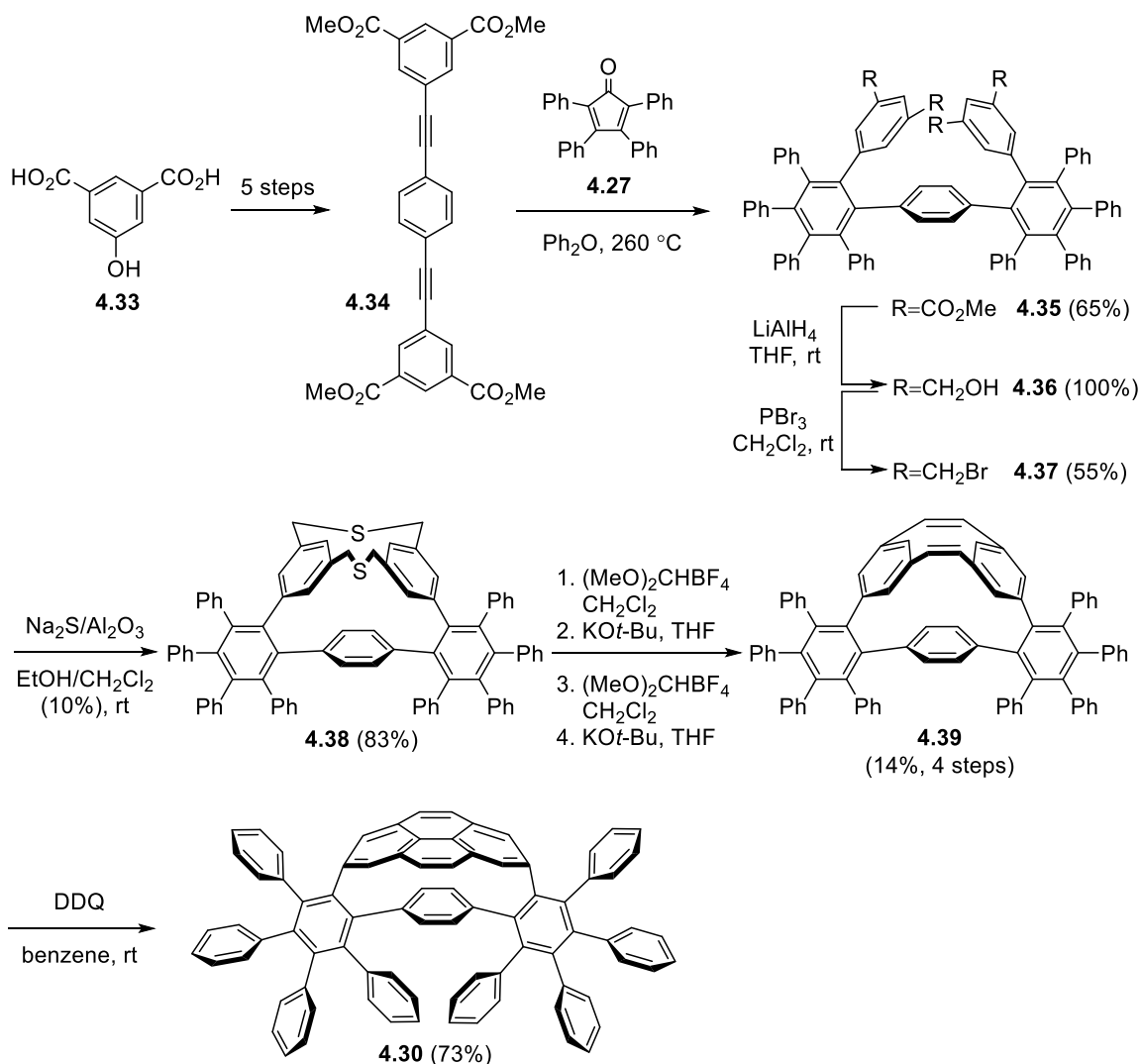


Figure 4.5 Pyrenophanes **4.30-4.32**.

Pyrenophanes **4.30-4.32** were identified as targets (Figure 4.5). These mixed [2,2]cyclophanes, which differed in the nature of the central aromatic system, were synthesized using the Sonogashira-based synthetic strategy (Scheme 4.4).

Tetraesterdiyne **4.34** (five steps from 5-hydroxyisophthalic acid **4.33**, Chapter 1, Scheme 1.16) was heated with tetraphenylcyclopentadienone (**4.27**, R=H) in diphenyl ether at reflux to afford tetraester **4.35** (65%). **4.35** was reduced with LiAlH₄ to furnish tetraol **4.36** in quantitative yield. Treatment of tetraol **4.36** with PBr₃ generated tetrabromide **4.37**



Scheme 4.4 Synthesis of pyrenophane **4.30**.

(55%). Compounds **4.35-4.37** were obtained as slowly equilibrating mixtures of *cis* and *trans* isomers. Reaction of **4.37** with $\text{Na}_2\text{S}/\text{Al}_2\text{O}_3$ afforded dithiacyclophane **4.38** (83%). Bridge contraction and double bond formation to give **4.39** (14%, 4 steps) was achieved using the usual four-step sequence involving *S*-methylation, thia-Stevens rearrangement, *S*-methylation and Hofmann elimination. Upon reaction with DDQ in benzene at room temperature, cyclophanediene **4.39** was converted into the corresponding pyrenophane **4.30** in 1.6% overall yield.

To date, only pyrenophanes containing 1,4-phenyl (**4.16**, **4.30**), 1,3-phenyl (**4.15**, **4.31**) and 2,5-thienylene unit (**4.32**) have been synthesized. Although the arenes vary in their size, shape and electronic nature, no pyrenophane containing an electron-deficient aromatic ring has been reported. Therefore, it was decided that replacement of some of the aliphatic bridge carbon atoms in both the pyrenophane and teropyrenophane systems (**4.11**, **4.40**) with pyridine (**4.41**, **4.42**, Figure 4.6) would be a worthwhile endeavour. This would not only provide the potential for the discovery of new compounds with unusual and exploitable optoelectronic properties, but also offers opportunities to investigate their host-guest chemistry and metal complexes. Along these lines, [*n.n*]cyclophanes **4.43**, **4.44** and

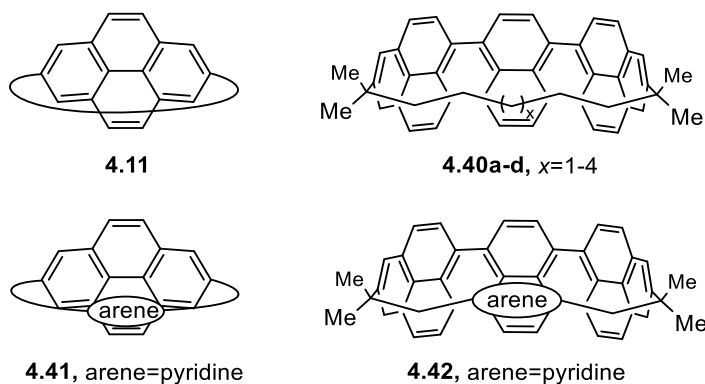


Figure 4.6 Incorporation of pyridine in the tether of **4.11** and **4.40**.

4.45 were identified as viable synthetic targets (Figure 4.7). Pyridine-containing teropyrenophane (pyridinophane) **4.43** was of particular interest due to the appreciable cavity within the cycle, therefore it was the first target of investigation.

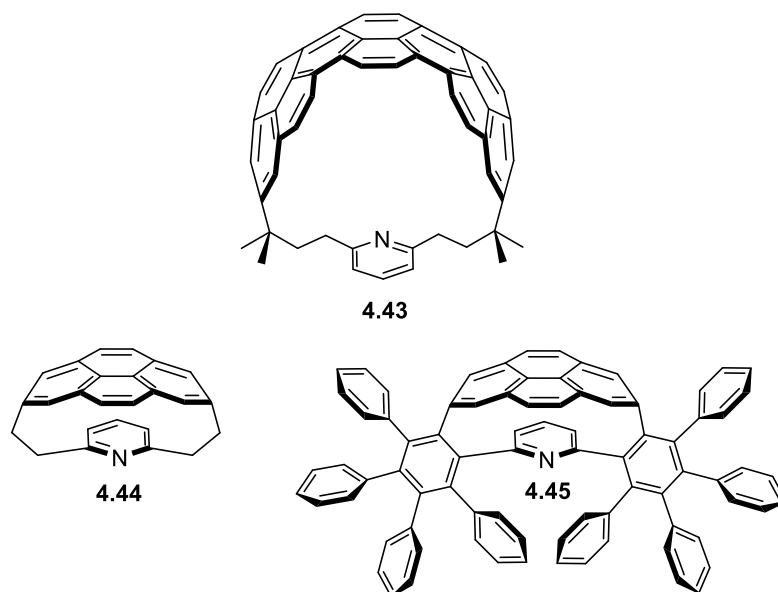


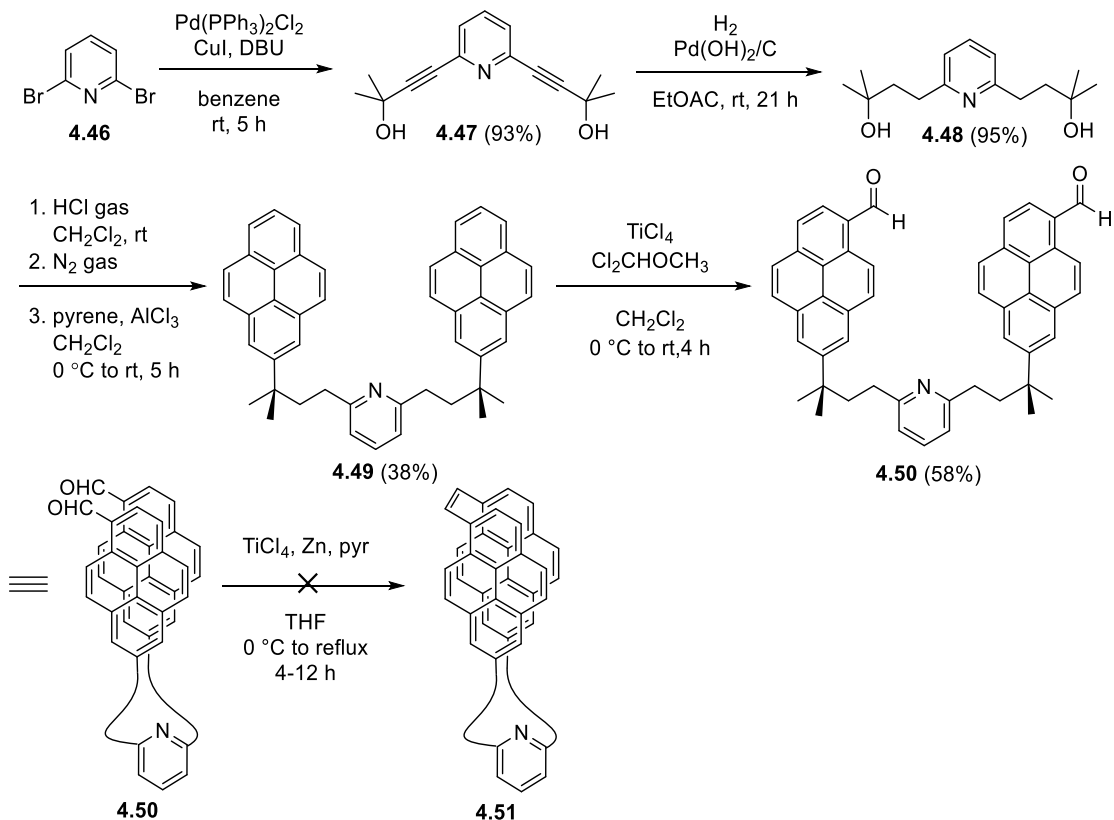
Figure 4.7 Target [m.n]cyclophanes **4.43**, **4.44** and **4.45**.

4.3 Results and Discussion

4.3.1 Attempted Synthesis of Pyridine-Containing Teropyrenophane **4.43** *via* both McMurry and Wurtz/McMurry Strategies

As described in Chapter 2, the Bodwell group has reported two different approaches (double-McMurry and Wurtz coupling/McMurry) for the synthesis of a series of 1,1,*n,n*-tetramethyl[*n*](2,11)teropyrenophanes **4.40a-d** (Chapter 2, Section 2.2).^{12,13} Therefore, it was decided to investigate both routes at the same time. The early stages of the synthesis of **4.43** necessarily differed from those of [*n*](2,11)teropyrenophanes (**4.40a-d**, Chapter 2, Schemes 2.3 and 2.5) due to the presence of the pyridine unit. Accordingly, synthetic work

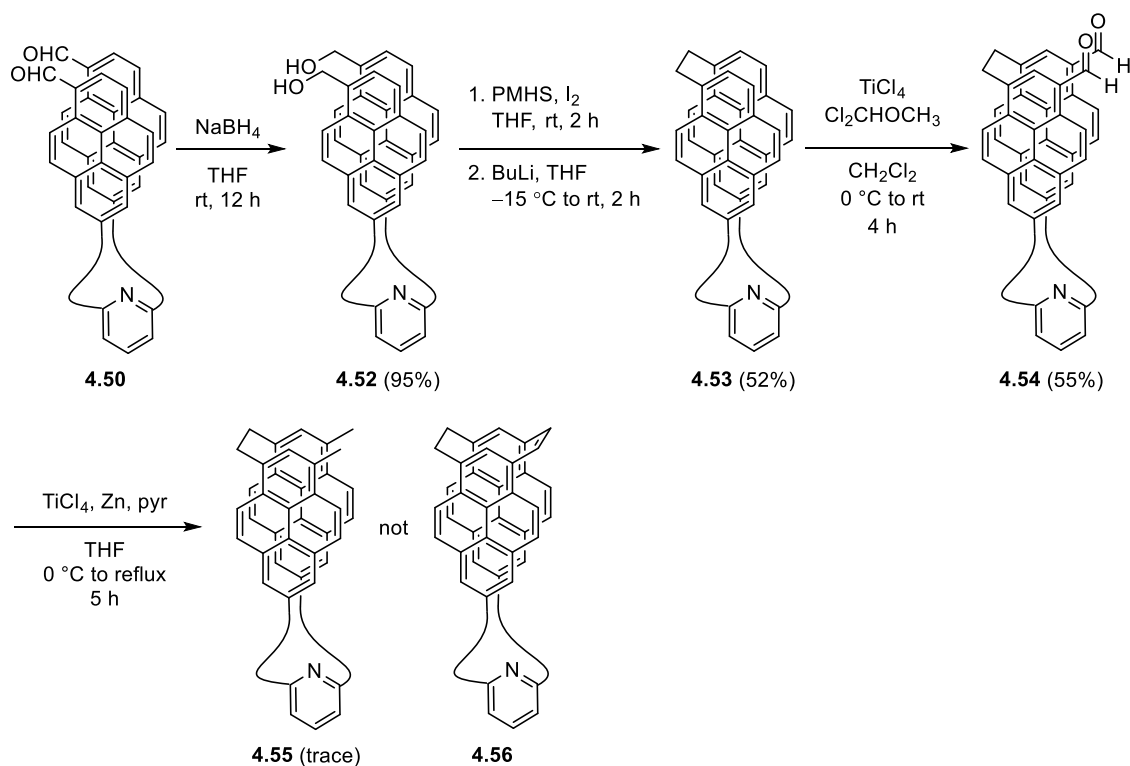
commenced with the construction of unsaturated diynediol **4.47** from 2,6-dibromopyridine (**4.46**) via a Sonogashira cross-coupling reaction (Scheme 4.5). Catalytic hydrogenation of



Scheme 4.5 Attempted synthesis of pyridinophane **4.43** using a double-McMurry route.

4.47 afforded diol **4.48** (95%) and this was used in a Friedel-Crafts alkylation of pyrene to furnish dipyren-2-ylalkane **4.49** in 38% yield. Rieche formylation of **4.49** gave dialdehyde **4.50** with complete regioselectivity in 58% yield. Several attempts at performing the McMurry reaction of dialdehyde **4.50** resulted in the formation of a mixture of products (TLC analysis), from which no distinguishable compound could be isolated. The failure of the McMurry reaction was unexpected, because the unit tethering the two pyrene systems was flexible and relatively long (9 atoms).

The failure of the double-McMurry strategy at the first hurdle prompted the investigation of the Wurtz/McMurry approach (Scheme 4.6). Hence, dialdehyde **4.50** was smoothly reduced to the corresponding diol **4.52** in high yield using NaBH₄. The diol **4.52** was then subjected to the iodination/Wurtz coupling sequence and cyclophane **4.53** was



Scheme 4.6 Attempted synthesis of pyridinophane **4.43** using a Wurtz/McMurry route.

obtained in 52% yield. Rieche formylation then furnished dialdehyde **4.54** in moderate yield, but with complete regioselectivity again. Attempted intramolecular McMurry reaction of **4.54** resulted in a complex mixture, in which a compound with the mass of the reduced product **4.55** ($m/z = 674.37$) could be detected (LCMS analysis).

During the work aimed at the synthesis of 1,1,6,6-tetramethyl[6](2,11)teropyrenophane (Chapter 2), it became clear that the conformational

behaviour of dialdehydes slated for McMurry reaction played an important role. With this in mind, the ^1H NMR spectrum of **4.54** was examined (Figure 4.8). High-field aromatic signals were observed at $\delta 6.90$ ppm, which indicates that the *anti* conformation is dominant in solution (see Section 2.4.3). On the other hand, the signal for the methyl groups appeared

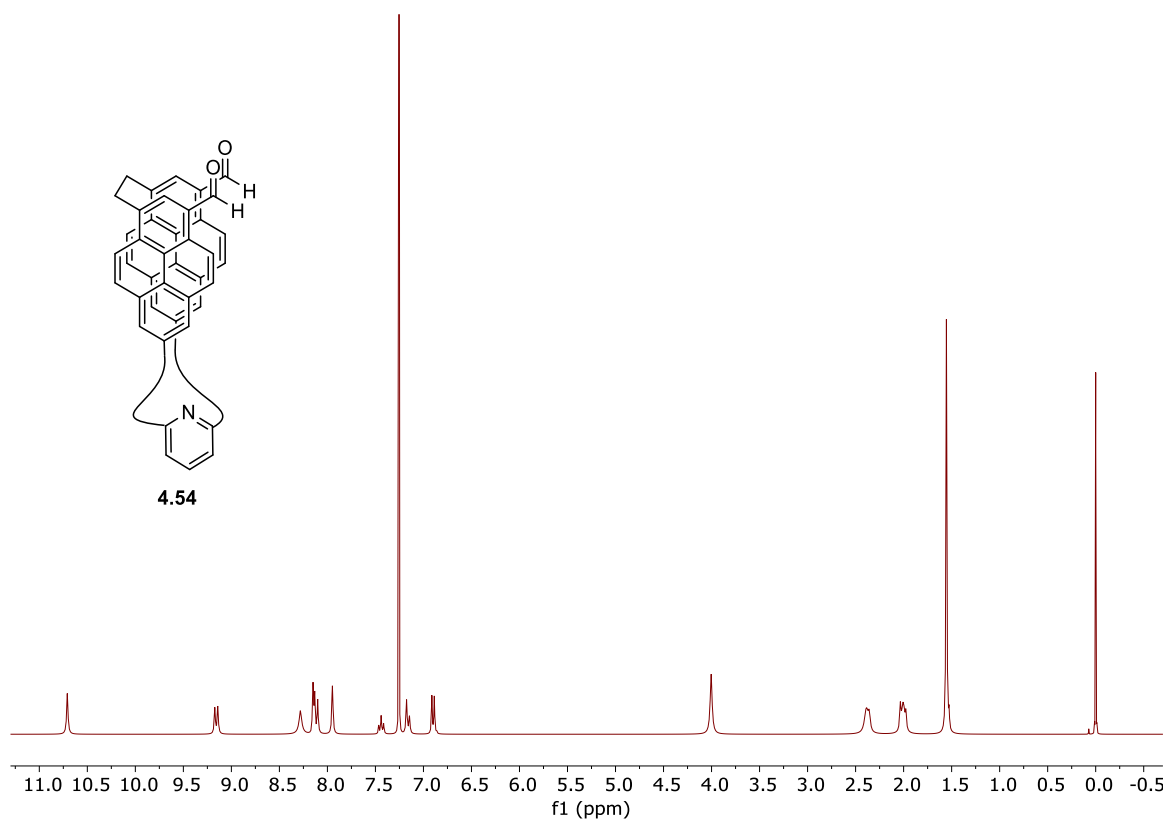


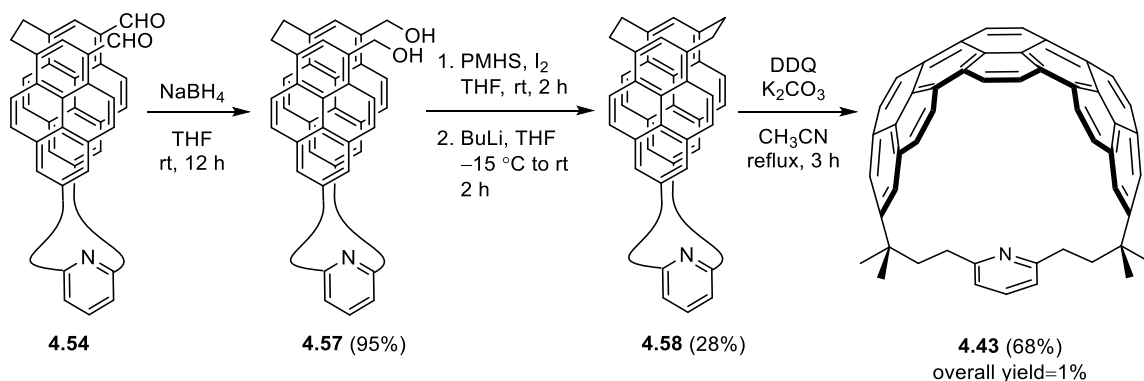
Figure 4.8 The ^1H NMR spectrum of cyclophane **4.54**.

as a sharp 12H singlet at $\delta 1.56$ ppm, which means that *anti/anti'* interconversion is rapid at room temperature. Since this process proceed through the *syn* conformation, the *syn* conformation must be readily accessible at the temperature of the McMurry reaction. This being the case, the failure of the McMurry reaction of **4.54** is surprizing.

4.3.2 Synthesis of Pyridine-Containing Teropyrenophane **4.43** via a Double-Wurtz Coupling Route

Both the double-McMurry and Wurtz/McMurry routes failed at a McMurry reaction. In both cases, the accessibility of conformation required for successful McMurry reactions appeared to be available. It therefore seemed likely that the failure of this McMurry reaction is attributable to a different phenomenon, but it is not yet clear what this is. The pyridine ring could affect the McMurry reaction by coordination of the lone pair of nitrogen to some sorts of Ti species, which might provide a steric barrier to the approach of the two formyl groups in **4.50** and **4.54**. Therefore, it was decided to replace the McMurry reaction in the Wurtz/McMurry approach with another Wurtz coupling. Dialdehyde **4.54** was reduced with NaBH₄ to furnish diol **4.57** in 95% yield (Scheme 4.7). It was then found that **4.57** could be converted into cyclophane **4.58** using the iodination/Wurtz coupling sequence, albeit in rather modest yield (28%). In view of the successful formation of a series of [*n*](2,11)teropyrenophanes **4.40b-c** (*x*=1-2, Figure 4.6) using DDQ in CH₃CN (see Chapter 3 for details), it was decided to reflux cyclophane **4.58** with DDQ in CH₃CN for 3 hours. This led to the formation of one new spot on the baseline (TLC analysis) and only partial consumption of starting material **4.58**. It was suspected that the reaction had indeed proceeded but underwent protonation by the hydroquinone resulting from the reduction of DDQ to form a TLC immobile salt. This made it problematic to monitor the progress of the reaction. In an effort to avoid the presumed protonation, the reaction of **4.58** was attempted with the addition of K₂CO₃ to the reaction mixture. In this case, the reaction afforded the target pyridine-containing teropyrenophane (pyridinophane)

4.43 in 68% yield (1% over 10 steps). The starting material was not consumed completely even after heating for 5 hours, so it means that higher yield may be achievable.



Scheme 4.7 Synthesis of pyridinophane **4.43** using a double-Wurtz coupling route.

The success of this reaction is noteworthy. There is no unsaturation in the two-atom bridges, so there can be no valence isomerisation. It is thus very likely that the reaction is an intramolecular Scholl reaction and not a VID reaction. This calls into question whether the reactions leading to the $[n](2,11)$ teropyrenophanes (**4.40a-d**) are VID reactions and not Scholl reactions.

The isolation of the desired product (**4.43**) in pure form was a challenging endeavour due to the very close R_f values of **4.58** and **4.43**, however it was eventually isolated (2 mg) as a slightly impure orange solid. The structure of **4.43** was determined by NMR and MS analysis.

The structure of **4.43** was calculated at the B3LYP/PM6 level of theory (calculations performed by Prof. Yuming Zhao, Memorial University). The bend angle in pyridinophane **4.43** was found to be 161.4° (Figure 4.9), which is smaller than the calculated angle of $[8](2,11)$ teropyrenophane **4.40b** (169.0°) and bigger than that of

[9](2,11)teropyrenophane **4.40c** (156.6°). It should be noted that the nitrogen atom of pyridine is predicted to point into the cavity of teropyrenophane, which suggest that the

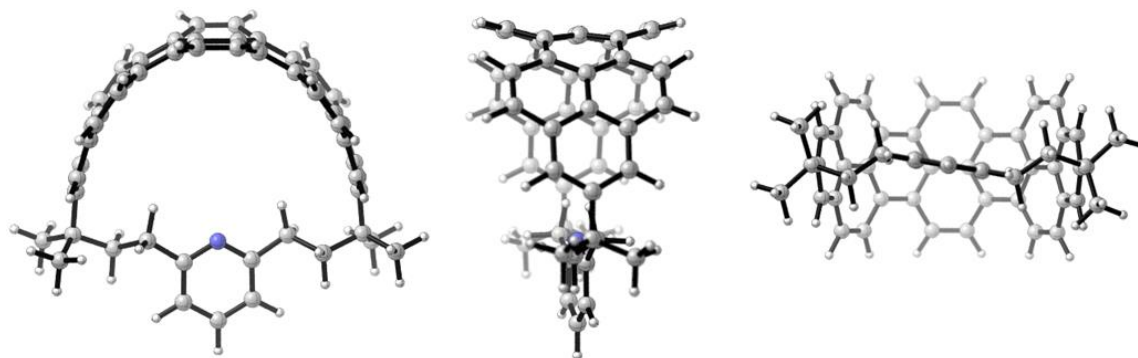


Figure 4.9 Calculated molecular structure of **4.43** at B3LYP/PM6 level of theory.

metal ions might be directed into the cavity. Work in this direction will require access to larger quantities of **4.43**. An intriguing feature of **4.43** is the difference in electronic nature between the teropyrene system and the pyridine system and how this difference could be made much larger by protonation of the nitrogen atom or complexation to a metal cation. Therefore, the absorption and emission spectra of **4.43** were investigated with an eye to how they change upon titration with Brønsted acid and metal cations.

4.3.3.1 Absorption and Emission Spectroscopy of Pyridinophane **4.43**

The absorption spectrum of **4.43** consists of three sets of bands, in the ranges of 330-377 nm, 457-473 nm and 491-527 nm. The longest wavelength absorption maxima of each range are observed at 345, 466, and 499 nm respectively (Figure 4.10). The λ_{max} of **4.43** is at larger wavelength than those for **4.40a** (484 nm), **4.40b** (489 nm) and **4.40c** (494). The emission spectrum for pyridinophane **4.43** is also very similar to what was observed

for teropyrenophanes **4.40a-c** and shows two overlapping fluorescence bands: $\lambda_{\text{max}} = 514$ (480-531 nm) and $\lambda_{\text{max}} = 541$ (534-600 nm).

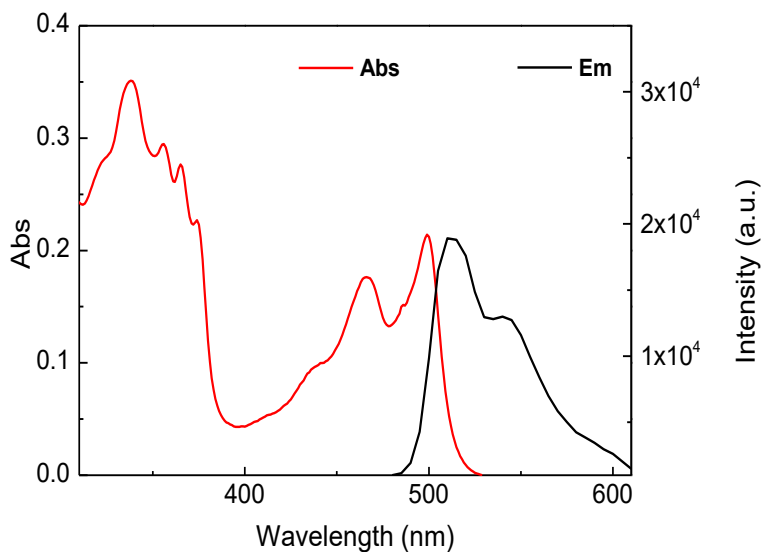


Figure 4.10 Normalized absorption and emission spectra of pyridinophane **4.43** measured in CH_2Cl_2 at room temperature.

To investigate the changes in pyridinophane **4.43** through protonation of pyridine in the system, titration with trifluoroacetic acid (TFA) was performed. TFA was chosen due to its strong acidity ($\text{p}K_{\text{a}}=0.23$) and good solubility in most common organic solvents. Addition of a large excess of TFA led to the complete loss of fluorescence. A titration using 0.043 equiv. of acid was then performed. The titration was stopped until no further change in the fluorescence spectrum was found (15.5 equiv.). Upon slow addition of acid, it was observed that fluorescence was quenched gradually. After addition of 1.0 equiv., the intensity had gone down to 80% of the original intensity and it went to 0% after the addition of 15.5 equiv. This would suggest that there must be some interactions, possibly an intramolecular charge transfer between the excited electron rich teropyrene system

(chromophore) and the electron deficient (pyridinium) system, which did not exist in neutral pyridine (Figure 4.11).

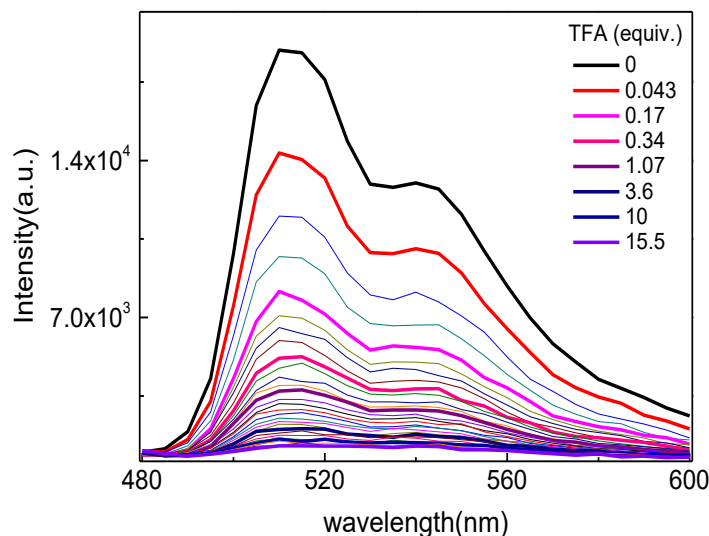


Figure 4.11 Changes in the emission spectra of pyridinophane **4.43** upon titration with TFA in CH_2Cl_2 at room temperature.

As shown in the absorption spectrum (Figure 4.12), no band was observed at 742 nm before the addition of TFA, but the trend started to increase upon the protonation. It seems likely that pyridine is not a strong enough acceptor, but it converts to a better acceptor upon protonation. Therefore, after excitation, instead of emission, energy would be released in a non-emissive pathway by a neighboring charge transfer mechanism. As might be expected, these bands are weak because the charge transfer from the highest occupied molecular orbital (HOMO) of teropyrene system to the lowest unoccupied (or unfilled) molecular orbital (LUMO) of pyridinium is perhaps a forbidden transition, however this transition is nevertheless able to quench the fluorescence (Figure 4.11).

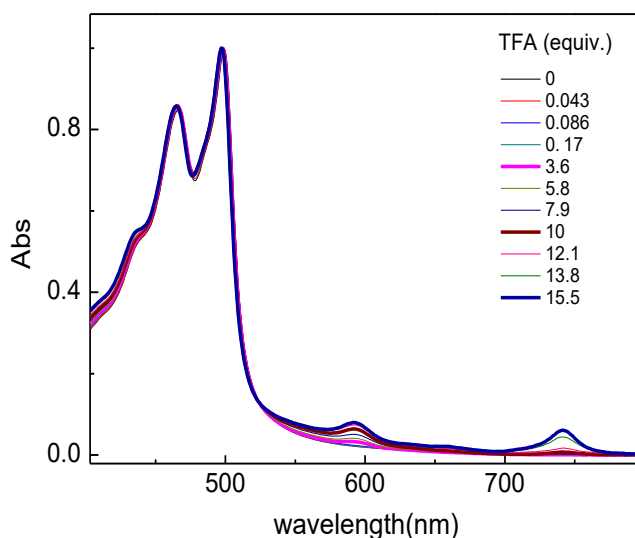


Figure 4.12 Changes in the absorption spectra of pyridinophane **4.43** upon titration with TFA in CH_2Cl_2 at room temperature.

To examine the potential of pyridinophane **4.43** to form metal complexes, titration of this cyclophane with copper(II) triflate was performed. Copper(II)triflate was selected due to its ability to form stable complexes (a soft Lewis acid, which can be coordinated to the pyridine as a base). Overall, 0 to 15.5 equiv. of copper(II) triflate was used (0.013 equiv. per injection). Pyridinophane **4.43** showed a similar response to the metal titration in its emission spectrum (Figure 4.13, second spectrum) as it did to the Brønsted acid, TFA. The fluorescence was quenched gradually with gradual addition of copper (II) triflate, but no major changes were observed in the UV-Vis absorption spectrum of **4.43**, which could indicate that the LUMO of a protonated pyridine unit is lower than the LUMO of a Cu-coordinated pyridine unit. There would be some interactions between the HOMO of the teropyrene system and the LUMO of coordinated pyridine unit due to the quenching effect. Although copper would not be able to bind strongly to nitrogen, probably due to the steric

hindrance, which could show that the cavity in this structure is well suitable to hold a proton but not bigger ions (metals).

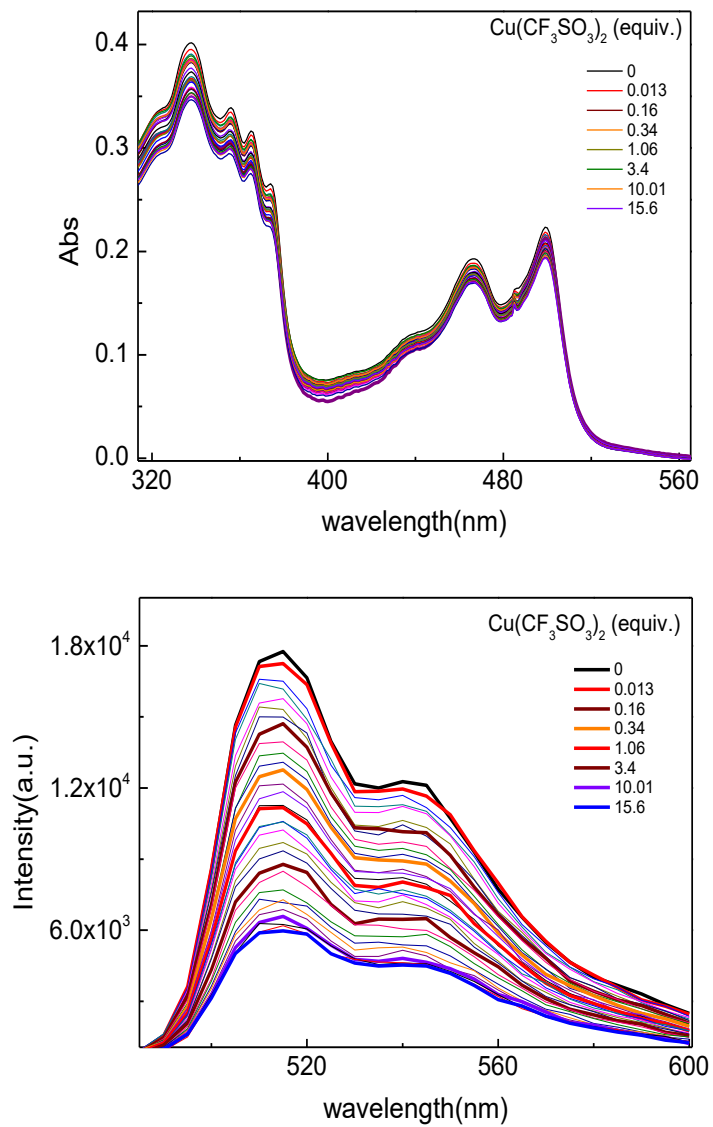


Figure 4.13 Absorption and emission spectra of pyridinophane **4.43** upon titration with copper(II) triflate in CH_2Cl_2 at room temperature.

4.3.3.2 DFT/TD-DFT Calculations Results of Pyridinophane 4.43

The geometries of compounds were first optimized at the B3LYP/6-31G(d) level and then subjected to single-point TD-DFT calculations at the CAM-B3LYP/6-31G(d) level (calculations performed by Prof. Yuming Zhao, Memorial University).¹⁴ Summary of TD-DFT calculated UV-Vis absorption bands of neutral pyridinophane **4.43** are shown in Table 4.1.

Table 4.1 Summary of TD-DFT calculated UV-Vis absorption bands and assignment of related MO contributions (neutral pyridinophane **4.43**).

λ_{calcd} (nm)	f	Major MO contributions
451	0.62	HOMO→LUMO (95%)
332	0.22	HOMO→L+1 (31%), HOMO→L+2 (59%)
321	0.13	H-2→LUMO (84%)
315	0.29	H-1→LUMO (47%), HOMO→L+1 (27%), HOMO→L+2 (17%)
287	0.81	H-1→L+1 (66%), H-1→L+2 (22%)
274	0.01	H-2→L+3 (14%), HOMO→L+7 (65%)

The TD-DFT results show that the lowest-energy absorption band observed in the experimental UV-Vis spectrum is mainly due to the HOMO to LUMO transition. MO plots indicate that the HOMO and LUMO are both populated on the teropyrene structure. The pyridyl unit, however, does not contribute to the UV-Vis absorption bands significantly (Figure 4.14).

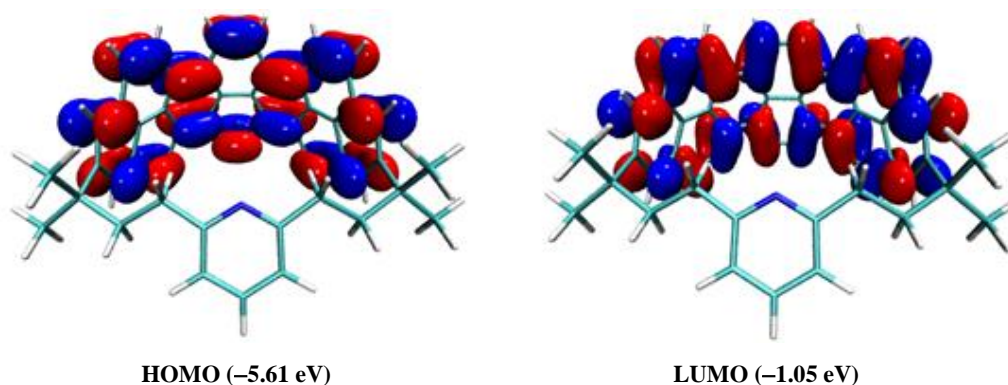


Figure 4.14 Contour plots (isovalue = 0.02) and eigenvalues of highest occupied molecular orbital (HOMO) and lowest unoccupied molecular orbital (LUMO) of neutral pyridinophane **4.43**. Calculations done at the B3LYP/6-31G(d)//CAM-B3LYP/6-31G(d) level of theory.

The TD-DFT results of the protonated pyridinophane **4.43** show that the strong low-energy $\pi \rightarrow \pi^*$ transition band in the experimentally measured UV-Vis spectrum essentially arises from the HOMO to LUMO+2 transition (Table 4.2). The contour plot of LUMO+2 resembles the LUMO of neutral pyridinophane. The HOMO to LUMO transition, on the other hand, is kind of forbidden, since they do not have significant spatial overlap. The LUMO of the protonated species is mainly on the pyridinium unit. Therefore, the HOMO

Table 4.2 Summary of TD-DFT calculated UV-Vis absorption bands and assignment of related MO contributions (protonated pyridinophane **4.43**).

λ_{calcd} (nm)	f	Major MO contributions
638	0.0002	HOMO \rightarrow LUMO (100%)
450	0.6035	HOMO \rightarrow L+2 (94%)
424	0.0024	H-1 \rightarrow LUMO (99%)
411	0.0005	H-2 \rightarrow LUMO (95%)
406	0.0009	H-1 \rightarrow L+2 (39%), HOMO \rightarrow L+3 (41%), HOMO \rightarrow L+4 (13%)
335	0.2132	HOMO \rightarrow L+3 (27%), HOMO \rightarrow L+4 (64%)
320	0.0033	H-3 \rightarrow LUMO (93%)
318	0.159	H-2 \rightarrow L+2 (72%), H-1 \rightarrow L+2 (14%)

to LUMO transition exhibits a significant charge transfer (CT) character. The oscillator strength of this band is calculated to be very small, which is in good agreement with the experimentally observed very weak CT band in the UV-Vis titration spectra. Overall, the TD-DFT results indicate that protonation of the pyridyl unit makes it more electron-withdrawing, and the interplays between the pyridinium and teropyrene units lead to observable CT absorption band in the UV-Vis data (Figures 4.15).

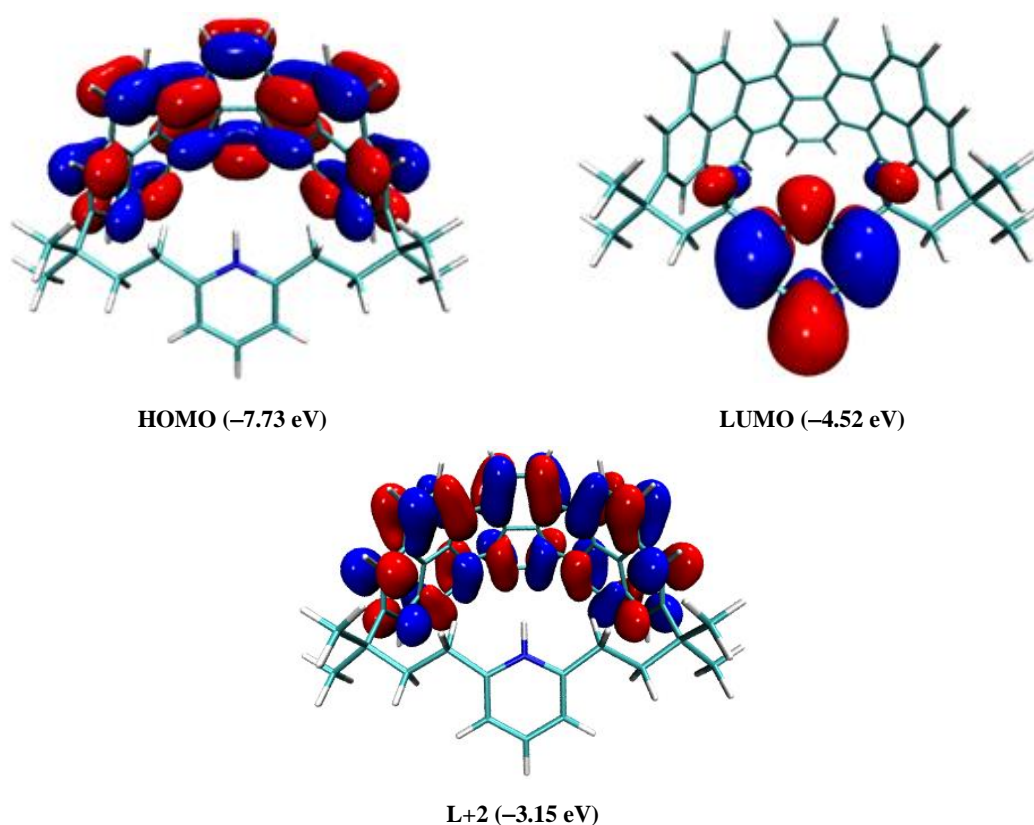


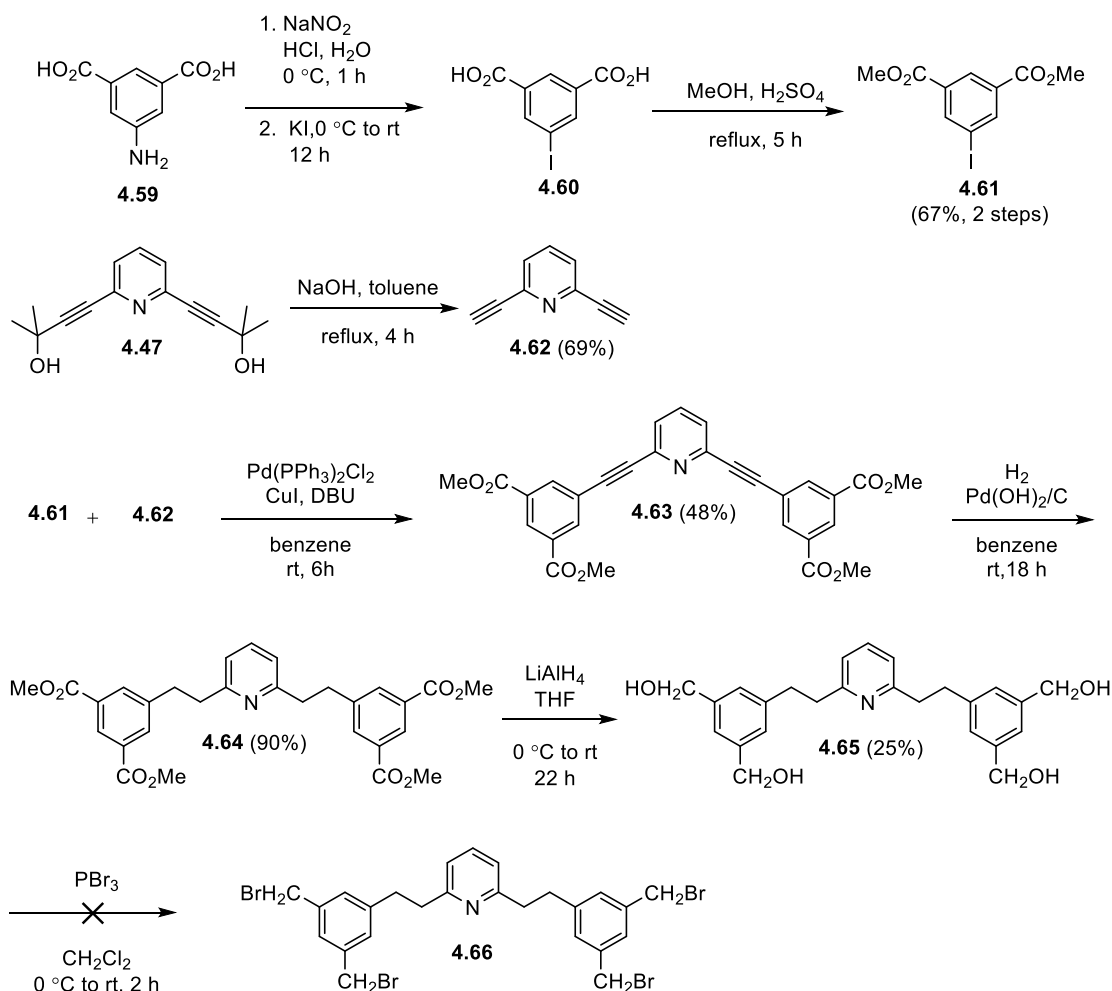
Figure 4.15 Contour plots (isovalue = 0.02) and eigenvalues of HOMO, LUMO, and LUMO+2 of protonated pyridinophane **4.43**. Calculations done at the B3LYP/6-31G(d)//CAM-B3LYP/6-31G(d) level of theory.

Synthesis of pyridinophane **4.43** as the first teropyrenophane containing an arene is remarkable and invites more investigation regarding the potential of this large cyclophane

in host-guest chemistry, and further its potential for application in the design of optoelectronic devices and solar cells.

4.3.4 Towards the Synthesis of Pyridine-Containing Pyrenophanes

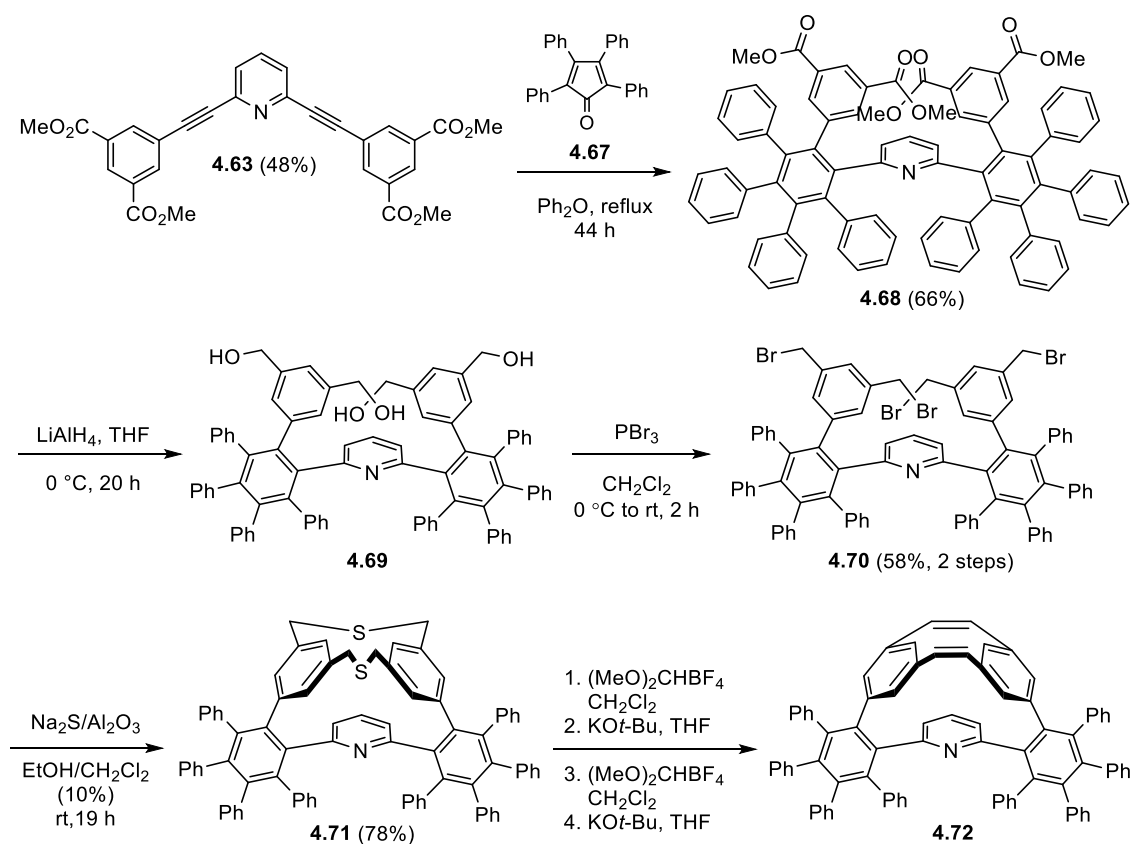
The success in synthesizing a novel pyridine-containing teropyrenophane (**4.43**) prompted the synthesis of related pyrenophane systems, which contains an electron deficient ring (pyridine). This could provide the opportunity to investigate the intramolecular charge transfer transition in pyrenophanes. Hence, **4.44** was identified as an attractive target. The synthesis of **4.44** commenced with the diazotization of commercially available 5-aminoisophthalic acid (**4.59**) followed by iodination to give **4.60**, esterification of which with methanol afforded **4.61** in 67% yield over 2 steps (Scheme 4.8). Separately, **4.62** was synthesized by deprotection of **4.67** with sodium hydroxide in toluene in 69% yield. Sonogashira cross-coupling of diester **4.61** with dialkyne **4.62** furnished tetraester **4.63** in 48% yield. With all of the carbon atoms in place, the remainder of the synthesis involved the manipulation of the present carbon skeleton. Catalytic hydrogenation of **4.63** afforded tetraester **4.64** in high yield (90%). Tetraester **4.64** was then reduced with LiAlH_4 to give tetraol **4.65** but in just 25%. The low yield of the reaction was likely related to the very poor solubility of the product in most common organic solvents. The tetraol was subjected to bromination using PBr_3 , which failed to provide the tetrabromide **4.66**. Using HBr/AcOH and $\text{CBr}_4/\text{PPh}_3$ also provided a complex mixture from which no distinguishable product could be obtained. A concern, which was never confirmed was self-alkylation. With bromination being problematic, it was decided to change the synthetic route by using Müllen's methodology that led to pyrenophane **4.45** as a new target (Figure 4.7).



Scheme 4.8 Attempted synthesis of pyridine-containing pyrenophane **4.44**.

Heating tetraphenylcyclophenadienone (**4.67**) with tetraester **4.63** in diphenyl ether at 260°C brought about the desired two-fold Diels-Alder reaction followed by *in-situ* decarbonylation reaction and furnished octaphenyl tetraester **4.68** in 66% yield (Scheme 4.9). Tetraester **4.68** was then reacted with LiAlH_4 and afforded tetraol **4.69**.¹⁵ Benzylic bromination of crude tetraol **4.69** using phosphorous tribromide yielded tetrabromide **4.70** (58% 2 steps), which could not be isolated in pure form and was taken through the next step without further purification. Treatment of **4.70** with $\text{Na}_2\text{S}/\text{Al}_2\text{O}_3$

afforded dithiacyclophane **4.71** in 78% yield. According to ^1H NMR and HRMS analysis dithiacyclophane is clearly present, but it is not as pure as would have been desired. At this stage, there were a serious concern about whether the standard protocol namely *S*-methylation, thia-Stevens rearrangement, *S*-methylation and Hofmann elimination could be used due to the possibility of the methylation of the nitrogen, which was very highly undesirable and need to be avoided. The thought was that nitrogen has two alkyl groups beside it, which makes the alkylation relatively slow. In addition, sulfur is more electrophilic and more accessible than the nitrogen atom. Consequently, it was decided to take the impure dithiacyclophane **4.71** through the afore-mentioned four-step sequence using a stoichiometric amount of Borch reagent. Unfortunately, only ~1 mg of product was



Scheme 4.9 Attempted synthesis of pyridine-containing pyrenophane **4.45**.

obtained, LCMS analysis of which indicated that the correct product may have been formed ($[M+1]^+$ $m/z=1040$ and the expected mass=1039). The synthesis of pyrenophane **4.45** demands more investigation and future work in this area should focus on building up the required materials to deliver the corresponding cyclophane diene **4.72**, which is only one step from the target pyrenophane **4.45**.

4.4 Summary

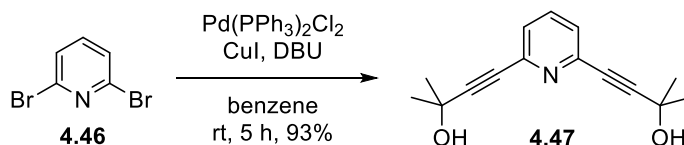
Sonogashira-based strategy for the synthesis of a variety of $[n](2,7)$ pyrenophanes and Wurtz/McMurry strategy for the synthesis of 1,1, n -tetramethyl $[n](2,11)$ teropyrenophanes **4.40a-d** evolved into the development of a new synthetic sequence to pyridinophane **4.43**. The new strategy exploits a Sonogashira reaction and two Wurtz coupling reactions to construct the three bridges of triply-bridged pyrenophane **4.58**, which can be converted into the corresponding pyridinophane **4.43** upon treatment with DDQ in CH_3CN .

To investigate the changes in pyridinophane **4.43** through protonation of pyridine and metal complex formation, titration of this cyclophane with TFA and copper(II) triflate were performed respectively. UV-Vis acid titration spectra showed a weak charge transfer band due to the intramolecular transition between the teropyrene and pyridinium units, which did not exist in neutral pyridinophane. In contrast, no CT band was observed in the UV-Vis metal titration spectra. Pyridinophane **4.43** showed a similar response to both acid and metal titrations in emission spectra and fluorescence was quenched gradually. These results are in good agreement with the TD-DFT calculation outcomes.

Remarkable progress was made towards the synthesis of pyridine-containing pyrenophane, but more investigation is required in this area. These new types of compounds offer opportunities to investigate their host-guest chemistry and have the potential for application in the design of optoelectronic devices.

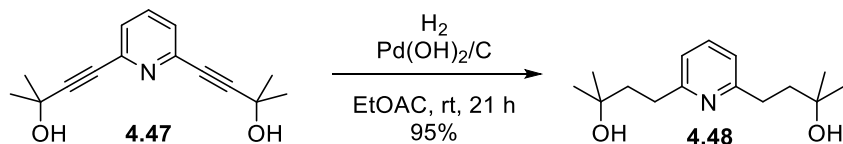
4.5 Experimental Procedures and Characterization Data

Diynediol **4.47**



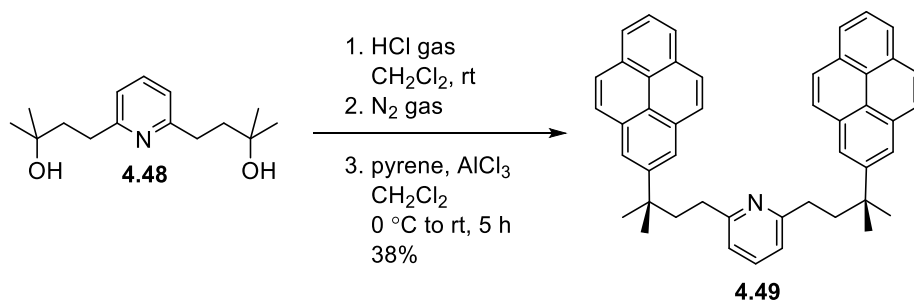
2,6-dibromopyridine (**4.46**) (10.1 g, 42.2 mmol) was added to a solution of $\text{Pd(PPh}_3)_2\text{Cl}_2$ (1.18 g, 1.69 mmol) and CuI (1.29 g, 6.75 mmol) in degassed benzene (200 mL, 250 mL Schlenk flask). The reaction mixture was stirred for 5 min and then DBU (18.93 mL, 126.4 mmol) and 2-methyl-3-butyn-2-ol (12.37 mL, 126.6 mmol) were added at 0 °C. The ice bath was removed and the green reaction mixture was stirred at room temperature for 5 h. The residue was dissolved in a mixture of ethyl acetate (100 mL) and Saturated ammonium chloride solution (150 mL). The layers were separated, and the aqueous layer was extracted with ethyl acetate (2×100 mL). The combined organic layers were washed with brine (70 mL), dried over Na_2SO_4 and the solvent was removed under reduced pressure. The dark brown residue was subjected to column chromatography (30×4.0 cm; 70% ethyl acetate/hexanes) to afford diynediol **4.47** as a brown solid (9.55 g, 93%); R_f =0.5 (50% ethyl acetate/hexanes); m.p. 112.9–113.8 °C (ethyl acetate/hexane); ^1H NMR (300 MHz, CDCl_3) δ 7.61 (dd, J =7.4 Hz, 1H), 7.32 (d, J = 7.8 Hz, 2H), 2.76 (s, 2H), 1.62 (s, 12H); ^{13}C NMR (75 MHz, CDCl_3) δ 161.46, 137.35, 120.31, 70.17, 42.53, 32.91, 29.84; HRMS (APPI) calculated for $\text{C}_{15}\text{H}_{17}\text{NO}_2$ $[\text{M}+\text{H}]^+$ 244.1356, found 244.1342.

Diol 4.48



A mixture of diynediol **4.47** (5.01 g, 20.6 mmol), 20% wet palladium hydroxide on carbon (Pearlman's catalyst) (0.871 g, 6.17 mmol), and degassed ethyl acetate (200 mL) was stirred at room temperature under an atmosphere of hydrogen for 21 h. The reaction mixture was suction filtered through a pad of celite, and the filtrate was concentrated under reduced pressure to afford diol **4.48** as a brown oil (4.90 g, 95%); $R_f=0.5$ (50% ethylacetate/hexanes); ^1H NMR (300 MHz, CDCl_3) δ 7.50 (t, $J = 7.7$ Hz, 1H), 6.99 (d, $J = 7.7$ Hz, 2H), 3.86 (s, 2H), 2.92 (t, $J = 7.4$ Hz, 4H), 1.90 (t, $J = 7.4$ Hz, 4H), 1.28 (s, 12H); ^{13}C NMR (75 MHz, CDCl_3) δ 161.33, 137.23, 120.18, 70.04, 42.40, 32.78, 29.72; HRMS (APPI) calculated for $\text{C}_{15}\text{H}_{25}\text{NO}_2$ $[\text{M}+\text{H}]^+$ 252.1979, found 252.1974.

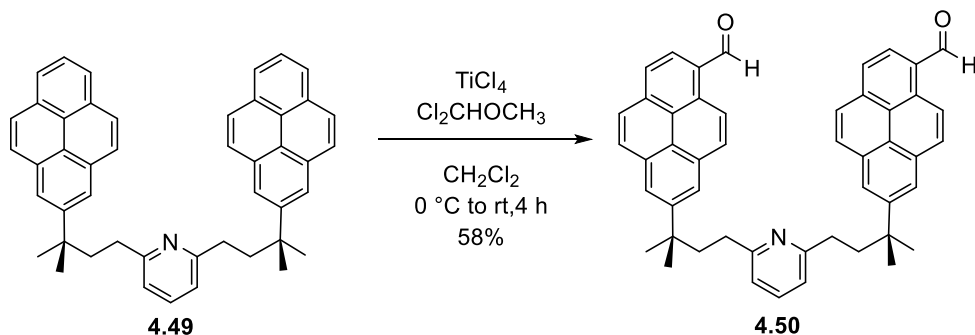
Dipyren-2-ylalkane 4.49



The crude diol **4.48** (3.10 g, 12.3 mmol) was dissolved in dichloromethane (350 mL) and HCl gas (generated by the dropwise addition of concentrated HCl into 98% sulfuric acid) was purged into the solution for a period of 4 h (complete conversion was

monitored by TLC analysis using a PMA stain). Nitrogen was purged into the reaction mixture for 30 min to remove the excess HCl. The solution was then cooled to 0 °C followed by the addition of pyrene (24.54 g, 121.3 mmol) and aluminium chloride (5.17 g, 38.8 mmol). The ice bath was removed, and the resulting dark brown mixture was stirred at room temperature for 5 h. The reaction mixture was poured into ice-cold water (200 mL) and extracted with dichloromethane (2×100 mL). The combined organic layers were washed with brine solution (1×100 mL), dried over sodium sulfate and solvents were removed under reduced pressure. The solid brownish orange residue was subjected to column chromatography (22×12 cm; 4% ethyl acetate/hexanes) to afford **4.49** as a dark orange solid (2.85 g, 38%): R_f =0.25 (10% ethyl acetate/hexanes); m.p. 180.9–181.5 °C; ^1H NMR (300 MHz, CDCl_3) δ 8.23 (s, 4H), 8.15 (d, J =7.9 Hz, 4H), 8.05 (s, 6H), 8.01–7.94 (m, 4H), 7.27 (t, J =7.7 Hz, 1H), 6.71 (d, J =7.6 Hz, 2H), 2.62–2.56 (m, 4H), 2.33–2.27 (m, 4H), 1.67 (s, 12H); ^{13}C NMR (75 MHz, CDCl_3) δ 161.94, 147.18, 136.36, 131.15, 131.12, 127.76, 127.37, 125.67, 124.88, 124.71, 123.11, 123.01, 119.41, 44.94, 38.58, 34.21, 29.66; HRMS (APPI) calculated for $\text{C}_{47}\text{H}_{41}\text{N}$ $[\text{M}+\text{H}]^+$ 620.3454, found 620.3440.

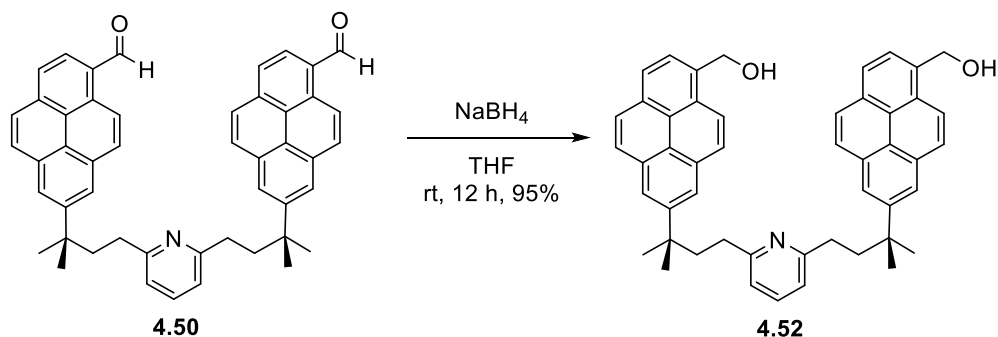
Dialdehyde **4.50**



Dipyrren-2-ylalkane **4.49** (0.151 g, 0.242 mmol) was dissolved in dry dichloromethane (10 mL) and dichloromethylmethyl ether (0.167 g, 1.45 mmol), titanium(IV) chloride (0.271 g, 1.45 mmol) was added at $0\text{ }^\circ\text{C}$. The ice bath was removed, and the deep purple reaction mixture was stirred at room temperature for 4 h. The reaction mixture was slowly poured (exothermic) into ice-cold water (20 mL). The layers were separated, and the aqueous layer was extracted with dichloromethane ($2\times 10\text{ mL}$). The combined organic layers were washed with brine (20 mL), dried over Na_2SO_4 and the solvent was removed under reduced pressure. The light brown residue was subjected to column chromatography (14 \times 4.0 cm; 15% ethyl acetate/hexane) to afford **4.50** as a bright yellow solid (0.0948 g, 58%): $R_f=0.16$ (30% ethyl acetate/hexane); m.p. 109–111 $^\circ\text{C}$ (ethyl acetate/hexane); ^1H NMR (300 MHz, CDCl_3) δ 10.71 (s, 2H), 9.30 (d, $J=9.3\text{ Hz}$, 2H), 8.34–8.30 (m, 6H), 8.20 (d, $J=9.3\text{ Hz}$, 2H), 8.14–8.10 (m, 4H), 8.01–7.94 (m, 2H), 7.29 (t, $J=7.7\text{ Hz}$, 1H), 6.73 (d, $J=7.7\text{ Hz}$, 2H), 2.63–2.45 (m, 4H), 2.34–2.20 (m, 4H), 1.65 (s, 12H); ^{13}C NMR (75 MHz, CDCl_3) δ 193.20, 147.93, 135.43, 131.19, 131.12, 131.01, 130.95, 130.42, 127.34, 127.09, 125.17, 124.85, 124.56, 124.40, 122.95, 122.45, 119.59, 44.82, 38.64, 34.06, 29.62 (a fewer-than-expected number of aromatic signals was

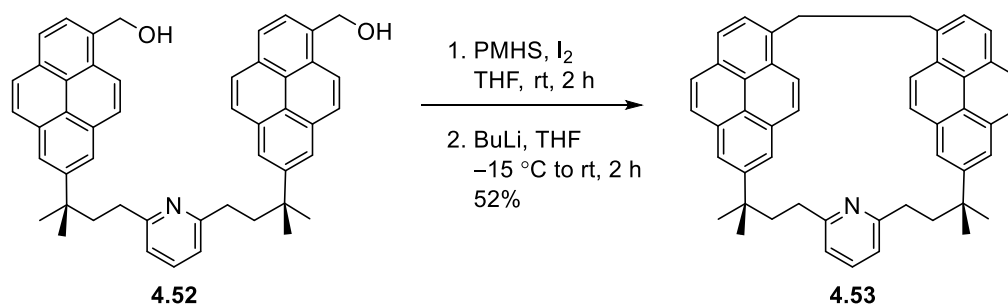
observed, presumably due to overlap); HRMS (APPI) calculated for $C_{49}H_{41}NO_2$ $[M+H]^+$ 676.3325, found 676.3345.

Diol **4.52**



Sodium borohydride (0.0201 g, 0.533 mmol) was added to a stirred solution of diol **4.50** (0.0601 g, 0.0891 mmol) in THF (10 mL). The reaction mixture was stirred at room temperature for 12 h and then cooled to 0 °C. The reaction mixture was neutralized using a 5.0 M aqueous HCl solution. Most of the THF was removed under reduced pressure. Dichloromethane (20 mL) and water (20 mL) were added to the resulting mixture. The layers were separated, and the aqueous layer was extracted with dichloromethane (2×20 mL). The combined organic layers were washed with brine (20 mL), dried over Na_2SO_4 , gravity filtered and concentrated under reduced pressure to afford diol **4.52** as a white solid (0.0574 g, 95%): R_f = 0.13 (50% ethyl acetate/hexanes); m.p. 100.6-101.9 °C (dichloromethane). HRMS, 1H and ^{13}C NMR analysis were not possible due to the very low solubility of diol **4.52** in most organic solvents. The compound was partially dissolved in $DMSO-d_6$ by heating, but a precipitate formed during the process of acquisition. Therefore, **4.52** was taken to the next step without purification.

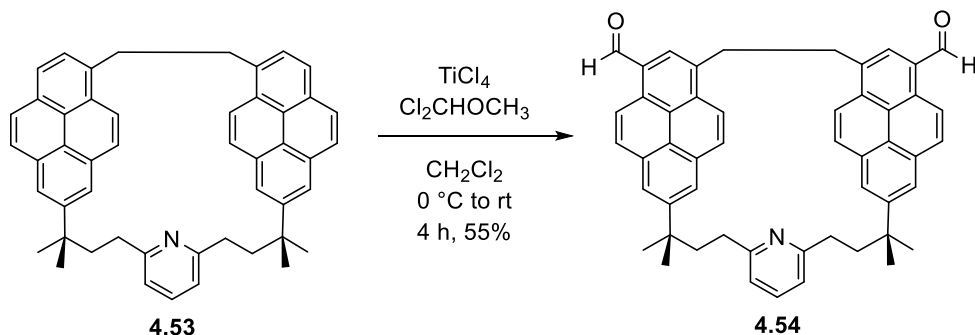
Pyrenophane **4.53**



Diol **4.52** (0.145 g, 0.213 mmol) was dissolved in THF (10 mL) and PMHS (0.819 g, 1.28 mmol) and then iodine (0.167 g, 0.660 mmol) were added under a nitrogen atmosphere. The reaction mixture was stirred at room temperature until the starting material was completely consumed (*ca.* 2 h, TLC analysis). The reaction mixture was diluted with THF (10 mL) and cooled to $-15\text{ }^{\circ}\text{C}$. BuLi (2.3 M, 0.6 mL, 1.4 mmol) was added gradually over a period of 5 min and left to stir for 2 h during which the brown solution turned to pale yellow. The solution was cooled to $0\text{ }^{\circ}\text{C}$ (ice bath) and quenched with ice-cold water, the reaction mixture was neutralized using 5.0 M aqueous HCl. Most of the THF was removed under reduced pressure and dichloromethane (20 mL) was added to the resulting mixture. The layers were separated, and the aqueous layer was extracted with dichloromethane (2 \times 20 mL). The combined organic layers were washed with brine (30 mL), dried over Na₂SO₄, gravity filtered and concentrated under reduced pressure. The yellow residue was subjected to column chromatography (25 \times 3.0 cm; 10% ethyl acetate/hexane) to afford compound **4.53** (0.071 g, 52%) as a fluffy white solid: R_f =0.38 (20% ethyl acetate/hexane); m.p. 199.1–201.6 $^{\circ}\text{C}$ (dichloromethane); ^1H NMR (300 MHz, CDCl₃) δ 8.13–7.97 (m, 4H), 7.89 (s, 6H), 7.83 (d, J =1.8 Hz, 2H), 7.43 (t, J =7.7 Hz, 1H), 7.18 (d, J =9.3 Hz, 2H), 7.03 (d, J =9.3 Hz, 2H), 6.89 (d, J =7.7 Hz, 2H), 3.95 (s, 4H),

2.42–2.36 (m, 4H), 2.01–1.95 (m, 4H), 1.55 (s, 12H); ^{13}C NMR (75 MHz, CDCl_3) δ 161.95, 146.03, 136.30, 131.12, 130.52, 129.62, 129.56, 127.63, 127.16, 126.95, 126.53, 124.72, 124.68, 123.22, 123.09, 122.67, 122.54, 119.08, 45.52, 38.41, 35.72, 34.19, 29.32 (a fewer-than-expected number of aromatic signals was observed, presumably due to overlap); HRMS (APPI) calculated for $\text{C}_{49}\text{H}_{43}\text{N}$ $[\text{M}+\text{H}]^+$ 646.3505, found 646.3499.

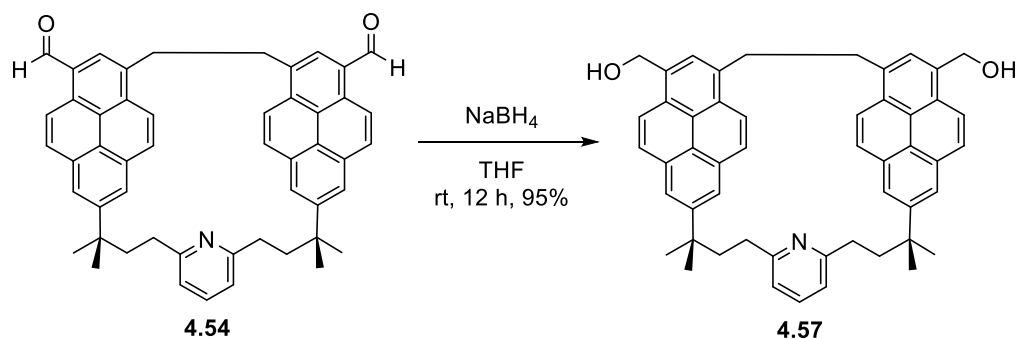
Dialdehyde **4.54**



Pyrenophane **4.53** (0.160 g, 0.247 mmol) was dissolved in dry dichloromethane (20 mL) and the solution was cooled to 0 °C under a nitrogen atmosphere. Titanium(IV) chloride (0.752 g, 3.96 mmol) and dichloromethyl methyl ether (0.455 g, 3.96 mmol) were added and the resulting deep purple solution was stirred at room temperature for 4 h. The reaction mixture was slowly poured (exothermic) into ice-cold water (20 mL). The layers were separated, and the aqueous layer was extracted with dichloromethane (2×10 mL). The combined organic layers were washed with brine (20 mL), dried over Na_2SO_4 and the solvent was removed under reduced pressure. The yellow residue was subjected to column chromatography (16×4.0 cm; 14% ethyl acetate/hexane) to afford pyrenophane dialdehyde **4.54** (0.095 g, 55%) as a yellow solid: R_f =0.18 (10% ethyl acetate/hexanes); m.p. >300 °C

(ethyl acetate/hexanes); ^1H NMR (300 MHz, CDCl_3) δ 10.71 (s, 2H), 9.16 (d, $J=9.2$ Hz, 2H), 8.28 (s, 2H), 8.15–8.10 (m, 6H), 7.95 (s, 2H), 7.44 (t, $J=7.6$ Hz, 1H), 7.17 (d, $J=9.1$ Hz, 2H), 6.90 (d, $J=7.6$ Hz, 2H), 4.01 (s, 4H), 2.42–2.33 (m, 4H), 2.08–1.95 (m, 4H), 1.56 (s, 12H); ^{13}C NMR (75 MHz, CDCl_3) δ 193.00, 178.67, 161.78, 147.17, 134.14, 132.55, 130.48, 130.18, 130.05, 129.73, 126.99, 124.93, 124.87, 124.76, 122.71, 122.47, 122.33, 119.30, 51.73, 45.34, 38.53, 34.17, 29.85 (a fewer-than-expected number of aromatic signals was observed, presumably due to overlap); HRMS (APPI) calculated for $\text{C}_{51}\text{H}_{43}\text{NO}_2$ $[\text{M}+\text{H}]^+$ 702.3429, found 702.3411.

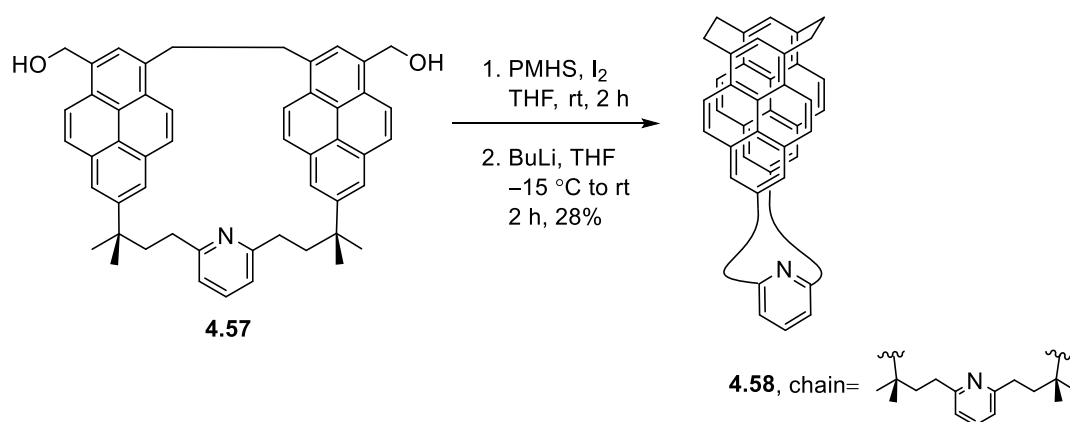
Diol 4.57



Sodium borohydride (0.029 g, 0.783 mmol) was added to a stirred solution of diol **4.50** (0.055 mg, 0.078 mmol) in THF (5 mL). The reaction mixture was stirred at room temperature for 12 h and then cooled to 0 °C. The reaction mixture was neutralized using a 5.0 M aqueous HCl solution. Most of the THF was removed under reduced pressure. Dichloromethane (20 mL) was added to the resulting mixture. The layers were separated, and the aqueous layer was extracted with dichloromethane (2×10 mL). The combined organic layers were washed with brine (10 mL), dried over Na_2SO_4 , gravity filtered and

concentrated under reduced pressure to afford diol **4.57** as a white solid (0.052 mg, 95%): R_f =0.23 (60% ethyl acetate/hexanes); m.p. >300 °C (dichloromethane). LCMS, ^1H and ^{13}C NMR analysis were not possible due to the poor solubility of diol **4.57** in most organic solvents. Hence, compound **4.57** was taken to the next step without further purification.

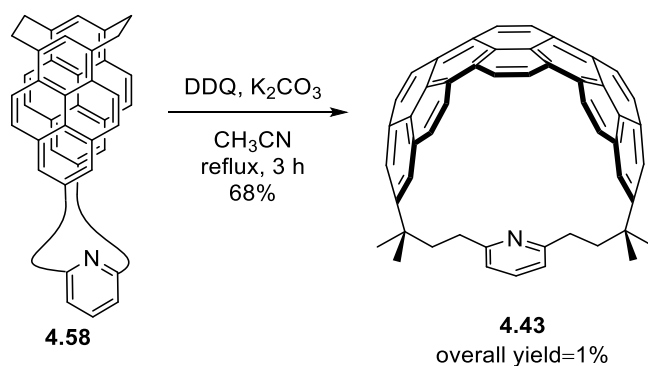
Pyrenophane **4.58**



Diol **4.57** (0.035 g, 0.049 mmol) was dissolved in THF (5 mL) and PMHS (0.013 g, 0.20 mmol) and then iodine (0.039 g, 0.15 mmol) were added under a nitrogen atmosphere. The reaction mixture was stirred at room temperature until the starting material was completely consumed (*ca.* 2 h, TLC analysis). The reaction mixture was diluted with THF (5 mL) and cooled to -15 °C. BuLi (2.3 M, 0.17 mL, 0.39 mmol) was added gradually over a period of 5 min and left to stir for 2 h during which the brown solution turned to pale yellow. The solution was cooled to 0 °C (ice bath) and quenched with ice-cold water, the reaction mixture was neutralized using 5.0 M aqueous HCl. Most of the THF was removed under reduced pressure and dichloromethane (10 mL) was added to the resulting mixture. The layers were separated, and the aqueous layer was extracted

with dichloromethane (2×10 mL). The combined organic layers were washed with brine (10 mL), dried over Na₂SO₄, gravity filtered and concentrated under reduced pressure. The yellow residue was subjected to column chromatography (25×3.0 cm; 5% ethyl acetate/hexanes) to afford compound **4.58** (0.0093 g, 52%) as a white solid: *R*_f = 0.45 (20% ethyl acetate/hexanes); m.p. >300 °C (ethyl acetate); ¹H NMR (300 MHz, CDCl₃) δ 7.81 (d, *J*=9.2 Hz, 4H), 7.66 (s, 4H), 7.50 (d, *J*=9.2 Hz, 4H), 7.45 (t, *J*=7.7 Hz, 1H), 6.89 (d, *J*=7.7 Hz, 2H), 4.30–4.24 (m, 4H), 3.78–3.71 (m, 4H), 2.53–2.47 (m, 4H), 1.87–1.81 (m, 4H), 1.46 (s, 12H); ¹³C NMR (75 MHz, CDCl₃) δ 161.72, 146.35, 136.46, 135.86, 131.15, 130.28, 127.55, 126.07, 124.47, 122.86, 122.21, 121.70, 119.08, 45.56, 37.99, 33.67, 32.05, 29.86, 27.85 (a fewer-than-expected number of aromatic signals was observed, presumably due to overlap); HRMS (APPI) calculated for C₅₁H₄₅N [M+H]⁺ 672.1816, found 672.1820.

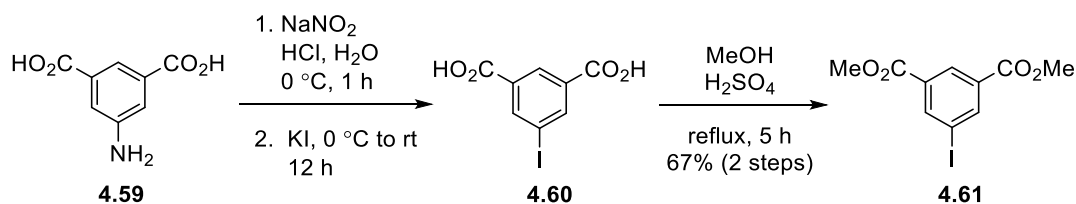
Pyridinophane **4.43**



Cyclophane **4.58** (0.0056 g, 0.0083 mmol) was dissolved in dry acetonitrile (2 mL) and K₂CO₃ (0.0056 g, 0.041 mmol) and DDQ (0.0095 g, 0.041 mmol) were added. The reaction mixture was stirred at reflux for 3 h. Solvent was then removed and the resulting solid residue was subjected to column chromatography (10×4.0 cm; 4% ethyl

acetate/hexanes) to afford pyridinophane **4.43** (0.0037 g, 68%) as a reddish brown solid: R_f = 0.42 (20% ethyl acetate/hexanes); m.p. >300 °C (ethyl acetate/hexanes); ^1H NMR (500 MHz, CDCl_3) δ 8.73 (s, 4H), 8.49 (d, J =9.5 Hz, 4H), 7.73 (d, J =9.5 Hz, 4H), 7.50 (s, 4H), 7.13 (t, J =7.7 Hz, 1H), 6.42 (d, J =7.8 Hz, 2H), 2.03–2.00 (m, 4H), 1.87–1.85 (m, 4H), 1.26 (s, 12H); ^{13}C NMR (75 MHz, CDCl_3) δ 164.72, 146.25, 129.99, 127.78, 125.47, 124.37, 122.91, 121.08, 119.85, 119.05, 117.19, 46.56, 40.89, 33.56, 29.99, 23.98 (a fewer-than-expected number of aromatic signals was observed, presumably due to overlap); HRMS (APPI) calculated for $\text{C}_{51}\text{H}_{39}\text{N}$ $[\text{M}+\text{H}]^+$ 666.2761, found 666.2729.

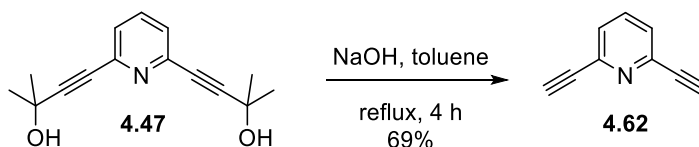
Dimethyl 5-iodoisophthalate (**4.61**)



To a 0 °C suspension of 5-aminoisophthalic acid (5.01 g, 27.4 mmol) in water (15 mL) and a 10% aqueous solution of HCl (100 mL) was added NaNO_2 (2.01 g, 28.7 mmol). The suspension was stirred at 0 °C for 1 h. KI (18.21 g, 109.6 mmol) was added portionwise over 15 minutes. The reaction mixture was warmed to room temperature and stirred for 12 h. The suspension was collected by suction filtration and washed with cold water (150 mL) to afford crude 5-iodoisophthalic acid (**4.60**). The collected solid was dissolved in MeOH (250 mL) and H_2SO_4 (100 mL) and heated at reflux for 5 h. The solvent was removed under reduced pressure and the resulting mixture was redissolved in ethyl acetate (150 mL) and poured in water (100 mL). The layers were separated, and the aqueous

layer was extracted with ethyl acetate (2×100 mL). The combined organic layers were washed with saturated aqueous NaHCO₃ solution (50 mL), washed with brine (100 mL), dried over Na₂SO₄, gravity filtered and concentrated under reduced pressure to afford dimethyl 5-iodoisophthalate (**4.61**) (3.38 g, 67%) as a pale yellow solid: *R*_f=0.41 (10% ethyl acetate/hexanes); m.p. 98.4–99.6 °C (ethyl acetate); ¹H NMR (300 MHz, CDCl₃) δ 8.62 (t, *J*=1.5 Hz, 1H), 8.53 (d, *J*=1.6 Hz, 2H), 3.94 (s, 6H); ¹³C NMR (75 MHz, CDCl₃) δ 164.93, 142.60, 132.32, 130.00, 93.56, 52.78; HRMS (APPI) calculated for C₁₀H₉IO₄ [M+H]⁺ 321.2721, found 321.2729.

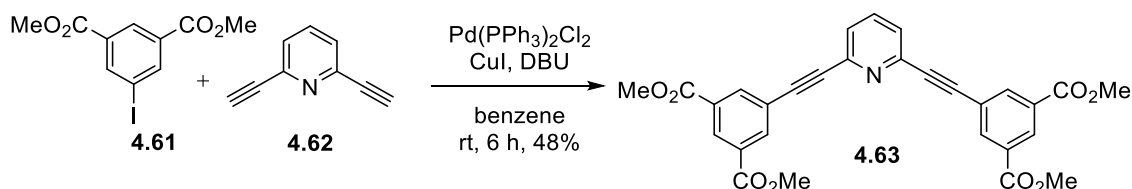
Dialkyne **4.62**



To a solution of diynediol **4.47** (5.02 g, 0.021 mmol) in toluene (210 mL) preheated to 80 °C, powdered NaOH (4.21 g, 0.123 mmol) was added. The reaction mixture was heated at reflux for 4 h then cooled to room temperature. The reaction mixture was poured into water (200 mL). The layers were separated, and the aqueous layer was extracted with diethyl ether (3×100 mL). The combined organic layers were washed with brine (100 mL), dried over Na₂SO₄, gravity filtered and concentrated under reduced pressure. The brown residue was subjected to column chromatography (20×5.0 cm; 20% ethyl acetate/hexanes) to afford compound **4.62** (1.79 g, 69%) as a brown solid: *R*_f=0.31 (20% ethyl acetate/hexanes); m.p. 85.4–87.1 °C (diethyl ether); ¹H NMR (300 MHz, CDCl₃) δ 7.64 (t, *J*=7.5 Hz, 1H), 7.43 (d, *J*=7.7 Hz, 2H), 3.15 (s, 2H); ¹³C NMR (75 MHz, CDCl₃) δ 142.86,

136.66, 127.22, 82.21, 77.87; HRMS (APPI) calculated for C_9H_5N $[M+H]^+$ 128.0921, found 128.0975.

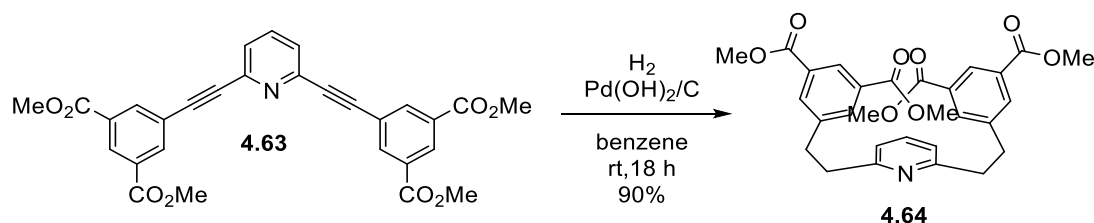
Tetraester **4.63**



Dimethyl 5-iodoisophthalate (**4.61**) (4.44 g, 13.8 mmol) was added to a solution of $Pd(PPh_3)_2Cl_2$ (0.156 g, 0.222 mmol) and CuI (0.169 g, 0.888 mmol) in degassed benzene (150 mL). The reaction mixture was stirred for 5 min and then DBU (2.48 mL, 16.6 mmol) and diyne **4.62** (0.706 g, 5.55 mmol) were added at 0 °C. The ice bath was removed and the green reaction mixture was stirred at room temperature for 6 h. The residue was dissolved in a mixture of ethyl acetate (100 mL) and Saturated ammonium chloride solution (150 mL). The layers were separated, and the aqueous layer was extracted with ethyl acetate (2×100 mL). The combined organic layers were washed with brine (70 mL), dried over Na_2SO_4 and the solvent was removed under reduced pressure. The dark brown residue was subjected to column chromatography (30×5.0 cm; 20% ethyl acetate/hexane to pure ethyl acetate) to afford tetraester **4.63** as a brown solid (1.38 g, 48%); R_f = 0.19 (20% ethyl acetate/hexanes); m.p. 164.9–166.4 °C (ethyl acetate); 1H NMR (300 MHz, $CDCl_3$) δ 8.68 (t, J =1.6 Hz, 2H), 8.45 (d, J =1.6 Hz, 4H), 7.75 (dd, J =8.3 Hz, 1H), 7.54 (d, J =8.1 Hz, 2H), 3.97 (s, 12H); ^{13}C NMR (75 MHz, $CDCl_3$) δ 165.56, 143.47, 137.12, 136.87, 131.27,

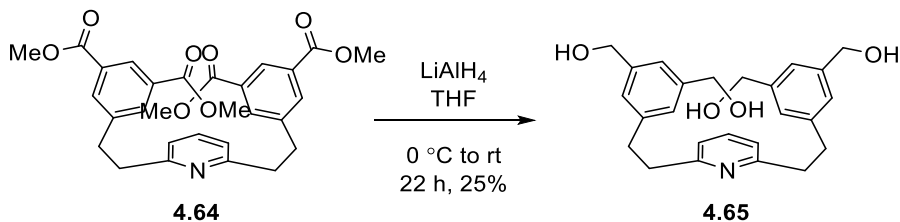
131.08, 126.97, 123.27, 89.77, 87.60, 52.75; HRMS (APPI) calculated for $C_{29}H_{21}NO_8$ $[M+H]^+$ 512.1366, found 512.1362.

Tetraester **4.64**



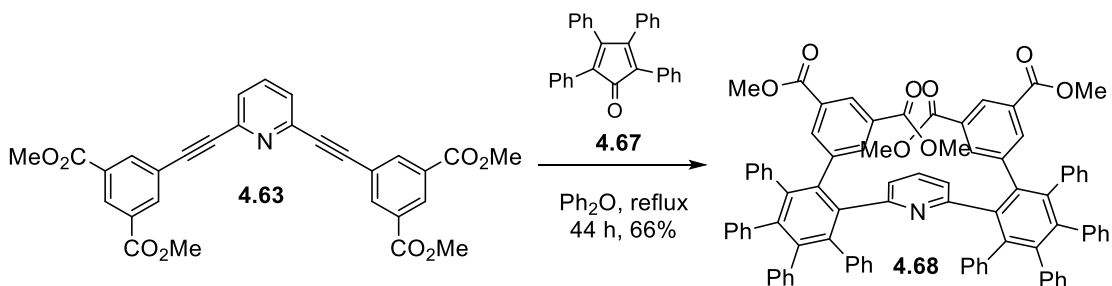
A mixture of tetraester **4.63** (0.503 g, 0.963 mmol), 20% wet palladium hydroxide on carbon (Pearlman's catalyst) (0.577 g, 0.0613 mmol), and degassed benzene (100 mL) was stirred at room temperature under an atmosphere of hydrogen for 18 h. The reaction mixture was degassed by bubbling nitrogen through the mixture for 20 min, suction filtered through a pad of celite, and concentrated under reduced pressure to afford tetraester **4.48** as a brown solid (0.452 g, 90%); $R_f=0.2$ (20% ethyl acetate/hexanes); m.p. 143.7–145.0 °C (benzene); ^1H NMR (300 MHz, CDCl_3) δ 8.49 (t, $J=1.6$ Hz, 2H), 8.07 (d, $J=1.6$ Hz, 4H), 7.44 (t, $J=7.6$ Hz, 1H), 6.89 (d, $J=8.2$ Hz, 2H), 3.91 (s, 12H), 3.21–3.07 (m, 8H); ^{13}C NMR (75 MHz, CDCl_3) δ 166.48, 160.10, 142.75, 134.12, 130.70, 128.58, 120.67, 52.40, 39.65, 35.48, 29.80; HRMS (APPI) calculated for $C_{29}H_{29}NO_8$ $[M+H]^+$ 520.1516, found 520.1502.

Tetraol **4.65**



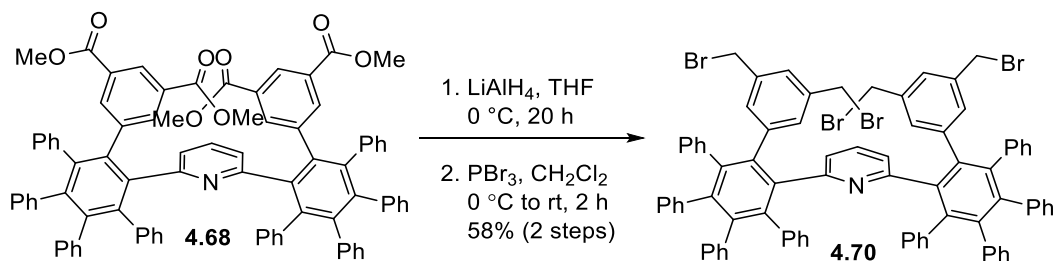
To well-stirred 0 °C solution of **4.64** (0.270 g, 0.512mmol) in dry THF (70 mL) was added LiAlH_4 (0.233 g, 6.14 mmol) under a nitrogen atmosphere. The mixture was stirred at room temperature for 22 h, cooled in an ice-bath, quenched with ethyl acetate (50 mL) and water (30 mL). The layers were separated, and the aqueous layer was extracted with ethyl acetate (2×30 mL). The combined organic layers were washed with brine (30 mL), dried over Na_2SO_4 and the solvent was removed under reduced pressure to afford tetraol **4.65** as a white solid (0.053 g, 25%); R_f =0.18 (20% ethylacetate/hexane); m.p. 130.7–132.0 °C (ethyl acetate); LCMS, ^1H and ^{13}C NMR analysis were not possible due to the poor solubility of diol **4.64** in most organic solvents. Hence, it was used without further purification.

Tetraester **4.68**



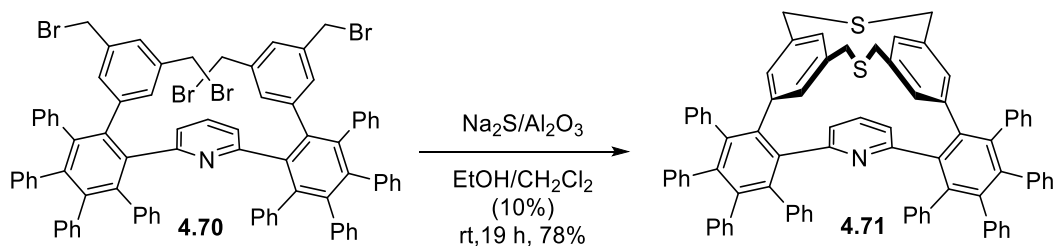
A solution of tetraester **4.63** (0.250 g, 0.489 mmol) and tetraphenylcyclopentadienone (**4.67**) (0.405 g, 1.07 mmol) in degassed diphenyl ether (10 mL) was heated at reflux (260 °C) for 44 h. The mixture was cooled to room temperature and (without removal of the solvent) purified by column chromatography (30×4.0 cm, 10% ethyl acetate/hexane) to give tetraester **4.68** as a yellow solid (0.394 g, 66%); $R_f=0.25$ (15% ethyl acetate/hexanes); m.p. >300 °C (ethyl acetate); ^1H NMR (300 MHz, CDCl_3) δ 8.37 (t, $J=1.6$ Hz, 2H), 6.92–5.70 (m, 44H), 6.36 (dd, $J=7.4$ Hz, 1H), 6.12 (d, $J=7.8$ Hz, 2H), 3.89 (s, 12H); ^{13}C NMR (75 MHz, CDCl_3) δ 166.41, 155.80, 142.62, 141.47, 141.01, 140.82, 140.44, 140.28, 139.96, 139.89, 139.83, 139.09, 137.86, 131.49, 131.26, 128.54, 128.10, 126.68, 125.67, 125.49, 125.40, 123.93, 52.34, 29.85; HRMS (APPI) calculated for $\text{C}_{85}\text{H}_{61}\text{NO}_8$ $[\text{M}+\text{H}]^+$ 1224.4495, found 1224.4504.

Tetrabromide **4.70**



To well-stirred 0 °C solution of **4.68** (0.181 g, 0.147 mmol) in dry THF (15 mL, 50 mL 3-neck RBF) was added LiAlH_4 (0.067 g, 0.0017 mmol) under a nitrogen atmosphere. The mixture was stirred at room temperature for 20 h, cooled in an ice-bath, quenched with ethyl acetate (20 mL) and water (10 mL). The layers were separated, and the aqueous layer was extracted with ethyl acetate (2×10 mL). The combined organic layers were washed with brine (15 mL), dried over Na_2SO_4 and the solvent was removed under reduced pressure to afford tetraol **4.69** as a white solid (0.129 g). Crude tetraol **4.69** was used without further purification. Crude **4.69** (0.129 g, 0.116 mmol) was dissolved in dry dichloromethane (10 mL), to which PBr_3 (0.046 mL, 0.174 mmol) was added dropwise. The reaction mixture was stirred at room temperature for 2 h. The reaction mixture was poured into water (10 mL). The layers were separated, and the aqueous layer was extracted with dichloromethane (2×10 mL). The combined organic layers were washed with brine (15 mL), dried over Na_2SO_4 and the solvent was removed under reduced pressure to afford **4.70** as an inseparable mixture of products (0.120, 58% over 2 steps). Since the isolation of dibromide **4.70** in pure form was problematic it was taken to the next step without further purification.

Dithiacyclophane **4.71**



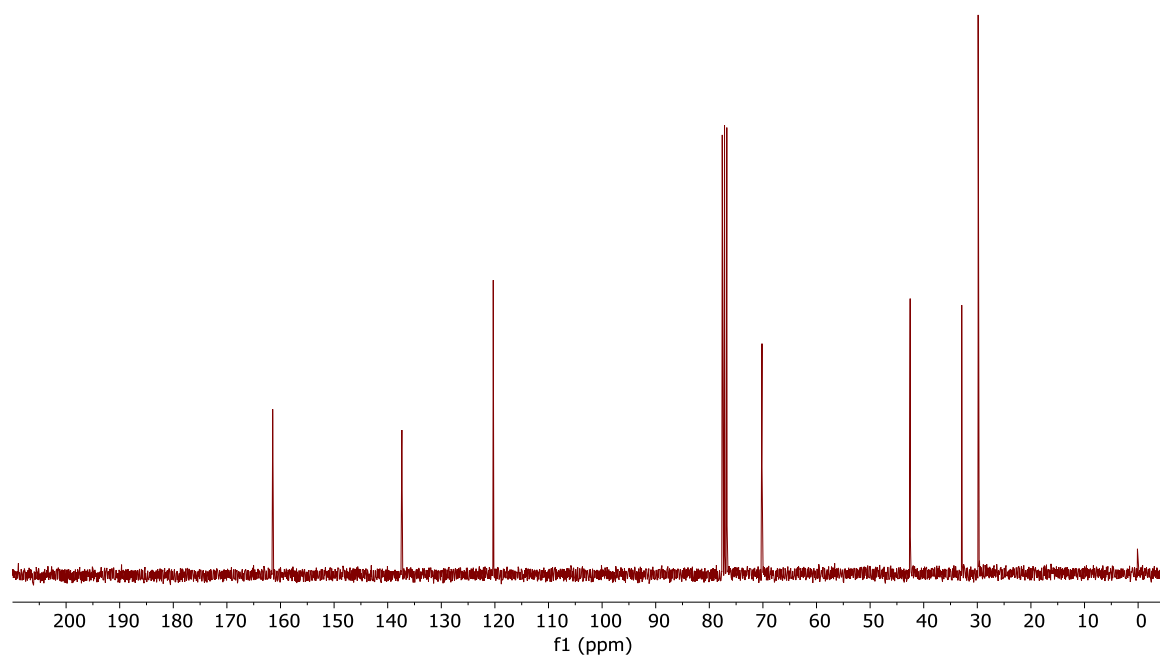
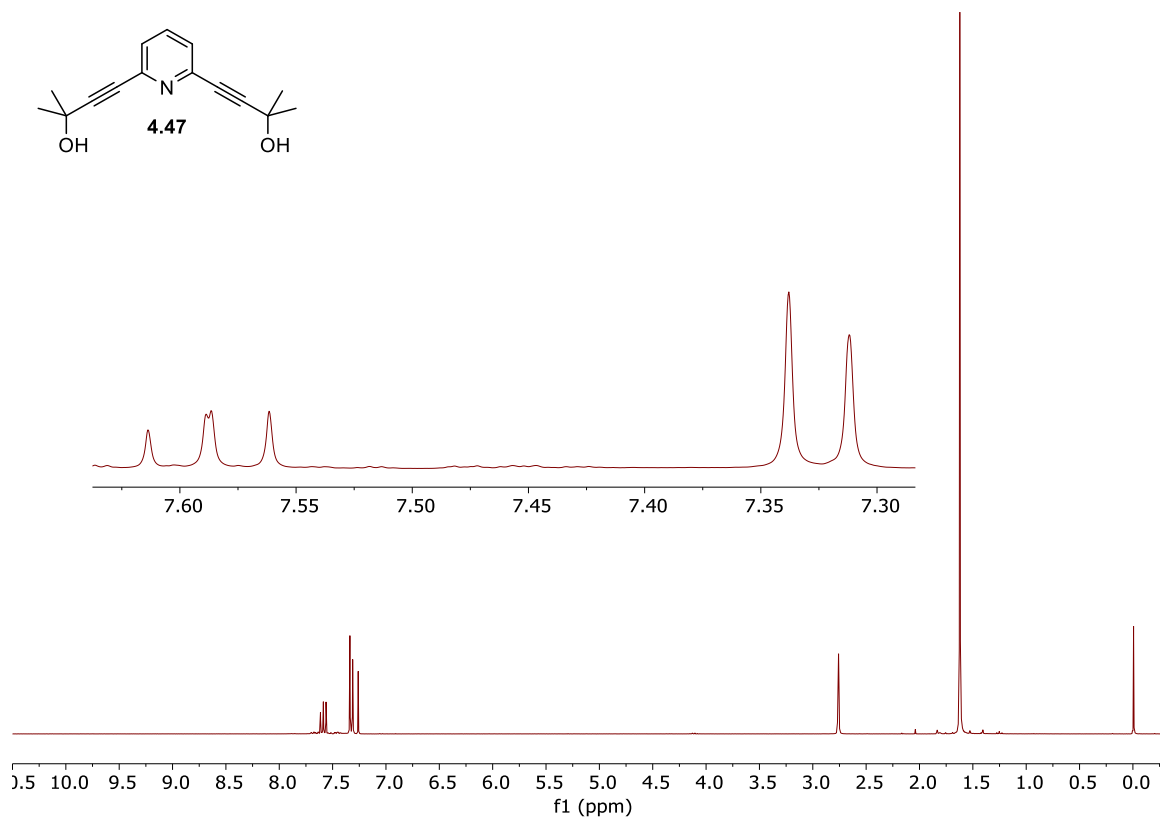
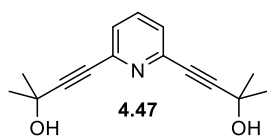
$\text{Na}_2\text{S}/\text{Al}_2\text{O}_3$ (0.098 g, 0.733 mmol) was added in four equal portions to a stirred room temperature solution of **4.70** (0.100 g, 0.073 mmol) in 1:9 (v/v) EtOH/dichloromethane (10 mL) over a 15 min period. The resulting slurry was stirred vigorously for 19 h and the reaction mixture was suction filtered through a plug of celite. The filtrate was concentrated under reduced pressure and the residue was subjected to column chromatography (20×2.5 cm; 50% dichloromethane/hexanes) to afford dithiacyclophane **4.71** (0.063 g, 78%) as an off-white solid: $R_f=0.40$ (40 % dichloromethane/hexanes); m.p. >300 °C (dichloromethane); ^1H NMR (300 MHz, CDCl_3) δ 7.14 (t, $J=7.7$ Hz, 1H), 6.97 (d, $J=7.7$ Hz, 2H), 6.55–6.78 (m, 40H), 6.52 (s, 2H), 6.29 (s, 2H), 6.20 (d, $J=7.6$ Hz, 2H), 3.58 (s, 4H), 3.13 (d, $J=15.0$ Hz, 2H), 2.89 (d, $J=15.0$ Hz, 2H); ^{13}C NMR (75 MHz, CDCl_3) δ 166.37, 155.77, 142.59, 141.44, 140.98, 140.79, 140.41, 140.25, 139.93, 139.86, 139.80, 139.06, 137.82, 132.57, 131.45, 131.23, 128.50, 128.08, 126.76, 126.65, 126.54, 125.64, 125.47, 125.38, 123.90, 28.15; HRMS (APPI) calculated for $\text{C}_{81}\text{H}_{57}\text{NS}_2$ $[\text{M}+\text{H}]^+$ 1108.4026, found 1108.4009.

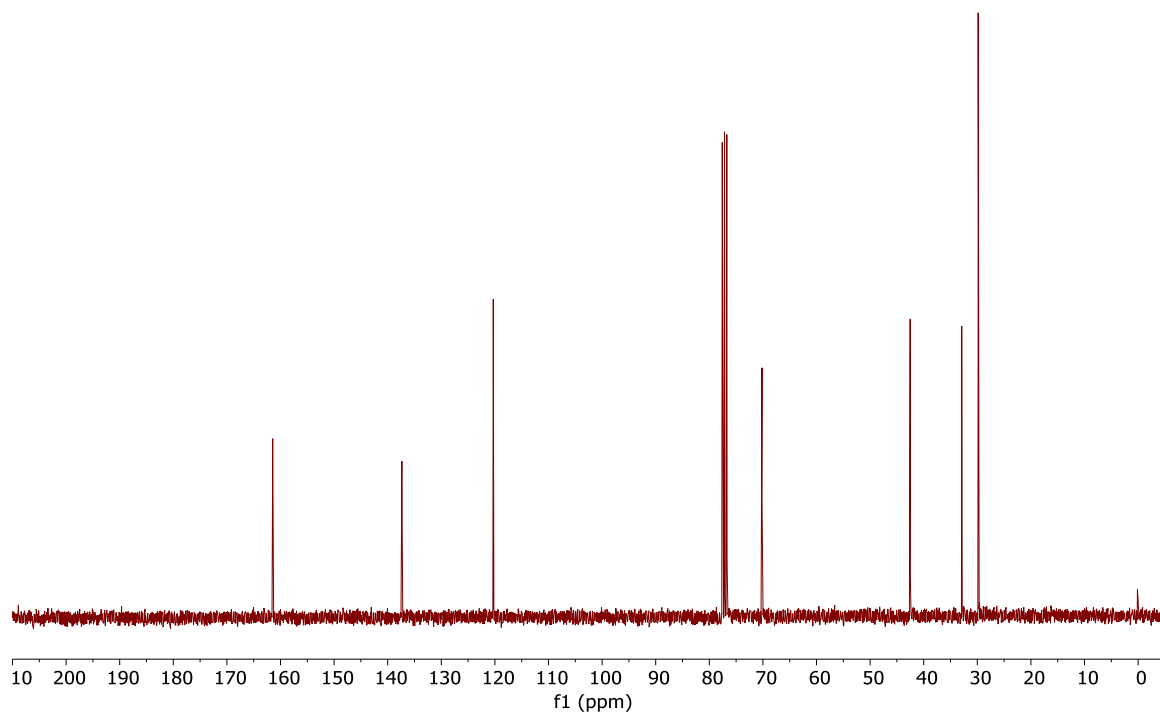
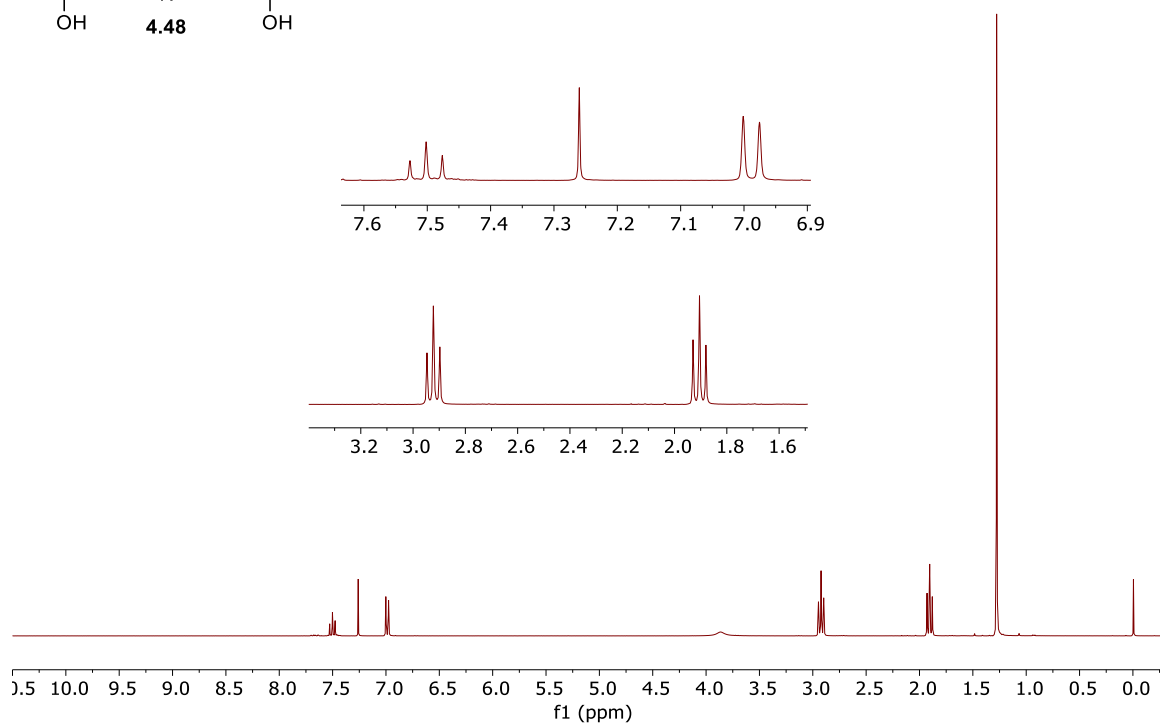
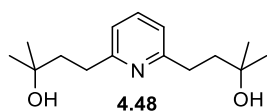
4.6 References and Notes

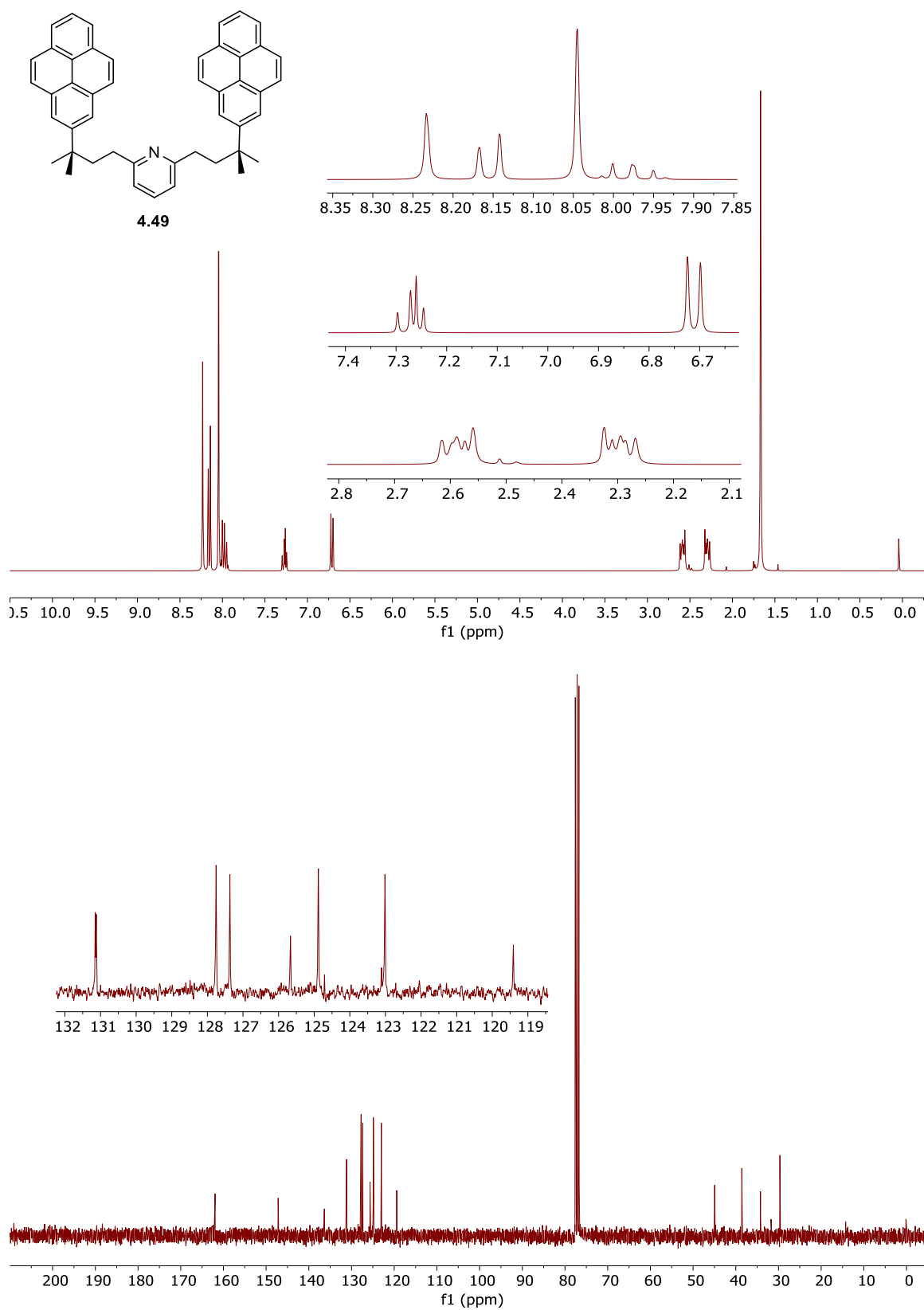
1. a) Gleiter, R.; Eckert-Mekic, M.; Schafer, W.; Trusedale, E. A. *Chem. Ber.* **1982**, *115*, 2009–2011. b) Haenel, M. W. *Chem Ber.* **1982**, *115*, 1425–1436. c) Kang, H. C.; Boekelheide, V. *J. Am. Chem. Soc.* **1984**, *106*, 2672–2680.
2. a) Pellegrin, M. M. *Rec. Trav. Chim. Pays-Bas.* **1899**, *18*, 457–465. b) Brown, C. J.; Farthing, A. C. *Nature* **1949**, *164*, 915–916. c) Cram, D. J.; Steinberg, H. *J. Am. Chem. Soc.* **1951**, *73*, 5691–5704.
3. a) Wang, H.; Predeus, A. V.; Wulff, W. D. *Chem. Eur. J.* **2013**, *19*, 8261–8267. b) Malcolm Sainsbury (Editor), *Aromatic Compounds: Polybenzenoid Hydrocarbons and Their Derivatives: Hydrocarbon Ring Assemblies, Polyphenyl-Substituted Aliphatic Hydrocarbons and Their Derivatives*, 1995.
4. a) Grave, C.; Schlüter, A. D. *Eur. J. Org. Chem.* **2002**, 3075–3098. b) Williams, R. V.; Edwards, W. D.; Mitchell, R. H.; Robinson, S. G. *J. Am. Chem. Soc.* **2005**, *127*, 16207–16214. c) Mitchell, R. H.; Iyer, V. S.; Mahadevan, R.; Venugopalan, S.; Zhou, P. *J. Org. Chem.* **1996**, *61*, 5116–5120.
5. Staab, H. A.; Binnig, F. *Tetrahedron Lett.* **1964**, *5*, 319–321.
6. Bodwell, G. J.; Bridson, J. N.; Houghton, T. J.; Kennedy, J. W. J.; Mannion, M. R. *Angew. Chem. Int. Ed.* **1996**, *35*, 1320–1321.
7. Bodwell, G. J.; Bridson, J. N.; Houghton, T. J.; Kennedy, J. W. J.; Mannion, M. R. *Chem. Eur. J.* **1999**, *5*, 1823–1827.
8. Bodwell, G. J.; Fleming, J. J.; Miller, D. O. *Tetrahedron* **2001**, *57*, 3577–3585.
9. Bodwell, G. J.; Miller, D. O.; Vermeij, R. J. *Org. Lett.* **2001**, *3*, 2093–2096.

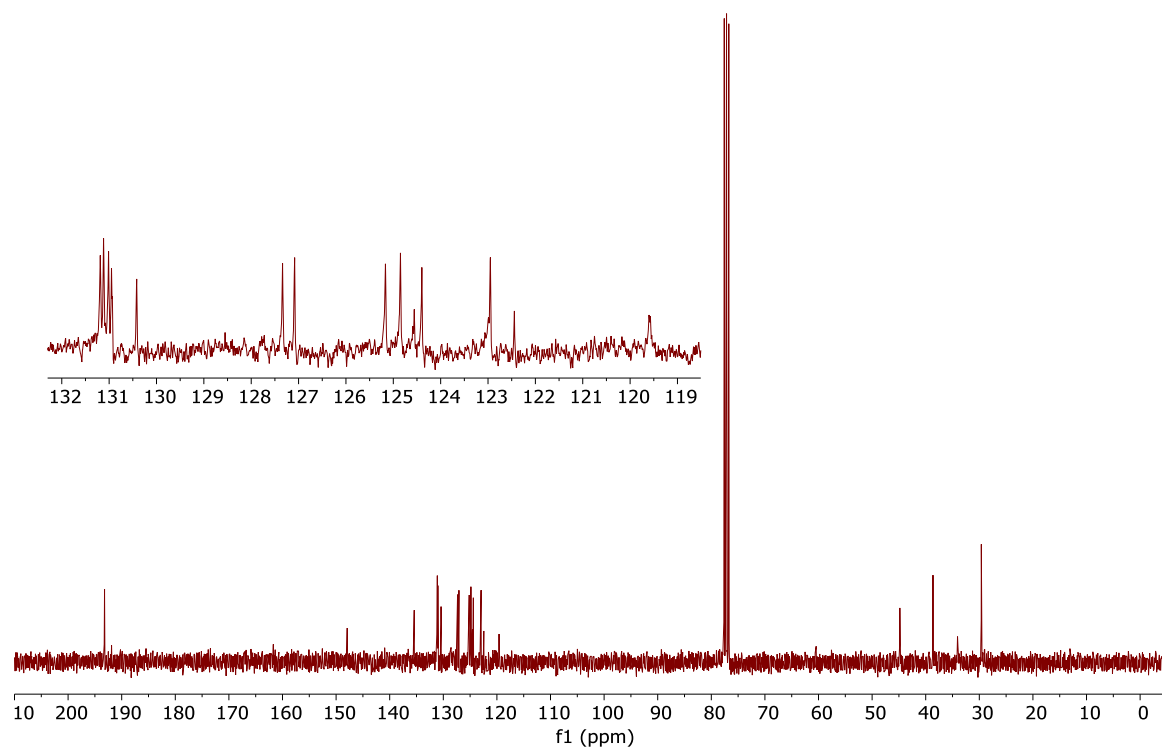
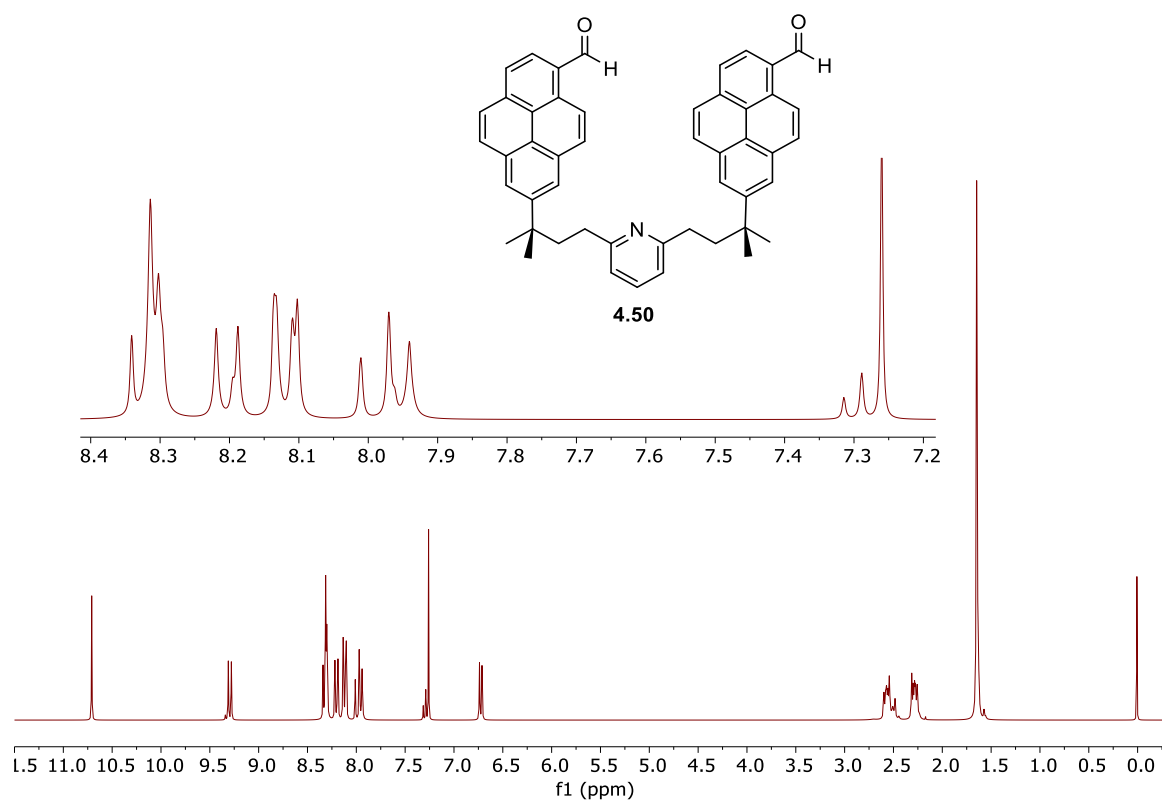
10. Zhang, B.; Manning, G. P.; Dobrowolski, M. A.; Cyranski, M. K.; Bodwell, G. B. *Org. Lett.* **2008**, *10*, 273–276.
11. a) Grimsdale, A. C.; Müllen, K. *Adv. Polym. Sci.* **2006**, *199*, 1–82. b) Wu, J. S.; Pisula, W.; Müllen, K. *Chem. Rev.* **2007**, *107*, 718–747. c) Watson, M. D.; Fechtenkötter, Müllen, K. *Chem. Rev.* **2001**, *101*, 1267–1300.
12. Merner, B. L.; Dawe, L. N.; Bodwell, G. J. *Angew. Chem. Int. Ed.* **2009**, *48*, 5487–5491.
13. Merner, B. L.; Unikela, K. S.; Dawe, L. N.; Thompson, D. V.; Bodwell, G. J. *Chem. Commun.* **2013**, *49*, 5930–5932.
14. Calculations were performed using the Gaussian 2016 software package and only singlet states were taken into consideration in the TD-DFT analysis. Molecular structures and orbitals were visualized by VMD software.
15. The solubility of tetraol **4.69** improved compared to tetraol **4.65** but, LCMS, ^1H and ^{13}C NMR analysis were not possible due to the precipitation of product during the process of acquisition.

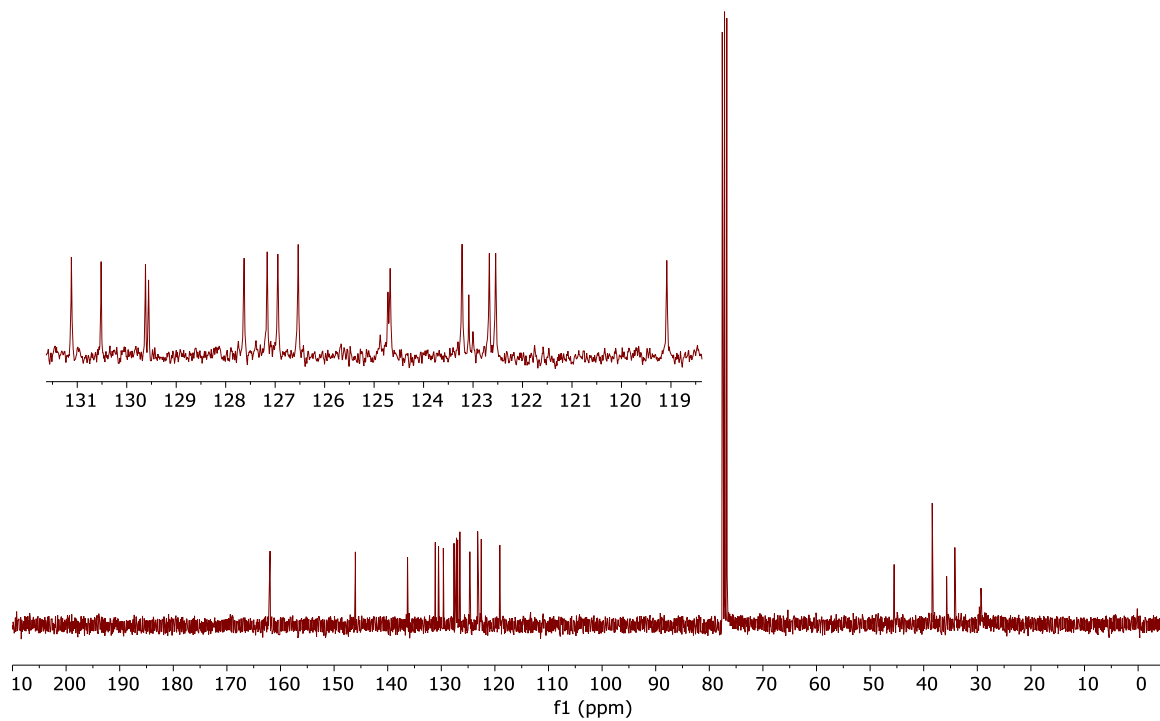
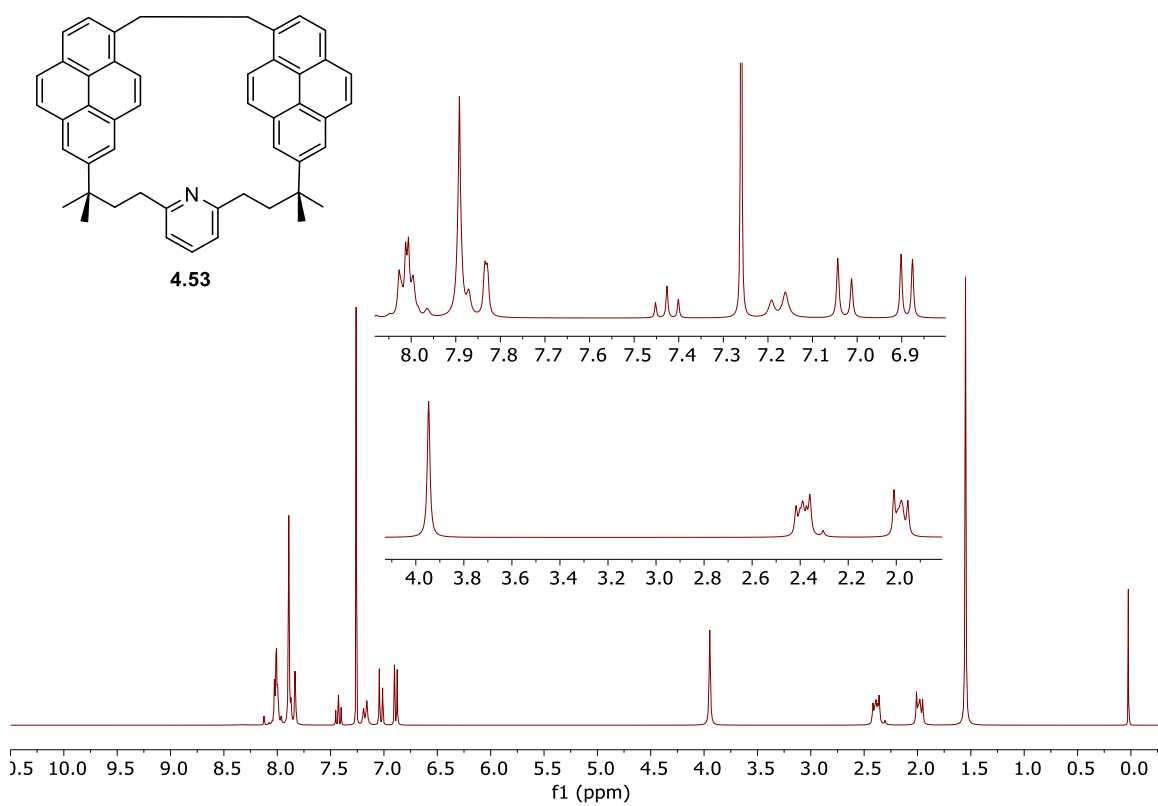
APPENDIX 3

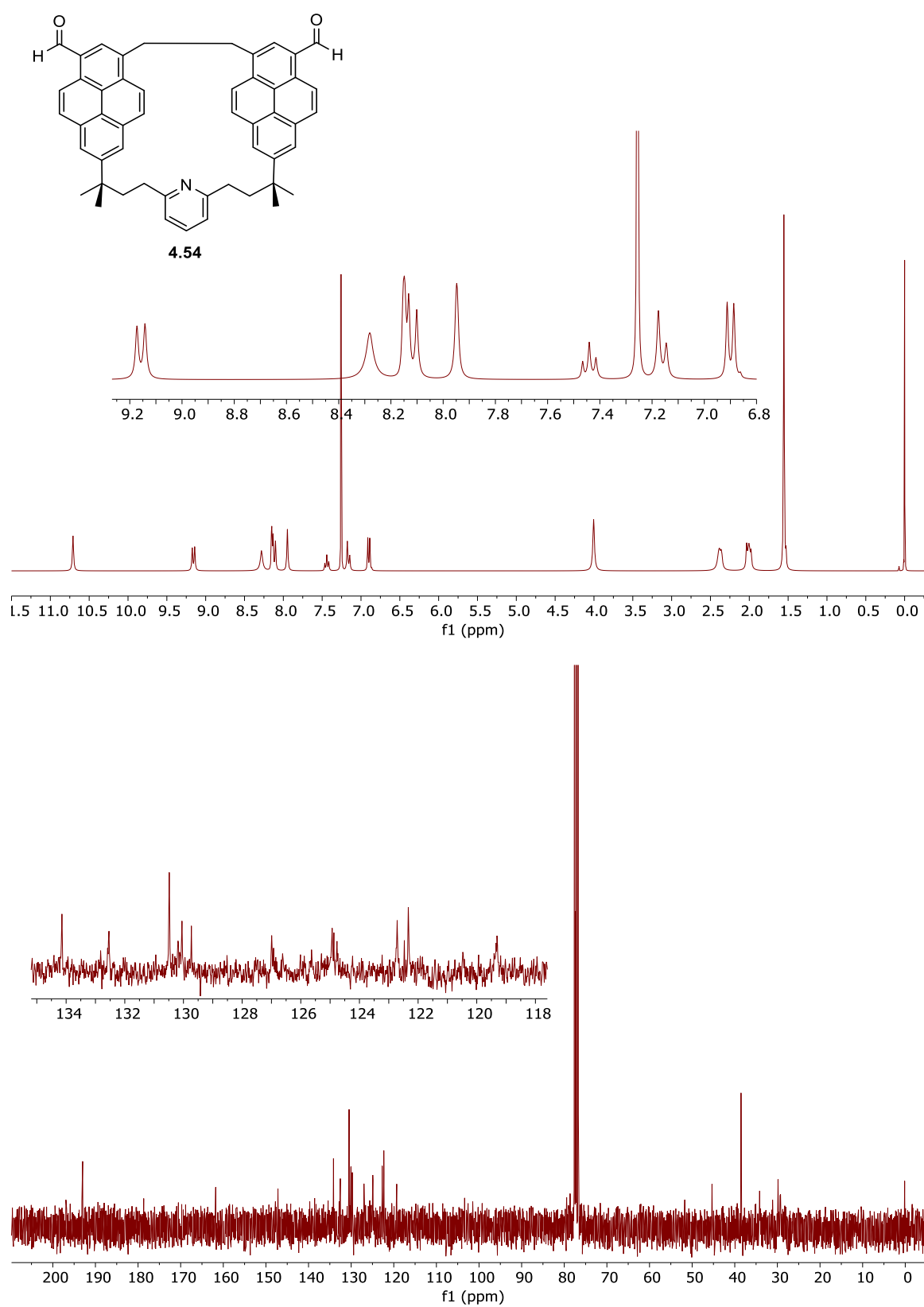


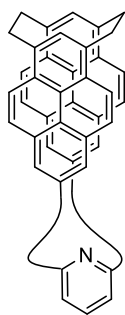












4.58

